Università degli Studi di Torino

Doctoral School of Sciences and Innovative Technologies

PhD Programme in Chemical and Materials Sciences XXXI Cycle

Thermodynamics of Boron-based Complex Hydrides for Energy Storage

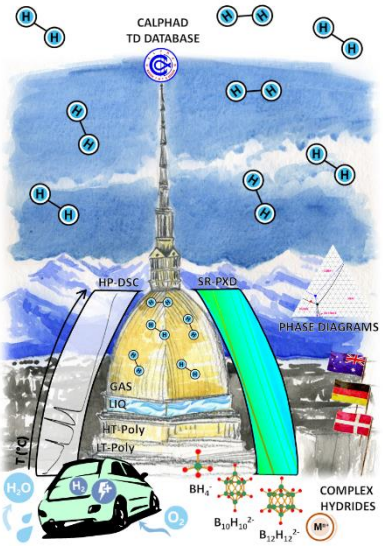

Erika Michela Dematteis

Supervisor:

Prof. Marcello Baricco

Università degli Studi di Torino

Doctoral School of Sciences and Innovative Technologies

PhD Programme in Chemical and Materials Sciences XXXI cycle

Thermodynamics of Boron-based Complex Hydrides for Energy Storage

Candidate: **Erika Michela Dematteis**

Supervisor: Prof. **Marcello Baricco**

Jury Members:

Prof. **Giuseppe Spoto**
Università degli Studi di Torino
Department of Chemistry

Prof. **Torben Renè Jensen**
Aarhus University
Department of Chemistry

Prof. **Chiara Milanese**
Università degli Studi di Pavia
Department of Chemistry

Head of the Doctoral School: Prof. Massimo Maffei
PhD Programme Coordinator: Prof. Mario Chiesa

Torino, September 2018

to Debora and Simone

"Sapienza, scienza e gioia"

"Wisdom, knowledge and happiness"

Ecclesiastes 2:26

"Il cuore intelligente acquista la scienza,
l'orecchio dei saggi ricerca il sapere."

"The heart of the discerning acquires knowledge,
for the ears of the wise seek it out."

Proverbs 18:15

Table of Contents

Preface

This dissertation entitled "Thermodynamics of Boron-based Complex Hydrides for Energy Storage" has been submitted to the Doctoral School of Sciences and Innovative Technologies at the University of Turin to fulfil the requirements for obtaining the PhD. degree in Chemical and Material Science.

The results presented in this dissertation were obtained in the last 3 years as a Ph.D. student of the XXXI cycle (from October 2015 to September 2018) in the Metallurgy research group, under the supervision of Prof. Marcello Baricco, at the Department of Chemistry and NIS centre at the University of Turin.

In the beginning, PhD courses, schools, seminars, workshops and conferences attended, together with teaching activities, periods abroad, publications, oral and poster presentation presented during these 3 years are reported in a short bullet-point overview.

Chapter 1 introduces the field of energy storage in complex hydrides, in particular in boron-based materials, and presents the motivation and goal of these studies.

Chapter 2 summaries the experimental and theoretical methods used in this thesis.

Chapter 3-6 contains the main results obtained during the PhD with an overview of the literature, discussions and conclusions. In details, the thermodynamic properties of pure boron-based complex hydrides such as borohydrides' heat capacities values and closo-boranes' polymorphic transition mechanisms are reported in **Chapter 3**.

The thermodynamic assessment of binary and ternary phase diagrams as a function of composition and temperature for the $LiBH_4$-$NaBH_4$-KBH_4 system are described in **Chapter 4**. More complex systems and possible cationic substitution are explored in **Chapter 5**, including the description of $Mg(BH_4)_2$-$Ca(BH_4)_2$ system, and ternary, quaternary and quinary mixtures in the $LiBH_4$-$NaBH_4$-KBH_4-$Mg(BH_4)_2$-$Ca(BH_4)_2$.

Furthermore, to improve hydrogen release properties, mixture of reactive hydride composite with eutectic borohydrides were investigated and described in **Chapter 6**.

Conclusions and outlook are reported in the final **Chapter 7**.

Acknowledgements

I want to gratefully acknowledge my supervisor Prof. Marcello Baricco for giving me the opportunity of doing research in such a great international network and in a wonderful research group at UNITO, you were more than a supervisor, a personal mentor that constantly revised and helped me to upgrade my academic career and work, always involving me in interesting projects and events.

Furthermore, I want to thank all the people of the metallurgy group at UNITO: the staff, Livio for the fruitful discussion especially during the lab meeting, Paola for the teaching activities and gender seminar initiative, Federico, Alberto and Gianluca for their constant support in the lab; all the students of the Island, my FRIENDS Francesco, Anna, Maria, Nadia, Matteo, Silvia, Dario, Bine, Sofia, Silvère, and my best master student ever, Jus and Valerio. Thanks to all the Via Quarello mates, for the coffes, nice lunch and scientific discussions, especially to Giorgia, Cesare, MichelOne, Matteo, Ale, Giulio, Valentina, and Prof. Silvia Bordiga, Prof. Elena Groppo and Prof. Francesca Bonino.

It would be impossible to cite all the great collaborators in the hydrogen community, but I want to spend few lines.
Special thank in particular to Prof. Torben Renè Jensen, your group is always source of inspiration in the field of inorganic chemistry synthesis methods and crystallographic characterizations, thanks to Mark, Kasper, Steffen, Mathias, Jakob, Bjarne, Arash and Priscilla, for welcoming me for 3 months in Aarhus.

A big thanks to Prof. Martin Dornheim, for hosting me 2 months in Geesthacht at the HZG, a super big thank to Dr. Claudio Pistidda for always helping me with measurements and data evaluation, I furthermore thank all the collaborators in Martin's group, especially Antonio, Giovanni, Anna-Lisa, Gökhan and Hujun. Many thanks to all the friends from the guesthouse for the happy times passed together in Hamburg!

Many thanks to the ECOSTORE fellows, for making me feel part of your international family, special thanks to Matteo, Filippo, Michael, Efi, Joe and Nicola.

Last but not least, thanks to my family: my beloved husband Giacomo, my parents Paola and Bruno and my parent in law Roberta and Mimmo, for their constant love and support.

Abstract

The study performed during this PhD project investigated many boron-based compounds, such as borohydrides and closo-boranes, and mixture of them.
The heat capacity of some borohydrides have been experimentally determined, and an insight on different polymorphs of closoboranes have been performed studying the polymorphic transition mechanism and enthalpies by HP-DSC.
Those values are important and useful information for the thermodynamic assessment of these compounds. Correlations and structure-properties relations have been evidences and discussed.
The $LiBH_4$-$NaBH_4$-KBH_4 ternary system was deepen combining experimental and theoretical investigations. The Calphad method was used to assess the thermodynamics of $LiBH_4$-$NaBH_4$, $LiBH_4$-KBH_4 and $NaBH_4$-KBH_4 pseudo binary systems, as well as a full investigation and assessment of the ternary system for the first time. The evaluation of the hydrogen release reactions from different mixtures in the system was not deeply investigated. A prediction of the decomposition reactions in the system can be done with the current optimised database. However, it should be coupled with experimental evaluation of these reactions. Further studies can be performed and would be of interest.
Extended experimental investigation of the interaction between borohydrides in equimolar ratio in ternary or higher mixtures (up to quinary) were performed in the $LiBH_4$-$NaBH_4$-KBH_4-$Mg(BH_4)_2$-$Ca(BH_4)_2$ system. Furthermore, the $Mg(BH_4)_2$-$Ca(BH_4)_2$ binary system, which was still unstudied, was characterized in function of temperature and composition.
Eutectic mixtures of borohydrides have been mixed with Mg_2NiH_4 to form reactive hydride composite and tailor their hydrogen storage properties to improve hydrogen release temperatures and cyclability. However only a slight improvement of the hydrogen release reactions have been evidenced.
In conclusion, it has been demonstrated that a combined use of *ab-initio* and Calphad thermodynamic calculations, supported and confirmed by experimental measurements, especially *in-situ* techniques, is a powerful tool for a complete description of thermodynamic properties of mixtures of borohydrides. The proficient results from this PhD project have been possible thanks to a wide scientific network and many international collaborations.

Riassunto (Italian Abstract)

Lo studio condotto durante questo progetto di dottorato ha esaminato molti composti a base boro, come ad esempio boroidruri e closoborani, o miscele di questi.
Il calore specifico di alcuni boroidruri è stato determinato sperimentalmente in funzione della temperatura e sono stati effettuati approfondimenti su diversi polimorfi di closoborani studiando il meccanismo delle loro transizioni polimorfe e le relative entalpie mediante HP-DSC.
I valori ottenuti sono informazioni importanti e utili per la valutazione termodinamica di questi composti. Correlazioni e relazioni struttura-proprietà sono state evidenziate e discusse.
Il sistema ternario $LiBH_4$-$NaBH_4$-KBH_4 è stato approfondito combinando indagini sperimentali e teoriche. Il metodo Calphad è stato utilizzato per valutare la termodinamica dei sistemi pseudo binari $LiBH_4$-$NaBH_4$, $LiBH_4$-KBH_4 e $NaBH_4$-KBH_4, nonché una completa indagine e valutazione del sistema ternario per la prima volta. La valutazione delle reazioni di rilascio dell'idrogeno da diverse miscele nei sistemi non è stata approfondita. Una previsione delle reazioni di decomposizione nel sistema può essere eseguita con il corrente database ottimizzato. Tuttavia, dovrebbe essere associato alla valutazione sperimentale di queste reazioni. Ulteriori studi possono essere eseguiti e potrebbero essere di interesse.
Sono stati effettuati studi sperimentali dell'interazione tra boroidruri in rapporto equimolare in miscele ternarie o superiori (fino alla quinaria) nel sistema $LiBH_4$-$NaBH_4$-KBH_4-$Mg(BH_4)_2$-$Ca(BH_4)_2$. Inoltre, il sistema binario $Mg(BH_4)_2$-$Ca(BH_4)_2$, che non era ancora stato studiato, è stato caratterizzato in funzione della temperatura e della composizione.
Miscele eutettiche di boroidruri sono state mescolate con Mg_2NiH_4 per formare un composito di idruro reattivo e migliorare le loro proprietà di stoccaggio dell'idrogeno, le temperature di rilascio dell'idrogeno e la ciclabilità. Tuttavia, è stato evidenziato solo un leggero miglioramento delle reazioni in oggetto.
In conclusione, è stato dimostrato che l'uso combinato di calcoli termodinamici *ab-initio* e Calphad, supportati e confermati da misurazioni sperimentali, in particolare tecniche *in-situ*, è un potente strumento per una descrizione completa delle proprietà termodinamiche di miscele di idruri complessi. I risultati proficui di questo progetto di dottorato sono stati possibili grazie a un'ampia rete scientifica e numerose collaborazioni internazionali.

PhD Activities Report

Publications

1. Dematteis, E. M., Roedern, E., Pinatel, E. R., Corno, M., Jensen, T. R., & Baricco, M. - "A thermodynamic investigation of the $LiBH_4$–$NaBH_4$ system." - RSC Adv., **2016**, 6 (65), 60101–60108. Open Access.
http://doi.org/10.1039/C6RA09301A. IF (18/06/2018): 3.108
2. Dematteis, E. M., Pinatel, E. R., Corno, M., Jensen, T. R., Baricco, M. - "Phase diagrams in the LiBH4–NaBH4-KBH4 system." - PCCP, **2017**, 19, 25071-25079.
http://doi.org/10.1039/C7CP03816J. IF (18/06/2018): 4.123
3. Dematteis, E. M., Vaunois, S., Pistidda, C., Dornheim, M., Baricco, M. – "Reactive Hydride Composite of Mg2NiH4 with Borohydrides Eutectic Mixtures" - Crystals **2018**, 8 (2), 90. Open Access.
http://doi.org/10.3390/cryst8020090. IF (18/06/2018): 1.566
4. Dematteis, E. M., Santoru, A., Poletti, M. G., Pistidda, C., Klassen, T., Dornheim, M., Baricco, M. – "Phase stability and hydrogen desorption in a quinary equimolar mixture of light-metals borohydrides" – IJHE, **2018**, 43 (34), 16793-16803.
https://doi.org/10.1016/j.ijhydene.2018.05.048. IF (18/06/2018): 3.582
5. Milanese C., Jensen T. R., Hauback B., Pistidda C., Dornheim M., Yang H., Lombardo L., Zuettel A., Filinchuk Y., Ngene P., De Jongh P., Buckley C., Dematteis E. M., Baricco M. - "Complex Hydrides for Energy Storage", IJHE, **2018**, submitted. IF (18/06/2018): 3.582

Oral presentations

Presenting author is underlined.

1. Pinatel E. R., Dematteis E. M., Wolczyk A., Paruzzo F., Corno M., Ugliengo P., Civalleri B., Baricco M., ISHE2016, 10th int. Symposium hydrogen Energy, Japan, Sendai, 21-25/02/**2016** - "Assessment of phase diagrams in complex hydrides"
2. ***Dematteis E. M.*** - "The thermodynamics behind the hydrogen society" – – Annual Metallurgy Group Lab. Meeting, Skype Conference – Italy, Vaie (TO), 30/06/**2016**.

3. Dematteis E. M., Wolczyk A., Corno M., Rizzi P., Castellero A., Baricco M., AIMAT2016 & SIB2016, Italy, Ischia Porto, 13-15/07/**2016** - "Assessment of phase diagrams in complex hydrides"
4. Baricco M., Wolczyk A. R., Dematteis E. M., Belmonte N., Marano E., Castellero A., Rizzi P. - Thematic Meeting "Materials for Energy", Institute for Complex Systems, Italy, Rome, 09/09/**2016 -** "Hydrides for Energy Storage"
5. ***Dematteis, E. M.***, Pinatel, E. R., Corno, M., Jensen, T. R., Baricco, M. - To.Ska.Lake Summer School - Total Scattering for Nanotechnology – Italy, Como (CO), 02/06/**2017 -** "Coupling Synchrotron Radiation Powder X-Ray Diffraction and Thermodynamic modelling on Complex Hydrides for Energy Storage"
6. ***Dematteis, E. M.*** Metallurgy Lab. Seminar, Department of Chemistry, University of Turin – Italy, Turin (TO), 09/06/**2017**. – "Experimental investigation and thermodynamic modelling of mixtures of borohydrides for energy storage"
7. ***Dematteis E. M.***, Jensen S. R., Jensen T. R., Baricco M. - EMRS, Fall Meeting 2017, Warsaw University of Technology, Poland, 18-21/09/**2017** - "Heat capacity and Thermodynamic properties of borohydrides" - ***Awarded****: Best student oral presentation of symposium C.*
8. ***Dematteis E. M.***, Santoru A., Poletti M. G., Pistidda C., Dornheim M., Baricco M. - CIMTEC 2018 - 8th Forum on New Materials, Perugia (Italy), Symposium FC - "Thermodynamic Stability of Multi-Cation Complex Hydrides", 13/06/**2018**.
9. ***Dematteis E. M.*** - "Thermodynamic Stability of Multi-Cation Complex Hydrides" — Annual Metallurgy Group Lab. Meeting – Italy, Vaie (TO), 13/07/**2018**.

Poster presentations

Presenting author is underlined.

1. ***Dematteis, E. M.***, Roedern, E., Pinatel, E. R., Corno, M., Jensen, T. R., Baricco, M., "Thermodynamic investigation of the LiBH4-NaBH4 system." - 44th Danish Crystallographers & 7th DanScatt Annual Meeting, Denmark, Aarhus University, 28-29/05/**2015**

2. ***Dematteis, E. M.***, Roedern, E., Pinatel, E. R., Corno, M., Jensen, T. R., Baricco, M., "Experimental and computational investigations on the $LiBH_4$-$NaBH_4$ system" – 8èmes Journées Franco-Italiennes de Chimie / 8o Giornate Italo-Francesi di Chimica, France, Université d'Avignon, 25-26/04/**2016**
3. ***Dematteis, E. M.***, Pinatel, E. R., Corno, M., Jensen, T. R., Baricco, M., "$LiBH_4$-$NaBH_4$-KBH_4 pseudo-ternary system: experimental investigations and modelling" – HyDem 2016, Denmark, Aarhus University, 1-3/06/**2016**
4. ***Dematteis, E. M.***, Pinatel, E. R., Corno, M., Jensen, T. R., Baricco, M., "A first experimental and theoretical modelling of thermodynamic properties of pseudo-ternary $LiBH_4$-$NaBH_4$-KBH_4 system" – MH 2016, Switzerland, Interlaken, 7-12/08/**2016**
5. Baricco M., Wolczyk A., Dematteis E. M., Belmonte N., Marano E., Castellero A., Rizzi P., "Hydrides for Energy Storage"- Materials.it 2016, Italy, Catania, 12-16/12/**2016**
6. ***Dematteis E. M.***, Jensen S. R., Jensen T. R., Baricco M. - "Above room temperature heat capacity of alkali and alkaline earth borohydrides" – Gordon Research Seminar on Hydrogen-Metal System 2017, USA, Boston (MA), 15-16/07/**2017**
7. ***Dematteis, E. M.***, Santoru A., Pistidda C., Dornheim M., Baricco, M. – "Toward high entropy complex hydrides" - Gordon Research Conference on Hydrogen-Metal System 2017, USA,Boston (MA), 16-21/07/**2017**
8. Gulino, V., Dematteis, E. M., Wolczyk, A. R., Chierotti, M., Nervi, C., Baricco, M. - "Development of solid-state electrolytes by anion substitutions in lithium borohydride" - Giornate dell'elettrochimica italiana - GEI 2018, 21-25/01/**2018**, Sestriere, Torino, Italy
9. Gulino, V., Dematteis, E. M., Nervi, C., Baricco, M. - "Development of solid-state electrolytes by anion substitutions in lithium borohydride" - 1st International Symposium on Solid-State Batteries, 28-29/05/**2018**, EMPA, Dübendorf, Switzerland.
10. Barale J., Deledda S., Dematteis E. M., Sørby M. H., Baricco M., Hauback B. C. - "Synthesis and Characterization of Magnesium-Iron-Cobalt Complex Hydrides" - 1st Workshop on Mechanochemistry of Metal Hydride – University of Oslo, Science Park, Oslo, Norway, 30/05-01/06/**2018.**
11. ***Dematteis, E. M.***, Gulino V., Santoru A., Pistidda C., Dornheim M., Baricco, M. - "Solubility in Borohydrides: Role of Thermal Treatment in Mechanochemistry" - 1st Workshop on Mechanochemistry of Metal Hydride – University of Oslo, Oslo, Norway, 30/05-01/06/**2018.**

12. Dematteis E. M., Gulino V., Scaglione F., Santoru A., Pistidda C., Dornheim M., Nervi C., Baricco M. - "Solubility in nanostructured Borohydrides prepared by Mechanochemistry" – NanoInnovation 2018, Rome, Italy, 11-14/09/**2018**.

Teaching activities

1. European Researchers' Night, Let's bet on Chemistry!, Prof. Marco Ginepro – 25/09/**2015**, 6h
2. Metallic materials Laboratory, Prof. Paola Rizzi - 16-24/05/**2016**, 37h
3. European Researchers' Night, Let's bet on Chemistry!, Prof. Marco Ginepro – 30/09/**2016**, 6h
4. Metallic materials Laboratory, Prof. Paola Rizzi - 15-23/05/**2017**, 30h
5. Polymeric materials Laboratory, Prof. Valentina Brunella - 24-25/05/**2017**, 10h
6. European Researchers' Night, Let's bet on Chemistry!, Prof. Marco Ginepro – 23/09/**2017**, 6h
7. Laboratory of Inorganic Chemistry, Prof. Carlo Nervi, 23/10-03/11/**2017**, 40h

Periods Abroad

1. Erasmus Traineeship mobility period: 3 months (25/05-30/08/**2016**) at the Aarhus University, Denmark. Supervisor: Prof. Renè Jensen.
2. Beamtime at Diamond, Oxford, UK. Synchrotron measurements (June **2016**).
3. Erasmus Traineeship mobility period: 2 months (01/03-02/05/**2017**) at the Helmholtz Zentrum Geesthacht, Germany. Supervisor: Prof. Martin Dornheim and Dr. Claudio Pistidda.
4. Beamtime at ESRF, Grenoble, France. Synchrotron measurements (March **2017**).

Conferences attended

1. 44th Danish Crystallographers & 7th DanScatt Annual Meeting, Denmark, Aarhus University, 28-29/05/**2015**
2. HyDem 2016: Hydride as Energy Materials, Denmark, Aarhus, 01-03/06/**2016**
3. JFIC 2016 - 8th Journées Franco-Italiennes de Chimie. – France, University of Avignon, 25-26/04/**2016**
4. MH2016 - 15th International Symposium on Metal-Hydrogen System – Switzerland, Interlaken, 07-12/08/**2016**
5. Gordon Research Seminar & Conference, Hydrogen-Metal Systems 2017, USA, Boston (MA), 15-21/07/**2017**
6. EMRS, Fall Meeting 2017, Warsaw University of Technology, Poland, 18-21/09/**2017**
7. International Hydrogen Energy Agency meeting (IHEA), TASK32, San Servolo, Venice, Italy, 15-18/04/**2018**
8. 1st Workshop on Mechanochemistry of Metal Hydride – University of Oslo, Oslo, Norway, 30/05-01/06/**2018.**
9. CIMTEC 2018 - 8th Forum on New Materials, Perugia, Italy, Symposium FC, Hydrogen Storage and Production, 10-14/06/**2018**

Seminars, Schools and Workshop attended

1. Light and nanomaterials: see, understand, cure. – Luisa De Cola – Italy, University of Turin, Department of Chemistry, 29/09/**2015**
2. 2nd year PhD presentations. – Italy, University of Turin, Department of Chemistry, 15-18/12/**2015**
3. IV School on Raman Spectroscopy for Earth science and Enviroment, Italy, Turin, 19-21/01/**2016**
4. Darwin Day: How much chemistry there is in the evolution? – Italy, University of Turin, Department of Chemistry, 12/02/**2016**
5. New frontiers in NMR spectroscopy: from biochemistry to materials. – Italy, University of Turin, Department of Chemistry, 03/03/**2016**
6. From Molecular Switches to functional materials. – Silvia Giordani – Italy, University of Turin, Department of Chemistry, 04/03/**2016**

7. The Chemistry of your Documents: Creating texts people want to read. – Daniela Drago – Italy, University of Turin, Department of Chemistry, 04/03/**2016**
8. Metallurgy Group Lab. Meeting, Web Meeting, Italy, Vaie (TO), 30/06/**2016**
9. New materials for electrochemical energy conversion and storage. – Vito Di Noto – Italy, Politecnico di Torino, Department of Applied Science and Technology, 05/09/**2016**
10. Communicate the chemistry in the age of the web 2.0 - Ordine dei chimici del Piemonte e della Valle d'Aosta, 09/09/**2016**
11. 2nd year PhD presentations. – Italy, University of Turin, Department of Chemistry, 29-30/09/**2016**
12. Day for the valorization of PhD's and PostDoc's competences - Italy, University of Turin, 04/10/**2016**
13. Harnessing the power of light in hybrid materials. - Italy, University of Turin, Department of Chemistry, 06-07/10/**2016**
14. Energy: metallic materials and storage. Studying day. - Italy, AIM, Milan, 16/12/**2016**
15. Chemical Journeys – Italy, University of Turin, Department of Chemistry, 22/12/**2016**
16. To.sca.lake 2.0: Total Scattering for Nanotechnology on the Como Lake - Italy, Como, 29/05/2017-02/06/**2017**
17. Building your career in the EU – Italy, University of Turin, 09/05/**2017**
18. Overcoming limitations of Li-ion batteries with Multivalent Cathode Materials, Pieremanuele Canepa - Italy, University of Turin, Department of Chemistry, 05/07/**2017**
19. Metallurgy Group Lab. Meeting, Italy, Vaie (TO), 06/07/**2017**
20. 2nd year PhD presentations. – Italy, University of Turin, Department of Chemistry, 25/09/**2017**
21. Biosensors and Catalysis: Applications of Nanoporous Gold, Federico Scaglione, Department of Chemistry, University of Turin, 20/11/**2017**
22. Gender equality: don't change women, change the system, Department of Chemistry, University of Turin, 24/11/**2017**
23. The profession of Chemistry: a dialogue between generations inspired by Primo Levi. – **Invited Speaker** - Italy, University of Turin, Department of Chemistry, 20/12/**2017**
24. Chemical Journeys – Italy, University of Turin, Department of Chemistry, 22/12/**2017**

25. Effect of different processing routes on the properties of thermoelectric materials, Francesco Aversano - Italy, University of Turin, Department of Chemistry, 19/01/**2018**
26. The small and wonderful world of nanomaterials: synthesis and characterization of novel ferromagnetic nanostructures, Matteo Cialone - Italy, University of Turin, Department of Chemistry, 09/03/**2018**
27. Promotion of Basic Epistemological Understanding of Science, Christiane Reiners - Italy, University of Turin, Department of Chemistry, 16/03/**2018**
28. International Hydrogen Energy Agency meeting (IHEA), TASK32, San Servolo, Venice, Italy, 15-18/04/**2018**
29. Two hundred years of mixed crystals. – Accademia delle Scienze, Sala dei mappamondi, Turin, Italy, 22/05/**2018**
30. 1st Workshop on Mechano-chemistry of Metal Hydride – Oslo, University of Oslo, Science Park, 30/05-01/06/**2018**
31. Marie Sklodowska-Curie Individual Fellowships tenders: how to write a successful proposal. - Italy, University of Turin, 06/06/**2018**
32. Metallurgy Group Lab. Meeting, Italy, Vaie (TO), 13/07/**2018**
33. Event Energy Center Lab – Energy Storage Seminar – Prof. Silvia Bodoardo, Prof. Arnaldo Visintin, Prof. Ezequiel Leiva, Politecnico di Torino, Turin, Italy, 11/09/**2018**

PhD Courses Attended

1. Biomass wastes as renewable source of energy and chemicals - Various Teachers - University of Turin, Department of Chemistry, 4 CFU.
2. The Evolution of Heterogeneous, Homogeneous and Enzymatic Catalysis. Key Processes and Scientists. - Adriano Zecchina - University of Turin, Department of Chemistry, 2 CFU.
3. Bioinspired Materials. - Federico Bosia - University of Turin, Department of Chemistry and Physics, 2 CFU.
4. Basic Course – Solidification. – Various Teachers - Associazione Italiana Metallurgia, 3 CFU.
5. Statistical Thermodynamics in Chemistry and Materials Science. - Roberto Dovesi - University of Turin, Department of Chemistry, 5 CFU.
6. Research funding opportunities and international training and mobility. - Emilia Sannino - University of Turin, Department of Chemistry, 2 CFU.

7. English for Academic Purposes - Writing and Communication Skills. - Alice Spencer - University of Turin, 4 CFU.
8. Course in preparation for the state exam and qualification to practice the profession of chemist – Various Teachers - Ordine dei chimici del Piemonte e della Valle d'Aosta, 10 CFU. **National Abilitation in Chemistry**, November **2016**.
9. The Rietveld Method - Angelo Agostino - University of Turin, CRISDI, 2 CFU.
10. The Debye Scattering Equation: a Total Scattering Approach for Characterizing Nanomaterials - Federica Bertolotti - University of Turin, CRISDI, 1 CFU.
11. Solid State NMR - Michele Remo Chierotti - University of Turin, Department of Chemistry, 3 CFU.

List of Abbreviations

BM: ball milling
C_p, C_v: heat capacity at constant pressure or volume
DFT: Density Function Theory
DSC: Differential Scanning Calorimeter
DTA: Differential Temperature Analysis
FCH-JU: Fuel Cells and Hydrogen Joint Undertaking
GAP: Gender Action Plan
GFE: Gibbs Free Energy
HP: high pressure
HT: high temperature
JANAF: Joint Army-Navy-Air Force
LT: low temperature
NIST: National institute of Standard and Technology
NKR: Neumann –Kopp rule
PT: polymorphic transition
PXD: Powder X-ray Diffraction
RHC: Reactive Hydride Composites
RK: Redlich-Kister
RT: room temperature
SGTE: Substance Scientific Group Thermodata Europe
SR: Synchrotron Radiation
SS: stainless steel
UNCCC: United Nations Climate Change Conference
US-DOE: United State Department of Energy
WC: tungsten carbide
ZPE: zero-point energy

Chapter 1 - Introduction

Energy and climate crisis

In the XIX century, industrial revolutions brought impressive progress and development, starting from steam power and new machinery for production, which had transformed the world of work and manufacture.
The world population started to increase exponentially, human welfare and technological progress were often assumed to walk together.[1]
The second half of the nineteenth century brought a huge range of new techniques and new materials to the industrialised nations and the energy demand started to grow dramatically (**Figure 1**) together with the increase of population during the last fifty years.[2]
In the late twentieth century, industrialised societies entered an age of ambivalence, of mixed feelings about technology and its role in the world. As global temperatures rise, the climate change and pollution become the obvious side effects of the extreme use of fossil fuels for the production of energy and synthetic materials. The economic, energetic and climate crisis were started and this put stress on worldwide energy infrastructure.

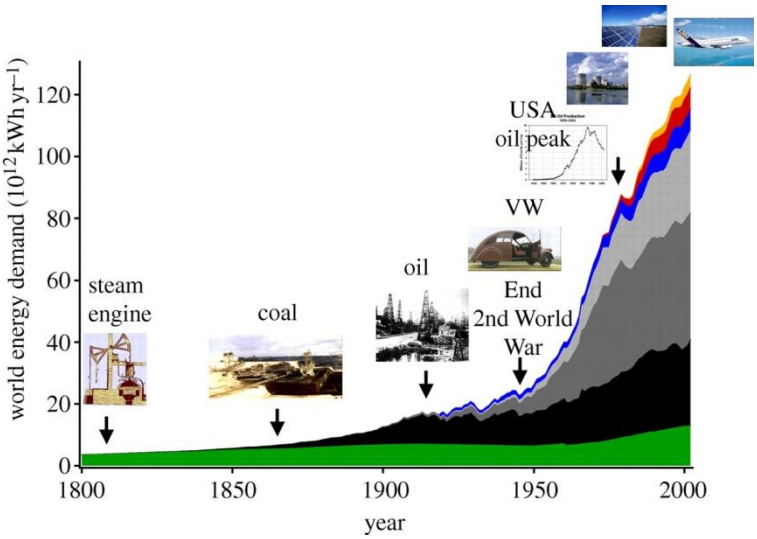

Figure 1 – Energy demand and energy carriers from the XIX century to nowadays. Orange, renewables; red, nuclear fission; blue, hydro power; grey, natural gas; dark grey, crude oil; black, coal; green, biomass.[2]

Gender and climate change

Climate change is making our world more dangerous, a changing climate affects everyone, but it is the world's poorest and most vulnerable, such as the elderly, immigrants, indigenous groups, but especially women and girls, who withstand the worst of environmental, economic, and social shocks. The reason why women and girls are more vulnerable to climate change is often socially constructed, in many developing countries, women and girls are predominantly responsible for food production, household, water supply, and energy supply for heating and cooking.[3–5] As climate change impacts increase, these tasks become more difficult and more time consuming. Nevertheless, women are also at the forefront of the solutions. Women are early adopters of climate-friendly agriculture and clean energy. Women also offer solutions and valuable insights into better managing climate risks.[6]

At the last United Nations Climate Change Conference (UNCCC), governments approved the Gender Action Plan (GAP), recognising the importance of involving men and women equally in climate action. With GAP we have entered in a new era in which we must enable women leadership in decision-making at all level of society. By empowering women and girls, we can both address a right issue, and give ourselves a better chance to meet the sustainable development goals and the Paris agreement. In fact, in the 2015 Paris agreement, calls for gender equality and women's empowerment were clearly established.

Sustainable energy is a human development enabler, which helps in the national development and advance social progress. The reduction of the carbon footprint of energy is imperative in the fight against climate change, and it plays a central role in climate change mitigation. Women have more sustainable consumption choices and, as household energy managers, tend to have a bigger say in household energy decisions. Thus, from the standpoint of consumption, the design, production, distribution and sales of sustainable energy technologies (for example, clean cooking stoves and lighting devices) would benefit from having women contribute to shaping the clean energy value chain. Their position in society equips them with an understanding of the cultural and community context, which is useful for introducing behavioural change with regard to energy consumption at the household level.[7,8]

Climate change can undo decades of development. It is not only a matter of clean and suitable technological development, but also genuine and suitable human development, which cannot be realised without gender equality.

Role of energy storage

Furthermore, to fight climate change, keeping the same welfare standard levels reached, the development of good, clean and efficient materials for energy storage is the bottleneck for using only renewable energies, instead of fossil fuel, because of their intermittent production of energy over time and geography.[1] It is therefore important to design a system that allows storing excess energy to meet future demand and utilisation at another place or time.

The phasing-out of the fossil fuels cannot be solved by a single technology but must involve the development of different approaches, which could offer economic and environmental benefits, and cover any requirements concerning application, cost and footprint, so taking into account all its life cycle assessment.

We entered in the clean energy revolution era.

Basic research and knowledge on new class of multifunctional materials will lead the way for the development of such flexible and efficient energy storage, the key to a reliable clean electricity supply.

The storage facilities that do exist use pumped hydropower,[9] a system that pumps water uphill to a reservoir when excess electricity is available and then lets the water flow downhill through turbines to generate electricity when it is needed. However, it can only be located in very limited areas.

Developing new energy storage technologies that are comparable in reliability and cost to pumped hydropower, and are deployable at any location could enable the storage of vast amounts of electricity anywhere on the grid worldwide.

Improved methods for storing and dispatching electricity would enable the increased use of renewable electricity generation while maintaining high reliability in electric supply.

A continuous flow of clean energy can be obtained with the development of smart grids connected with different energy storage systems such as batteries or heat storage systems.

Hydrogen is considered as potential future energy carrier for mobile and large-scale stationary applications, but it requires an efficient storage strategy and unfortunately lots of problem in using of hydrogen as energy vector still require solution.[10,11]

Furthermore, it can be used to reduce CO_2 and produce synthetic fossil fuel following the closed carbon cycle which is CO_2-balanced (**Figure 2**).[2,12,13]

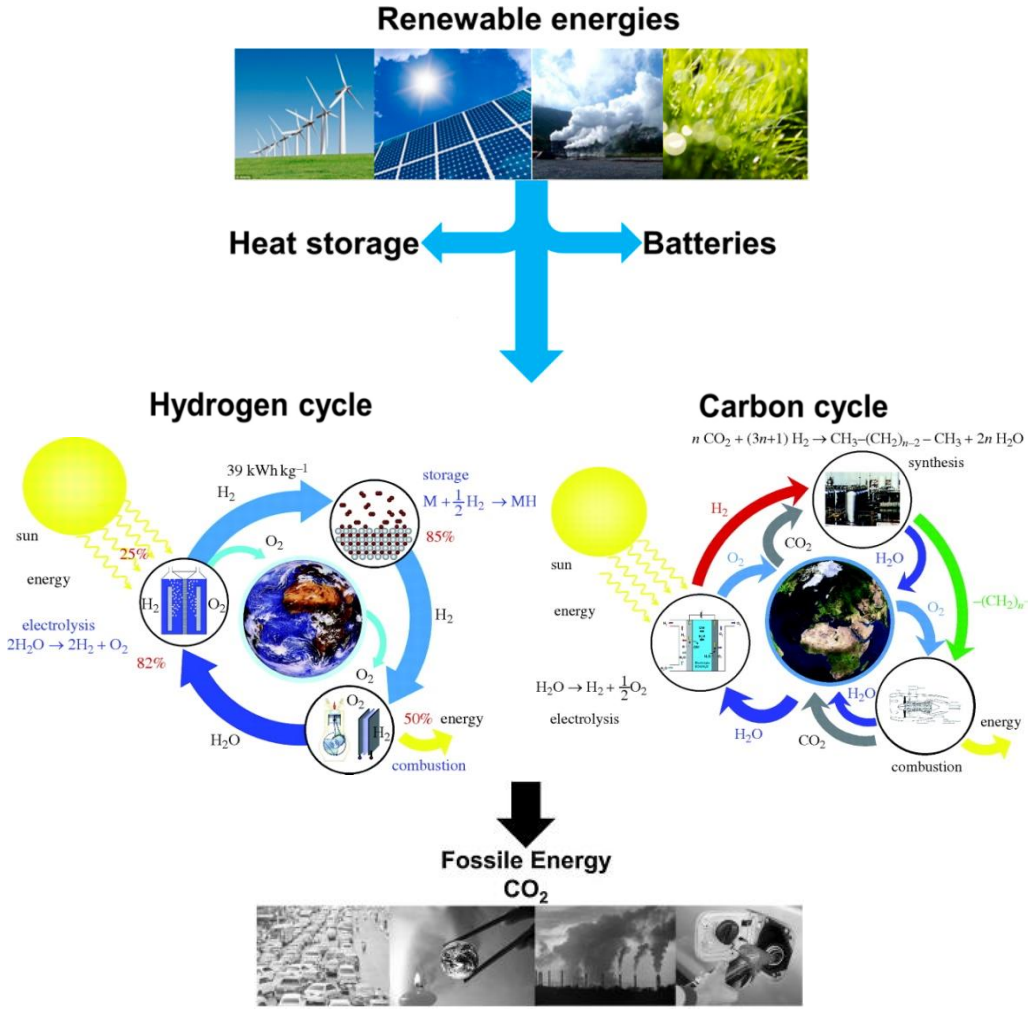

Figure 2 – Illustration of a suitable energy storage system based on different technologies and the hydrogen and carbon closed cycles, which are CO_2-free or balanced, while it is not in the case of fossil energy. Modified figures from[2,14,15]

Hydrogen economy

Hydrogen is the first element of the periodic table and the most abundant in the universe. Currently, most hydrogen is produced from fossil fuels, specifically natural gas. Electricity from the grid or from renewable sources such as wind, solar, geothermal, or biomass is also currently used to produce hydrogen. Thermochemical processes use heat and chemical reactions to release hydrogen from organic materials such as fossil fuels and biomass.

Renewable hydrogen can be obtained, in a complete CO_2-free cycle, by electricity from renewable sources and by splitting water (H_2O) into hydrogen (H_2) and oxygen (O_2) using electrolysis or solar energy as shown in **Figure 2**.[16]
Hydrogen can then be stored in gas, liquid or solid state and used whenever and wherever needed to produce energy and water in a fuel cell, closing the cycle, or to react with CO_2 and a proper catalyst to obtained synthetic fossil fuels.[5,6]
Hydrogen storage is a key enabling technology for the advancement of hydrogen and fuel cell technologies in applications including stationary power, portable power, and transportation. Hydrogen has the highest energy per mass of any fuel; however, its low ambient temperature density results in a low energy per unit volume, therefore requiring the development of advanced storage methods that have potential for higher energy density, such as in the case of solid-state hydrogen storage materials.
Solid-state hydrogen storage is a valid alternative to traditional methods and would overcome their problems.[17] The use of solids for hydrogen storage would allow the development of new lightweight and compact systems with high volumetric and gravimetric capacity of hydrogen and therefore the achievement of the objectives set by the Fuel Cells and Hydrogen Joint Undertaking (FCH-JU)[18] and the United States Department of Energy (US-DoE).[19]
FCH-JU supports research, technological development and demonstration on fuel cell and hydrogen technologies in Europe with the aim of accelerating commercialization and using its potential to achieve a low-carbon energy system,[20] while the DoE has established certain targets within the development of fuel cell vehicles.
The targets for the on-board hydrogen storage for light-duty fuel cell vehicles from the US-DOE are reported in **Table 1**:[19]

Table 1 – European and DOE targets for on-board hydrogen storage.[19]

Storage Parameters	2020	2025	Ultimate	Units
Gravimetric hydrogen density	4.5	5.5	6.5	[wt%]
Volumetric hydrogen density	30	40	50	[kg_{H2}/m^3]
Cost	333	300	266	[$/$kg_{H2stored}$]
Operating temperature	-40 / 60	-40 / 60	-40 / 60	[°C]
Min/Max delivery temperature	-40 / 85	-40 / 85	-40 / 85	[°C]
Operational cycle life	1500	1500	1500	[cycles]
Onboard efficienty	90	90	90	[%]
Refuelling time (5 kg)	3-5	3-5	3-5	[min]

Figure 3 compares different hydrogen storage systems as a function of their gravimetric and volumetric hydrogen density.

Physical-based hydrogen storage in gas and liquid phase both display low volumetric density, which is not suitable for mobile applications. In the gas phase, the hydrogen density is strongly related to the kind of material used for the tank and storage pressure. Liquid-state hydrogen storage has a constant volumetric density while the gravimetric density increases with the dimension of the tank; however, it requires cryogenic temperatures. Metal hydrides and complex hydrides are promising solid-state hydrogen storage materials owing to their high hydrogen density both gravimetric and volumetric, in a wide range of different values depending on the elements involved.

Material-based hydrogen storage can be performed on the surfaces of solids (adsorption) or within the solids (absorption). Example of material-based hydrogen storage are MOFs (adsorbent), organic liquids, chemical hydrides (i.e. NH_3BH_3), interstitial hydride or complex hydrides.

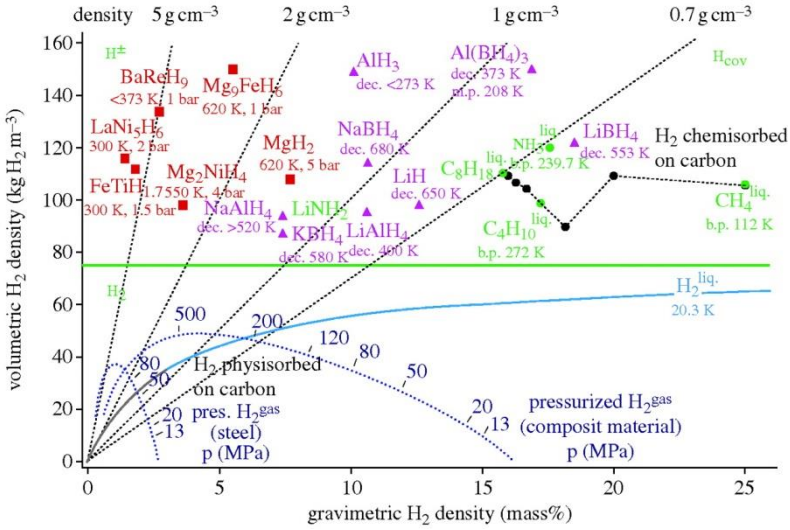

Figure 3 – Energy demand and energy carriers from the XIX century to nowadays. Orange, renewables; red, nuclear fission; blue, hydro power; grey, natural gas; dark grey, crude oil; black, coal; green, biomass.[2]

Energy storage in complex hydrides

Recent research has been focused on solid-state hydrogen storage materials, which allow storing hydrogen at low pressures. In particular, low cost and light weight complex hydrides have been considered and, among them, metal borohydrides are interesting compounds owing to their high gravimetric hydrogen content.[14,21–25] In this frame, the development of materials able to store hydrogen

close to room temperature and ambient pressure will enable the use of hydrogen in mobile and stationary large-scale applications.

However, light metal and complex hydrides absorb and release hydrogen through sluggish kinetics at relatively high temperatures (**Figure 4**).[26] In order to reduce their thermodynamic stabilities, transition metals have been added to form complex metal hydrides,[27] such as in the case of MgH_2 mixed with Ni to form Mg_2NiH_4, with a theoretical hydrogen content equal to 3.6%wt.

The so called Reactive Hydride Composites (RHC), for example, allows mixtures of metal hydrides and borohydride to release hydrogen in a reversible manner under moderate temperature and hydrogen pressure conditions.[28]

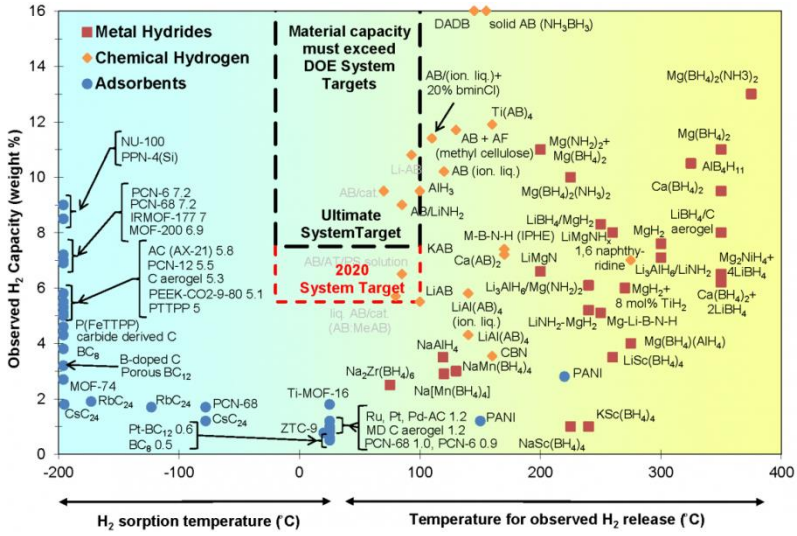

Figure 4 – Hydrogen gravimetric capacity as a function of hydrogen release temperature for different solid-state hydrogen storage systems.[26]

Borohydrides

Borohydrides are inorganic ionic compounds suitable for hydrogen storage in the solid state and they are a multifunctional class of materials that may also be used as fast ion conductors for new types of batteries, for gas adsorption or CO_2 capture and recycling.[25] They may also have optical, electronic and magnetic properties and can be used as reducing agents in organic synthetic chemistry.[25] Since they contain a large amount of hydrogen, they are promising materials as neutron shield from ionizing radiation such as high energy electrons and protons

in the space.[19] The most promising ones contain a light alkali or alkali-earth metal cation ionically bonded to the complex borohydride anion (BH_4^-).[25]
For their rich chemistry and tuneable properties in relation to their structures and interactions in mixtures, the attention of the latest research focused on the synthesis and characterization of new borohydrides.[23,25]
Since borohydrides show high hydrogen content, the research focus on studying their thermodynamic and hydrogen release properties.[22,30–32] The first group metal borohydride has shown the highest hydrogen content but also high thermodynamic stability and slow kinetic in hydrogen release and uptake.[33] The second group metal borohydride show low temperature of decomposition and release of hydrogen and when observed the melting of mixture turns into dark brown color instead of transparent liquid because of decomposition before melting.[34–36]
The theoretical hydrogen content of $LiBH_4$ is 18.5%wt, i.e. the highest among metal borohydrides, while it is equal to 10.7%wt for $NaBH_4$, 7.5%wt for KBH_4, 14.9%wt for $Mg(BH_4)_2$ and 11.6%wt for $Ca(BH_4)_2$. Observed values are usually lower, depending on the experimental conditions.[37]
The temperature of decomposition has been correlated with the Pauling electronegativity, a metal borohydride with a metal that has a Pauling electronegativity higher than 1.6 decomposes at low temperature, often releasing hydrogen and diborane, while, if the electronegativity is lower than 1.4, only hydrogen is released.[38,39]
However, the kinetic and thermodynamic limitation of these compounds has to be addressed and different approaches have been described in the literature to improve them.[28,40,41]
For instance, the melt infiltration of eutectic mixtures of borohydrides[31,32] into mesoporous carbon scaffolds improves the kinetic and reversibility of hydrogen release.[44–50] In this way, the kinetics and reversibility of hydrogen sorption/desorption reactions can be improved, because nanosized particles are preserved during cycling. Moreover, low melting mixtures of complex hydrides have been studied recently as ionic liquids, aiming to provide fast and convenient re-fuelling of hydrogen in fuel cell vehicles.[51,52] The use of eutectic mixtures is strongly related to the stability of the liquid phase, therefore the characterization of their thermodynamic properties is of fundamental importance.[44,53,54] Recently, a systematic study of hydrogen release in pure and eutectic mixtures of borohydrides was reported by Paskevicius et al..[34]
Among many tailoring routes, cation and anion substitution in borohydrides has been demonstrated to provide solid solutions[55–64], i.e. cationic or anionic fully

disordered structures, as well as hydrogen-fluorine exchange which improved the hydrogen desorption reactions.[64–67]
On the other hand, by mixing different light-metals borohydrides, the formation of bimetallic and trimetallic compounds, i.e. cationic or anionic fully ordered structures, were evidenced. New applications of bimetallic compounds have recently been suggested.[25]

Closo- deca and dodeca- boranes

Boron hydrides belong to a wide family of different compounds characterized by many different stoichiometry. The borane can also be considered complex anions. The borohydride anion, whose compounds were described before, is a particular class of polyhedral borane called *nido*-borane. During decomposition and hydrogen release, borohydrides can form higher boranes, which are another class of boron-based compounds with an extremely rich chemistry and broad application fields.
Closo-boranes (i.e. $B_nH_n^{2-}$) are the most stable class of anions among boranes, which have a closed polyhedral cluster where *n* boron atoms occupied all corners together with *n* terminal hydrogen atoms.
Metal-$B_{10}H_{10}$ and metal-$B_{12}H_{12}$ are considered to be reaction intermediates in the decomposition of many metal borohydrides[68,69] and are widely studied as solid-state ionic conductors as well. Moreover, they are promising for boron neutron capture therapy, for cancer treatment, owing to the large neutron scatter cross section of 10B and since their chemical stability in biological systems make them relatively nontoxic.[70]
It is fascinating that many of the current synthesis methods and applications were developed over 50 years ago, yet fundamental questions regarding structure, dynamics and reaction mechanisms continue to intrigue scientists today in many research fields and for many technology applications.
All the alkali metal-$B_{10}H_{10}$ and metal-$B_{12}H_{12}$ displays a polymorphic transition at different temperatures depending on the cation ionic radius, showing a reorientational motion of the boron cage complex anion.[70]
The anion reorientation and/or the order-disorder polymorphic transition are coupled by fast cation conduction in the high temperature polymorph making these material extremely promising as fast solid-state ion conductors.[71]
Some hypothesis behind this sudden ion conductivity jump were described by the paddle-wheel or percolation-type mechanism.[72,73]

Aim of the thesis

As said before, mixture of borohydride were studied in order to obtain better condition of release and uptake of hydrogen by means of cation or anion substitution, infiltration into nanoscaffold and studies of eutectic mixture for tailoring properties.[28]
The investigation of thermodynamic properties is the first step for a better understanding of these several systems and first of all a deep knowledge of pure compound is needed for a better planning for experimental design of mixture,[74,75] though many fundamental thermodynamic parameters or properties have not been assessed yet. Calculation of thermodynamic properties with the Calphad method,[76] together with a critic revision of the literature values reported and ab initio or experimental determination of missed values, allows the optimization of systems or compounds in order to design and predict new experiment or investigate multicomponent systems.[77]
The use of the Calphad approach, as it will be shown later on, for the assessment of the phase diagrams in complex hydrides allowed the determination of different thermodynamic properties and possible decomposition routes or hydrogen release reactions, together with the enthalpy of mixing in the liquid and solid solutions, which cannot be easily determined experimentally.[63,78–80]

The present thesis aims to fill the gap between numerous experimental studies and assessment of thermodynamics of complex systems, from binary up to quinary combination of borohydrides.
Thermodynamic properties of pure boron-based compounds, i.e. borohydrides and closoborane, were experimentally determined ad assessed, with an insight on new structures, polymorphic transition and melting mechanism, and heat capacities.
Cationic substitutions in binary and higher mixture have been investigated to define the stability of phases upon mixing and upon heating, together with the study of their decomposition. A tailoring of decomposition temperature has been performed by mixing eutectic borohydride with Mg_2NiH_4 complex hydride.
The final goal of this study is to define the nature of interactions in the solid and liquid state, finding correlations between thermodynamic parameters, structures and energy storage properties of complex boron-based hydrides.

Chapter 2 – Synthesis and Characterisation Methods

Mechanochemistry

Mechanochemical treatment, i.e. ball milling (BM), is a well established solid-state unconventional synthesis method. It is widely used to reduce and modify the morphology and size of materials by high-energy impacts. The dimension and diameter of vials and balls, together with speed rotation or vibration frequency, are important parameters in the definition of synthesis conditions and impact energy values. Mechanochemistry is considered an unconventional and green synthesis route because it could not imply solvents and, thanks to the high energy involved, it can be used to drive reaction in the solid state, leading to different products, including metastable ones.
Ball milling is widely used to obtain miscibility among immiscible elements (i.e. metallic solid solutions by mechanical alloying), metastable compounds, nanostructured or amorphous phases; thus, metathesis and addiction reaction can be performed as well.[81,82]
Together with morphology, microstructural changes and grain size, which generally decreases and creates new highly reactive surfaces, high energy ball milling introduces a severe plastic deformation because of the interaction between milling balls and powders, introducing stress and strain in the material, increasing defect concentration and the interface area.[83]
Using special vials, mechanically-induced solid/gas reactions can be performed. During reactive ball milling under hydrogen pressure, ternary and quaternary complex hydrides can be synthetized.[84] Furthermore, the use of diborane or ammonia gas allows to synthetize borohydrides and amides, respectively. Pressure and temperature sensors allow to record reaction condition inside the vial during the milling.[84,85]
This powerful tool was widely used in the past to synthetize new complex hydrides, among whom many borohydrides, and to tailor their kinetics and thermodynamics by nanosizing.[81,82]

During this study, pure borohydrides were purchased from Sigma-Aldrich, Rockwood Lithium, KatChem, ABCR, Merck or synthetized by combination of ball milling and wet chemistry, in collaboration with the Aarhus University.
The purity of each borohydride was generally higher than 95%: lithium borohydride ($LiBH_4$) >95%, sodium borohydride ($NaBH_4$) >98%, potassium

borohydride (KBH_4) >97%, magnesium borohydride ($Mg(BH_4)_2$) >95% and calcium borohydride ($Ca(BH_4)_2$) >95%.
Fine grinded homogenous mixture were obtained by milling and mixing the reactants in the right molar composition in a Fritsch Pulverisette 6 planetary mill under an inert atmosphere of argon or nitrogen in 80 mL tungsten carbide (WC) or stainless steel (SS) containers and with WC or SS balls (o.d. 5, 6 or 10 mm).
A balls-to-sample mass ratio of 30:1 was used; around 0.5 up to 2 g of powder ware milled for 5 min, and followed by 2 min pause for 24 repeated sequences, using a speed of 350 r.p.m. and a total milling time of 120 minutes.
Mg_2NiH_4 was synthesized by reactive ball milling MgH_2 and Ni in a molar ratio 2:1. Approximately 5 g of powder were milled for 10 h at 350 r.p.m. in a custom-made stainless steel 250 ml vial, under 10 bar of hydrogen and a ball-to-powder mass ratio of 5:1, using 15 mm SS balls. After milling, the powder was transferred in a Parr Reactor and heated under 10 bar of hydrogen up to 370 °C for 10 h.
All preparations and manipulations of the samples were performed in argon-filled or nitrogen-filled glove boxes with a circulation purifier, with O_2 and H_2O levels lower than 1 ppm because of their reactivity to moisture.

X-ray Diffraction

Powder X-ray Diffraction (PXD) is a useful nondestructive analysis, which allows the determination of crystallographic structure of crystalline materials, providing information on chemical composition and physical properties of samples.
The interaction of a monochromatic electromagnetic radiation within energies, thus wavelength, comparable with the interplanar distance of a crystal produces diffraction if the Bragg equation is satisfied.[86,87]
The collection of the diffracted beam, which produces a constructive interference, generates a diffraction pattern.
Any crystalline material have a characteristic diffraction pattern, that can be used to get information about different phases present in mixtures or structural information of the material, so both for qualitative and quantitative analysis.
The intensity of the peaks is related with the amount of the phase, the scattering factor of the material, its electron density, the intensity of the beam and preferred orientations. The position of the peak is related to the wavelength of the radiation, the specimen displacement and unit cell parameters, while the shape of the peak is related to thermal parameters, and sample shape, size and strain. The peak shapes observed are a function of both the sample (e.g. domain size,

stress/strain, defects) and the instrument (e.g. radiation source, geometry, slit sizes).
X-rays generated from a laboratory source allows *ex-situ* analysis at room temperature, but it usually requires long exposure or pattern collection time to obtain reliable data to be further analysed by the Rietveld Method.
Synchrotron Radiation (SR) sources display high brilliance and allow collecting, within seconds, high resolution PXD patterns for *in-situ* time resolved studies or structure resolution of unknown phases or new compounds.[88,89]
For this reason, SR-PXD is a powerful technique for the study of complex hydrides stabilities as a function of temperature, decomposition mechanism or reactions.
Different beamlines at synchrotron radiation facilities have been used for this study, allowing the investigation of structure of boron-based complex hydrides as a function of time, temperature and pressure and, as a consequence, to determine phases stability, transitions or reactions in the solid state. The raw 2D diffraction datasets collected were transformed to a 1D powder patterns with the FIT2D program and a mask was used to remove the undesired spots from the single-crystal sapphire tube and shadow from the sample holder.[90,91] The detector distance was calibrated using LaB_6 as a standard.
Generally laboratory source have been widely used for the first screening and investigation of the synthetized sample and as a check after any significant treatment of the samples.

Rietveld Refinement

The Rietveld refinement is a computer-based analytical technique for the characterisation of crystalline materials. The Rietveld method uses a least squares approach to refine a theoretical line profile until it matches the measured profile (best fit). It considers and treats the whole pattern in order to match peak position, intensity and profile. At first, for a Rietveld refinement, it is essential to collect a good powder diffraction pattern. Factors to consider prior to data collection are the geometry of the diffractometer, the quality of the instrument alignment and calibration (i.e. instrumental function to be obtained with a standard material), the most suitable radiation and its wavelength, appropriate sample preparation and thickness, slit sizes, and necessary counting time. As much as possible on the sample composition, size, absorption or microstructure should be known in order to carry on the refinement with a good starting model. The first step of the Rietveld analysis should be the identification of the phases present in the sample, considering both crystalline and amorphous contributions,

and a first estimation of the relative amount considering the intensity of the peaks. Then, knowing the instrumental function, which takes into account various instrumental contributions to the pattern, the background should be carefully modelled. Either the background can be estimated by linear interpolation between selected points between peaks or it can be modelled by a polynomial function containing several parameters. When a good starting model it is manually obtained, the refinement can be run in order to optimise the background parameters and intensity. Then, the scale factor can be adjust and refined. After the background, the parameters related to the sample can be refined.

Among the analytical peak-shape functions, the pseudo-Voigt approximation of the Voigt function is probably the most widely used.[92] The pseudo-Voigt function is a linear combination of Lorentzian and Gaussian components. An additional function to allow a more precise description of asymmetry due to axial divergence of the diffracted beam at low angles can be refined as well. With a complete structural model and good starting values for the background contribution, the unit-cell parameters and the profile parameters, the Rietveld refinement of structural parameters can begin. It is usually advisable to start the refinement of structural parameters with the positions of the heavier atoms and then to proceed with the lighter atoms. The scale, the occupancy parameters and the thermal parameters are highly correlated with one another, and are sensitive to the background correction. The thermal factor B is a thermal motion factor that can slightly tune the results, modifying the intensity and broadening of the reflections. In addition, the modification of size and strain of the crystallites can affect the broadening of the reflections.

In conclusion, structure refinement using the whole-pattern Rietveld method is a powerful technique for extracting structural details from powder diffraction data but it is essential to proceed with careful and precise approach to obtain a good and reliable best fit.

In this work, the Rietveld refinement of selected diffraction patterns has been performed using the MAUD program.[93] The instrumental function was determined using LaB_6 or Si as a standard.

Laboratory X-ray diffraction

To analyse the phase mixtures and decomposition products, powder X-ray diffraction measurements were performed at room temperature. A Panalytical X-

pert (Cu K_α = 1.54059 Å, K_β = 1.54446 Å; K_α/K_β = 0.375) in capillary transmission set-up (Debye-Scherer geometry) was used. Patterns were collected between 5° to 130° 2θ range, step size 0.016, time step 60 or 90 seconds. Samples were inserted, in the glove box, in 0.5 mm glass capillaries and sealed with plastiline, then moved out of the glove box and sealed with flame.

Max-Lab

The measurements performed at beamline I711 at the MAX-II synchrotron in the MAXIV laboratories, Lund, Sweden, with a Titan CCD detector system,[94] and using single crystal sapphire capillaries and a special setup.[95]
The setup for *in-situ* measurements was a sample cell specifically developed to study solid-gas reactions, applying a pressure or a heating ramp.[95] The samples were packed in a single-crystal sapphire tube (o.d. 1.09 mm, i.d. 0.79 mm) and mounted on the sample cell in the glove box. To guarantee an inert environment around the sample, graphite ferrules were used to tighten the sapphire tube. A hot air blower heated the sample from RT to 500 °C at 5 °C/min in an argon atmosphere; the temperature was recorded by a thermocouple. Both the blower and the thermocouple were connected to a programmable PID temperature controller and the temperature was calibrated using the thermal expansion coefficient of NaCl and Ag as a standard.

Petra III

The *in situ* SR-PXD measurement performed at the diffraction beamline P02, in the Petra III storage ring of DESY (Hamburg, Germany), used few milligrams of sample packed in a single crystal sapphire capillary (inner diameter ca. 0.6 mm). The capillary was then mounted in an in-house-built synchrotron cell and sealed using Vespel ferules and Swagelok connections. This cell is equipped with a heating element (electric resistance) and thermocouples allowing varying the temperature between room temperature (RT) and 450 °C during the experiment. Moreover, the cell can be connected to an external gas line and loaded with inert or reactive gases at different pressures.[96,97] The sample was heated up and cooled down at 5 °C/min under a hydrogen pressure of 1 bar. The beamline provides a monochromatic X-ray beam (λ = 0.207157 Å) and is equipped with a PerkinElmer XRD 1621 plate detector (pixel size 200 µm x 200 µm, array 2048x2048 pixels). The diffraction images, collected every 15 seconds, were integrated with the software Fit2D.

ESRF

Measurements at ESRF, Grenoble (France), were performed at the beamline BM01, with a wavelength of 0.7129 Å and 5 s exposure time.
Sample were packed and manipulated in a glove box, and sealed in borosilicate capillary (o.d. 0.5 mm). A hot air blower, equipped with a PID controller, was used to anneal the sample from RT up to the desired temperature at 5 °C/min.

Diamond

Measurements at Diamond Light Source, Didcot (UK), were performed at the beamline I11, with a wavelength of 0.8259 Å and 5 s exposure time.
As for ESRF, sample were packed and manipulated in a glove box, and sealed in borosilicate capillary (o.d. 0.5 mm). A hot air blower, equipped with a PID controller, was used to anneal the sample from RT up to the desired temperature at 5 °C/min.

Thermal analysis

The analysis of the thermal behaviour of the material is of fundamental importance to understand any physical or chemical transition and define its thermodynamic properties. Thermal analysis allows quantifying temperature and enthalpy of phase transitions and reactions, together with the determination of other thermal properties such as the heat capacity. Thermal analysis can also be coupled with other techniques, such as thermogravimetric analysis, volumetric apparatus or mass spectroscopy to define the mass loss or gain due to decomposition, gas release or oxidation and the kind and quantity of released gas.
The standard thermal analysis measurement is the Differential Temperature Analysis (DTA), which measures the difference of temperature between the sample and a reference upon heating. It is characterized by a programmable furnace and two thermocouples connected in series close to the reference and sample to measure their temperatures. The results are reported as a temperature difference (ΔT), expressed as a differential potential (in Volt) generated between the thermocouples, as a function of the temperature of the programmed furnace, as in the heat flux calorimeter (**Figure 5, a**).
On the other hand, in a power compensation Differential Scanning Calorimeter (DSC) two furnaces are used to control the temperature of a reference and the

sample separately. Two thermoresistances are placed under both the reference and sample to heat and constantly record their temperatures. The same temperature in the reference and sample cell is maintained by tuning the power of the two furnaces, so that the differential power used (in W) is recorded as a function of the programmed temperature (**Figure 5, b**).

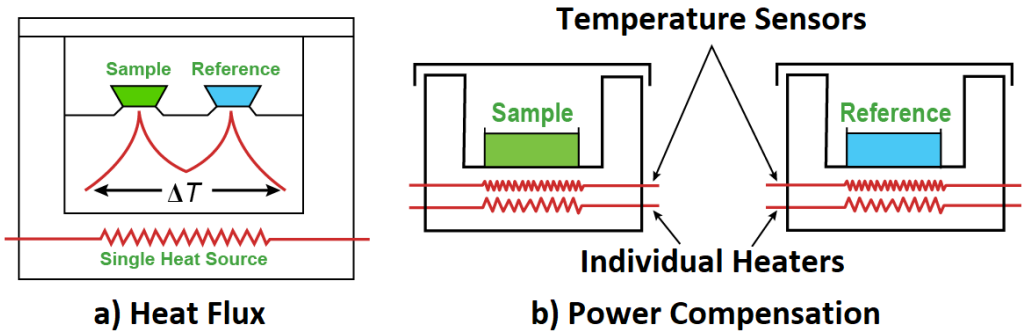

Figure 5 – a) Heat Flux calorimeter, similar to a DTA; b) Power compensation DSC.

Differential Temperature Analysis coupled with Mass Spectroscopy

A DTA Netzsch STA 409 coupled with a Hiden Analytical Hal 201 Mass Spectrometer was used to analyse hydrogen and diborane release in the mixture as a function of temperature. The instrument is placed inside the glove box to ensure sample handling under inert atmosphere. Approx. 2 mg of sample were heated from RT up to 500 °C at 5 °C/min under an argon gas flow of 50 mL/min, which was used also to transport the gases to the MS analyser.

High Pressure Differential Scanning Calorimetry

A high-pressure 204 Netsch DSC (HP-DSC) was used to analyse the thermal behaviour the samples. A backpressure of hydrogen was loaded in the chamber in order to avoid the decomposition, obtaining accurate values of temperature and enthalpy of phase transformations at a definite thermodynamic condition. Few milligrams of sample were loaded into alumina or aluminium crucibles with a lid with a hole for gas release. The HP-DSC was placed inside the glove box to ensure sample handling under inert atmosphere. Samples were heated and cooled in the desired temperature range at 5 °C/min under a static pressure of 1, 2, 10 or 50 bar of H_2. Sometimes, to clarify reversibility and phase transformation, various cycling were performed.

Calibration

The accurate calibration of the instrument is indeed necessary to measure reliable values of temperature and enthalpy.
The instruments were calibrated in temperature and heat flow using the melting enthalpy and temperature of high purity standards (Bi, CsCl, In, Sn, Zn) and the same conditions used for different experiments, so using the same crucible, heating rate, gas flow or pressure. Furthermore, sapphire has been used as a reference for the heat capacity measurements, as described below.
The T_{onset} and integration of melting peak of the standard materials during heating were provided to the software in order to compare them with literature values and generate a sensitivity and temperature calibration curve.

Heat Capacity

Calorimetry, as said before, measures essentially the amount of heat necessary to rise the temperature of the sample to a desired value. For this reason, DSC is a powerful technique to evaluate heat capacity.
The heat capacity is dependent on the size of the system and is therefore an extensive thermodynamic property. However, in normal usage, it is more convenient to use the heat capacity per unit quantity of the system. Thus, the specific heat of the system is the heat capacity per gram at constant pressure (or constant volume), and the molar heat capacity is the heat capacity per mole at constant pressure (C_p) or at constant volume (C_v).
The experimental determination of the molar heat capacity require a well defined temperature program which consists in a linear ramp or several heating or cooling ramps divided by isotherms, used as equilibrium point and baseline. Once the temperature program is defined, three measurements need to be performed. The measurement on the empty crucible (ΔY_0) works as baseline, then a well known heat capacity reference material is measured (ΔY_{std}) and, finally, the measurement is performed on the sample (ΔY_s).
Usually, a short heating or cooling step is programmed and any endothermic or exothermic events should be inside of the range of temperature chosen for the ramp. Between each ramps an isothermal holding is imposed for a suitable time to get stabilization in the DSC signal.
During this study, the chosen temperature program consists in linear temperature ramps at different temperature, in 2 bar hydrogen atmosphere, at 5 K/min with

a temperature step of 30 degrees, and an isotherm of 20 minutes before and after each step (**Figure 6**).

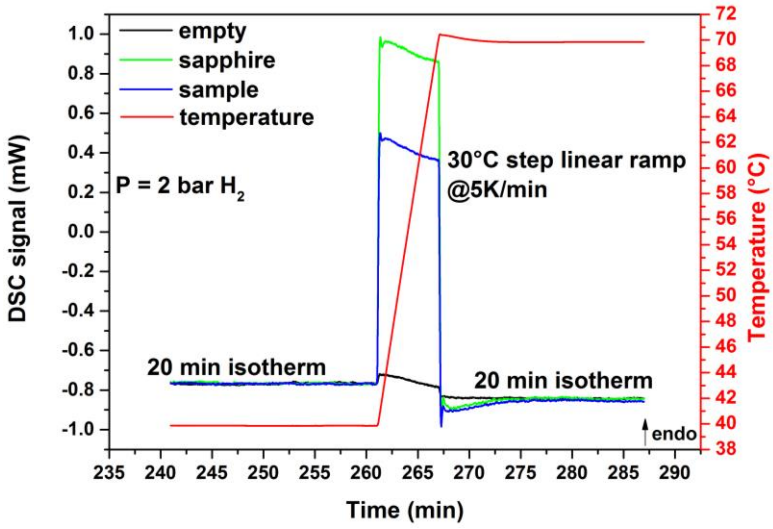

Figure 6 – DSC measurement of empty crucible, reference sapphire disk and sample in a selected temperature ramp between 40 °C and 70°C. Each ramp of 30 °C step was performed at 5 °C/min with a 20 min isotherm before and after the step.

The C_p determination can be performed with two different method: the linear temperature ramp (height) method (**Figure 7, a**) and the enthalpy (area) method (**Figure 7, b**).[98]

The evaluation of heat capacity of boron-based materials was calculated by the height method, using the following formula:[98]

$$C_{p,m}^{s} = C_{p,m}^{ref} \cdot \frac{\Delta Y_0 + \Delta Y_{std}}{\Delta Y_0 + \Delta Y_{ref}} \cdot \frac{n_{ref}}{n_{std}} \qquad \boldsymbol{Eq.1}$$

Where ΔY_0, ΔY_{std}, ΔY_s are the height of empty crucible, standard and sample; n_{ref} and n_{std} are the mole numbers of the reference and sample.
Basically, after the baseline subtraction to the sample and sapphire, comparing the height of the sample signal with the sapphire, which as a known heat capacity, the heat capacity of the sample has been calculated.

The value for the molar heat capacity of the reference is taken from thermochemical tables[99] and calculated using the following formula:

$$Cp = \frac{4.1868 \cdot ((25.48 + 0.00425 \cdot T) - 682000 \cdot T - 2)}{101.961} \quad \boldsymbol{Eq.2}$$

Using a sapphire (Al_2O_3) disk as a reference, the good calibration of the instrument was validate by the calculation of the cell constant, which turns out to be 1 with an experimental error of 2% on each measurement. For this reason, all the data reported in the results have an error bar of 2% (**Figure 8**).

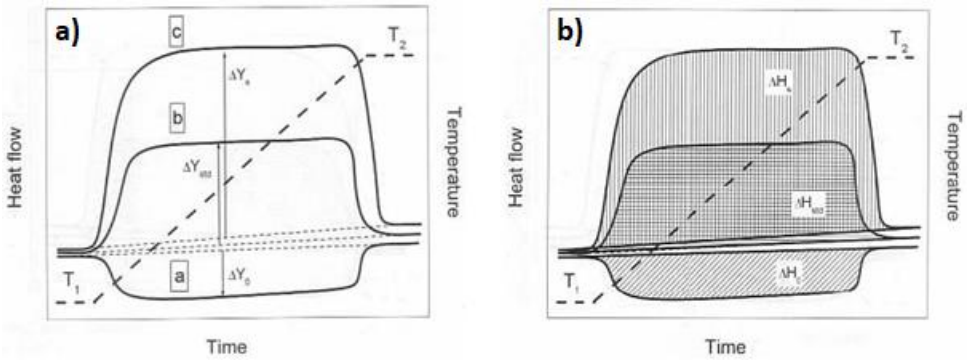

Figure 7 – Methods to determine the heat capacity: a) height method, linear temperature ramp, and b) area method, enthalpy method.[98]

The average of the molar heat capacity of the sample in a chosen temperature range determined with the enthalpy method can be calculated by this formula:[98]

$$\overline{C_{p,m}^{s}} = \overline{C_{p,m}^{ref}} \cdot \frac{\Delta Q_0 + \Delta Q_{std}}{\Delta Q_0 + \Delta Q_{ref}} \cdot \frac{n_{ref}}{n_{std}} \quad \boldsymbol{Eq.3}$$

Where ΔQ_0, ΔQ_{ref}, ΔQ_{std} are the enthalpies measured by the integration of each step for the empty crucible, reference and sample; $\overline{C_{p,m}^{ref}}$ is the average of the molar heat capacity of the reference.

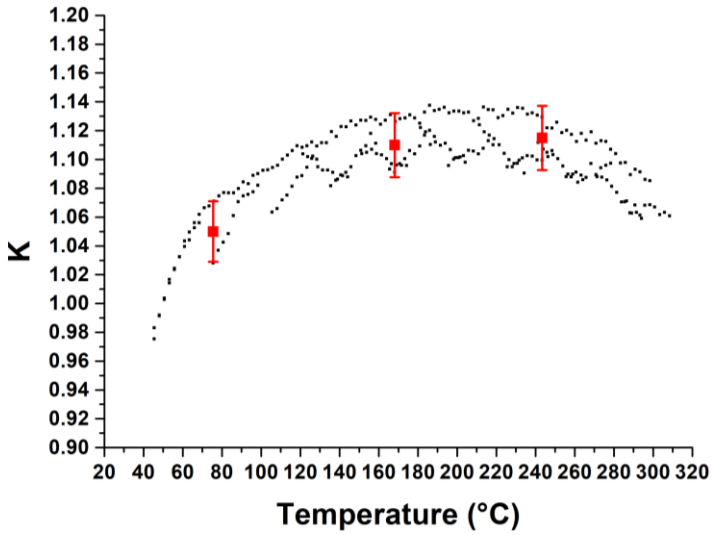

Figure 8 – Calculated DSC cell constant using sapphire disk as a reference. Calculation performed both on heating and cooling. Error on cell constant value turns out to be equal to 2%.

Spectroscopies

Spectroscopies are useful characterization methods owing to their sensibility towards both crystalline and amorphous materials, and different physical state of the material (i.e. solid, liquid, gas). Furthermore, they can support interpretation of data from diffraction techniques to identify phases, define structures and details about local bonding environment.
Vibrational frequency in boron-based materials are quite well known and experimental values can be compared to tabulated or calculated one in the literature.[100–108]

Infrared Spectroscopy

The infrared spectra (2 cm^{-1} resolution, average on 64 scans) were collected in Attenuated Total Reflection (ATR) mode on loose powder with a Bruker Alpha-P spectrometer, equipped with a diamond crystal. All the spectra were recorded in the 5000−400 cm^{-1} range, in a protected atmosphere since the instrument is placed inside a nitrogen filled glove-box (MBraun Lab Star Glove Box supplied with pure 5.5 grade Nitrogen, <1 ppm O_2, <1 ppm H_2O).

Raman Spectroscopy

Raman spectra were collected using a WITec alpha300 confocal Raman spectrometer (Ulm, Germany) using a 633 nm (red) excitation wavelength in backscattering mode, with exposure times of 0.5 s and 200 accumulations per spectrum over a 2600–1000 cm^{-1} range.

Modelling

Nowadays, with increasing computational power and software development, modelling techniques are becoming more and more popular, and widely used for a screening of material properties. The experimental investigation of thermodynamic properties for all compositions and conditions would be based on many experiments and measurements, that are too expensive and time consuming. Therefore, the combination of experimental investigation, *ab-initio* calculations and mathematical modelling of thermodynamic properties, able to be extended in region out of the feasible experimental investigation will enable the full understanding of complex systems and their further developement and tailoring towards real applications.
A full evaluation of the thermodynamic properties of borohydrides and their mixtures is indeed fundamental for tailoring hydrogen storage materials, as well as for further improvements and insight on complex hydrides. The use of the Calphad approach for the assessment of the phase diagrams in complex hydrides allows the determination of different thermodynamic properties and possible decomposition routes or hydrogen release reactions, together with the enthalpy of mixing in the liquid phase and solid solutions, which cannot be easily determined experimentally.[63,78–80]

Calphad Method

The Calphad method for the assessment of thermodynamic properties in condensed systems is based on a parametric description of the Gibbs free energy as a function of temperature and composition that generates a thermodynamic database. Literature data and new experimental results on thermodynamic properties for the studied system should be critically collected and used as input data. In order to establish the Gibbs free energy of compounds with crystal

structures different from the stable one (end-members), *ab-initio* calculations are often necessary. A process of optimization by best fitting allows the assessment of parameters in order to have the most reliable description of Gibbs free energy for all phases in the system based on the input values and following the flowchart reported in **Figure 9**.

The daily use of the Calphad method includes the calculation of multicomponent and multiphase systems for extended region of compositions and conditions. Starting from an assessed database, the evaluation and interpolation of thermodynamic properties of binary or higher systems can be performed to calculate equilibrium points, reactions, and graphical outputs such as pseudo-binary and pseudo-ternary phase diagrams (**Figure 9**).

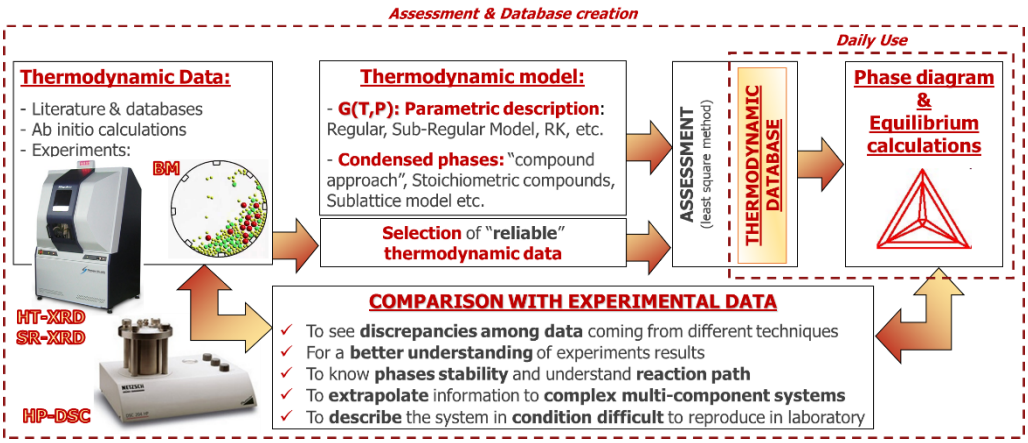

Figure 9 – Flowchart of the CALPHAD method.

According to the Calphad approach, the Gibbs Free Energy (GFE) of a phase can be expressed as:[76]

$$^{\varphi}G = {}^{\varphi}G^{ref} + {}^{\varphi}G^{id} + {}^{\varphi}G^{exc} \quad \boldsymbol{Eq.4}$$

where φ is the considered phase, $^{\varphi}G^{ref}$ is the reference contribution (so the contribution of the components of the system), $^{\varphi}G^{id}$ is the contribution given by the ideal mixing entropy and $^{\varphi}G^{exc}$ is the excess Gibbs free energy, that considers all the contributions due to non-ideal interactions between the components.

Thermodynamic functions for missing end-members can be evaluated adding to the Gibbs energy of the stable phase the *ab-initio* calculated enthalpy difference between the stable and the metastable structures.

The GFE of a stoichiometric compound with chemical formula A_xB_y can be described as:

$$^{\varphi}G_{A_xB_y} = x^{\varphi}G_A + y^{\varphi}G_B + \Delta H_{for}(T,P) - T\Delta S_{for}(T,P) \quad \boldsymbol{Eq}.5$$

where $\Delta H_{for}(T,P)$ and $\Delta S_{for}(T,P)$ are the enthalpy and entropy of formation of the compound.
In the case of an ideal A-B binary solution, which means there are no interactions between the components, the $^{\varphi}G^{exc}$ is equal to zero and the GFE can be expressed as:

$$^{\varphi}G = {}^{\varphi}G^{ref} - TS^{id} \quad \boldsymbol{Eq}.6$$

$$^{\varphi}G^{ref} = x^{\varphi}G(A) + (1-x)^{\varphi}G(B) \quad \boldsymbol{Eq}.7$$

$$S^{id} = -R[x\,ln\,x + (1-x)\,ln(1-x)] \quad \boldsymbol{Eq}.8$$

where x is the molar fraction of A, T is the temperature.
Ideal solution can be widely applied to gas phases, however, for real condensed phases, some additional terms must be considered and more complex models have to be adopted, such as the regular and sub-regular solutions models.
Considering a binary system of two components A and B in the regular solution model, it can be described in terms of bonding energies between first neighbours ($E_{A\text{-}B}$, $E_{A\text{-}A}$ and $E_{B\text{-}B}$) and the following expression for the excess Gibbs energy can be derived:

$$^{\varphi}G^{exc} = x(1-x)L \quad \boldsymbol{Eq}.9$$

$$^{\varphi}G^{ref} = x^{\varphi}G(A) \quad \boldsymbol{Eq}.10$$

$$L = {}^{1}a + {}^{1}bT \quad \boldsymbol{Eq}.11$$

where L is the regular solution interaction parameter that can be temperature dependent (^{1}a and ^{1}b are optimized parameters). The temperature dependence of interaction parameters is usually constant or linear, as it can be observed above in the equation describing L.
In this model, the bonding energies are assumed to be composition independent.

If instead a linear dependence on the composition is assumed, the excess GFE can be described according to the sub-regular solution model where:

$$^{\varphi}G^{exc} = [^{0}L + {}^{1}L(x_a - x_b)]x_a x_b \quad \boldsymbol{Eq.}\,12$$

$$^{\varphi}G^{exc} = x(1-x)(^{1}a + {}^{1}bT) + x(1-x)(2x-1)(^{2}a + {}^{2}bT) \quad \boldsymbol{Eq.}\,13$$

Excess Gibbs energy can be furthermore modelled with a Redlich-Kister (RK) expansion series:[109]

$$^{\varphi}G^{exc} = x_a x_b \sum_{\nu} {}^{\varphi}L_{A,B} \cdot (x_a - x_b)^{\nu} \quad \boldsymbol{Eq.}\,14$$

It has to be noticed that if the RK expression is truncated to v=0, only the parameter relative to $^{0}L_{A,B}$ is used, obtaining a regular solution, when instead also v=1, and so $^{1}L_{A,B}$, is considered, a sub-regular behaviour is described.
The truncation of the expansion series needs to be decided considering when a satisfactory agreement between experimental and calculated thermodynamic data is reached.

Thermo-Calc Software and databases

There are several commercial packages (e.g. Thermocalc[110,111], Pandat[112], Factsage[113]) able to handle thermodynamic databases and calculate phase diagrams.
The Thermo-Calc Software[110] based on the Calphad approach was used in this study for the thermodynamic calculations or simulations.
The software is a general and flexible command line software based on different modules with specific functions as describe below:

- **TDB** for database retrieval and management;
- **GES** for thermodynamic model handling and data treatments for various phases;
- **TAB** for thermodynamic property tabulations of phases and reactions;
- **POLY** for multicomponent heterogeneous equilibrium and stepping/mapping calculations (core of the program);
- **POST** for post-processing of various phase diagrams and property diagrams;

- **PARROT** for parameter optimizations in data assessments;
- **ED_EXP** for experimental points editing and equilibrium calculations;
- **BIN** and **TERN** for binary and ternary phase diagram calculations;
- **POURBAIX** for Pourbaix diagram;
- **SCHEIL** for Scheil-Gulliver solidification; and
- **REACTOR** for steady-state reaction simulations.

The modules can interact with each other and are linked as shown in **Figure 10**.

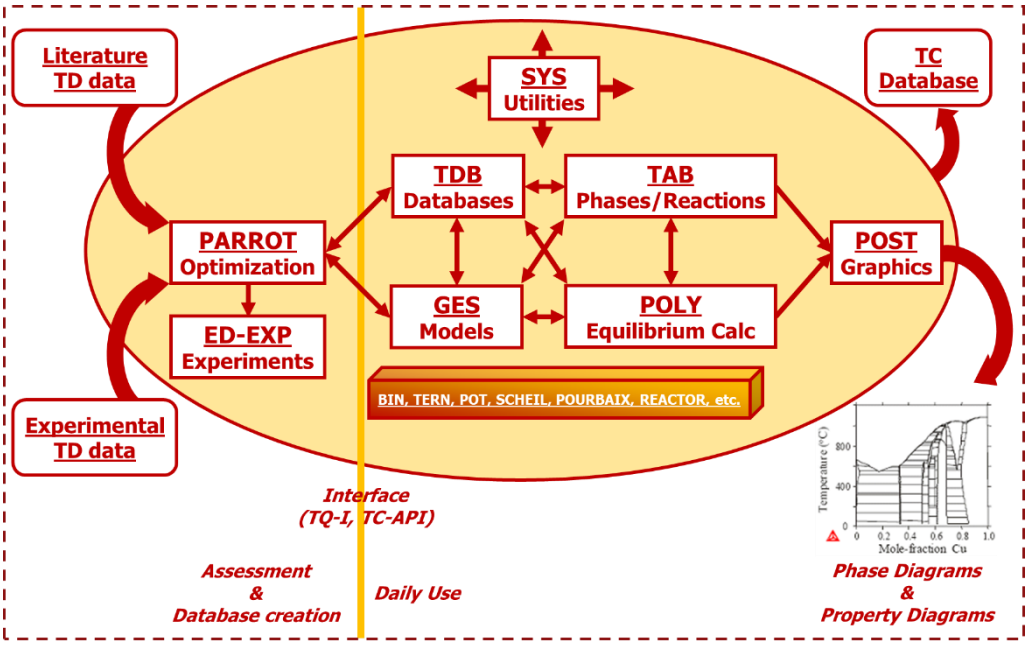

Figure 10 – The structure of the Thermo-Calc software.

The Substance Scientific Group Thermodata Europe (SGTE) database[114,115] and already published thermodynamic functions[78] were used, in this study, as a starting point for the thermodynamic assessment, providing thermodynamic functions for stable stoichiometric compounds. Assessed parameters of thermodynamic functions for different phases (hexagonal, cubic, orthorhombic and liquid) have been used, in order to explore and characterize the pseudo-binary and pseudo-ternary phase diagrams in the $LiBH_4$-$NaBH_4$-KBH_4 system.
Among databases, the Joint Army-Navy-Air Force (JANAF) Thermochemical Tables[99] are one of the most important collections of thermodynamic data,

reporting temperature-dependent thermochemical properties (such as the heat capacity) of many elements and compounds.
Another important collection of thermodynamic functions is available on the National institute of Standard and Technology (NIST) website.[116]

Ab-initio

Periodic quantum-mechanical calculations were performed by Dr. Marta Corno, using the periodic quantum-mechanical software CRYSTAL14[117,118] within the Density Functional Theory. The CRYSTAL software has been developed by the theoretical group of the University of Turin.
The structure and stabilities of investigated compounds or end-members can be evaluated. Internal coordinates and lattice parameters need to be first fully optimized using experimental observed structure as a starting point.
Both GGA (PBE[119]) and hybrid (PBE0[120], B3LYP[121,122]) functionals have been tested, with and without Grimme's D2 correction to the electronic energy.[123] The PBE0-D2 level of theory was chosen, as the best compromise in terms of accuracy and cost of the calculations. The CRYSTAL code utilizes localized Gaussian functions to describe electrons. Localized Gaussian functions of double-ζ quality were applied as basis sets for the description of electrons.
In detail, for the cations, the following sets were used: 5–11G(d) basis set (α_{sp} = 0.479 bohr^{-2} for the most diffuse shell exponent and α_{pol} = 0.600 bohr^{-2} for polarization) to describe lithium; a 8-511G (α_{sp} = 0.323 bohr^{-2} for the most diffuse shell exponent) for sodium and 86-511G (α_{sp} = 0.389 and α_{d} = 0.394 bohr^{-2} for the most diffuse shell exponent of sp and d functions) in the case of potassium.[124,125] Boron was described by a 6–21G(d) set (α_{sp} = 0.124 bohr^{-2} for the most diffuse shell exponent and α_{pol} = 0.800 bohr^{-2} for polarization) and for hydrogen, a 31G(p) set (α_{sp} = 0.1613 bohr^{-2} for the most diffuse shell exponent and α_{pol} = 1.1 bohr^{-2} for polarization) was adopted.[125]
Phonons at Γ point in the harmonic approximation were computed to derive the thermodynamic functions. Within the CRYSTAL code, frequencies are computed by diagonalizing the associated mass-weighted Hessian matrix. More details on the specific procedure can be found in references.[126,127] Enthalpy data were obtained by computing the electronic energy, inclusive of the zero-point energy correction (ZPE), and the thermal factor at T = 25 °C.[65]

Chapter 3 – Thermodynamic properties of pure borohydrides and closoboranes

A wide variety of borohydrides and closoboranes, and their relative polymorphs, have been investigated in the past years as promising compounds for both solid-state hydrogen storage and solid-state electrolytes in batteries.[25,70] Furthermore, thermochemical energy storage systems based on metal hydrides gained great interest for having high energy densities and good reversibility.[128]

Borohydrides

Borohydrides possess a wide range of attractive properties and were widely studied.[25] The precise knowledge of their thermodynamic properties is crucial to evaluate their stability and to describe phase transitions in the temperature range of interest.

Introduction

The heat capacity is a basic thermodynamic property for any material and its knowledge is necessary for many engineering applications. In addition, C_p experimental values are highly desirable for a full thermodynamic description of these compounds.
Considering the polynomial expression of the GFE:[76]

$$G = A + BT + CT\ln T + DT^2 + ET^3 + \frac{F}{T} + \cdots \qquad \boldsymbol{Eq}.15$$

Since:

$$C_p = -T\left(\frac{\delta^2 G}{\delta T^2}\right)_{p,N_i} \qquad \boldsymbol{Eq}.16$$

The following reported expressions of the heat capacity are suitable for expressing the Gibbs energy and heat capacity for a limited temperature range and above the Debye temperature.
At low temperatures, a more complex expression of GFE, based on the Einstein or Debye models for the molar heat capacity has to be used.[76]

For compounds with no measured heat capacity, it is common to apply the Neumann–Kopp rule (NKR)[129] which suggests that the heat capacity of a compound is equal to the stoichiometric average of the heat capacities of the constituent pure elements.

The heat capacity can be described by the following polynomial expression:

$$C_p = -C - 2DT - 6ET^2 - \frac{2F}{T^2} + \cdots \qquad \boldsymbol{Eq.}\,17$$

where the parameters A–F are optimized on the basis of the available experimental or computed data.

In this chapter, new insight on polymorphic transition (PT), melting reaction and calorimetric measurements of molar heat capacity of various borohydrides (MBH_4, M = Na, K, Rb, Cs, Mg, Ca), performed by DSC, will be described.
C_p data have been obtained as a function of temperature for different polymorphs using the height method. As described in the Experimental, the same temperature program was ran on each sample, empty pan (baseline) and reference (sapphire) on heating and cooling. It consists in linear temperature ramps at different temperature at 5 °C/min with a temperature step of 30 °C and an isotherm of 20 minutes before and after each step.
The above room temperature measured C_p values have been compared with available extrapolated literature data[130,131], and they have been modelled as a function of temperature according to the Calphad method with the polynomial expression reported above.[76]
The variation of the C_p values for different polymorphs were studied in details and they have been related to the corresponding crystal structures, considering the mobility of the BH_4^- group.
From the whole set of assessed thermodynamic data, possible correlations with dynamics, structural and electronic properties have been estimated.

Literature Survey

Concerning borohydrides, only few data are available, the low temperature (LT) heat capacity, below 350 K, was determined in the 50s for the alkali borohydrides,[130] while the high temperature (HT), above room temperature, heat

capacity was investigated only for $LiBH_4$.[131] The literature data are reported in **Figure 11**.

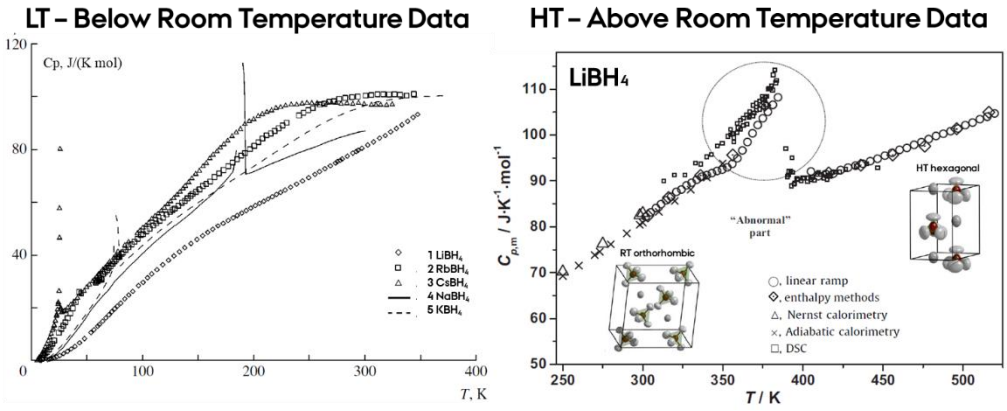

Figure 11 – Available literature data about heat capacities of borohydrides; LT alkali borohydrides data (left)[130] and above RT $LiBH_4$ data (right).[131–133]

All alkali borohydrides show a polymorphic transition (PT).
Starting from $CsBH_4$ that has the lowest PT temperature at 26 K, than the transitions can be observed in $RbBH_4$ at 48 K, KBH_4 at 77 K, $NaBH_4$ at 190 K and in $LiBH_4$ at 385 K.
$LiBH_4$ is the only compound that shows a PT above room temperature, it transforms from an orthorhombic to a hexagonal structure. They all present anomalies of heat capacity through the PT.

Heat capacity and Polymorphic transition

The experimental heat capacity values of cubic $NaBH_4$ are similar to the one reported in the literature,[132,134–136] but they present lower values and a different slope (**Figure 12, a**). It has to be noticed that the literature value are estimated and has not been experimentally determined. However, as it will be described later on, since they were the only available data, they have been used for further estimations and calculation of heat capacity of borohydrides such as $Mg(BH_4)_2$[137] and $Ca(BH_4)_2$.[138]
For KBH_4,[99,135,136] $RbBH_4$,[139] and $CsBH_4$,[140] an unexplained inflection towards lower values is observed (**Figure 12, b,c,d,** respectively), then the heat capacity is stabilized to a nearly constant value.

At temperatures higher than 300 K, a plateau, where a constant heat capacity is reached in function of temperature, seems to be present.

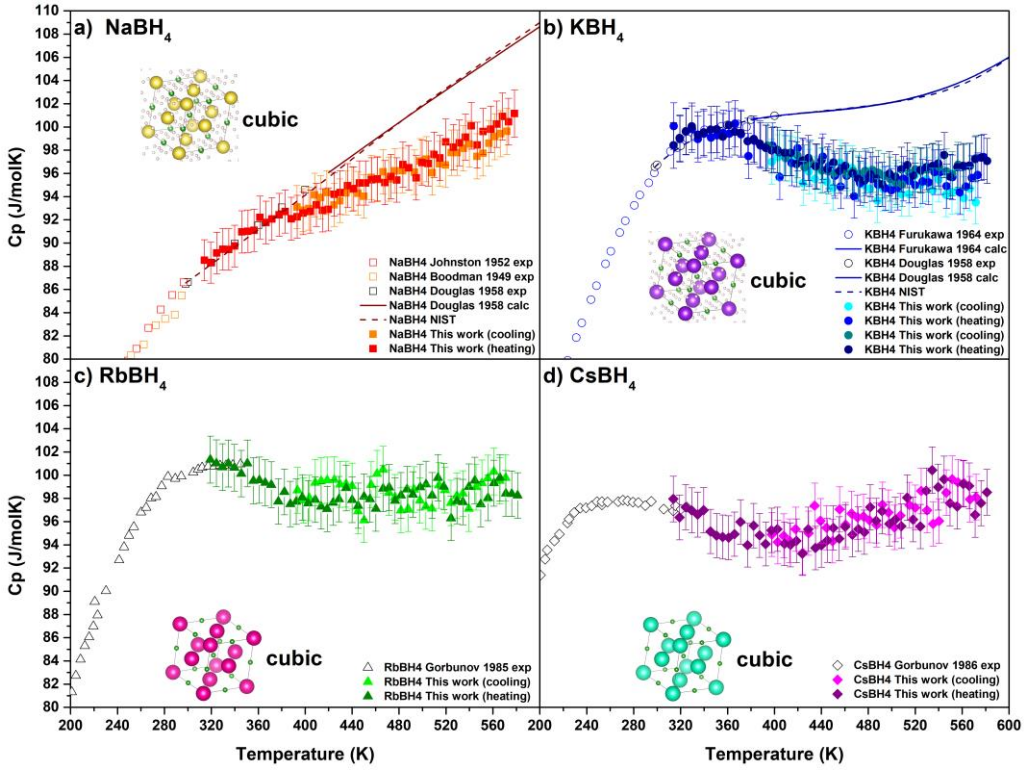

Figure 12 – Literature and experimental C_p values of a) $NaBH_4$, b) KBH_4, c) $RbBH_4$, d) $CsBH_4$. Open points show experimental literature data, closed points the new experimental data from this study and the lines the extrapolated calculate values from the literature. Error bars of 2% are reported, taking into account the variation of the cell constant reported in **Figure 8**.

Regarding the second group borohydrides, no experimental literature data were available for $Mg(BH_4)_2$ and $Ca(BH_4)_2$. The C_p of $Mg(BH_4)_2$ was estimated by Pinatel et al.[137] using a modified Neumann-Kopp rule, where the contribution to the heat capacity of the BH_4^- anion was define in function of temperature as:

$$Cp(BH_4^-) = Cp(NaBH_4) - Cp(Na) = 35.22 + 0.072 \cdot T \quad \boldsymbol{Eq.}\,18$$

Then the heat capacity of $Mg(BH_4)_2$ and $Ca(BH_4)_2$ can be estimated as:

$$Cp(Mg(BH_4)_2) = 2 \cdot Cp(BH_4^-) + Cp(Mg) \quad \boldsymbol{Eq.}\,19$$

$$Cp(Ca(BH_4)_2) = 2 \cdot Cp(BH_4^-) + Cp(Ca) \quad \boldsymbol{Eq}.20$$

The modified Neumann-Kopp rule was also used by Udovic et al.[138] to estimate the hat capacity of $Ca(BH_4)_2$, the results have been compared with the standard Neumann-Kopp rule using the heat capacity of gaseous hydrogen and DFT calculations, as will be reported later on.

Several $Mg(BH_4)_2$ polymorphs are known: α, β, γ, δ, ε and ζ;[141] and from this point of view $Mg(BH_4)_2$ presents an analogy with silica (SiO_2). Its structure can always be described as arrangement of tetrahedra in which the magnesium, in the centre of the tetrahedron, is coordinated to four anions BH_4^-, similarly to Si and O in the units SiO_4^{4-} of the silicates.[142] The Mg-BH_4 interaction is directional and partially covalent.[143]

The α polymorph, stable at room temperature, has a large hexagonal unit cell and a *$P6_122$* symmetry. It can be described as constituted by MgH_8 polyhedra linearly coordinated by H_2BH_2 units and organized in a 3D network of five terms ring $(-Mg-BH_4-)_n$.[141] It contains an unoccupied volume equal to 6.4% and turns into the β polymorph at around 457 K, with a polymorphic transition enthalpy (ΔH_{PT}) equal to 11.3 kJ/mol.[79,144]

The β polymorph is metastable at room temperature and less dense than α-$Mg(BH_4)_2$.[143] It displays an orthorhombic primitive cell with symmetry *Fddd*, characterized by two different types of MgH_8 polyhedra, coordinated by $(-Mg-BH_4-)_n$ rings, for which n cannot assume odd values.[141]

α-$Mg(BH_4)_2$ also turns into the stable high-pressure polymorph δ (tetragonal, *$P4_2nm$*) at 1.1-1.6 GPa.[143]

Wet-chemistry methods of synthesis have led to the discovery of γ-$Mg(BH_4)_2$ (cubic, $Ia\bar{3}d$).[143] Its structure is highly porous (33% of the material volume is not occupied) and it is responsible for its high surface area (1160 m^2/g), which makes it capable of storing hydrogen also as a physisorbed molecule.[145]

γ-$Mg(BH_4)_2$ transforms into a not crystalline phase between 0.4-0.9 and 2 GPa, called δ-$Mg(BH_4)_2$.[146]

The ζ polymorph is hexagonal with symmetry *$P3_112$*. Finally, ε-$Mg(BH_4)_2$ has been observed for the first time by Paskevicius et al.[147] in a study on the decomposition of γ-$Mg(BH_4)_2$.[147]

The γ phase used for this study was prepared by wet-chemistry by Steffen R. Jensen at the Aarhus University.

Concerning the heat capacity of the studied $Mg(BH_4)_2$ polymorphs, α and γ $Mg(BH_4)_2$ show similar values and a linear heat capacity as a function of

temperature. It was possible to measure the heat capacity of β phase below the PT in metastable conditions, down to RT. β-$Mg(BH_4)_2$ displays also a linear behaviour, but at lower values, compared to α and γ (**Figure 13, a**). The assessed values by Pinatel et al.,[137] obtained by the modified Neumann-Kopp rule (**Figure 13, green solid line**), are comparable to the experimental one of the α and γ phase, however the experimental data have a different slope in function of temperature.

$Ca(BH_4)_2$ presents the polymorphs α, β and γ, which are structurally related to those of titanium dioxide (TiO_2), containing all Ca^{2+} ions in octahedral coordination with six BH_4^-. Although these structures might show an ionic bond, the existence of non-compact packaging polymorphs suggests a certain degree of directionality in the Ca-BH_4 bond.[143]
α-$Ca(BH_4)_2$ is characterized by an orthorhombic cell, with a *F2dd* symmetry, and it turns into β-$Ca(BH_4)_2$ at 437 K (ΔH_{PT} = 8.6 kJ/mol),[144] which presents a tetragonal cell with $P\bar{4}$ symmetry, so it is metastable at room temperature.[148]
γ-$Ca(BH_4)_2$ is orthorhombic (*Pbca*) as well.[149] According to the Riktor et al. study about phase transitions and decomposition of $Mg(BH_4)_2$ and $Ca(BH_4)_2$,[150] γ-$Ca(BH_4)_2$ should transform into a new polymorph (δ) at high temperature. However, it was later discovered, that the δ phase is actually an oxidation product of $Ca(BH_4)_2$ at high temperature.[151]
Pure α-$Ca(BH_4)_2$ can be obtained by wet chemistry and it was prepared by Steffen R. Jensen at the Aarhus University as well.
The heat capacity of the α phase shows really high values and a fast increase close to the PT can be observed (**Figure 13, b**). This transition was reported to be of a second order type,[150] however it was confirmed to be a first order transition later on, because of no simple order parameter to describe these transition, furthermore, the impact of low-energy phonons at high temperature was discovered to be the origin of a vibrational entropy driven phase transition.[152]
Also the β phase of $Ca(BH_4)_2$ is metastable below its PT and present a linear heat capacity with the same room temperature value of the α. Solid lines in **Figure 13, b** report the estimated $Ca(BH_4)_2$ heat capacity values reported in the NIST report by Udovic et al.,[138] and obtained from DFT calculations, Neumann-Kopp rule and modified Neumann-Kopp rule. The best estimation of the heat capacity is obtained with the modified Neumann-Kopp rule which is quite in good agreement with experimental values of the β phase.

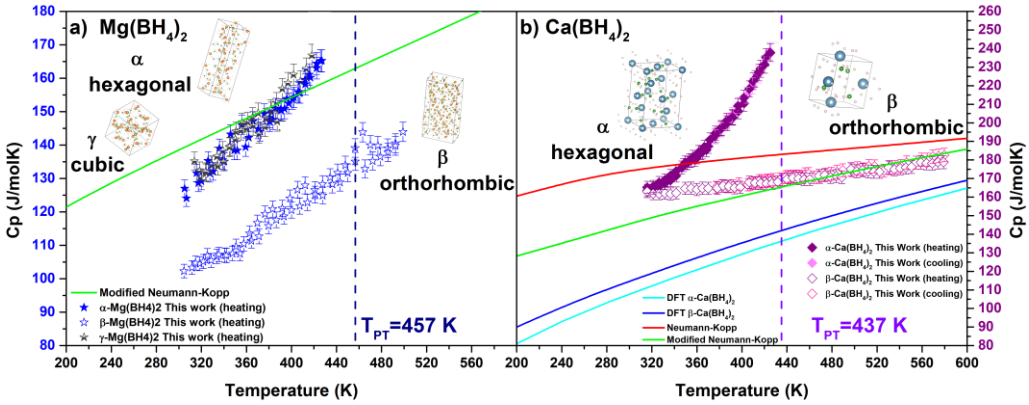

Figure 13 – Literature and experimental C_p values of a) α,β,γ-$Mg(BH_4)_2$ and b) α,β-$Ca(BH_4)_2$. Open points show experimental data of the β phase, while closed points refer to the α phase. The lines report the literature estimated values obtained from DFT calculation or the Neumann-Kopp equation. Literature data of $Mg(BH_4)_2$ from [137], and $Ca(BH_4)_2$ from [138]. Error bars of 2% are reported, taking into account the variation of the cell constant reported in **Figure 8**.

From experimental measurements reported in **Figure 13**, it can be generally observed that the α and γ polymorphs show an higher value of heat capacity than the β polymorph, while there is a change in the C_p value around the temperature of the polymorphic transition toward lower values (β phase). C_p values of the β phase have a linear dependence as a function of temperature, and can be measured down to room temperature because of the metastability of these phases.

According to the Calphad approach, the heat capacity can be modelled by a parametric equation. The number of parameter to be introduced in the equation depends on the behavior of the heat capacity as a function of temperature and should be chosen to obtain with a good grade of agreement with the experimental data. For this reason, the number of modelled parameter reported in **Table 2** have been chosen to obtain a good fit.
As an example, **Figure 14** and **15** show a comparison of three different fit on experimental data reported before. The assessed expression is valid in the limited temperature range in which the fit is determined (i.e. from 300 to 600 K), and the extrapolation of heat capacity data at higher temperature generates values, which are not always reliable, should always be confirmed by experimental data. Starting from $NaBH_4$, **Figure 14 a**, the linear behavior of the heat capacity can be easily assessed by using a two-parameter equation (FIT 1). A better fit can be obtained by a four parameters equation (FIT 3), however the extrapolation to

higher temperature show a fast increase of heat capacity to really high values which are not expected for $NaBH_4$. The best fit assessed equations for all investigated samples are reported in **Table 2**. For $NaBH_4$ the estimation of heat capacity at higher temperature with FIT 1 generates values lower than the one reported in the JANAF table, as in the case of a three parameters assessment (FIT 2).

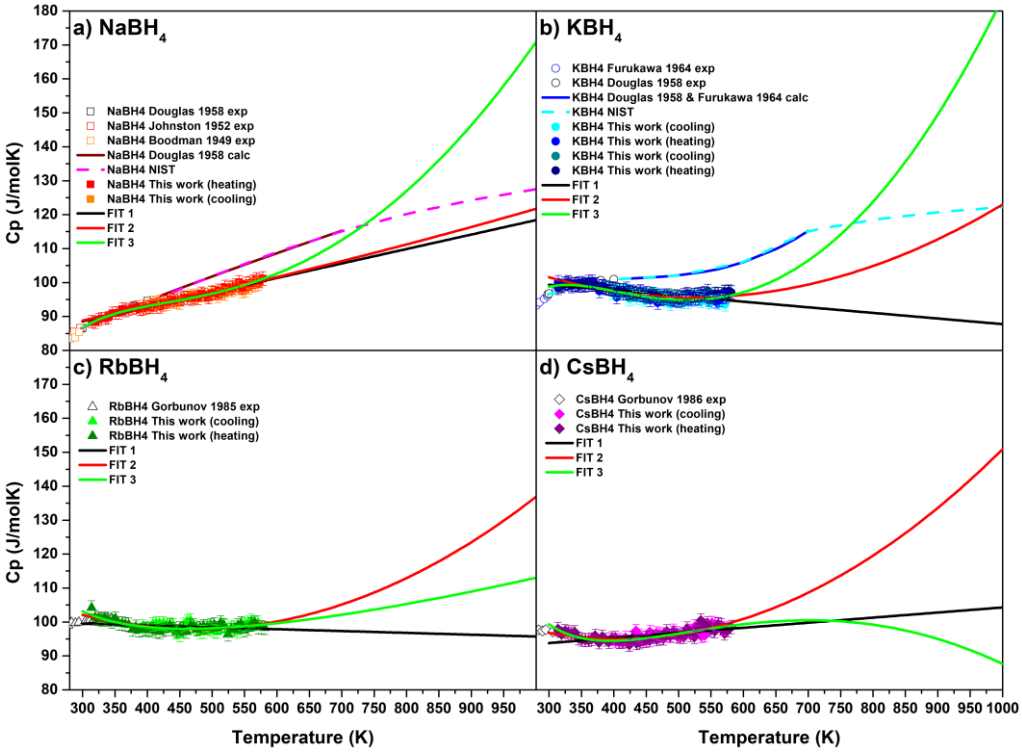

Figure 14 – Comparison of different fit of experimental heat capacity data in function of temperature, and their extrapolation to higher temperature. a) $NaBH_4$, b) KBH_4, c) $RbBH_4$ and d) $CsBH_4$. FIT 1: linear fit (two parameter C,D), FIT 2: three parameters fit (C,D,E), FIT 3: four parameter fit (C,D,E,F).

For KBH_4, $RbBH_4$ and $CsBH_4$, **Figure 14 b, c, d**, a four-parameter equation should be used to well fit the experimental heat capacity values in the temperature range 300-600 K, in order to well describe the particular inflection that was measured. For these compounds, the assessed equations should not be used outside of the reported temperature range, neither the linear, nor the three-parameter equation seems to describe reasonably the heat capacity outside of the experimental temperature range. The data can be part of a large plateau and so constant values of heat capacity seems to be the best description of the data above the

experimental temperature range, possibly all active mode have been enabled and a constant value of heat capacity is observed.

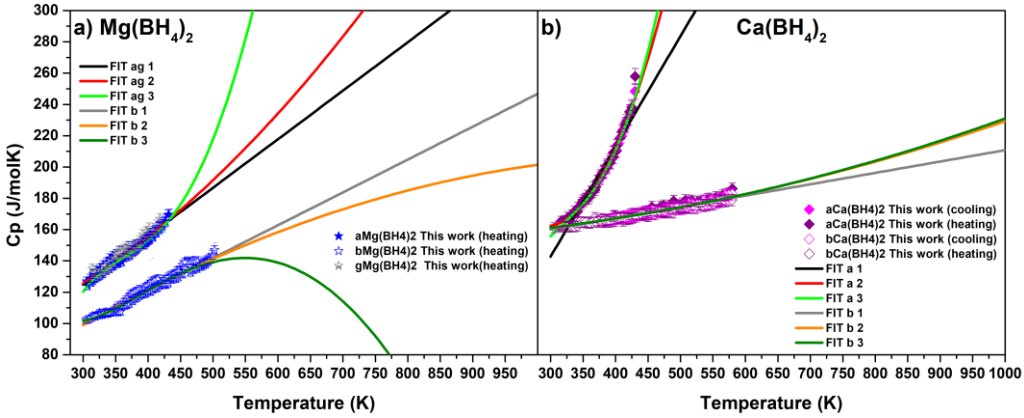

Figure 15 – Comparison of different fit of experimental heat capacity data in function of temperature, and their extrapolation to higher temperature. a) α,β,γ-$Mg(BH_4)_2$ and b) α,β-$Ca(BH_4)_2$. FIT 1: linear fit (two parameter C,D), FIT 2: three parameters fit (C,D,E), FIT 3: four parameter fit (C,D,E,F).

α,β-$Mg(BH_4)_2$ and β-$Ca(BH_4)_2$ have an almost linear behavior that can be described by a two parameters equation (**Figure 15**). In the case of α-$Ca(BH_4)_2$, a three or four parameters equation should be use, to have a best fit of the rapidly growing heat capacity values towards the polymorphic transition (**Table 2**).

Table 2 – Values of the parameters used for the best fit of the experimental heat capacities of $M(BH_4)_x$ (M= Li, Na, K, Rb, Cs, Mg, Ca) and relative polymorphs.

	C [J/molK]	D·10^{-3} [J/molK^2]	E·10^{-6} [J/molK^3]	F·10^5 [JK/mol]	R^2
$NaBH_4$	-75.8	-21.3			0.97
KBH_4	-258.4	260	-74.9	19.85	0.79
$RbBH_4$	-79.4	-9.27	-2.26	-7.62	0.48
$CsBH_4$	10.6	-135	29.3	-20.13	0.65
α,γ-$Mg(BH_4)_2$	-31.8	-155			0.96
β-$Mg(BH_4)_2$	-36.8	-105			0.97
α-$Ca(BH_4)_2$	-538.6	1282	-728		0.99
β-$Ca(BH_4)_2$	-138.2	-36.3			0.93

Discussions

An enlarged view of the C_p close to the polymorphic transition of the studied borohydrides is proposed in **Figure 16** and **17**. Experimental and literature data are reported in points, while the full or dashed line are a guide of the eyes.
In the case of $Mg(BH_4)_2$ and $Ca(BH_4)_2$ points at higher temperatures have been inserted as a guide for the eyes to drive the trend of the C_p as a function of temperature outside of the investigated temperature range.
The shape of the C_p trends around the PT is rather similar for investigated compounds, reminding a λ shape, especially in $CsBH_4$, $RbBH_4$, $LiBH_4$, $Ca(BH_4)_2$ and $Mg(BH_4)_2$. This could suggest a role of the BH_4^- anion in the structural transition across the PT. In the case of $RbBH_4$ there are not that enough experimental points to well define the shape of the Cp across the PT.

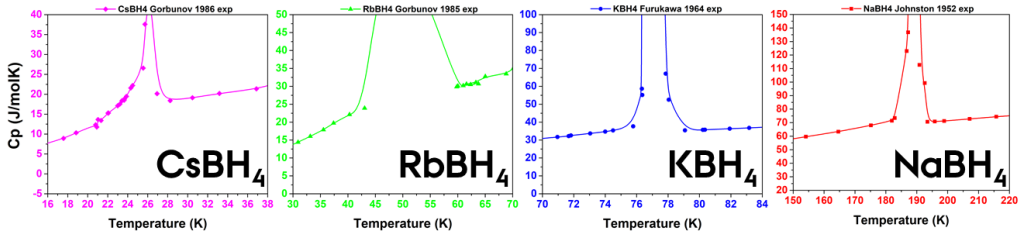

Figure 16 – Enlarged view of the heat capacities values as a function of temperature in the temperature range close to the polymorphic transition of $CsBH_4$, $RbBH_4$, KBH_4 and $NaBH_4$. The line is a guide for the eyes.

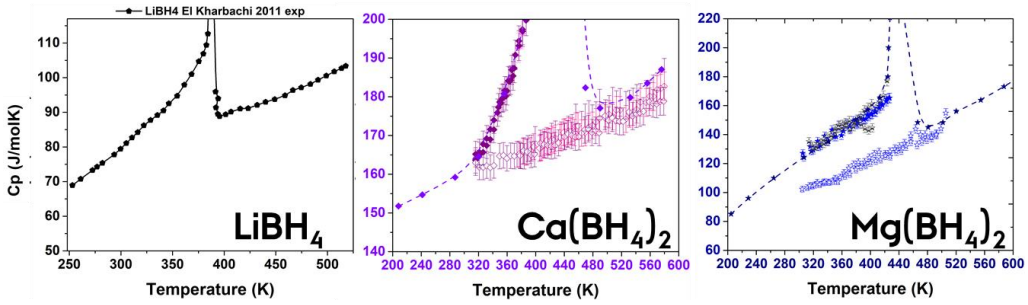

Figure 17 – Zoom in on the heat capacities values in function of temperature in the temperature range of the polymorphic transition of $LiBH_4$, $Ca(BH_4)_2$ and $Mg(BH_4)_2$. The solid and dashed lines are a guide for the eyes.

A resume of $M(BH_4)_x$ (M= Li, Na, k, Rb, Cs, Mg, Ca) literature and experimental heat capacities values as a function of temperature is reported in **Figure 18**. It can be observed that, in general, the C_p of borohydrides can be described as a

function of temperature by three segments. The first segment has an almost linear trend and a PT is present. Then there is an inflection or change in the slope and the last segment shows an almost constant value of C_p.
Depending on the PT temperature, a shift in temperature of the trend/segment of the C_p as a function of temperature for the different borohydrides is observed. The values for $Ca(BH_4)_2$ and $Mg(BH_4)_2$ are higher likely because of the presence of two BH_4^- groups and are related to the linear segment of the C_p containing the PT.

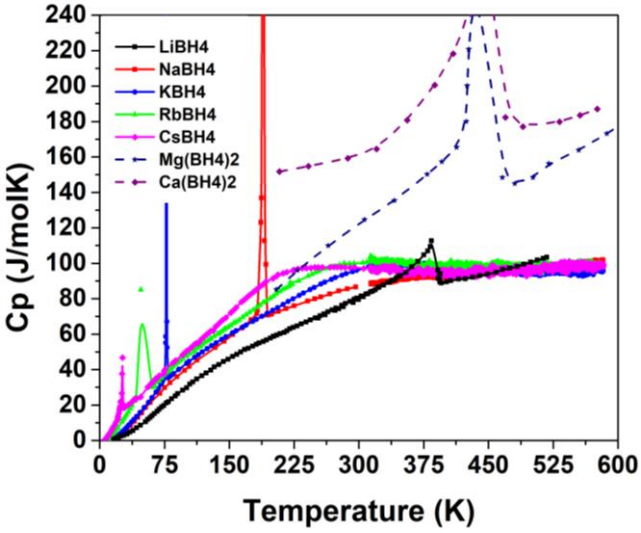

Figure 18 – Resume of $M(BH_4)_x$ (M= Li, Na, K, Rb, Cs, Mg, Ca) literature and experimental heat capacities values as a function of temperature. The line is a guide for the eyes.

The Neumann-Kopp rule is widely used in metal systems to calculate the heat capacity of different alloys, since the heat capacity of a solid compound is the sum of the atomic heat capacities of the elements composing it. In the case of a borohydrides, we should take into account the contribution of the metal, of the boron and of hydrogen. However, since H is in a gas phase, the contribution to the heat capacity at room temperature of the BH_4^- anion was calculated by subtracting the C_p^0 of the metal to the C_p^0 of the metal borohydride, as it was done previously with the modified Neumann-Kopp rule.
Table 3 reports the values for the investigated samples and from the graph in **Figure 19** we can observe an almost constant value, which is slightly increasing along the alkali borohydrides, while the α-$Mg(BH_4)_2$ show low values, similar to the $LiBH_4$ one, and the $Ca(BH_4)_2$ has values comparable with $CsBH_4$ and $RbBH_4$.

Table 3 – C_p^0 values of the studied $M(BH_4)_x$ (M= Li, Na, K, Rb, Cs, Mg, Ca), of the metal and of the BH_4^- anion, calculated by the Neumann-Kopp rule. Red values are the new experimental values, while the others were already reported in the literature.[130]

Compound	C_p^0 [J/molK] MBH_4	C_p^0 [J/molK] M	C_p^0 [J/molK] BH_4
$LiBH_4$	80.46	24.62	55.84
$NaBH_4$	86.48	28.15	58.33
KBH_4	96.06	29.57	66.49
$RbBH_4$	100.30	31.03	69.27
$CsBH_4$	97.35	29.80	67.55
α,γ-$Mg(BH_4)_2$	124.10 ± 2.5	24.85	49.63
β-$Mg(BH_4)_2$	102.31 ± 2.0		38.73
α,β-$Ca(BH_4)_2$	161.23 ± 3.3	25.93	67.65

The use of the modified Neumann-Kopp equation to estimate the C_p values of borohydride it is convenient in case of unknown experimental values. However, because of the variety of crystal structures, coordination number, temperature and type of polymorphic transition of these materials it is not always reliable and the values obtained should be used with care. Generally, experimental values are highly desirable and their parametric description can be used in the declared temperature range, because above and below that range the use of parametric description can fail or deviate significantly as was described previously.

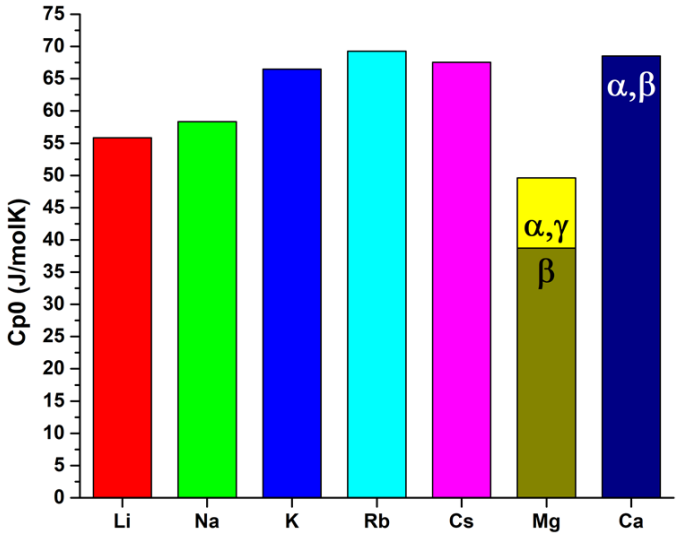

Figure 19 –Contribution to the C_{p0} values of the BH_4^- anion, calculated by the Neumann-Kopp rule for $M(BH_4)_x$ (M= Li, Na, K, Rb, Cs, Mg, Ca).

The temperature of the PT shows an inverse proportion with the size of the cation and the study of the heat capacity of the 1st group metal borohydrides[130] showed that the polymorphic transition is related to the orientation of the BH_4^- anion and its temperature increases when the distance of B-B atom decreases (**Figure 20**).[133]

Concerning the temperature of the polymorphic transition of different borohydrides, even for $Mg(BH_4)_2$ and $Ca(BH_4)_2$, a linear correlation between the minimum B-B distance and the temperature of the PT can be observed, as reported in **Figure 20**.[153] The correlation is related with the coordination of the cation in the high temperature polymorph structure and can be extended to $Mg(BH_4)_2$ and $Ca(BH_4)_2$.

This correlation evidenced that the complex anion play a role in the occurrence of the polymorphic transition, and different rotation and reorientation of the complex anion in the crystal lattice can explain the improved ion mobility and enhanced conductivity.[130] In fact, the study and understanding of the behavior of complex ions, as it will be discussed with closoboranes later on, is aimed to assess parameters of ionic motion in lattice sites for further improvement of those compounds as solid-state electrolytes.

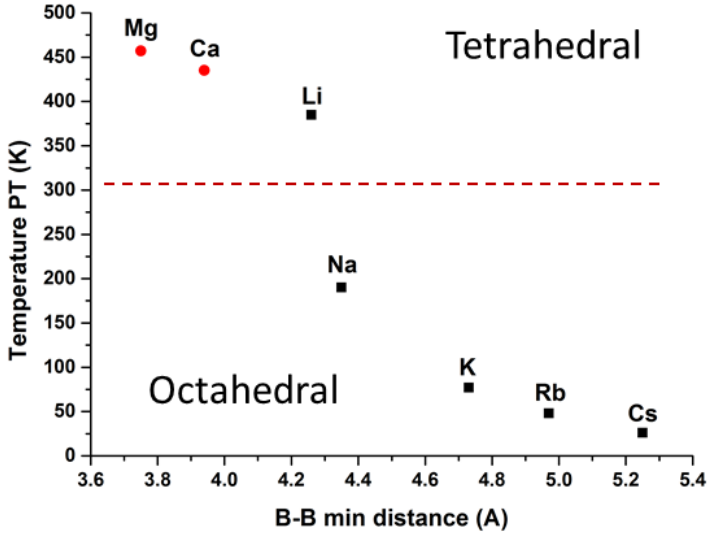

Figure 20 – Correlation between the PT temperatures of different borohydrides [$M(BH_4)_x$, M= Li, Na, K, Rb, Cs, Mg, Ca] as a function of the minimum B-B distance in the high temperature structure and coordination of the cation. Adapted from [133].

Furthermore the observed inflection in the heat capacity values in KBH_4, $RbBH_4$, and $CsBH_4$ could be related to a continuous reorientation of the BH_4^- group.[136] In fact, the heat capacity reflects the lattice dynamics, lattice expansion in function of temperature, and it is strictly related to vibrational characteristics (transational, rotational, librational, intraionic vibration), especially of the complex anion in ionic compounds. In solids, different vibrational modes are excited consecutively as the temperature is raised, after the polymorphic transition, the BH_4^- complex anion orientation disordering give way to hindered rotation which explain the plateau of heat capacity values.[133] The rotational disorder of the BH_4^- complex anion is also responsible of the first order phase transition in all studied borohydrides.[154] Structural order-disorder transition is evidenced from the orthorhombic to the hexagonal structure of $LiBH_4$, from the tetragonal to the cubic structure of $NaBH_4$, KBH_4, $RbBH_4$ and $CsBH_4$, because of the increase in the dynamic reorientational disorder and short-range ordered arrangements of BH_4^-.[154] Higher temperature of the phase transition are observed with smaller cation because the entropic term needs to compensate energy as the lattice parameter decreases.

In conclusion, the Dulong–Petit law states the classical expression for the molar specific heat capacity of chemical elements at high temperature.[155] Dulong and Petit found that the heat capacity of a mole of many solid elements is about 3R, where R is the gas constant, so the heat capacity of certain solid elements per mole of atoms they contained is approximately equal to 25 J/K.

As described before, the heat capacity of solids states is due to lattice vibrations in the solid. In the classical theory of heat capacity, the heat capacity of solids approaches a maximum of 3R per mole of atoms because full vibrational-mode degrees of freedom amount to 3 degrees of freedom per atom, each corresponding to a quadratic kinetic energy term and a quadratic potential energy term. Despite its simplicity, Dulong–Petit law offers good prediction for the specific heat capacity of many elementary solids with relatively simple crystal structure at high temperatures. Indeed, the maximum reachable value of the heat capacity is equal to 25 J/K multiply for the number of atoms in the molecule.

$$Cp\ max = n° \cdot 3R \quad \boldsymbol{Eq}.21$$

where: $C_{p\ max}$ is the maximum value that the C_p can reach in a compound (plateau), n° is the number of atoms involved in the compound, and R is the gas constant.

In the case of alkali borohydride a total of 6 atoms are present in the compound and the plateau in the heat capacity reached in KBH_4, $RbBH_4$ and $CsBH_4$, is approximately equal to 100 J/molK. This suggest that the BH_4^- anion should be considered as a "3 atoms unit" following the Dulong-Petit law. In fact:

$$n^\circ = \frac{Cp\ max}{3R} \sim \frac{100}{25} \sim 4 \quad \boldsymbol{Eq}.22$$

Excluding the metal cation involved in the compound, the borohydride anion should be considered as a "3 atoms unit". The presence of a relative strong bond between boron and hydrogen may be related to the apparent fault of the Dulong-Petit law. In fact, the BH_4^- group cannot be easily considered as composed by five independent oscillators. The presence of strong chemical bonds may induce a limitation of single degrees of freedom for the oscillation of single atoms, contributing less (i.e close to half) to the heat capacity of the complex anion.

Conclusions

Experimental C_p values above room temperature for pure borohydrides have been compared with available literature data and modelled as a function of temperature, according to the Calphad method. The Neumann-Kopp rule has been used to define the heat capacity of the borohydride anion.
Phase transitions and trends of the heat capacities as a function of temperature have been compared and could be linked to different role and dynamics of the borohydrides anion and related to the shape of the C_p across the polymorphic transition. The observed inflection in C_p could be related to a continuous order-disorder orientation of the BH_4^- group and the observed plateau at 300 K to a hindered rotation of BH_4^- anion. The temperature of the polymorphic transition is related to the coordination of the BH_4^- anion to the metal cation in the HT phase and its spacing (B-B distance). No further correlations have been observed suggesting a key role of crystal structure and ion coordination in the polymorphic transition mechanism.

Closo deca and dodeca-borane

Boranes are molecular compounds that can be subdivided in different classes, among which closo-boranes are the most stable anions with general formula

$B_nH_n^{2-}$, where n=6-12. Recently, Paskevicius et al. reviewed their synthesis routes, structure, coordination, properties and applications.[70]
Despite these compounds were discovered and studied from the beginning of the XX century, still many structures and details about their polymorphic transitions are missing. The present study aims to systematically investigate into details their LT and HT crystal structures, thermal properties and polymorphic transition mechanism.
The project is part of a collaboration between the University of Turin (Italy), the Curtin University (Australia) and the Aarhus University (Denmark). Synthesis of pure water-coordinated compounds was performed at the Curtin University by Mark Paskevicius. Mark Paskevicius and Mathias Jørgensen are performing *in-situ* SR-PXD studies and resolution of new crystal structures is ongoing.
At the University of Turin, as received/synthesized compounds have been dried by heating up to 200 °C under dynamic vacuum for several hours. The treatment was stopped when detected pressure was stable and equal to $4 \cdot 10^{-5}$ bar.
After thermal treatment, the compounds have been analysed by ATR-IR to ensure the complete removing of water. In fact, no O-H signal have been observed in any spectra around 3000 cm^{-1} (not reported). Then, their thermal behaviours and thermodynamics have been investigated by HP-DSC.

Introduction

The nomenclature of solid-state phase transitions is very discussed since in the literature more than 300 types/mechanisms of solid state phase transitions are reported.[156,157]
Generally, the assignment of type/mechanism of phase transition can be done knowing the thermodynamics of the compound and the structures of the low and high temperature phase.
In a first order transition,[158] at least one of the first derivatives of the Gibbs Free Energy experiences a discontinuous change, i.e. $\Delta S \neq 0$ or $\Delta V \neq 0$. The specific heat of the system is effectively infinite at the transformation temperature and a latent heat of transformation must be defined. Therefore, this transitions are discontinuous and presents jumps in physical properties. Crystal structure changes abruptly, latent heat is absorbed or released, symmetries of the phases are not related, and overheating or overcooling is possible. Generally, this type of transition is the most common one; its mechanism is characterized by nucleation, that can be homogeneous or heterogeneous, and growth. Antiphase boundaries can be formed, long-range diffusion processes in the solid state have

an important role and a two-phase region, where the low temperature and the high temperature phase coexist, can be observed. First order diffusionless transformations, such as martensitic ones, occur without atom diffusion but by cooperative small movements (military) and homogeneous lattice deformation leading to a new crystal structure. They are reversible and present hysteresis.[158] In a second order transition,[158] at the equilibrium transformation temperature, the second derivatives of the Gibbs free energy are discontinuous, while the first derivatives are continuous. No latent heat can be defined and the specific heat usually presents high values. Generally, the transition is continuous and occurs with a gradual loss of long-range order and an increase of disordering approaching the critical temperature, in a range of temperature (order-disorder transition). There is a continuous increase of short-range order by homogenous local arrangements in the crystal. No two-phase region is observed and no hysteresis is usually present (neither overheating nor overcooling). In ordering transformations, the degree of order must be quantified, for example by defining a long-range order parameter that approaching the critical temperature varies from 1 (related to the full ordered structure) to 0 (fully disordered one, random distribution), or any other specific property that shows a change approaching the critical temperature. The λ-type phase transition is a particular case of second order transition, where the specific heat presents a finite change/discontinuity and particular shape remembering a λ.[158]

Literature Survey

Few details are reported in the literature about LT and HT crystal structures, thermal properties and polymorphic transition mechanism for closo-boranes, and they will be reported hereafter.

$Li_2B_{10}H_{10}$ displays at room temperature a $P6_422$ structure with a nominally hexagonal-close-packed arrangement of $B_{10}H_{10}^{2-}$ anions and a trigonal planar coordination of the Li^+ cations.[159] A lower order in the high temperature phase could be expected, and an entropically driven order-disorder polymorphic transition has been suggested bu Wu et. al,[159] with an onset temperature of 367 °C at 5 °C/min under He flow, and it presents a hysteresis upon cooling.[159] However, the crystal structure of the high temperature phase has not been reported yet.

$Na_2B_{10}H_{10}$ has a room temperature monoclinic ($P2_1/c$) structure,[160] while the crystal structure of the high temperature phase is not reported in the literature. Phase transition was reported at T=109 °C, with an enthalpy of 9.81 kJ/mol.[161]
$K_2B_{10}H_{10}$ has a room temperature monoclinic ($P2_1/c$) structure,[160] and it has been reported to have a low temperature polymorph of unknown structure below 0 °C, but crystal structures of both the low and the high temperature phases are not reported in the literature.
$Rb_2B_{10}H_{10}$ has a room temperature monoclinic ($P2_1/c$) structure and it loses crystallinity when cooled below room temperature. It suffers from strong texture effects.[160]
The crystal structure of $Cs_2B_{10}H_{10}$ is unknown. In the literature,[160] it has been reported that it cannot be crystallised solvent-free at all. At room temperature, crystals with the composition $Cs_2B_{10}H_{10}\cdot 2H_2O$ loose water within 20 minutes and turn to an amorphous structure.[160] Heating under vacuum at 5 °C/min, it showed small endotherms peaks at 143 and 268 °C, together with a large endotherm at 606 °C, which could be related to melting.[162]
$Cs_2B_{10}H_{10}$ has an IR spectra[162] very similar to the one of $Na_2B_{10}H_{10}$,[160] $K_2B_{10}H_{10}$ and $Rb_2B_{10}H_{10}$.[162] The only difference stays in a splitting of frequencies in $Na_2B_{10}H_{10}$ and $Cs_2B_{10}H_{10}$ spectra around 2500 cm^{-1}, meaning that some distortion of B-H bonds can be present. A monoclinic structure could be expected also for $Cs_2B_{10}H_{10}$.

Moving to metal-$B_{12}H_{12}$, $Li_2B_{12}H_{12}$ has a cubic ($Pa\bar{3}$, ccp/fcc) structure at room temperature, where the Li^+ cation is displaced from the tetrahedral site. It lies on a near-trigonal-planar site formed by three $B_{12}H_{12}^{2-}$ anions, each of which resides in the octahedral cage defined by six Li^+ cations. Each $B_{12}H_{12}^{2-}$ anion orients two H atoms to each of the Li^+ cations, resulting in a strongly distorted octahedral coordination of the Li^+ cation with six H atoms.[163] A first-order phase transition (high temperature structure: $Fm\bar{3}m$, ccp/fcc) was reported for $Li_2B_{12}H_{12}$ at T_{onset}= 342 °C (1 °C/min), with an enthalpy of approx. 20 kJ/mol, and at T= 323 °C (2 °C/min) upon cooling.[164] The transition seems to be irreversible after 367 °C because of a decomposition and release of hydrogen. Experimental *in-situ* studies are also present in the literature.[68,71,165]
A monoclinic-to-cubic phase transition was reported for $Na_2B_{12}H_{12}$ (RT: $P2_1/n$, ccp/fcc, HT: various bcc or ccp/fcc structures) at T_{onset}= 256 °C (at 1 °C/min) with an enthalpy of approx. 6 kJ/mol and an hysteresis down to 210 °C upon cooling.[164] The transition seems to be a λ type order-disorder/martensitic transformation, because on cooling a first broad peak is reported to start at 262

°C and then the main phase transformation is reported at 272 °C. However, three high temperature polymorphs have been reported.[165] The first structure possesses a $Pm\bar{3}n$ symmetry, with bcc arrangement of orientationally disordered $B_{12}H_{12}^{2-}$ anions and it is related to a transition around 256 °C. The disordered Na^+ cations are located, with reduced occupancies, at higher-multiplicity, off-center sites within the distorted tetrahedral sites of the anion sublattice. The second high-temperature structure ($Im\bar{3}m$, bcc) existing above 272 °C is the result of an order–disorder transition yielding more extensive disorder of the bcc anions (orientationally) and cations.[164,165] Moreover, it appears that a minor amount of a third high temperature structure coexists with the other two phases. It has been suggested that this structure may resemble a fcc, orientationally disordered anion lattice with Na^+ cations populating a variety of sites, including the planar three-fold sites ($Fm\bar{3}m$, ccp/fcc).[165]

In the case of $K_2B_{12}H_{12}$, the room temperature crystal structure is fcc ($Fm\bar{3}$), where the $B_{12}H_{12}^{2-}$ anion is surrounded by eight K^+ cations within the cubic geometry, while the K^+ cation is tetrahedrally surrounded by four $B_{12}H_{12}^{2-}$ anions.[163,166] A reversible phase transition was reported for $K_2B_{12}H_{12}$ at T= 538°C of second-type order-disorder. Above that temperature, partial decomposition could be possible. The enthalpy of PT is reported to be between 50-270 J/mol for the compounds with K, Rb and Cs, where the enthalpy is higher for smaller cations, so probably for K is around 270 J/mol.[167] Around 630 °C it was reported to melt.[166]

$Rb_2B_{12}H_{12}$ has a room temperature fcc crystal structure ($Fm\bar{3}$).[10] A polymorphic order-disorder transition was reported at T_{onset}= 469 °C, at 10 °C/min.[167] Around 672 °C it was reported to melt.[166]

The room temperature crystal structure of $Cs_2B_{12}H_{12}$ is fcc ($Fm\bar{3}$).[10] In the literature, corresponding DSC trace was reported to show a large endothermic signal, beginning at 652 °C, which peaked at 666 °C (heated under vacuum at 5 °C/min). Other small endotherms of undetermined origin were observed at T_{peak} 157, 569, and 721 °C. The recovered sample appeared to have been molten, it was not darkened, and its infrared spectrum was unchanged.[162,166] Furthermore, a second order phase transition was reported at T_{onset}= 256 °C, at 10 °C/min.[167]

Polymorphic transition

It is clear that the classification suggested so far for closo-borane phase transitions still misses a deep description of the thermodynamics (especially specific heat determination) and mechanism of transitions from the low

temperature crystal structure to the high temperature one, that will be included in this study to classify the observed phase transitions.

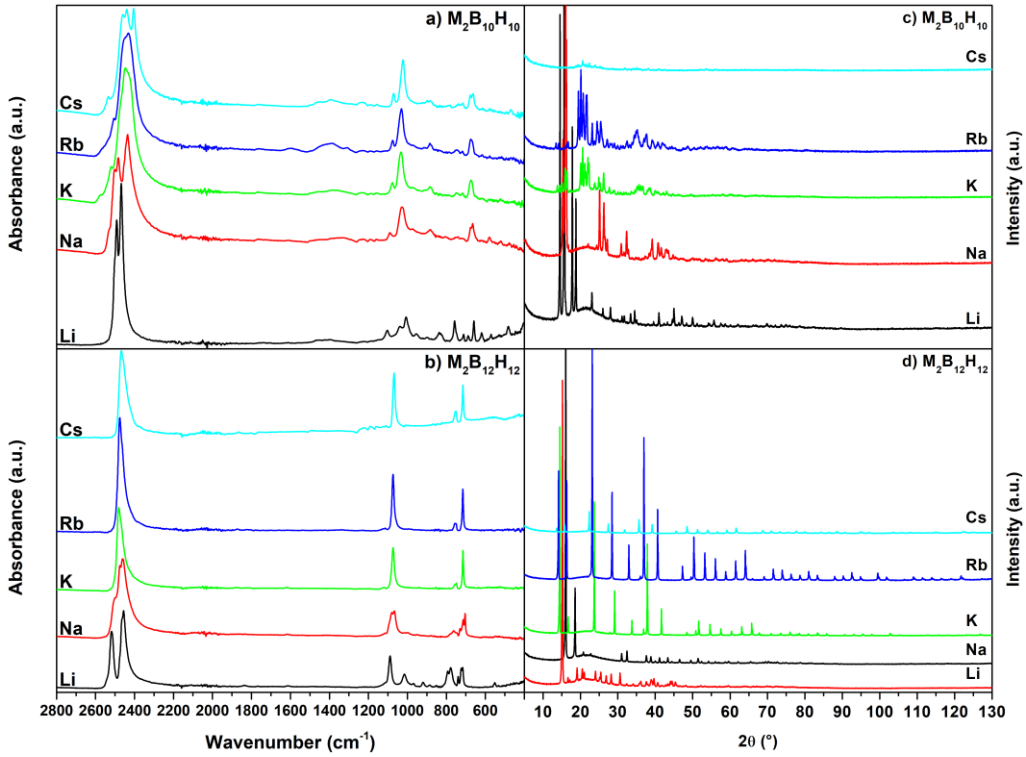

Figure 21 – Characterisation of as synthesized water-free closo-boranes $M_2B_{10}H_{10}$ and $M_2B_{12}H_{12}$ (M=Li, Na, K, Rb, Cs), investigated by ATR-IR (a,b) and XRD (c,d).

Figure 21 reports an overview of water-free closoboranes investigate in this study by ATR-IR and XRD.

Generally, the ATR-IR spectra (**Figure 21 a,b**) are in good agreement with the literature.[160,162] In fact, in ATR-IR spectra of $Na_2B_{10}H_{10}$ all known frequencies can be observed: 2445 (νB-H), 1031, 745, and 665 cm^{-1} (δB-B), as well as for $Rb_2B_{10}H_{10}$ ATR spectra: 2453 (νB-H), 1075, 1031, 745, and 675 cm^{-1} (δB-B).[160]

Figure 21 c,d reports all the PXD pattern of the analysed compounds.

In the $Rb_2B_{10}H_{10}$ sample, some excess of $Rb_2B_{12}H_{12}$ used as a starting reactant in the synthesis is present in 3%wt, determined by Rietveld refinement.

As reported before, a monoclinic structure could be expected also for $Cs_2B_{10}H_{10}$, but PXD shows very low intensity (**Figure 21, c**) and the structure cannot be solved, SR-PXD are needed.

All PXD after DSC (not reported) are the same as the one reported below (**Figure 21 c,d**) confirming the non-decomposition of the sample, except for the $Li_2B_{10}H_{10}$ (better described later).

In relation to the thermal behaviour of closo-boranes, DSC analysis of $Li_2B_{10}H_{10}$ under 10 bar of H_2 (**Figure 22 a**) reveals a thermal event at T_{onset}= 369 °C (at 5 °C/min, T_{peak}= 379 °C) with an enthalpy of 27.8 kJ/mol that could be related both to polymorphic transition or decomposition.

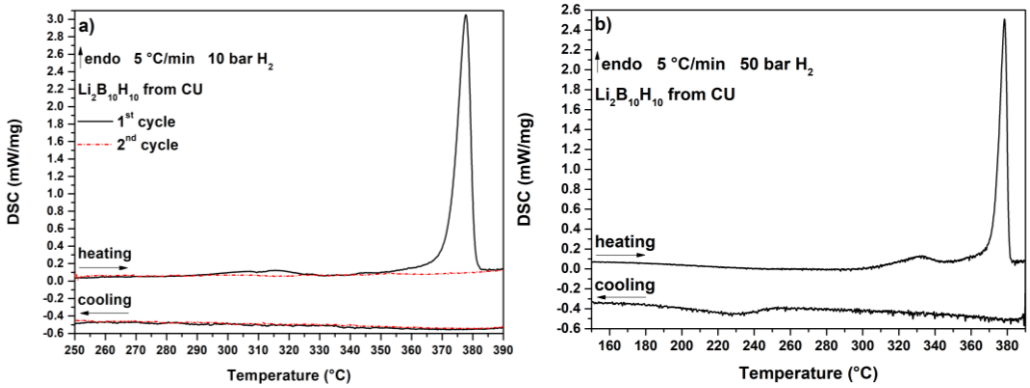

Figure 22 – HP-DSC analysis of $Li_2B_{10}H_{10}$ under a) 10 bar and b) 50 bar H_2, at 5 °C/min.

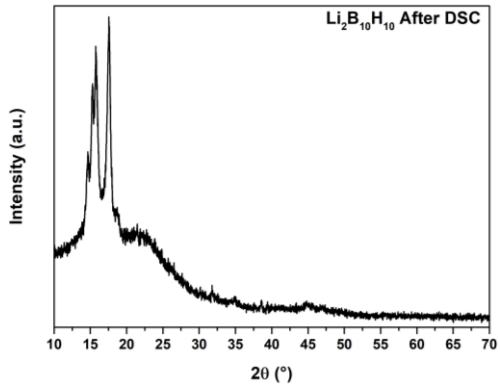

Figure 23 – PXD pattern after HP-DSC analysis of $Li_2B_{10}H_{10}$.

In fact, after the first heating, the transition is not reversible and PXD pattern evidenced decomposition to an unknown phase (**Figure 23**). Analysis under 50 bar of H_2 (**Figure 22 b**) shows the event at T_{onset}= 370 °C (at 5 °C/min, T_{peak}= 378 °C) with an enthalpy of 24.0 kJ/mol. No shift in peak temperature is recorded,

meaning that it could be related to a reversible polymorphic transition. Small extra peaks can be observed before the transition, and upon cooling in the 50 bar run. They could be related to an order-disorder transition confirming the assignment done in the literature.[159]

In the DSC analysis of $Na_2B_{10}H_{10}$ (**Figure 24**), the polymorphic transition is reversible and clearly detected at T_{onset}= 107 °C (at 1 °C/min, T_{peak}= 110 °C, 94 °C on cooling). The shape of the peak could indicate the presence of two overlapping peaks, one more intense and thin and a second one less intense and broad. In fact, upon cooling, a hysteresis is present and the peak of the transition presents a shoulder, evidencing the presence of two different transitions. The total enthalpy of the transition is equal to 14.0 ± 0.1 kJ/mol, higher than the previous value reported in the literature.[161]

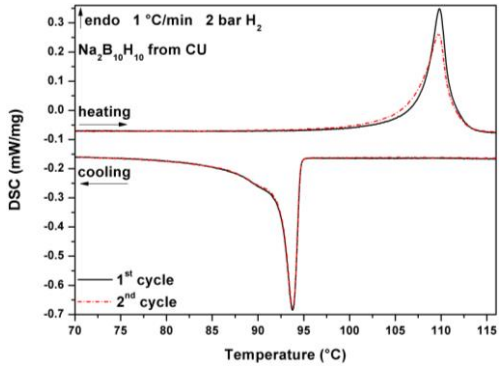

Figure 24 – HP-DSC analysis of $Na_2B_{10}H_{10}$ under 2 bar H_2, at 1 °C/min. Two cycles have been performed.

$K_2B_{10}H_{10}$, on the first heating (**Figure 25**), an intense peak can be detected at T_{onset}= 422 °C (at 5 °C/min, T_{peak}= 430 °C), which shape is similar to that of $Na_2B_{10}H_{10}$. Second and third cycles are overlapping and they show the peak at T_{onset}= 394 °C (T_{peak}= 408 °C) on heating and at T_{peak}= 391 °C on cooling, without a significant hysteresis. Comparing the heating ramps, the peak observed on the first heating is recorded at higher temperature, maybe because of overheating.
The peak observed on the first heating ramp has a higher enthalpy compared to the following cycles, equal to 6.2 kJ/mol. However, since the transition has no significant hysteresis, it seems to be of second order type and no latent heat should be defined. It could also be described as λ-type transition because of the shape of the DSC peak.

Figure 26 shows the DSC analysis of $Rb_2B_{10}H_{10}$. On the first heating, approaching the polymorphic transition, the baseline is not perfectly flat. The main peak can be detected at T_{onset}= 477 °C (at 5 °C/min, T_{peak}= 484 °C). Second and third cycles are overlapping and they present a flat baseline and a clear DSC peak, without any shoulder. The peak observed on the first heating is recorded at slightly higher temperature. In fact, on second and third heating the peak is observed at T_{onset}= 475 °C (T_{peak}= 482 °C). On cooling, the transition is reversible, the peak is broader and it is recorded at T_{peak}= 466 °C, with a small hysteresis. Similarly to $K_2B_{10}H_{10}$ the transition can be assign to a second order, λ-type.

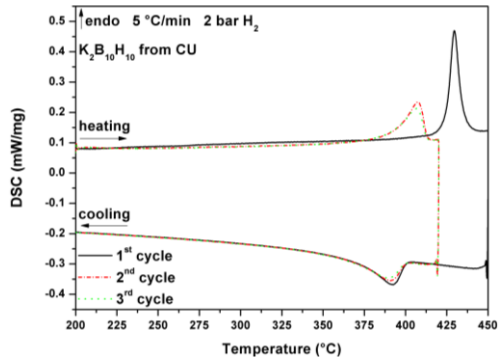

Figure 25 – HP-DSC analysis of $K_2B_{10}H_{10}$ under 2 bar H_2, at 5 °C/min. Three cycles have been performed.

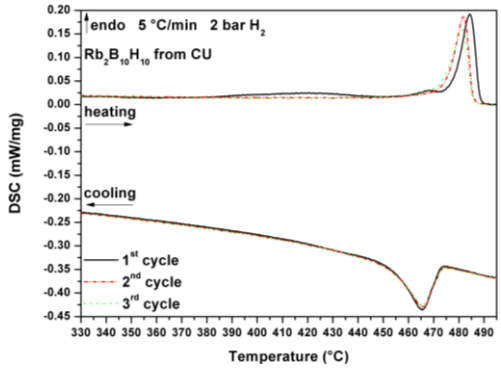

Figure 26 – HP-DSC analysis of $Rb_2B_{10}H_{10}$ under 2 bar H_2, at 5 °C/min. Three cycles have been performed.

To conclude the alkali series of deca-boranes, $Cs_2B_{10}H_{10}$ shows no endotherms nor exotherms in the investigated temperature range (from RT up to 500 °C, not reported).

With reference to dodeca-boranes, **Figure 27** shows DSC analysis of $Li_2B_{12}H_{12}$ under 10 bar of H_2 and reveals, on the first heating, an event at T_{onset}= 349 °C (at 5 °C/min, T_{peak}= 357 °C) with an enthalpy of 22.0 kJ/mol, related to the polymorphic transition. On cooling, the transition is reversible and it is detected at T_{peak}= 321 °C (hysteresis).
On the second and third cycle, the transition is recorded progressively at lower temperature, T_{onset}= 341 °C (T_{peak}= 347 °C) and T_{onset}= 338 °C (T_{peak}= 344 °C) respectively. It maintains the same shape, but the peak is wider and less intense. The peak is asymmetric and a shoulder seems to be present. On cooling, the reversible transformation is observed at the same temperature of the first cooling and with similar area and shape.
The averaged enthalpy of the transition, taking into account both heating and cooling is equal to 20.5 ± 1.0 kJ/mol, in good agreement with literature value.

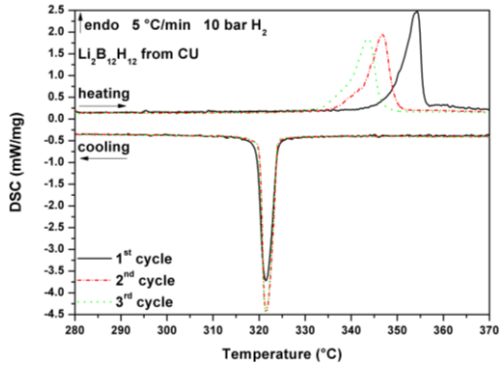

Figure 27 – HP-DSC analysis of $Li_2B_{12}H_{12}$ under 10 bar H_2, at 5 °C/min. Three cycles have been performed.

On the first heating of $Na_2B_{12}H_{12}$ (**Figure 28**), a peak that present a shoulder can be detected at T_{onset}= 262 °C (at 5 °C/min, T_{peak}= 266 °C), the shape of the peak is similar to the one of $Li_2B_{10}H_{10}$. Second and third cycles are overlapping at T_{onset}= 257 °C (at 5 °C/min, T_{peak}= 263 °C). Comparing the DSC traces in heating ramps, the peak observed on the first heating is recorded at higher temperature. On cooling, two events are clearly observed, related to the polymorphic transitions from a fully disordered phase to a partially ordered one and then to the ordered phase, which could be the origin of the shoulder upon heating and that were mentioned in the literature.[164,165]
The first DSC peak, which is the less intense and could be related to a second order transition, can be observed at T_{peak}= 255 °C (enthalpy 1.93 ± 0.03 kJ/mol), while the second is recorded at T_{peak}= 197 °C (enthalpy 9.4 ± 0.3 kJ/mol) but a

clear assignment to which structure transition they correspond to, cannot be done. The second peak occurs in a rather wide temperature range, but it shows an evident latent heat of transformation and could be assigned to a first order transition.

The averaged enthalpy of the transition, taking into account both heating and cooling, is equal to 11.8 ± 0.7 kJ/mol, a value that is almost double than that reported in the literature.[164,165]

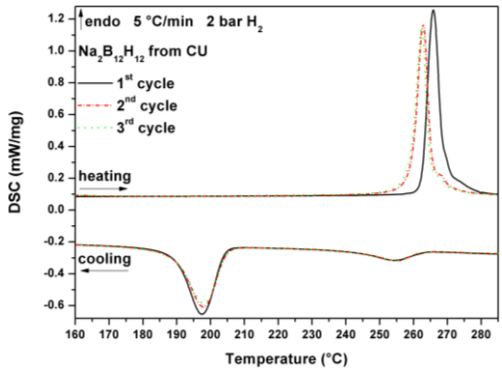

Figure 28 – HP-DSC analysis of $Na_2B_{12}H_{12}$ under 2 bar H_2, at 5 °C/min. Three cycles have been performed.

In the case of $K_2B_{12}H_{12}$, the polymorphic transition is clearly detected in **Figure 29** at T_{peak}= 541 °C (at 5 °C/min, T_{peak}= 540 °C on cooling), but it seems to take place in a broad temperature range. The shape of the DSC signal suggests a λ type transition, the broad temperature range could correspond to an order-disorder transition, and it has no hysteresis upon cooling.

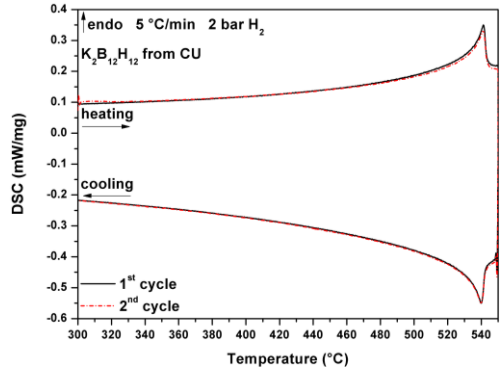

Figure 29 – HP-DSC analysis of $K_2B_{12}H_{12}$ under 2 bar H_2, at 5 °C/min. Two cycles have been performed.

The DSC analysis of $Rb_2B_{12}H_{12}$ shows a trace and transition similar to that of $K_2B_{12}H_{12}$. First and second thermal cycles are overlapping (**Figure 30**) and they present a clear peak with T_{peak}= 476 °C, reversible and without hysteresis on cooling. The transition could be of second order, since it seems to happen in a broad temperature range, or order-disorder or λ type.

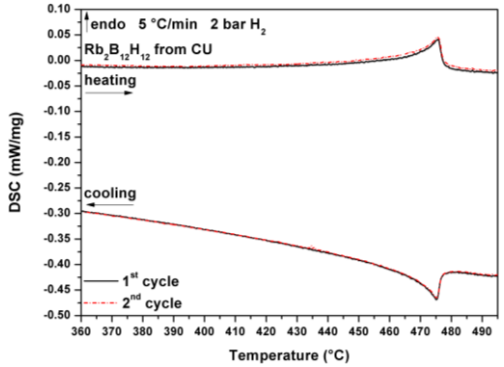

Figure 30 – HP-DSC analysis of $Rb_2B_{12}H_{12}$ under 2 bar H_2, at 5 °C/min. Two cycles have been performed.

To conclude, from the DSC analysis of $Cs_2B_{12}H_{12}$, the polymorphic transition is hardly visible and it takes place in a broad temperature range (**Figure 31**), starting above 230 °C (at 5 °C/min, T_{peak}= 256 °C), with no hysteresis upon cooling and in good agreement with the literature and confirming a second order transition.[167]

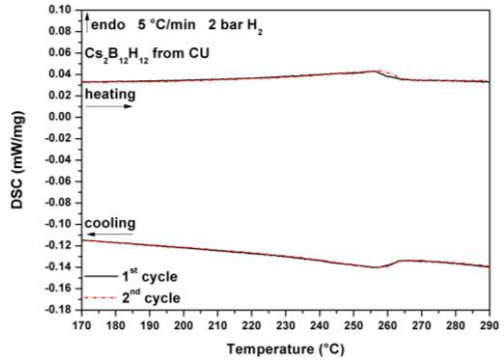

Figure 31 – HP-DSC analysis of $Cs_2B_{12}H_{12}$ under 2 bar H_2, at 5 °C/min. Two cycles have been performed.

Discussions and Conclusions

Table 4 resumes the polymorphic transition details of investigated closoboranes comparing literature information and new experiments. Lithium and sodium closoboranes usually show first order phase transitions and present many polymorphs at high temperature. Potassium, rubidium and caesium display second order transitions with order-disorder phenomena that need to be further studied and described in details.

Most of the investigated closoboranes show a tetrahedral coordination of the cation in the low temperature phase but different crystal structures. In particular when the Li^+ cation is involved the crystals rearrange in a completely different space group, while in the case of Na^+, K^+, Rb^+ and Cs^+ the space group at low temperature is the same.

Table 4 – Summary of classification of phase transitions type from the literature and from the present study, together with and missing information.

	$B_{10}H_{10}$	$B_{12}H_{12}$
Li_2	➢ Entropically driven PT ➢ Order-disorder ✓ Possible decomposition × Determination of HT phase or decomposition product	➢ First order ✓ First order ✓ 2 possible transitions × Determination of HT phases
Na_2	✓ First order ✓ 2 possible transitions × Determination of HT phases	➢ λ-type ➢ Order-disorder ➢ Martensitic ✓ 2 possible transitions: *Order-disorder* and First order × Determination of HT phases
K_2	✓ Second order ✓ λ-type × Determination of LT phase; temperature and enthalpy of LT-PT × Determination of HT phase × Determination of enthalpy of melting	➢ Second order ➢ Order-disorder ✓ Second order, possibly *Order-disorder* or λ-type × Determination of HT phase × Determination of enthalpy of melting
Rb_2	✓ Second order ✓ λ-type × Determination of HT phase × Determination of enthalpy of melting	➢ Order-disorder ✓ *Order-disorder* ✓ Second order ✓ λ-type × Determination of HT phase × Determination of enthalpy of melting
Cs_2	➢ Not crystalline × Determination of crystal structures × Determination of enthalpy of melting	➢ Second order ✓ Second order × Determination of HT phase structure × Determination of enthalpy of melting
Legend: ➢ Literature ✓ New Experiments × Still missing (ongoing investigation)		

As evidenced in borohydrides the polymorphic transition is strongly influenced by the crystal structure and atomic distance between boron or metal atoms in the structures. Also the values of polymorphic transition temperatures in function of B-B and M-M minimum distances in high temperature structures of borohydrides are reported and compared with the closoboranes one in **Figure 32 and 33**. However, since for closoborane the high temperature structures are not known yet, the relative distances where obtained from the known low temperature structures.

Some correlations between the B-B (**a**) or M-M (**b**) distance and the peak polymorphic transition temperature can be observed in **Figure 32**, especially in the case of potassium, rubidium and caesium. While the lithium compounds stay outside of correlations trends.

In $M_2B_{10}H_{10}$ compounds the minimum distances between the complex anion cage (B-B) seems not to influence the polymorphic transition temperatures (**Figure 32 a**), while considering the M-M distance, it shows a relationship with the polymorphic transition temperature (**Figure 32 b**). Whereas, in borohydrides and $M_2B_{12}H_{12}$ compounds, the temperature of the polymorphic transition display an inverse proportion with the B-B and M-M minimum distances (**Figure 32 a,b**). The same trends are observed as a function of ionic radius of the metal cation (**Figure 32**).

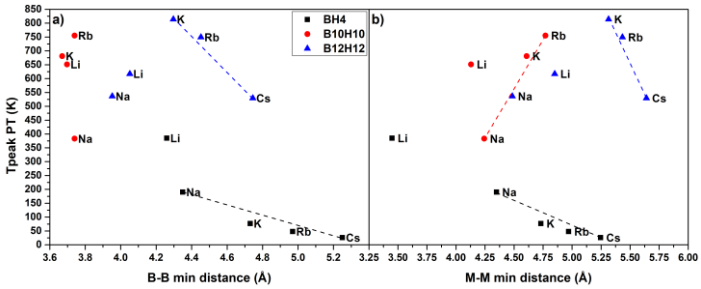

Figure 32 – Possible trends in the peak temperature of closoboranes and borohydrides polymorphic transitions as a function of B-B and M-M minimum distances. Dashed lines are a guide for the eyes.

As for borohydride, structural features play a role in the polymorphic transition mechanism of closoboranes. The direct or inverse proportion could be related to possible reordering phenomena or changes in volume involved in the transition, which can be better understood if the high temperature crystal structure will be determined, for instance by *in-situ* measurements.

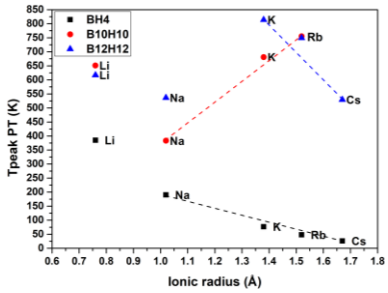

Figure 33 – Possible trends in the peak temperature of closoboranes and borohydrides polymorphic transitions as a function of the ionic radius. Dashed lines are a guide for the eyes.

Taking into account electronic features, some trends can be observed as a function of different electronegativity scales (**Figure 34**).

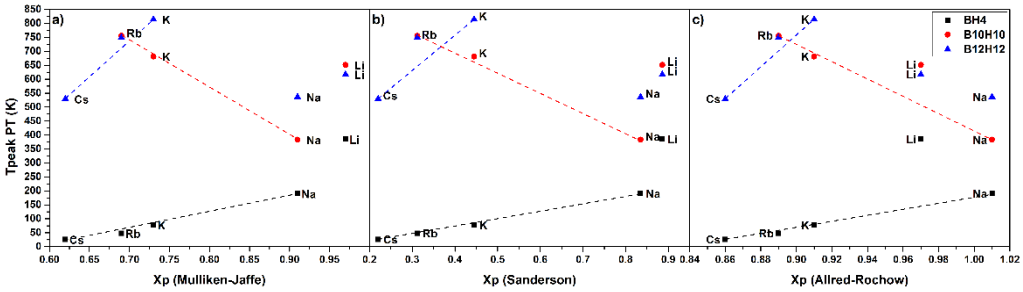

Figure 34 – Possible trends in the peak temperature of closoboranes and borohydrides polymorphic transitions, as a function of different electronegativity scales. Dashed lines are a guide for the eyes.

The Mulliken-Jaffe electronegativities referred to the arithmetic mean of the first ionization energy and the electron affinity. It measures of the tendency of an atom to attract electrons.[168,169]

Sanderson electronegativity is calculated on the basis of the reciprocal atomic volume. This electronegativity underlies the concept of electronegativity equalization, which suggests that electrons distribute themselves around a molecule to minimize or to equalize the Mulliken electronegativity.[170,171]

Allred–Rochow electronegativity is related to the charge experienced by an electron on the "surface" of an atom: the higher the charge per unit area of atomic surface the greater the tendency of that atom to attract electrons.[170]

These scales of electronegativity seem to evidence some electronic constrain involved in the polymorphic transition mechanism that should be taken into account.

Despite these compounds have been known and studied from almost 50 years, quite a lot of information are still missing. High temperature structure are often

not reported. *In-situ* SR-PXD could help in the determination of phase structure and polymorph stability, even at low temperatures, where other phase transitions could take place. *In-situ* SR-PXD studies are currently ongoing in collaboration with Mark Paskevicius (Curtin University, Australia) and Mathias Jørgensen (Aarhus University, Denmark).

Furthermore, vibrational studies as a function of temperature would help in the understanding of polymorphic transition mechanism in details, in order to define an order parameter to describe the order-disorder phase transitions. DFT calculations could help in the determination of frequencies and heat capacities estimation.

The determination of heat capacities and assessment of thermodynamic properties should be performed, to define, for the first time, a complete database on this compounds, implementing the current database of complex hydrides.

In conclusion, determination of missing crystal structures and heat capacities are necessary to further confirm and to determine the type and mechanism of all phase transitions and to fully describe their thermodynamics.

Chapter 4 – Thermodynamic assessment of $LiBH_4$-$NaBH_4$-KBH_4 system

Following the assessment and characterization of pure borohydrides and boranes, the study have been expanded with an insight into binary and more complex systems of borohydrides.
In the literature, it was showed that binary combination of $LiBH_4$, $NaBH_4$ and KBH_4 present eutectic melting[54,124] or a thermal minimum.[172] Starting from the presented experimental values, and new *ab-initio* calculation or experiments, the thermodynamic assessment and optimisation of binary systems will allow the modelling of solid and liquid phases, leading to a description of the pseudo-ternary phase diagrams using the Calphad approach.[76]
The full assessment in all temperature and composition range of the $LiBH_4$-$NaBH_4$-KBH_4 (LiNaK) system allows developing a Calphad database for complex hydride to be used for further interpolation or calculation on decomposition reactions and understanding of interaction among mixtures and their relative thermodynamics.

Introduction

Metal borohydrides are interesting compounds for hydrogen storage in the solid-state owing to their high gravimetric hydrogen content.[14,21–23] When mixed, owing to their low temperature of melting, eutectic mixtures of complex hydrides can easily be infiltrated into porous scaffolds.[49,50] In this way, the kinetics and reversibility of hydrogen sorption reactions can be improved, because nanosized particles are preserved during cycling. The knowledge of the thermodynamics of those system and discovery of even lower eutectic systems will open the way for new promising hydrogen storage systems.
Since some reported phase diagrams are not coherent and the experimental points are not fully described, further investigations are necessary and a full assessment of systems of interest is necessary.

Literature

As reported before, mixtures of metal borohydrides often show eutectic melting, *e.g.* the mixture of lithium and potassium borohydride, $0.72LiBH_4$–$0.28KBH_4$, with a melting point as low as T_e = 105 °C.[34,54,173] For the $LiBH_4$-$NaBH_4$ system, an

eutectic composition 0.62$LiBH_4$-0.38$NaBH_4$, melting at 220 °C, was reported more than 40 years ago.[174,175]

A partial pseudo-binary $LiBH_4$-$NaBH_4$ phase diagram was proposed by Adams in 1961, describing the system as eutectic and reporting experimental liquidus points in the $LiBH_4$-rich mixtures, however without detailing the experimental method used for their determination.[174] In 1971, Semenenko et al. conducted a study of the pseudo-binary phase diagram by coupling thermographic and X-ray investigation on annealed samples. The system was described without any eutectic point, but it was characterized by the formation of solid solutions with a miscibility gap and a minimum melting temperature at the same composition previously proposed by Adams as eutectic (0.62$LiBH_4$-0.38$NaBH_4$).[175] It is worth noting that solid solutions of metal borohydrides have recently received attention, especially those of $LiBH_4$ with alkali metal halides, since it was reported that $LiBH_4$-LiI shows fast-ion conduction, owing to the stabilization of the hexagonal HT-structure of $LiBH_4$ at room temperature.[57,60–63,65,176–178]

The $LiBH_4$-$NaBH_4$ system was recently experimentally studied[124] showing the formation of solid solutions on both lithium and sodium rich side and a eutectic melting at 216 °C for the composition 0.70$LiBH_4$-0.30$NaBH_4$. In this system, the polymorphic transition from the orthorhombic to the hexagonal structure is observed at 95 °C in mixtures (i.e. 15 °C lower than pure $LiBH_4$).

The $LiBH_4$-KBH_4 system was reported as eutectic by Ley et al.[54] and Huff[179] with a melting temperature of 105 °C for the composition 0.72$LiBH_4$–0.28KBH_4. The same phase diagram, but with a different eutectic composition, was reported by Adams in 1961.[174] In this system, no solid solutions were observed. A bimetallic compound $LiK(BH_4)_2$ has been recently reported, which at 96 °C decomposes into $LiBH_4$ and KBH_4.

Two experimental studies have been reported for the $NaBH_4$-KBH_4[172,175] system. Jensen et al. showed the formation of a solid solution with full solubility above 200 °C and a minimum melting temperature at 458 °C for the composition 0.68$NaBH_4$-0.32KBH_4.[172] Below 200 °C, a miscibility gap has been evidenced by Jensen et al., but it was not reported from the previous study by Semenenko et al.[175]. The solid solution can be quenched at room temperature and the de-mixing kinetic of the solid solution at room temperature was studied by NMR by Jensen et al.[172].

Considering the ternary $LiBH_4$-$NaBH_4$-KBH_4 system, Huff[179] reported a ternary eutectic melting at 96 °C for the 0.65$LiBH_4$-0.08$NaBH_4$-0.27KBH_4 composition, but Paskevicius et al.[34] reported no eutectic melting for that mixture.

No $LiBH_4$-$NaBH_4$-KBH_4 pseudo-ternary phase diagram nor full characterization of ternary system are present in the literature so far.
The exploration of this ternary system, combining experimental and theoretical techniques will enable the assessment of the thermodynamics by the Calphad method. First the $LiBH_4$-$NaBH_4$, $LiBH_4$-KBH_4 and $NaBH_4$-KBH_4 binary systems must be optimized. For the assessment of solid solutions, the regular solution model was used, whereas the Redlich-Kister model was considered to describe the liquid phase, allowing to further explore the entire temperature and composition range of the ternary system and establish phase stabilities and limits of solubility.
The experimentally investigated sample and the corresponding synthesis method are reported in **Table 5**, furthermore the composition are graphically represented in the ternary phase diagram in **Figure 35**.

Table 5 – Investigated compositions in the ternary system. M = Manual mixing; BM = Ball Milled.

Sample	Composition (Molar Fraction)	Synthesis
T50Li	$0.50LiBH_4$-$0.25NaBH_4$-$0.25KBH_4$	BM
T50Na	$0.25LiBH_4$-$0.50NaBH_4$-$0.25KBH_4$	BM
T50K	$0.25LiBH_4$-$0.25NaBH_4$-$0.50KBH_4$	BM
T1	$0.65LiBH_4$-$0.08NaBH_4$-$0.27KBH_4$	BM
T2	$0.68LiBH_4$-$0.08NaBH_4$-$0.24KBH_4$	BM
T3	$0.66LiBH_4$-$0.11NaBH_4$-$0.23KBH_4$	BM
s1	$0.10LiBH_4$-$0.05NaBH_4$-$0.85KBH_4$	M
s2	$0.20LiBH_4$-$0.05NaBH_4$-$0.75KBH_4$	M
s3	$0.30LiBH_4$-$0.05NaBH_4$-$0.65KBH_4$	M
s4	$0.40LiBH_4$-$0.05NaBH_4$-$0.55KBH_4$	M
s5	$0.60LiBH_4$-$0.05NaBH_4$-$0.35KBH_4$	M
s6	$0.70LiBH_4$-$0.05NaBH_4$-$0.25KBH_4$	M
s7	$0.80LiBH_4$-$0.05NaBH_4$-$0.15KBH_4$	M
s8	$0.90LiBH_4$-$0.05NaBH_4$-$0.05KBH_4$	M

Experimental screening of ternary system

Three different compositions close to the centre of the pseudo-ternary phase diagram were synthesized by ball milling and have been characterized by *in-situ* SR-PXD (**Figure X**,T50Li, T50Na and T50K).

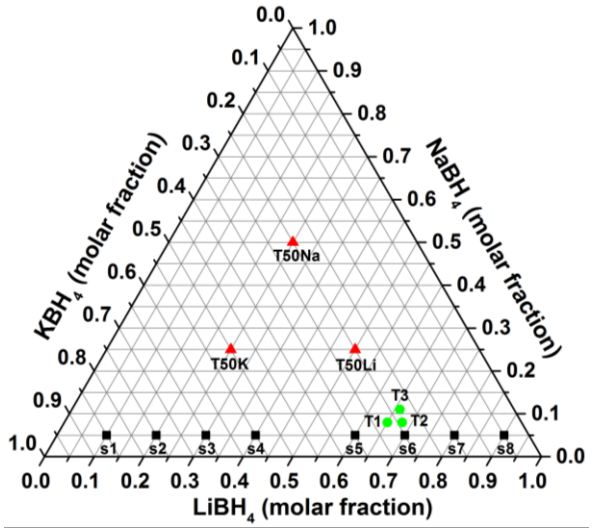

Figure 35 – Investigated compositions in the ternary system. For more details, see **Table 5**.

Samples T50Li, T50Na and T50K were annealed with a heating rate of 5 °C/min to investigate the formation of different phases in the system.

In T50Li (**Figure 36**), the polymorphic transition orthorhombic to hexagonal $LiBH_4$ is recorded at 109 °C, and at 112 °C the $LiBH_4$-KBH_4 eutectic melts. There is no evidence of any ternary eutectic melting or solid solutions in the temperature range 112 °C to 323 °C, where the melting of the sample is observed to start.

In T50Na (**Figure 37**), the polymorphic phase transition of $LiBH_4$ is not clearly observed, and the orthorhombic $LiBH_4$ melts at 114 °C. The formation of a cubic solid solution between the remaining $NaBH_4$ and KBH_4 is observed in the temperature range 114 °C to 215 °C as two sets of Bragg diffraction peaks merge into one. At 215 °C, diffraction peaks of KBH_4 disappear, and a single cubic solid solution is observed. An excess of $NaBH_4$ is also recorded, which disappears at 274 °C. The liquidus temperature is observed at 375 °C.

In T50K sample (**Figure 38**), the polymorphic transition of $LiBH_4$ is recorded at 110 °C, at which point the onset of the eutectic melting of $LiBH_4$-KBH_4 is also observed. At 185 °C, the crystalline fraction of the sample consists of a cubic solid solution of $NaBH_4$-KBH_4, which is rich in $NaBH_4$. The solid solution starts to melt at 352 °C and the liquidus temperature is recorded at 479 °C.
In none of these samples the bimetallic $LiK(BH_4)_2$ is observed.

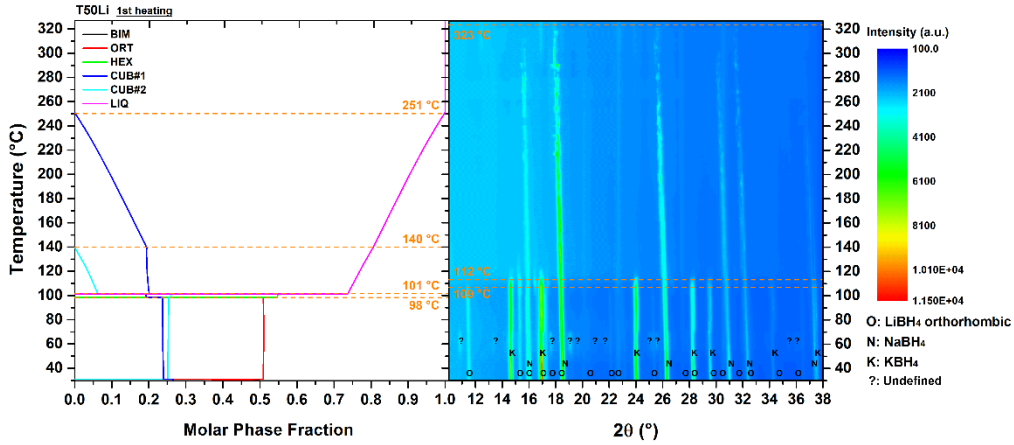

Figure 36 – Amount of calculated phases (CALPHAD, left) and SR-PXD (right) of T50Li, 0.50$LiBH_4$-0.25$NaBH_4$-0.25KBH_4 (λ = 0.9938 Å, ΔT/Δt = 5 °C/min, argon atmosphere).

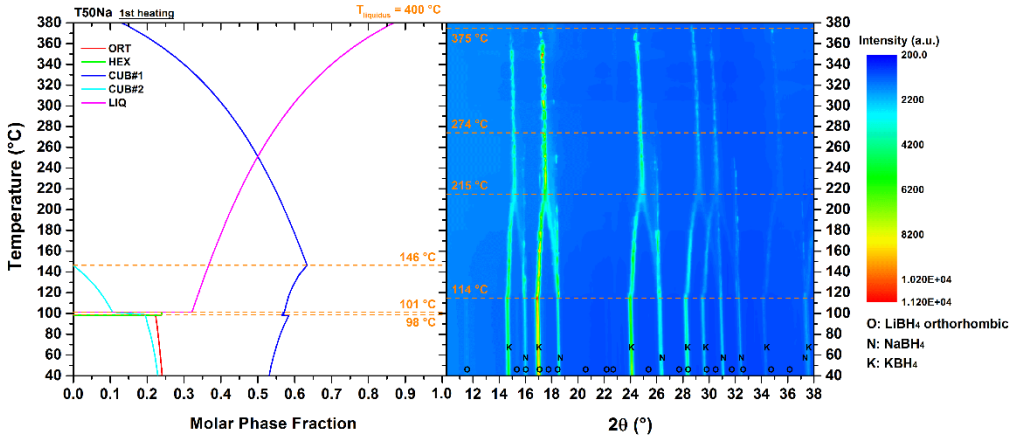

Figure 37 – Amount of calculated phases (CALPHAD, left) and SR-PXD (right) of T50Na, 0.25$LiBH_4$-0.50$NaBH_4$-0.25KBH_4 (λ = 0.9938 Å, ΔT/Δt = 5 °C/min, argon atmosphere).

This first screening of the $LiBH_4$-$NaBH_4$-KBH_4 ternary system, conducted by *in-situ* SR-PXD, did not allow identifying any ternary eutectic composition. So, data collected in this experimental study will be used for a preliminary thermodynamic assessment of the system, leading to a first approximation of the pseudo-ternary phase diagram and to give a hint of the ternary eutectic composition, as will be discussed later.

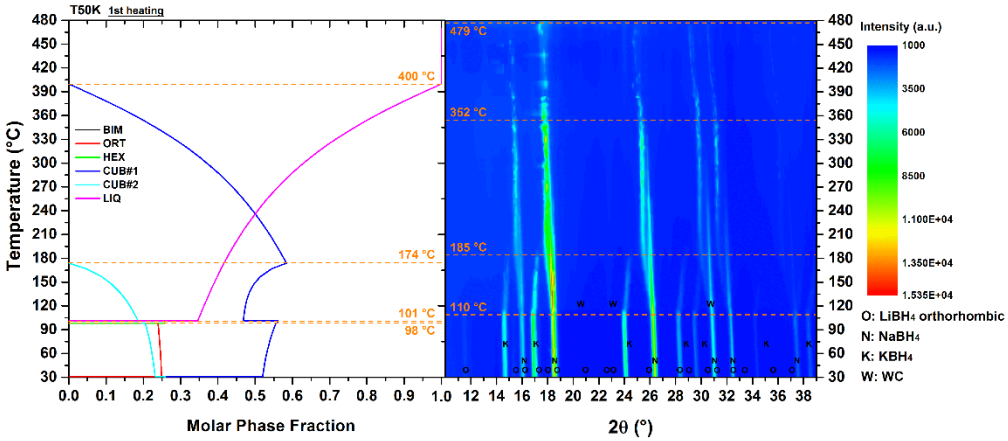

Figure 38 – Amount of calculated phases (CALPHAD, left) and SR-PXD (right) of T50K, 0.25$LiBH_4$-0.25$NaBH_4$-0.50KBH_4 (λ = 0.9938 Å, ΔT/Δt = 5 °C/min, argon atmosphere).

Assessment of binary systems

The thermodynamic assessment of the possible binary combinations in the $LiBH_4$-$NaBH_4$-KBH_4 system allowed the modelling of solid and liquid solution phases. Consistent literature and experimental data together with *ab-initio* calculations and available database have been used as input for the full assessment and description of pseudo-binary phase diagrams and for a first investigation of the ternary system.

$NaBH_4$-KBH_4

The $NaBH_4$-KBH_4 system was modelled considering experimental data obtained by both Jensen et al.[172] and Semenenko et al.[175] The cubic phase was modelled considering the formation of a solid solution with a miscibility gap, as confirmed experimentally by Jensen et al.,[172] so that a positive value of the enthalpy of mixing was assessed (**Table 6**).

Table 6 – Assessed excess Gibbs free energy functions for all investigated systems.

Assessed Excess Gibbs Free Energy (J/mol)
$LiBH_4$-$NaBH_4$
$^{LIQ}G^{exc} = X_{LiBH4}\cdot X_{NaBH4}\cdot(-11291 + 17\cdot T) + X_{LiBH4}\cdot X_{NaBH4}\cdot(X_{LiBH4} - X_{NaBH4})(-308)$
$^{CUB}G^{exc} = X_{LiBH4}\cdot X_{NaBH4}\cdot(5887)$
$^{ORT}G^{exc} = {}^{HEX}G^{exc} = 0$
$LiBH_4$-KBH_4
$^{LIQ}G^{exc} = X_{LiBH4}\cdot X_{KBH4}\cdot(-13016)$
$^{CUB}G^{exc} = X_{LiBH4}\cdot X_{KBH4}\cdot(10000)$
$^{ORT}G^{exc} = {}^{HEX}G^{exc} = X_{LiBH4}\cdot X_{KBH4}\cdot(5000)$
$NaBH_4$-KBH_4
$^{LIQ}G^{exc} = X_{NaBH4}\cdot X_{KBH4}\cdot(1056)$
$^{CUB}G^{exc} = X_{NaBH4}\cdot X_{KBH4}\cdot(7893)$
$^{ORT}G^{exc} = {}^{HEX}G^{exc} = X_{NaBH4}\cdot X_{KBH4}\cdot(10000)$
$LiBH_4$-$NaBH_4$-KBH_4
$^{LIQ}G^{exc} = X_{LiBH4}\cdot X_{NaBH4}\cdot(-11291 + 17\cdot T) + X_{LiBH4}\cdot X_{NaBH4}\cdot(X_{LiBH4} - X_{NaBH4})(-308) + X_{LiBH4}\cdot X_{KBH4}\cdot(-13016) + X_{NaBH4}\cdot X_{KBH4}\cdot(1056) + X_{LiBH4}\cdot X_{NaBH4}\cdot X_{KBH4}\cdot(-14162)$

For a proper modelling of the liquid phase, in order to optimise the enthalpy of melting for the composition with the lowest melting point, a revision of the thermodynamic description of the liquid phase of pure $NaBH_4$ was necessary. Pure $NaBH_4$ was previously described to have an enthalpy of melting equal to 26.9 kJ/mol,[124] as obtained experimentally in ref.[180] Considering that a lower value equal to 16.9 kJ/mol was reported by Milanese et al.,[181] a new function for the liquid phase of $NaBH_4$ was considered (**Table 7**).

Table 7 – Gibbs Free Energy for the liquid phase of $NaBH_4$, KBH_4 and Gibbs free energy for the bimetallic compound $LiK(BH_4)_2$.

Gibbs free energy (J/mol)	Temperature Range (°C)
$^{LIQ}G(NaBH_4) = {}^{CUB}G(NaBH_4) + 16926 - 21.756 \cdot T$	RT-505
$^{LIQ}G(NaBH_4) = -217735 + 693 \cdot T - 119.233 \cdot T \cdot Ln(T)$	505-1000
$^{LIQ}G(KBH_4) = {}^{CUB}G(KBH_4) + 19176 - 21.841 \cdot T$	RT-1000
$G(LiK(BH_4)_2) = {}^{CUB}G(LiBH_4) + {}^{CUB}G(KBH_4) - 1300 + 3.53 \cdot T$	RT-1000

The enthalpy of melting for pure KBH_4 has never been reported in the literature and it is not easy to measure, since it melts and decomposes at the same time.[182] A melting temperature equal to 605 °C was considered, as experimentally observed by Paskevicius et al.[34] and Stasinevich et al.[182] The enthalpy of melting for KBH_4 was first estimated and then progressively refined during the whole assessment process, leading to a value of 19.2 kJ/mol.

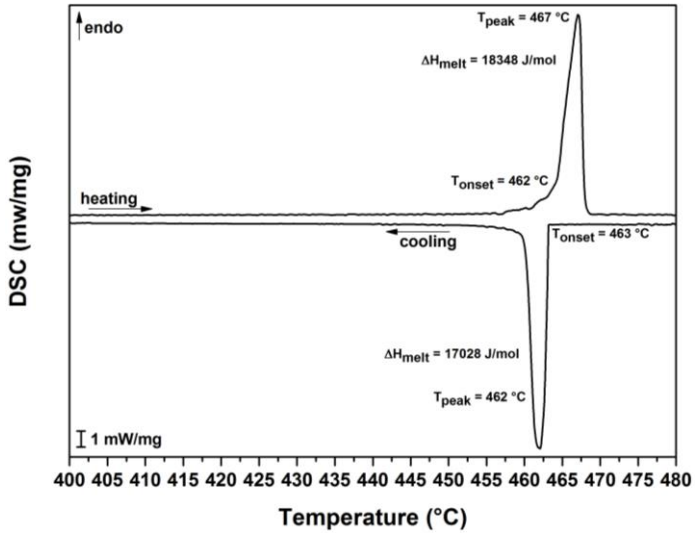

Figure 39 – DSC of $0.682NaBH_4$-$0.318KBH_4$ mixture, heating and cooling at 5 °C/min under 10 bars of H_2.

On the basis of assessed thermodynamic functions for pure $NaBH_4$ and KBH_4, the liquid phase in the $NaBH_4$-KBH_4 system has been described with a slightly positive interaction parameter, obtaining a calculated enthalpy of melting for the

composition $0.68NaBH_4$-$0.32KBH_4$ higher than that reported in the literature.[172] The same sample was measured again under 10 bar of hydrogen, and an enthalpy of melting of 17.0 kJ/mol was obtained during cooling (**Figure 39**), in good agreement with the calculated value (**Table 8**).

Table 8 – Comparison of experimental and calculated data of composition, melting temperatures and enthalpies for eutectics or minimum in the ternary $LiBH_4$-$NaBH_4$-KBH_4 system.

Experimental	**Calculated**
$LiBH_4$-$NaBH_4$	
Ref. [23]	
T = 216 °C	T = 219 °C
70.0 mol% $LiBH_4$	70.3 mol% $LiBH_4$
ΔH_{melt} = 6990 J/mol	ΔH_{melt} = 6520 J/mol
$LiBH_4$-KBH_4	
Ref. [24]	
T = 104 °C	T = 109 °C
72.5 mol% $LiBH_4$	72.3 mol% $LiBH_4$
ΔH_{melt} = 11025 J/mol	ΔH_{melt} = 9828 J/mol
$NaBH_4$-KBH_4	
T = 462 °C	T = 468 °C
68.2 mol% $NaBH_4$	68.2 mol% $NaBH_4$
ΔH_{melt} = 17028 J/mol	ΔH_{melt} = 15331 J/mol
$LiBH_4$-$NaBH_4$-KBH_4	
T = 103 °C	T = 101 °C
$0.66LiBH_4$-$0.11NaBH_4$-$0.23KBH_4$	$0.66LiBH_4$-$0.11NaBH_4$-$0.23KBH_4$
ΔH_{melt} = 4155 J/mol	ΔH_{melt} = 5701 J/mol

Assessed functions of Gibbs free energy are reported in **Table 7**. The calculated $NaBH_4$-KBH_4 pseudo-binary phase diagram is shown in **Figure 40 a**, together with available experimental data. The miscibility gap in the cubic phase is well

reproduced, as well as the melting temperatures. For KBH_4-rich compositions, the calculated values are higher than the experimental ones, suggesting an underestimation of solidus temperatures, which turned out rather constant as a function of composition.[172]

$LiBH_4$-$NaBH_4$

Considering the new thermodynamic description of pure $NaBH_4$, the $LiBH_4$-$NaBH_4$ binary system was re-assessed and a good agreement with the experimental value of enthalpy of melting for the eutectic mixture was achieved (**Table 8**), leading to a lower calculated enthalpy of mixing for the liquid phase with respect to the previous assessment.[124] Available experimental data and calculated pseudo-binary phase diagrams are reported in **Figure 40 b**, confirming the good agreement obtained with the new thermodynamic description.

$LiBH_4$-KBH_4

Since the $LiBH_4$-KBH_4 system was recently experimentally characterised, only the data from Ley et al.[54] were considered for the assessment, while Adams' values[174] have been taken into account only for comparison. *Ab-initio* results reported in **Table 9** were used to describe the Gibbs free energy of the KBH_4 end-members (i.e. orthorhombic and hexagonal phase).

Table 9 – All *ab-initio* calculated Gibbs free energy of end members for the compounds involved in the ternary $LiBH_4$-$NaBH_4$-KBH_4 system.

Gibbs free energy (J/mol)	
$^{CUB}G(LiBH_4) = G(LiBH_4) + 3600$	**ref. [124]**
$^{ORT}G(NaBH_4) = G(NaBH_4) + 8400$	**ref. [124]**
$^{HEX}G(NaBH_4) = G(NaBH_4) + 6200$	**ref. [124]**
$^{ORT}G(KBH_4) = G(KBH_4) + 15200$	
$^{HEX}G(KBH_4) = G(KBH_4) + 11100$	

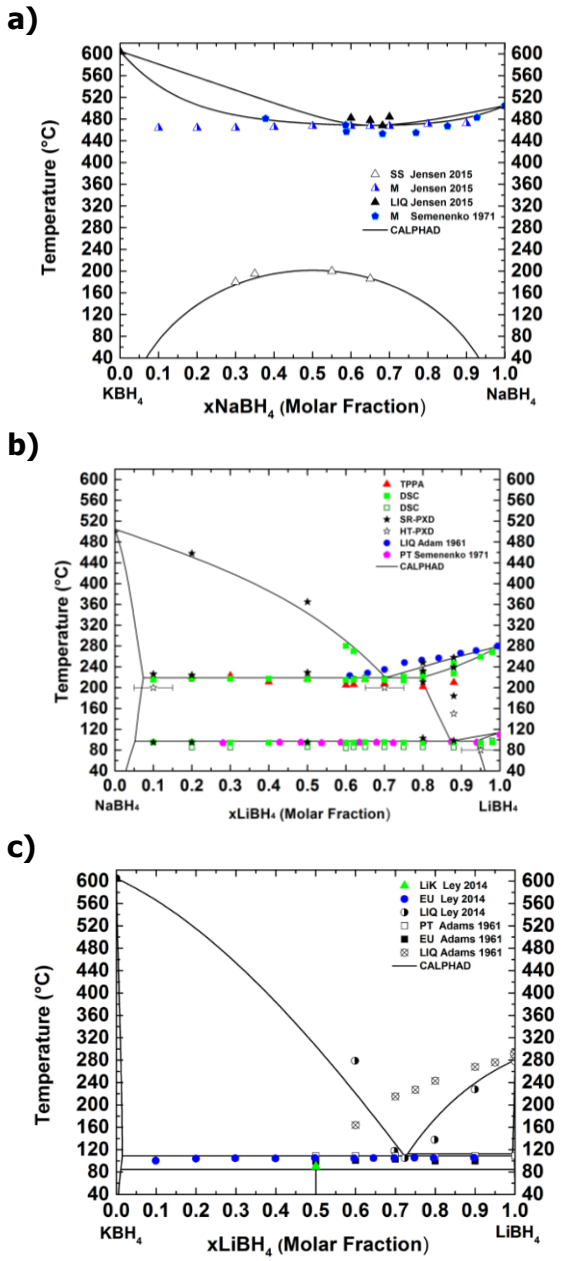

Figure 40 – Literature data and assessed phase diagrams for the $NaBH_4$-KBH_4 (a), $LiBH_4$-$NaBH_4$ (b), $LiBH_4$-KBH_4 (c) systems. (SS = Temperature of miscibility gap in the solid solution, M = Melting temperature of the solid solution, LIQ = Liquidus temperature, EU = Eutectic melting temperature, PT = Polymorphic Transition temperature, LiK = temperature of decomposition of the bimetallic $LiK(BH_4)_2$ compound, TPPA = Temperature Programmed Photographic Analysis temperature data, DSC = Differential Scanning Calorimetry temperature data, SR-PXD = Synchrotron Radiation Powder X-ray Diffraction temperature data, HT-PXD = High Temperature Powder X-ray Diffraction temperature data, CALPHAD = calculated phase diagram).

In the solid state, three phases are present in this system: orthorhombic, hexagonal, and cubic. In addition, up to 96 °C, also the bimetallic compound $LiK(BH_4)_2$ is present. The Gibbs free energy function for the bimetallic compound has been determined combining the calculated value of the enthalpy of formation from $LiBH_4$ and KBH_4 reported by Kim at al.[183] with the temperature of decomposition reported by Ley et al.[54] This is reported in **Table 7**. Since no solid solutions are observed experimentally, the solid phases were described with a positive interaction parameter to reduce the solubility limit (**Table 6**). In the frame of the regular solution model, a negative value of the interaction parameter has been used for the liquid phase in order to describe the deep eutectic. It has been optimized on the basis of the temperature and enthalpy of melting of the eutectic composition. The calculated pseudo-binary phase diagram is reported in **Figure 40 c**, together with available experimental data. Experimental data of eutectic composition and temperatures reported by Ley et al.[54] are in good agreement with calculations. Liquidus temperatures reported by Ley et al.[54] are reasonably reproduced, whereas those observed by Adams[174] appear significantly different.

Ternary system

A ternary eutectic composition has been reported by Huff et al.,[179] as indicated by a red triangle (T1) in the pseudo-ternary $LiBH_4$-$NaBH_4$-KBH_4 phase diagram shown in **Figure 41**, but it was evidenced as not eutectic by Paskevicius et al.[34] Therefore, the T1 composition was investigated by DSC and *in-situ* SR-PXD. A first heating up-and-down to melting was necessary to homogenise the sample. The DSC traces and SR-PXD patterns during the second cycle of heating and cooling of the mixture are shown in **Figure 42**. During heating, the orthorhombic-to-hexagonal polymorphic transition can be observed at 97 °C (DSC) and 95 °C (SR-PXD). It appears at lower temperature with respect to pure $LiBH_4$[78] because of the presence of $NaBH_4$, and possibly of KBH_4, in the orthorhombic solid solution. An eutectic melting temperature of T_{onset}=103 °C (DSC) and 104 °C (SR-PXD) was observed, whereas the liquidus temperature observed at 155 °C (SR-PXD) was difficult to defined by DSC (**Figure 42**). During cooling, the liquidus temperature was estimated at 148 °C and 146 °C by DSC and SR-PXD, respectively, and other phase transformations were also observed at lower temperatures because of undercooling.

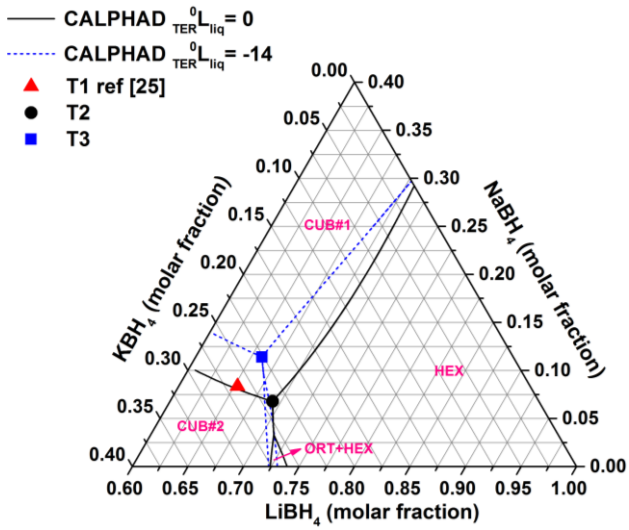

Figure 41 – Calculated minima of the liquidus surface for the $LiBH_4$-$NaBH_4$-KBH_4 system. Solid black lines and circle: simple extrapolation of binary systems; dashed blue lines and square: including a ternary interaction parameter ($_{TER}^{0}L_{liq}$) for the liquid phase equal to -14162 J/mol. Literature datum (triangular red point) is also reported for comparison. (CUB#1 and CUB#2 = cubic, ORT = orthorhombic, and HEX = hexagonal phases).

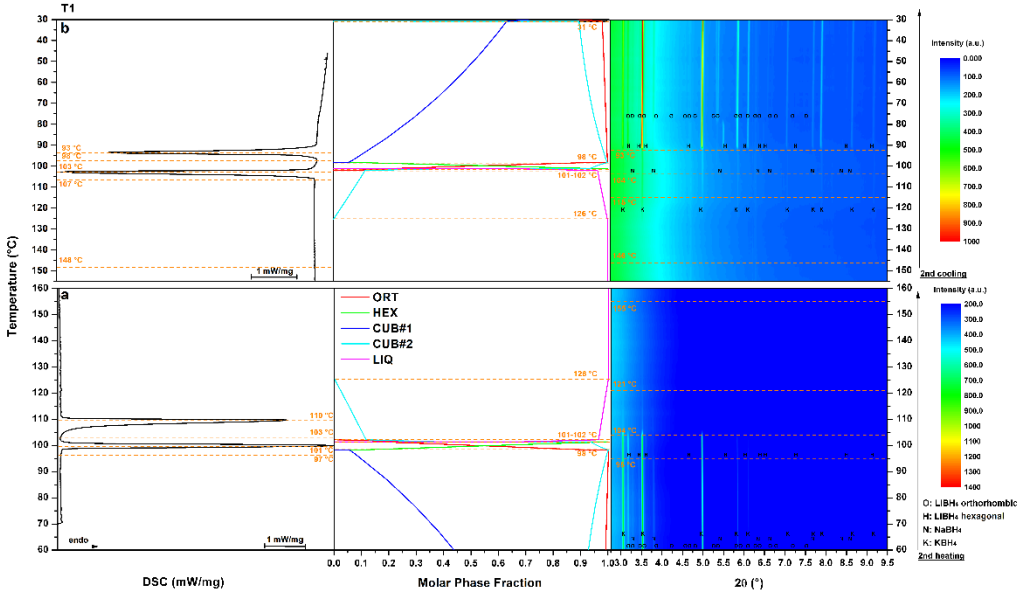

Figure 42 – DSC (left), amount of calculated phases (CALPHAD, middle) and SR-PXD (right) of T1, 0.65$LiBH_4$-0.08$NaBH_4$-0.27KBH_4 (λ = 0.2072 Å, ΔT/Δt = 5 °C/min, argon atmosphere, 2nd cycle of heating (a) and cooling (b)).

Initially, the enthalpy of mixing of the liquid phase for the ternary system was simply interpolated from those of the binary systems by using the Muggianu's rule.[76,184] The assessment of the pseudo-ternary phase diagram allowed the calculation of the minima of the liquidus surface, as shown by black solid lines in **Figure 41**. The ternary composition at the crossing of lines was calculated at $0.68LiBH_4$-$0.08NaBH_4$-$0.24KBH_4$, and it is shown as a black circle (T2) in **Figure 41.** The corresponding calculated melting temperature of 116 °C turned out higher than that of the eutectic in the $LiBH_4$-KBH_4 system, excluding a eutectic reaction. For this reason, the $0.68LiBH_4$-$0.08NaBH_4$-$0.24KBH_4$ composition was investigated by DSC and *in-situ* SR-PXD, and results are reported in **Figure 43**. From the SR-PXD data, it is clearly observed that the sample is not eutectic and that it contains an excess of KBH_4. In fact, on heating, we observed a strong reduction of X-ray intensity at 104 °C representative of melting onset, where most of the $NaBH_4$ transforms into liquid (**Figure 43**).

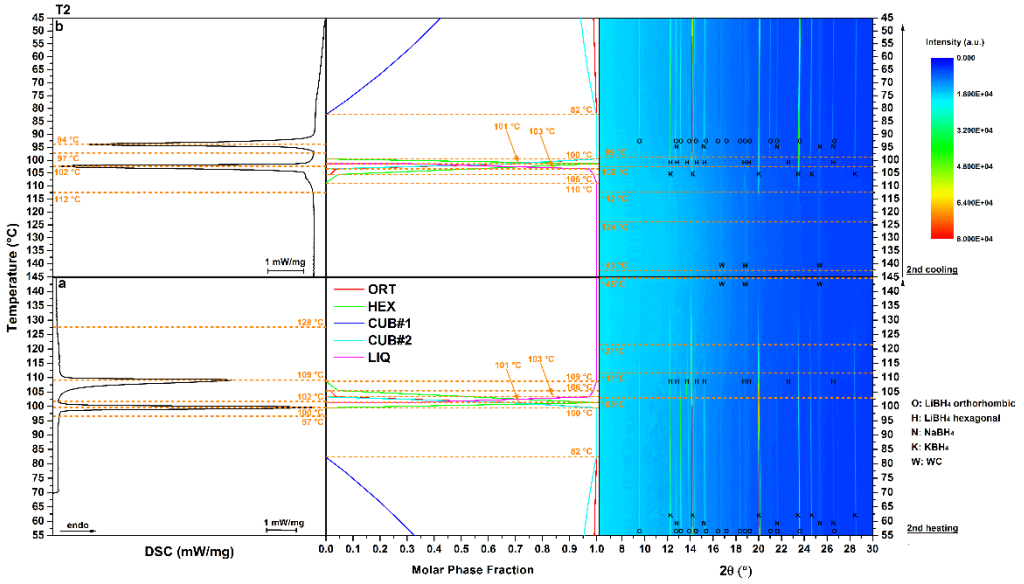

Figure 43 – DSC (left), amount of calculated phases (CALPHAD, middle) and SR-PXD (right) of T2, $0.68LiBH_4$-$0.08NaBH_4$-$0.24KBH_4$ (λ = 0.8259 Å, $\Delta T/\Delta t$ = 5 °C/min, argon atmosphere, 2nd cycle of heating (a) and cooling (b)). Presence of WC due to ball milling.

In a small, higher temperature range, both orthorhombic and hexagonal $LiBH_4$ have been observed, which melted at 121 °C, so that only KBH_4 was left up to 145 °C, corresponding to the liquidus temperature. On cooling, the excess of KBH_4 crystallized at 143 °C, then hexagonal $LiBH_4$ and cubic $NaBH_4$ appeared at

102 °C and a fully solid mixture was observed at 99 °C. The DSC data confirmed the phase transformations observed by SR-PXD, allowing the liquidus temperature to be better observed around 128 °C. The observed phase transformations confirm that the 0.68$LiBH_4$-0.08$NaBH_4$-0.24KBH_4 mixture is not eutectic and suggest that the real ternary composition should contain less $LiBH_4$ and KBH_4.

These results motivated the assessment of the ternary system introducing an interaction parameter for the liquid phase in order to obtain a ternary eutectic temperature of 102 °C. So, a further interaction parameter for the liquid phase was added, according to Redlich-Kister-Muggianu equation:[184]

$$
\begin{aligned}
{}_{TER}G_m^{exc} = {} & x_a x_b \left\{ {}^0L_{ab} + {}^1L_{ab}(x_a - x_b) \right\} + x_a x_c \left\{ {}^0L_{ac} + {}^1L_{ac}(x_a - x_c) \right\} \\
& + x_b x_c \left\{ {}^0L_{bc} + {}^1L_{bc}(x_b - x_c) \right\} + x_a x_b x_c \left\{ {}^0L_{abc} \right. \\
& \left. + {}^1L_{abc}(x_a - x_b) \right\} \quad Eq.\,23
\end{aligned}
$$

where x is the molar fraction, a: $LiBH_4$, b: $NaBH_4$, c: KBH_4, and L = a + bT which is a parameter containing the interaction parameters for binary and ternary systems.

A ternary interaction parameter was added in the description of the liquid phase, and the calculated eutectic temperature and composition were optimized step by step to obtain a eutectic melting at 102 °C.

The ternary interaction parameters necessary to obtain a calculated eutectic melting temperature of 102 °C turned out to be ${}^0L_{abc}$ = -14162 J/mol and ${}^1L_{abc}$ = 0 (**Table 6**). The optimized parameter turned out to be negative, confirming the occurrence of an interaction in the liquid phase for the ternary system, leading to a deep eutectic. The corresponding minima of the liquidus surface are reported in **Figure 41** as blue dashed lines. The new ternary eutectic composition is calculated at 0.66$LiBH_4$-0.11$NaBH_4$-0.23KBH_4 and it is shown as a blue square (T3) in **Figure 41**. The new calculated T3 composition confirms an excess of KBH_4 and $LiBH_4$ in T2 sample, as suggested by the occurrence of an off-eutectic transformation.

The 0.66$LiBH_4$-0.11$NaBH_4$-0.23KBH_4 composition was investigated by DSC and *in-situ* SR-PXD and the results are shown **Figure 44**, where experimental results are compared with the phase fraction calculated from the Calphad assessment.

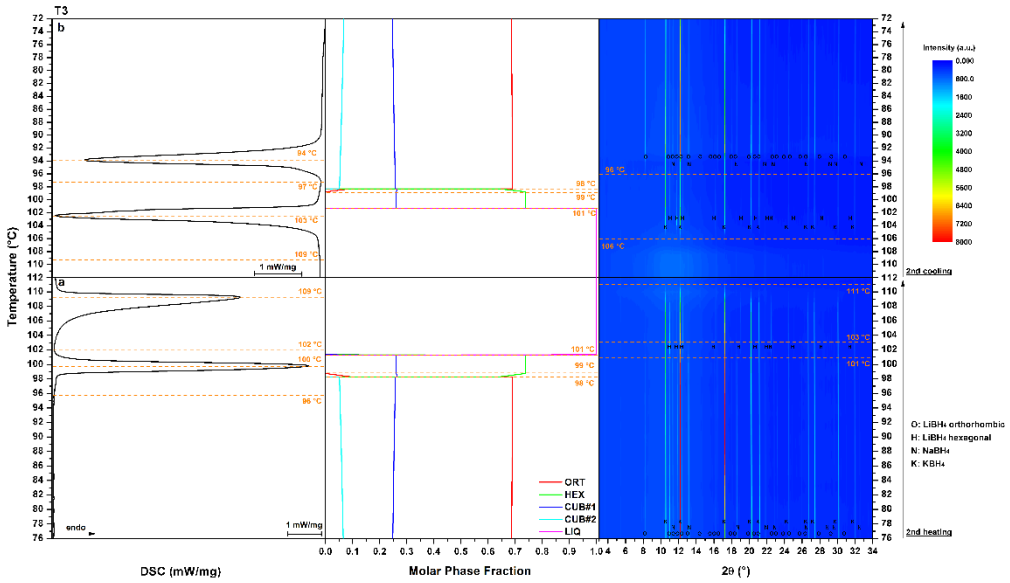

Figure 44 – DSC (left), amount of calculated molar fraction of phases (CALPHAD, middle) and SR-PXD patterns (right) of sample T3, $0.66LiBH_4$-$0.11NaBH_4$-$0.23KBH_4$ (λ = 0.7129 Å, $\Delta T/\Delta t$ = 5 °C/min, argon atmosphere, 2nd cycle of heating (a) and cooling (b)). (ORT = orthorhombic phase, HEX = hexagonal phase, CUB#1 and CUB#2 = cubic phases, LIQ = liquid phase).

In the middle panel of **Figure 44**, the calculated molar fraction of phases is reported as a function of temperature, clearly showing the calculated values for the temperature of phase transformations (e.g. polymorphic transitions, eutectic melting, liquidus). These values are in good agreement with the experimental ones. The $LiBH_4$ polymorphic transition is observed at 101 °C and melting starts at 103 °C. SR-PXD data revealed a liquidus temperature at 111 °C during heating and at 106 °C during cooling, suggesting the occurrence of an almost pure ternary eutectic mixture, as confirmed by DSC data. The enthalpy of melting of the ternary eutectic mixture is equal to 4.2 kJ/mol, in reasonable agreement with the calculated value of 5.7 kJ/mol (**Table 8**).
Calculated molar fraction of phases, generated from the optimized database, have been reported in each investigated sample, and they will be discussed later.

Validation of the assessed pseudo-ternary phase diagram

The pseudo-ternary phase diagram and corresponding thermodynamic properties were assessed in all temperature and composition ranges, allowing the

determination of the $0.66LiBH_4$-$0.11NaBH_4$-$0.23KBH_4$ ternary eutectic composition, which was experimentally confirmed. From the assessed thermodynamic functions, phase diagram sections related to the samples T50Li, T50Na, and T50K have been obtained, and the results are shown in **Figure 45**, where experimental and calculated temperatures of phase transformation are compared as a function of composition.

The calculated temperatures for the orthorhombic-to-hexagonal polymorphic transition (black squares, **Figure 45**) are in good agreement with experiments, as well as for the occurrence of a single cubic solid solution (red circles, **Figure 45**). The calculated liquidus temperatures are not fully matching the experimental ones (blue triangles, **Figure 45**), suggesting possible kinetic constraints during SR-PXD measurements. Phase fractions have been calculated as a function of temperature for T50Li, T50Na, and T50K compositions, and they are in good agreement with experimental SX-XRD results, as shown in **Figures 36, 37** and **38**, respectively. It is worth noting that the temperature for the formation of a single-phase cubic solid solution is calculated at 140 °C, 146 °C and 176 °C for T50Li, T50Na, and T50K compositions, respectively. These values are slightly different from the experimental ones, suggesting possible improvements of the thermodynamic description of the cubic solid solution in the ternary system by the introduction of an interaction parameter. Because of the lacking of experimental data, no further parameters have been considered for this phase.

Furthermore, to validate the thermodynamic assessment of the system, the database was used to calculate various isopleths, i.e. sections of the pseudo-ternary phase diagram at a constant molar fraction of $NaBH_4$ equal to 0.05 (**s1-s8**, see **Table 5** for composition), and new experiments were carried out to confirm the calculations.

The results are presented in **Figure 46**, together with the first heating and cooling DSC traces of the different mixtures prepared by manual mixing, which promotes the intimate interaction of the parent compounds. It is expected that the results from the manual mixed samples s1-s8 are not different from the ones of ball-milled samples. The calculated isopleths reveal that many phase transformations are taking place in the temperature range from 90 °C to 120 °C. The onset temperature of the peak recorded on the first heating is observed at 102 °C for all compositions, in good agreement with the calculated eutectic temperature. The DSC peak is broader for $LiBH_4$-rich samples, suggesting that, apart from melting, other reactions are taking place.

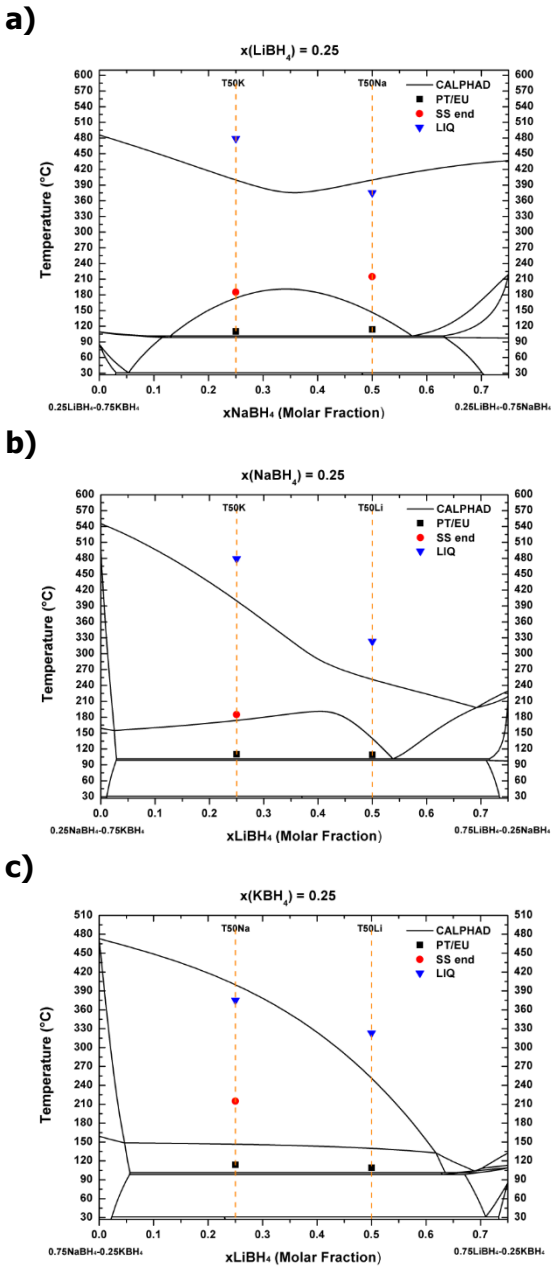

Figure 45 – Comparison between experimental data of mixtures T50Li, T50Na, T50K and calculated pseudo-binary phase diagrams (CALPHAD), section at constant composition of one component. (PT = Polymorphic Transition, EU = Eutectic melting, SS end = upper critical solution temperature, end of the miscibility gap and starting of single phase solid solution region, LIQ = Liquid phase).

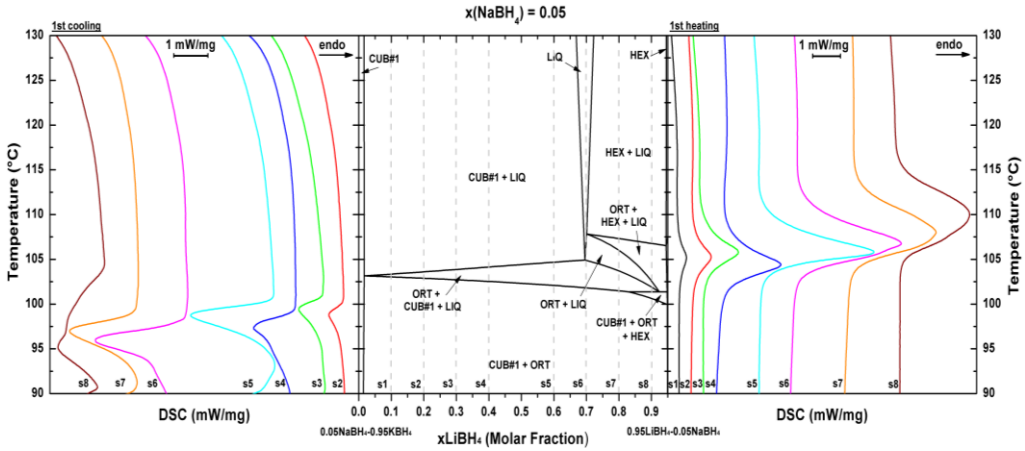

Figure 46 – Comparison between calculated isopleths for the $LiBH_4$-$NaBH_4$-KBH_4 system at constant composition ($xNaBH_4$ = 0.05) (CALPHAD, middle) and experimental data of mixtures s1-s8. DSC traces during 1st heating (right) and cooling (left), $\Delta T/\Delta t$ = 5 °C/min, 40 ml/min argon flow.

The calculations show that the orthorhombic-to-hexagonal polymorphic transition is observed, on heating, rather close to beginning of melting.
The area of the DSC peaks is related to the amount of heat required for the phase transformation, and it is proportional to the fraction of eutectic composition that is melting in the sample. Sample s5 presents the biggest peak because the entire sample is melting on heating, while in other samples only a fraction of the mixture is melting crossing the eutectic line. A slight undercooling of the liquid phase is observed on DSC traces measured on cooling.

To compare previous experimental results, calculation on all the other samples were made using the final optimized database and are reported together with previous experimental results already shown.
In T50Li (**Figure 36**), polymorphic transition of $LiBH_4$ is observed at 109 °C (calculated temperature 98 °C), followed by eutectic melting at 112 °C (calculated temperature 101 °C). At 140 °C the calculations reveals the complete melting of the cubic phase two (KBH_4) that is no more visible in the *in-situ* data after the eutectic melting. Experimental temperatures are higher with respect to calculated one probably because of kinetic reasons. Liquidus temperature is recorded at 323 °C (calculated temperature 251 °C).
In T50Na (**Figure 37**), at 98 °C and 101 °C calculated temperature, polymorphic transition of $LiBH_4$ and eutectic melting are taking place respectively, but they are not clearly revealed by the *in-situ* investigation.

At 185 °C (174 °C calculated temperature), the cubic phase two (KBH_4) disappear because of the formation of a single-phase cubic solution. In the experiment, the solid solution between $NaBH_4$ and KBH_4 starts to form at 114 °C and one phase solid solution is observed at 215 °C. Liquidus temperature is recorded at 375 °C (calculated temperature 400 °C).
As reported before, also in T50K (**Figure 38**), at 98 °C and 101 °C calculated temperature, polymorphic transition of $LiBH_4$ and eutectic melting are taking place respectively, from *in-situ* investigation the eutectic melting can be observed at 110 °C. At 185 °C (174 °C calculated temperature), the cubic phase two (KBH_4) disappear because of the formation of a single-phase cubic solution. Liquidus temperature is recorded at 352 °C (calculated temperature 400 °C).
Concerning the calculations on sample T1 (**Figure 42**), the polymorphic transition of $LiBH_4$ and eutectic melting reaction are calculated to occur at 98 °C and 101 °C. From *in-situ* investigation, the transitions can be observed at 95 °C and 104 °C respectively, in good agreement also with DSC measurement (start of DSC peak at 97 °C and 103 °C, on heating, respectively). At 121 °C $NaBH_4$ disappears (melting), and the liquidus temperature is recorded at 155 °C (calculated temperature 125 °C) but it cannot be clearly reveal by DSC measurements, only a noisy baseline is recorded after the eutectic melting. On cooling, the same transitions can be observed under undercooled conditions.
In T2 (**Figure 43**), at 82 °C calculated temperature, a single cubic solid solution phase is formed, but it is not revealed by *in-situ* investigation. At 100 °C and 101 °C calculated temperature, polymorphic transition of $LiBH_4$ and eutectic melting are taking place respectively, while from *in-situ* investigation from 103 °C to 111 °C both orthorhombic and hexagonal $LiBH_4$ are present and then melt. Calculations predict that the cubic phase is the first to melt (103 °C), followed by the orthorhombic (106 °C) and hexagonal phase (109 °C). Experimentally orthorhombic and hexagonal phase are completely melted at 111 °C, followed by the melting of $NaBH_4$ (121 °C) and KBH_4 (145 °C, liquidus temperature, 109 °C calculated liquidus temperature. On cooling, the same transitions can be observed under undercooled conditions.

Conclusions

The thermodynamics of $LiBH_4$-$NaBH_4$-KBH_4 ternary system was fully described combining experimental and theoretical investigations. The Calphad method, together with *ab-initio* calculations to determine the end-members, was used to

assess the $LiBH_4$-$NaBH_4$, $LiBH_4$-KBH_4, and $NaBH_4$-KBH_4 pseudo-binary phase diagrams. A screening of the ternary system allowed an investigation in all temperature and composition ranges in order to understand which phases could be formed as well as their limit of solubility.

The assessed binary systems are in good agreement with experimental data and the ternary system has been assessed and validated based on new experiments. A reconsideration of the thermodynamic description of the liquid phase of pure $NaBH_4$, together with the reassessment of the $LiBH_4$-$NaBH_4$ system, has been necessary, confirming the importance to obtain reliable data for the enthalpy of melting of pure compounds, in order to describe binary or ternary mixtures. In the case of KBH_4, the enthalpy of mixing was not known, but it has been obtained by a combined assessment of different binary systems ($LiBH_4$-KBH_4, and $NaBH_4$-KBH_4), and a melting enthalpy of 19.2 kJ/mol has been estimated for the first time. Negative enthalpies of mixing or low positive value have been obtained for the liquid phase, suggesting attractive interactions among ions in the molten state. On the other hand, positive or close-to-zero enthalpy of mixing have been calculated for the solid solutions, suggesting a combined role of electronic and size effects in the solubility among borohydrides.

In conclusion, it has been demonstrated that a combined use of *ab-initio* and Calphad thermodynamic calculations, supported and confirmed by experimental measurements, is a powerful tool for a complete description of thermodynamic properties of mixtures of borohydrides. An estimation of the decomposition reactions in the investigated system can be obtained with the current optimised database. However, it should be coupled with experimental evaluation of decomposition products.

Chapter 5 – Cationic substitution in the $LiBH_4$-$NaBH_4$-KBH_4-$Mg(BH_4)_2$-$Ca(BH_4)_2$ system

In the present chapter, the approach is to design combinations of borohydrides with multiple cations in equimolar ratio following the concept of high entropy alloys[185,186] or exploring interesting new systems and compositions to collect useful thermodynamic information to define phase diagrams.
In High Entropy Alloys (HEAs) at least five elements should be present in concentrations between 5 and 35 atomic percent, so that the high entropy of mixing can stabilise the formation of solid solutions with simple crystal structures. However, if the formation enthalpy of an intermetallic compound is high enough to overcome the effect of entropy, that intermetallic compound will be present in the equilibrium mixture.
As an overview, **Figure 47** shows a pentagram in which all possible combination in the LiNaKMgCa system can be observed and are reported as a list divided in column as binary, ternary and quaternary combinations. In the picture, segment are referred to binary systems, triangles visualise ternary combinations and trapezoidal shape are quaternary systems.
Pure compounds and some bimetallic or trimetallic compounds have been extensively studied in the literature,[25] so they will not be discussed here, nevertheless they will be compared when useful for the understanding of the systems' properties.

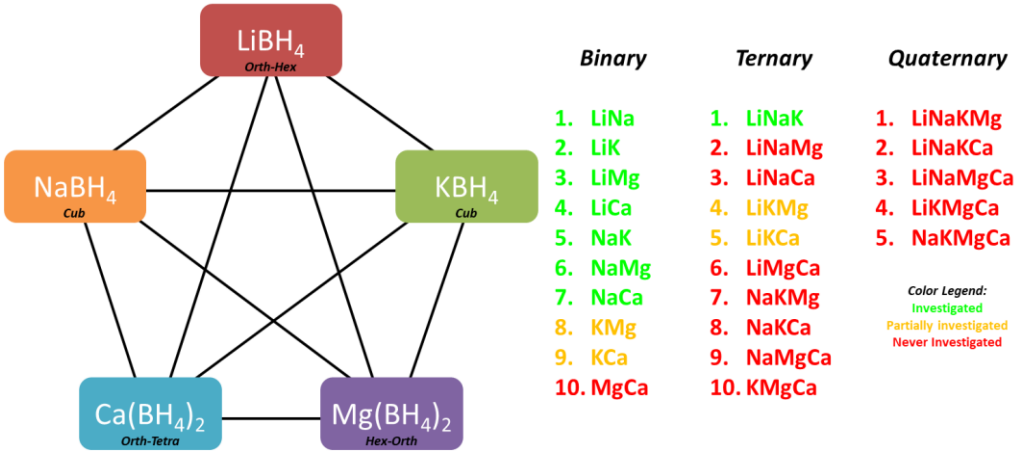

Figure 47 – Graphical representation and list of all possible binary, ternary and quaternary combination in the $LiBH_4$-$NaBH_4$-KBH_4-$Mg(BH_4)_2$-$Ca(BH_4)_2$ system (LiNaKMgCa).

The possible binary combinations in the system are ten, and have been widely experimentally investigated, apart from the KMg, KCa, MgCa system. Details on experimental studies reported in the literature are summarized ahead in the literature survey chapter and in **Table 10**. In this study we will explore as a function of composition and temperature, the MgCa system, and we will investigate in details the thermodynamics of the $KCa(BH_4)_3$ bimetallic compound. Among ternary systems, which possible combination are ten and are listed in **Figure 47**, only the LiNaK system have been characterized in details and assessed as described in **Chapter 4**. Few details are reported on the LiKMg and LiNaCa system in the literature and will be described ahead.
Quaternary combinations in the system are five and have not been explored yet.

Introduction

HEAs and relative concepts were born within the metallurgy community. In 2004 Cantor[185] and Yeh[187] suggested to discover new properties and alloys exploring the central region of the phase space in systems with at least five components. This leaded to the findings of microstructures mainly composed of *fcc* or *bcc* multicomponent solid solutions.[188,189] Since 2004, many HEAs have been explored, finding in some cases very interesting properties for compositions containing high entropy phases. In particular, mechanical behaviour of HEAs has been investigated.[190,191] An operative way to define a high entropy phase is to start from the calculation of the configurational entropy, ΔS_{conf}, of a completely disordered solid solution with the Boltzman formula,

$$\Delta S_{conf} = -R \cdot \sum^{i} x_i \ln x_i \qquad \boldsymbol{Eq}.24$$

being x_i the atomic fraction of the *i-th* elements. Commonly, the disordered solid solutions with $\Delta S_{conf} > 1.5$ R, where R is the gas constant, are defined high entropy phases.[192] Complex Concentrated Alloys (CCAs) are alloys showing a nominal composition with a configurational entropy of a hypothetical completely random state, i.e. $\Delta S_{conf} > 1.5$ R, but composed of more complex microstructures, i.e. constituted by different phases and intermetallics, but representative of the inner part of multicomponent phase space.[193]

In the case of equimolar compositions, the value of ΔS_{conf} can be obtained, for a system with a defined number of components N, as:

$$\Delta S_{conf} = R \ln N \quad \textbf{Eq.}\ 25$$

The higher the number of components N, the higher the value reachable by ΔS_{conf} in the system, i.e. for N = 5, ΔS^{max}_{conf} = 1.61 R, for N = 6, ΔS^{max}_{conf} = 1.79 R and for N= 7, ΔS^{max}_{conf} = 1.95 R.

Ordering in high entropy phases have been experimentally found in the exploration of CCAs.[194–196] Ordering decreases the entropy of the phase, since, following the Compound Energy Formalism (CEF),[197] the configurational entropy ΔS_{conf} should be decomposed into the contributes of the respective sub-lattices. Considering, for example, a system containing two different sub-lattice *h*, with a number of sites X, and *k,* with a number of sites Y, the configurational entropy of the ordered structure can be defined as:

$$\Delta S_{conf}^{ORD} = -R \cdot \left(\frac{X}{X+Y} \cdot \sum^{i} y_i^h \ln y_i^h + \frac{Y}{X+Y} \cdot \sum^{i} y_i^k \ln y_i^k \right) \quad \textbf{Eq.}\ 26$$

where y_i^h and y_i^k are the mole fractions of the constituent *i* in the sublattice *h* and *k*, respectively.[194] For instance, in a AB compound with atoms A and B in two different sub-lattices *h* and *k* with X and Y equal to 1, the respective disordering of each sublattices (considering random mixing within each sub-lattice) obtained replacing half atoms of A with C in sub-lattice *h* and half atoms of B with D in sub-lattice *k*, leading to an (ACBD) solid solution, increases the configurational entropy of 0.69 R, a value comparable to the configurational entropy of a equimolar binary system completely disordered. Such a situation can be observed in ionic compounds, which are characterized mainly by two sub-lattices, a cationic and an anionic one.

Literature survey

Recently, the formation of entropy stabilized mixtures of oxides[198] and borides[199] was reported, together with the description of a entropy driven polymorphic transition as a function of the composition of the solid solution. In ionic compounds, a structure containing one sub-lattice with random cation occupancy can be obtained at a sufficient high temperature if it does not melt before such

a transition. In the case of oxides, electroneutrality and geometrical parameters must be taken into account to succeed in the formation of a solid solution.

Table 10 – Borohydrides structures and details on pure compounds, binary mixtures, bimetallics, solid solutions (SS), enthalpy [kJ/mol] and temperature [°C] of polymorphic transition (PT), eutectic melting (EU), thermal minima (TM), and decomposition (DEC).

	$LiBH_4$	**$NaBH_4$**	**KBH_4**	**$Mg(BH_4)_2$**	**$Ca(BH_4)_2$**
$LiBH_4$	Orthorhombic (*Pnma*) Hexagonal ($P6_3mc$) $T_{PT\ ORT-HEX}$ = 115 ΔH_{PT} = 5.3 T_M = 280 ΔH_M = 7.2[78] T_{DEC}>400[200]	0.70$LiBH_4$-0.30$NaBH_4$ $T_{PT\ ORT-HEX}$ = 95 T_{EU} = 216 ΔH_M = 7.0[124] T_{DEC}>400[201] SS cubic, orthorhombic, hexagonal[124]	0.725$LiBH_4$-0.275KBH_4 T_{EU} = 104 ΔH_M = 11.0[54] T_{DEC}>400[49] $LiK(BH_4)_2$: Orthorhombic (*Pnma*)[54]	0.55$LiBH_4$-0.45$Mg(BH_4)_2$ T_{EU} = 180[202] T_{DEC}>250[44,202,203]	0.68$LiBH_4$-0.32$Ca(BH_4)_2$ T_{EU} = 200[173] ΔH_M = 9.1[42] T_{DEC}>350[173]
$NaBH_4$		Cubic ($Fm\bar{3}m$) T_M = 505 ΔH_M = 16.9[181] T_{DEC}>505[181]	0.682$NaBH_4$-0.328KBH_4 T_{TM} = 462 ΔH_{TM} = 17.0[172] SS cubic[172] T_{DEC}>465[172]	0.40$NaBH_4$-0.60$Mg(BH_4)_2$ T_{EU} = 205 ΔH_M = 7.0[36] T_{DEC}>205[36]	Partial Melting[36] T_{DEC}>350[36]
KBH_4			Cubic ($Fm\bar{3}m$) T_M = 605 ΔH_M = 19.2[204] T_{DEC}>605[182]	$K_2Mg(BH_4)_4$: Monoclinic ($P2_1/n$)[205] $K_3Mg(BH_4)_5$: Tetragonal ($P4_2/mbc$)[205]	$KCa(BH_4)_3$: Orthorhombic (*Pba*2)[206]
$Mg(BH_4)_2$				α : Hexagonal ($P6_122$) β : Orthorhombic (*Fddd*) γ : Cubic ($Ia\bar{3}d$) metast. $T_{PT\ \alpha-\beta}$ = 184[79] ΔH_{PT} = 11.3[79] T_{DEC}>290[182]	
$Ca(BH_4)_2$					α: Orthorhombic (*F*2*dd*) β: Tetragonal ($P\bar{4}$) $T_{PT\ \alpha-\beta}$ = 162[152] ΔH_{PT} = 8.6[152] T_{DEC}>300[207]

Generally, cations chosen for the equimolar mixture should come from compounds with the same crystal structures, should have similar ionic radii and

coordination number. In addition, they should be isovalent among them and with the counter anion. The formation of a multi cation solid solution can be correlated with the Goldschmidt tolerance factor (t), which should be close to 1.[208] The cation-size difference (δ_R) or average size difference using the lattice constant of individual component (δ_a and δ_c) should also be considered as important factor for the formation of one-phase solid solution if the compounds have mixed ionic and covalent characteristics. In the case of borides, δ_a and δ_c should be in the range of 4-12%. In addition, enthalpy of mixing, entropy of mixing and melting temperature play a role as for HEAs, but they usually are thermodynamic parameters unknown for all phases and of difficult experimental determination.
Unlike alloys, oxides and diborides, the most common and studied borohydrides presents different crystal structures, polymorphs, and many bi- or trimetallic compounds are present in binary or higher mixtures, as reported in **Table 10**.
Their crystal structures are characterized by the presence of cations surrounded by the complex BH_4^- anion. The presence of multiple cations is expected to promote the formation of solid solutions as observed for oxide systems or multi-cations eutectics. On the other hand, when the formation enthalpy of a multi-metallic compounds is high enough to overcome the entropy contribution to the free energy of solid solutions, their formation will be hindered.
The occurrence of solid solutions, multi cation eutectics and multi-metallic compounds leads to differences in the hydrogen desorption reactions, depending on the interaction among the components however only few ternary system have been explored in the literature, while no quaternary nor quinary mixture have never been investigated.

Binary systems

Table 10 reviews details about pure borohydrides and their interaction in binary systems. As it can be observed, regarding the liquid phase, most of the binary system show eutectic or thermal minima. In the solid state, solid solutions or bimetallic compound are formed.
In **Chapter 4**, the $LiBH_4$-$NaBH_4$, $LiBH_4$-KBH_4 and $NaBH_4$-KBH_4 system were critically reviewed and assessed. Nevertheless, other binary systems need to be assessed as well. The $Mg(BH_4)_2$-$Ca(BH_4)_2$ system have never been systematically studied in all temperature and composition range, while most of the other binary systems were characterized. When a bimetallic compounds is involved not many details about its enthalpy of formation, of polymorphic transition or melting, together with decomposition mechanism are reported, neither the study of an

extended composition range in the binary system have been explored, as in the case of the KMg and KCa systems. These thermodynamic values and investigations are necessary for a further assessment and full description of the system by the Calphad method.

$Mg(BH_4)_2$-$Ca(BH_4)_2$ system

Magnesium borohydride, $Mg(BH_4)_2$, and calcium borohydride, $Ca(BH_4)_2$, have a gravimetric hydrogen content of 14.9%, or 11.6% respectively, therefore they are very promising materials for the storage of hydrogen. However, little is known about their thermodynamic properties and their decomposition mechanisms.
Theoretical calculations predict decomposition reactions at not too high temperatures,[209] but the kinetics of such reactions can be very slow, thus hindering their practical use. In this scenario, it became essential an in-depth understanding of their decomposition reactions mechanisms, which include phase transitions, intermediate species and gaseous species.[143]
Concerning pure metal boronhydrides, hydrogen release decomposition reactions are very complex and characterized by different steps, which occur at high temperatures and they are reversible only at high pressures and temperatures. Often the decomposition reactions also involve the development of diborane gas (B_2H_6) which, due to its toxicity, hinders the practical use of such materials.[143,210]
$Mg(BH_4)_2$ and $Ca(BH_4)_2$ decompose at a temperature above 290 °C and 300 °C, respectively.[144]
Several different mechanisms have been proposed in the literature to explain their decomposition, including the following reactions:[137,211,212]

1. $Mg(BH_4)_2 \rightarrow MgB_2 + 4H_2$
2. $Mg(BH_4)_2 \rightarrow Mg + 2B + 4H_2$
3. $Mg(BH_4)_2 \rightarrow MgH_2 + 2B + 3H_2$
4. $Ca(BH_4)_2 \rightarrow \frac{1}{3}CaB_6 + \frac{2}{3}CaH_2 + \frac{10}{3}H_2$
5. $Ca(BH_4)_2 \rightarrow CaH_2 + 2B + 3H_2$
6. $Ca(BH_4)_2 \rightarrow Ca + 2B + 4H_2$

Experimentally it has been shown that decomposition can occur according to multiple mechanisms and in several steps, which can involve simultaneous reactions and different intermediates.[213]

Mechanisms and decomposition products depend on experimental conditions; several intermediates have been observed, including those containing the anions $B_3H_8^-$, $B_{10}H_{10}^{2-}$ and $B_{12}H_12^{2-}$,[142,212,214–219] which, probably, hindered the reversibility of the reaction.

The decomposition of $MgB_{12}H_{12}$ and $CaB_{12}H_{12}$, synthesized from $Mg(BH_4)_2$ and $B_{10}H_{14}$, and $Ca(BH_4)_2$ and $B_{10}H_{14}$, were studied by He et al..[220] In fact, these borohydride react at 400 ° C under helium flow, releasing hydrogen and forming $MB_{12}H_{12-x}$ (M = Mg, Ca) with icosahedral skeletons B_{12}, which later polymerize producing $(MB_yH_z)_n$. Finally, at 800 ° C, the formation of amorphous boron was also observed. This reaction does not show clear correlations with the decomposition of $Mg(BH_4)_2$ and $Ca(BH_4)_2$, for which the formation of further intermediates could probably be responsible for a different mechanism.[220]

$MB_{12}H_{12}$ species are difficult to be identified with clarity; *ab-initio* calculations have shown that these species can be amorphous,[209,211] as confirmed by XRD.[142,212,215,216] However, the formation of multiple isoenergetic crystalline phases is also probable, which hindered their exact recognition.[211,212]

The role of different additives on the decomposition reactions of $Mg(BH_4)_2$ and $Ca(BH_4)_2$ has also been investigated. Rueda et al.,[221] showed that silica airgel is able to lower the decomposition temperature of $Mg(BH_4)_2$ by 60 °C with partial reversibily at 390 °C under 110 bar of H_2. According to Kim et al.,[222] $Ca(BH_4)_2$ is reversible at 350 °C and 90 bar of H_2 using NbF_5 as a catalyst. Though, the exact role of these additives has not been fully understood yet.

Mixtures of different borohydrides are the subject of numerous researches as can be observed in **Table 10**, however the $Mg(BH_4)_2$-$Ca(BH_4)_2$ system (MgCa system) was the only one left behind in the characterization of binary systems.

Mixtures of borohydrides may have better thermodynamic properties than those of the individual constituents as regards the release of hydrogen: the formation of solid solutions can lead to the stabilization of certain phases present in the system, to lower decomposition temperatures and to reversible reaction mechanisms.[55,223]

For this reason the MgCa system (**Figure 48**) was experimentally investigated, analysing both the two pure compounds and three different mixtures (Mg:Ca - 1:2 , 1:1, 2:1) by means of DSC, in order to study its thermal behaviour, XRD, to determine the present phases, and ATR-IR. In fact, in the literature nothing is reported on the state diagram of this system, which however appears particularly promising for the storage of hydrogen.

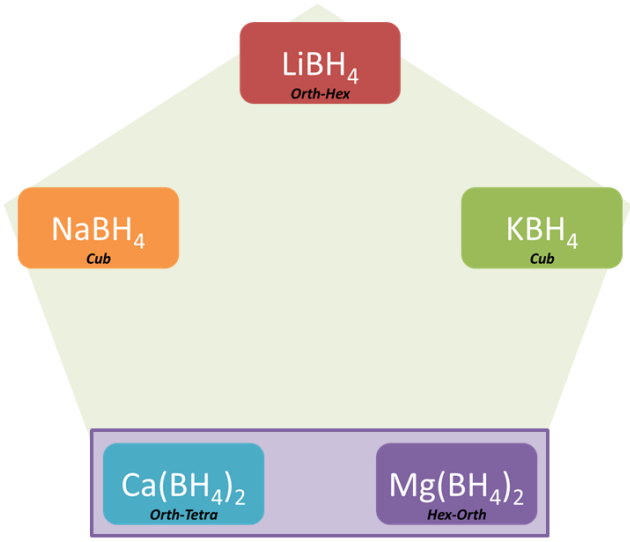

Figure 48 – Schematic representation of the binary $Mg(BH_4)_2$-$Ca(BH_4)_2$ system.

According to the Density Functional Theory (DFT) calculations of Ozolins et al.,[209] mixtures of $Mg(BH_4)_2$ and $Ca(BH_4)_2$ have better thermodynamic properties than those of the individual components. For the 5:1 $Mg(BH_4)_2$:$Ca(BH_4)_2$ mixture the release of 7.73%$_{wt}$ of hydrogen is expected at -18 °C and 1 bar with an enthalpy of about 25 kJ/mol H_2, according to the following reaction:

$$5Mg(BH_4)_2 + Ca(BH_4)_2 \rightarrow CaB_{12}H_{12} + 5MgH_2 + 13H_2$$

Besides, the experiments of Ibikunle et al.,[223,224] showed that the 5:1 mixture, after BM, releases hydrogen at a lower temperature[38] and with a fast kinetic[37] compared to the pure borohydrides. These studies showed that the 5:1 mixture begins to decompose at a temperature of 150 °C, but the system is only partially reversible, probably due to the formation of intermediates containing the $B_{12}H_{12}^{2-}$ anion, that probably causes a kinetic barrier for rehydrogenation.[38] The presence of Ca^{2+} in the mixture seems to have a beneficial effect on the mobility of the species that diffuse in the $Mg(BH_4)_2$ leading to an improvement of kinetic.

Synthesis, Structural and Thermal characterization

Pure and mixtures of $Mg(BH_4)_2$ and $Ca(BH_4)_2$ in a molar ratio 2:1, 1:1 and 1:2 were ball milled for 30 minutes at 500 rpm.

From the diffraction patterns shown in **Figure 49** it is possible to notice that only the α phase of $Mg(BH_4)_2$ is present after ball-milling, while both α and β polymorphs of $Ca(BH_4)_2$ are clearly visible. In the XRD pattern of the mixtures the three phases are present, underling their immiscibility after mechanical-chemical treatment.

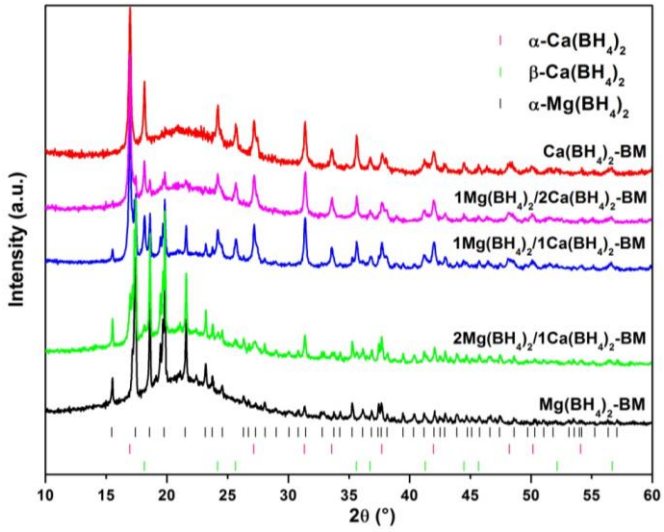

Figure 49 – PXD pattern of pure $Mg(BH_4)_2$, $Ca(BH_4)_2$ and their mixtures (2:1, 1:1, 1:2 molar ratio) after ball milling.

In the ATR spectra reported in **Figure 50**, bands in the 2500-2000 cm^{-1} range are related to the stretching of the B-H bond, while between 1500-100 cm^{-1}, they are referred to the H-B-H bending of the BH_4^- anion.[100,102,144] For $Ca(BH_4)_2$ is evident a splitting of the bands for the presence of both polymorphs α and β.[100] The band (d) at 2319 cm^{-1} is associated with α-$Ca(BH_4)_2$, while the (a) at 2253 cm^{-1} is related to β-$Ca(BH_4)_2$.[225] The spectra of the mixture 2:1, 1:1, 1:2 appear to be very similar to the one of pure compounds which suggest and confirm that all mixtures contain α-$Ca(BH_4)_2$ and β-$Ca(BH_4)_2$, as evident from the diffraction patterns (**Figure 49**). However, for the mixture 2:1 the separation of the two bands at about 2300 cm^{-1} (**Figure 50**) is less clear, while they are quite separate in the 1:1 and 1:2 mixture. Furthermore the band (a) are slightly shifted to larger wave numbers, thus overlapping to (b), at 2272 cm^{-1}. In addition, for 2:1 and 1:2, (c) is clearly observed at 1254 cm^{-1}. Therefore, it can be concluded that the spectroscopic analysis confirms the immiscibility of α-$Mg(BH_4)_2$, α-$Ca(BH_4)_2$ and

β-$Ca(BH_4)_2$, since the observed signals are the combination of those of the separated phases.

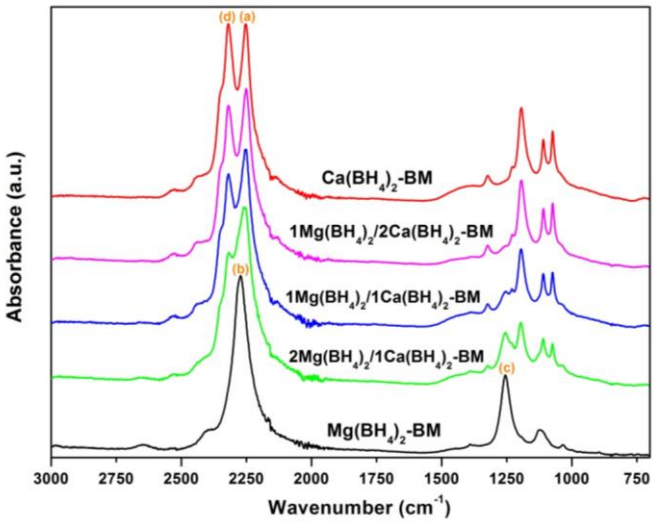

Figure 50 – ATR-IR spectra of pure $Mg(BH_4)_2$, $Ca(BH_4)_2$ and their mixtures (2:1, 1:1, 1:2 molar ratio) after ball milling.

The mechano-chemical treatment was followed by a thermal treatment realised in the DSC. Three cycles of heating and cooling from room temperature to 215 °C at 5 °C/min with a hydrogen pressure of 2 bar were performed.

The α to β phase transitions of $Mg(BH_4)_2$ and $Ca(BH_4)_2$ are not reversible, in fact no reversible signals were recorded in DSC during cooling (not shown). In the diffraction pattern after heat treatment (**Figure 51**) only the peaks of β-$Mg(BH_4)_2$, metastable at room temperature, are distinguished. The $Mg(BH_4)_2$ α-β transition temperature is recorded at T_{peak}=191 °C (T_{onset}=181 °C), as it can be observed in **Figure 52**.

In the DSC trace of $Ca(BH_4)_2$, on the other hand, there is a large peak around 168 °C (T_{onset}=157 °C), corresponding to its partial and partially irreversible α-β transformation. In fact, after the cycling, at room temperature, these two phases are present, as shown in **Figure 51**, similarly to the post-ball-milling pattern. It should be noted, however, that the ratio between the intensities of the peaks around 17° and 18° of the β-$Ca(BH_4)_2$ and the α-$Ca(BH_4)_2$ $\left(\frac{I_{\beta\,Ca}}{I_{\alpha}Ca}\right)$ increases considerably, as it is clearly observed comparing the pattern in **Figure 49** and **Figure 50**.

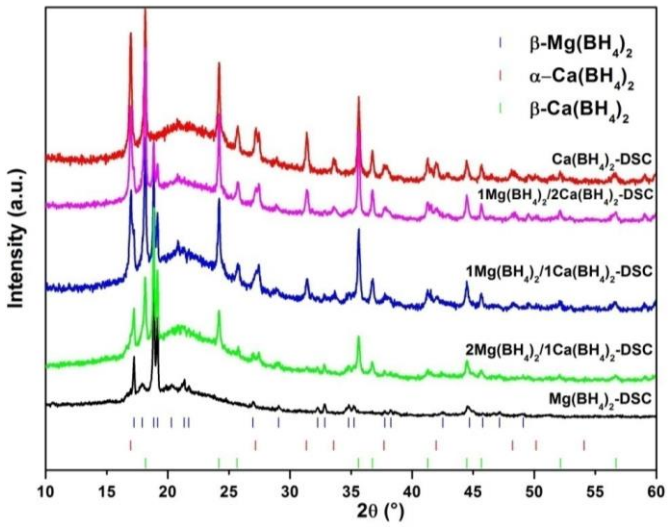

Figure 51 – Room temperature PXD pattern of pure $Mg(BH_4)_2$, $Ca(BH_4)_2$ and their mixtures (2:1, 1:1, 1:2 molar ratio) after DSC cycling up to 215 °C.

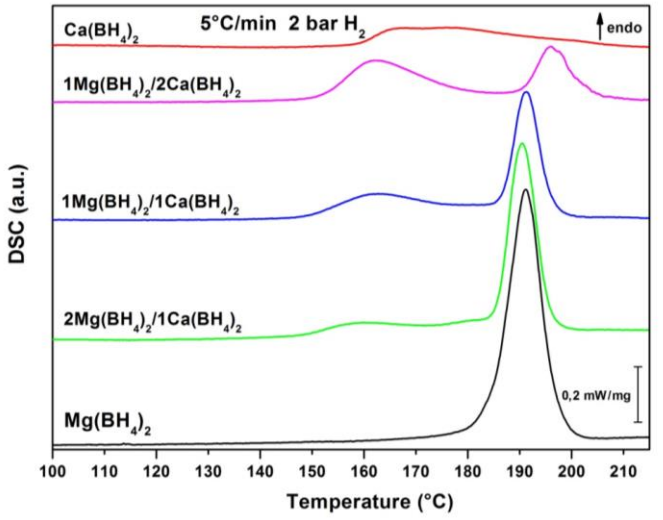

Figure 52 – DSC analysis up to 215 °C at 5 °C/min, under 2 bar of H_2, of pure $Mg(BH_4)_2$, $Ca(BH_4)_2$ and their mixtures (2:1, 1:1, 1:2 molar ratio). Only the first heating ramp is reported.

In the DSC traces of the mixture (**Figure 52**) always two peaks are observed, where at lower temperature the broad peak refers to the α-β transition of $Ca(BH_4)_2$, while the second more intense and narrow peak is referred to the α-β polymorphic transition of $Mg(BH_4)_2$ as described before. In the PXD pattern

(**Figure 51**) β-$Mg(BH_4)_2$, α-$Ca(BH_4)_2$ and β-$Ca(BH_4)_2$ are observed, with an increase of the $\frac{I_{\beta\ Ca}}{I_{\alpha\ Ca}}$ intensity ratio, after DSC cycling, as for the pure $Ca(BH_4)_2$.

The presence of both the Mg^{2+} and Ca^{2+} cations could influence the mechanism of the individual phase transitions. When $Mg(BH_4)_2$ is present, the α-β transition of $Ca(BH_4)_2$ occurs at a slightly lower temperature (**Table 11**) and in a narrower interval, as it can be observed in **Figure 52**. The α-β transformation of $Mg(BH_4)_2$, on the other hand, does not evidence any particular changes. The peak temperature is slightly higher only for the 1:2 mixture (**Figure 52** and **Table 11**). In conclusion, the signals of the mixtures do not changed significantly and no solid solutions should be formed.

Table 11 – Onset and peak temperatures of α-β polymorphic transition, decomposition and rehydrogenation of pure $Mg(BH_4)_2$, $Ca(BH_4)_2$ and their mixtures (2:1, 1:1, 1:2 molar ratio), obtained in the DSC analysis reported in **Figure X** and **X**.

	T_{onset} (°C) $Ca(BH_4)_2$ α-β PT	T_{peak} (°C) $Ca(BH_4)_2$ α-β PT	T_{onset} (°C) $Mg(BH_4)_2$ α-β PT	T_{peak} (°C) $Mg(BH_4)_2$ α-β PT	T_{peak} (°C) Dec.	T_{onset} (°C); T_{peak} (°C) Re-H_2
$Mg(BH_4)_2$			181	191	299, 340, 355,386	278; 254
2:1	149	160		191	272, 326, 346, 398	288; 273
1:1	149	163		191	282, 390	
1:2	149	162		196	280, 387	
$Ca(BH_4)_2$	157	168			355, 376	

The cell parameters and volumes per formula unit (V/z) of α-,β-$Mg(BH_4)_2$ (**Table 12**) and α-,β-$Ca(BH_4)_2$ (**Table 13**), for all samples after BM and DSC cycling were obtained by Rietveld refinement. Cell volumes per formula unit remain substantially unchanged, thus underlining the immiscibility of $Mg(BH_4)_2$ and $Ca(BH_4)_2$.

The hindered formation of solid solutions can be justified on the basis of the structural diversity of α,β-$Mg(BH_4)_2$[141] and α,β-$Ca(BH_4)_2$,[226] differences in the coordination number (CN) of cations (CN=4 for $Mg(BH_4)_2$ and CN=6 for $Ca(BH_4)_2$) and ionic radius (r_{Mg2+}= 0.57 and r_{Ca2+}= 1.00). Compounds with similar crystalline structures, electronegativity and cation size imply minimum distortions and maximum packaging.[144] Furthermore, Mg^{2+} and Ca^{2+} ions are isovalent whereby the immiscibility of $Mg(BH_4)_2$ and $Ca(BH_4)_2$ cannot be explained by electronic factors.[144]

Table 12 – Cell parameters and volumes per formula unit obtained from Rietveld Refinement of α (z=30) and β (z=64) $Mg(BH_4)_2$ after BM and DSC cycling for pure $Mg(BH_4)_2$ and mixtures (2:1, 1:1, 1:2 molar ratio $Mg(BH_4)_2$:$Ca(BH_4)_2$). Before the thermal treatment only the α polymorph is present, while after DSC on the β polymorphic is observed.

		α-$Mg(BH_4)_2$			β-$Mg(BH_4)_2$			
		a (Å)	c (Å)	V/z (Å³)	a(Å)	b(Å)	c (Å)	V/z (Å³)
$Mg(BH_4)_2$	BM	10,347	37,115	475				
	DSC				37,098	18,626	10,917	118
2:1	BM	10,344	37,102	475				
	DSC				37,105	18,640	10,921	118
1:1	BM	10,345	37,103	475				
	DSC				37,107	18,647	10,921	118
1:2	BM	10,342	37,088	474				
	DSC				37,089	18,667	10,921	118

Table 13 – Cell parameters and volumes per formula unit obtained from Rietveld Refinement of α (z=30) and β (z=64) $Ca(BH_4)_2$ after BM and DSC cycling for pure $Ca(BH_4)_2$ and mixtures (2:1, 1:1, 1:2 molar ratio $Mg(BH_4)_2$:$Ca(BH_4)_2$). Before the thermal treatment only the α polymorph is present, while after DSC on the β polymorphic is observed.

		α-$Ca(BH_4)_2$				β-$Ca(BH_4)_2$		
		a(Å)	b(Å)	c (Å)	V/z (Å³)	a (Å)	c (Å)	V/z (Å³)
2:1	BM	8,776	13,127	7,497	108	6,911	4,350	65
	DSC	8,744	13,104	7,480	107	6,918	4,348	65
1:1	BM	8,777	13,125	7,496	108	6,914	4,346	65
	DSC	8,754	13,105	7,497	108	6,917	4,348	65
1:2	BM	8,775	13,125	7,499	108	6,915	4,347	65
	DSC	8,760	13,116	7,503	108	6,917	4,347	65
$Ca(BH_4)_2$	BM	8,775	13,125	7,499	108	6,915	4,346	65
	DSC	8,762	13,119	7,496	108	6,917	4,348	65

Decomposition

The decomposition of $Mg(BH_4)_2$ occurs in four steps. In fact, during heating, endothermic peaks at peak temperature of 299 °C (T_{onset}=269 °C), 340 °C, 355 °C and 386 °C can be observed in **Figure 53**, in addition to the peak at 193 °C, corresponding to the transition α-β as reported before. Upon cooling an exothermic peak at 254 °C (T_{onset}=278 °C). The phases identified after the decomposition of $Mg(BH_4)_2$ are Mg and MgH_2 (**Figure 54**).

Experimental data seem to confirm the investigation reported in the literature. $Mg(BH_4)_2$ has a complex, partially reversible decomposition mechanism, in which several intermediates are involved, creating an obstacle to the complete reversibility of the reaction.[143,210,216,227] Intermediate compounds have not been clarified yet and they depend on experimental conditions.[213]

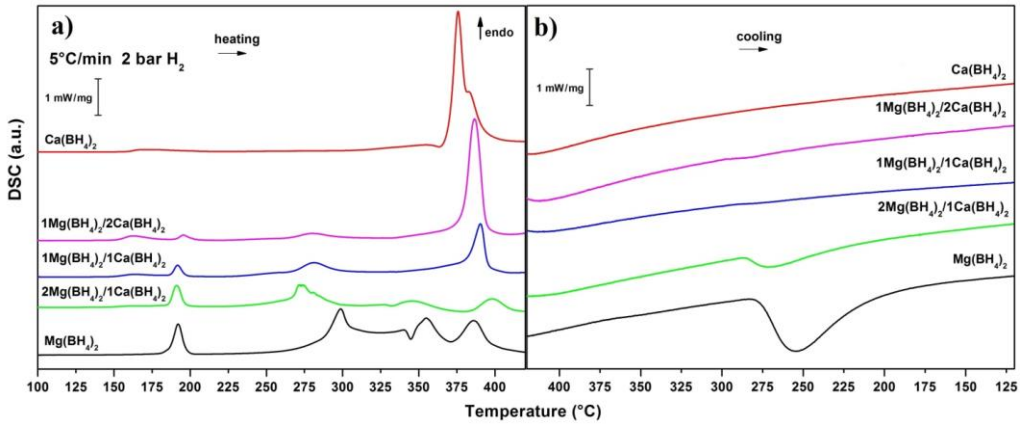

Figure 53 – DSC analysis up to 440 °C at 5 °C/min, under 2 bar of H_2, of pure $Mg(BH_4)_2$, $Ca(BH_4)_2$ and their mixtures (2:1, 1:1, 1:2 molar ratio). a) heating and b) cooling ramp.

In some studies the formation of $Mg(B_3H_8)_2$ was observed,[228,229] however, its formation does not seem to be spontaneous,[137] even though from DFT calculations it results very stable.[214] Other intermediate phases proposed are $MgB_{10}H_{10}$,[142,219] MgB_4H_{10},[142] $MgB_{12}H_{12}$[216] and a generic phase MgB_xH_y.[215]
From the collected data it is possible to confirm a four-step process,[216] which starts at 270 °C. In the first two steps intermediate products are formed, which, according to some studies, could be amorphous phases.[142,215,216] At 355 °C, MgH_2 could have been formed, which then decomposes into Mg following the reaction:[216]

$$MgH_2 \rightarrow Mg + H_2$$

The exothermic peak observed on cooling, is probably related to the rehydrogenation reaction of Mg:[216]

$$Mg + H_2 \rightarrow MgH_2$$

Because of the low hydrogen pressure applied (2 bar), it was not possible to fully hydrogenated all magnesium. In fact, both Mg and MgH_2 are observed in the PXD pattern after decomposition (**Figure 54**).

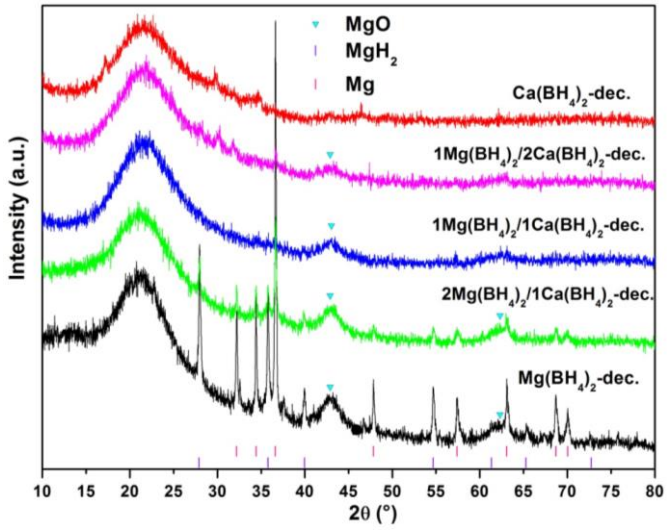

Figure 54 – Room temperature PXD pattern of pure $Mg(BH_4)_2$, $Ca(BH_4)_2$ and their mixtures (2:1, 1:1, 1:2 molar ratio) after decomposition (DSC analysis up to 440 °C).

The formation of Mg and MgH_2 has been observed in several studies.[142,150,215,216] Moreover, it seems that MgH_2 does not appear as a product of the first reaction steps, but it is formed at temperature higher than 280 °C.[215] Nevertheless the decomposition of $Mg(BH_4)_2$ cannot be explained simply through the reactions:

$$Mg(BH_4)_2 \rightarrow MgH_2 + 2B + 3H_2$$

$$MgH_2 \rightarrow Mg + H_2$$

The formation of particularly stable intermediates could be the reason of the incomplete reversibility of the reaction.[142,209,211,215,220]

The decomposition of $Ca(BH_4)_2$ proceeds through two steps, as observed by Mao et al.[207] and Riktor et al..[150] In the DSC trace, in addition to the α-β transition at 168 °C (not evident from **Figure 53**)), two signals at peak temperature equal to 355 °C (low intensity) and at 376 °C can be evidenced. In this case, it is difficult to determine the decomposition products since no peaks are clearly visible in the PXD pattern after decomposition (**Figure 54**). Since no crystalline phase are not clearly observed, amorphous products could be involved such as $CaB_{12}H_{12}$ or other compounds containing Ca, B and H, which, however, do not have long-range order.[211,212,217]

In the literature, two different decomposition mechanisms have been hypothesized for $Ca(BH_4)_2$:[209]

a) $6Ca(BH_4)_2 \rightarrow CaB_{12}H_{12} + 5CaH_2 + 13H_2$
   $CaB_{12}H_{12} + CaH_2 \rightarrow 2CaB_6 + 7H_2$
b) $3Ca(BH_4)_2 \rightarrow CaB_6 + 2CaH_2 + 10H_2$

In the present investigation, the mechanism a) could be probable, however no peaks associated to the CaB_6 can be observed in the PXD analysis. This can support the funding of Kim et al.,[230] where $Ca(BH_4)_2$ decomposes into nanocrystalline CaB_6, which cannot be easily identified. Additionally, the decomposition could follow a different path and form amorphous phases containing Ca, B and H, such as amorphous $CaB_{12}H_{12}$.[231] $Ca(BH_4)_2$ could follow both mechanisms reported before simultaneously, thus producing $CaB_{12}H_{12}$, CaB_6 and CaH_2.[218]

In the 2:1 mixture, MgH_2 and Mg can be identified from the diffraction pattern (**Figure 54**). The decomposition follows four steps as for pure $Mg(BH_4)_2$ (**Figure 53**). DSC trace upon heating is similar, even if the peak temperatures result at lower values for the mixture than for $Mg(BH_4)_2$, while the last peak is shifted to higher value (**Table 11**). The decomposition is partially reversible, as can be seen from the exothermic peak upon cooling at 273 °C (T_{onset} = 288 °C), corresponding to the rehydrogenation of magnesium, similarly to pure $Mg(BH_4)_2$.[216] Also in this case it is not possible to exclude the formation of amorphous phases which prevent the full reversibility $Mg(BH_4)_2$,[142,209,211,215,220] nevertheless in presence of $Ca(BH_4)_2$, the decomposition begins at lower temperature and involves a wider temperature range, as it can be seen from **Figure 53**. Ibikunle et al.[223] studying the 5:1 mixture underlined how the mixture of these two borohydrides result in a hydrogen release at lower temperature than pure compounds. Since no crystalline phase containing calcium has been found, $Ca(BH_4)_2$ has likely decomposes independently, thus being responsible for peaks widening in the DSC trace.

In the 1:1 and 1:2 mixtures the decomposition mechanism is characterized by two steps with T_{peak} equal to 280 °C and 390 °C, where the second peak is more pronounced than the first. Temperature in the 1:1 mixture are shifted to slightly higher values (**Table 11**). The identification of decomposition products is difficult from PXD pattern (**Figure 54**) since no crystalline peak can be observed. Similarly to pure $Ca(BH_4)_2$, the formation of amorphous or nano-crystalline phases could take place. Since substantial correspondence of DSC signals (**Figure 53**)

and diffraction patterns (**Figure 54**), in these two cases, it is reasonable to hypothesize similar mechanisms and reaction products. As $Ca(BH_4)_2$ decomposes after $Mg(BH_4)_2$, it is probable that the species formed by the first decomposition step of $Mg(BH_4)_2$ react with $Ca(BH_4)_2$ to form phases that result stable up to 390 °C. If MgH_2 is formed from the first decomposition process, the mechanism could be traced back to that of $Ca(BH_4)_2$-MgH_2 mixture.[218,230,232] According to Kim et al.[230] and Minella et al.,[218,232] it decomposes forming Mg-Ca-H phases firstly, and then $CaB_{12}H_{12}$, amorphous CaB_6 and CaH_2, and crystalline Mg.
However, the decomposition of the 1:1 and 1:2 mixture is not reversible in the present experimental conditions, as it can be seen from the absence of peaks in the DSC traces upon cooling (**Figure 53**).
Comparing the patterns in **Figure 54**, a wide peak at 43° and a second peak at 62° are present, whose intensities decrease with the content of $Mg(BH_4)_2$. They correspond to a trace of MgO, due to the oxidation of magnesium. The formation of MgO may be due to contamination of the starting sample; its formation during heating is in fact extremely favoured and could have influenced the reaction mechanism, limiting or preventing its reversibility.[142]

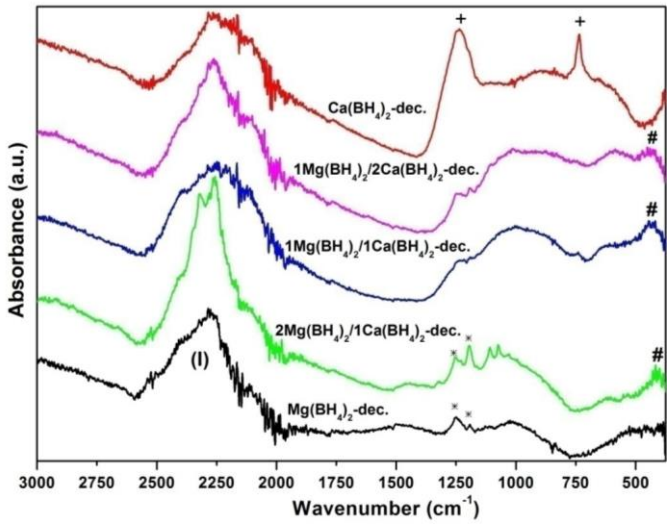

Figure 55 – ATR-IR spectra of pure $Mg(BH_4)_2$, $Ca(BH_4)_2$ and their mixtures (2:1, 1:1, 1:2 molar ratio) after decomposition.

ATR spectra shown in **Figure 55** provide some further indication regarding the decomposition products. In fact, in all of them there is a large band (I), in the 2590-2000 cm^{-1} region. This refers to the B-H stretching[144,217] and therefore

indicates the presence of species still containing the B-H bond. Therefore the the decomposition is not complete, hydrides and borides are not the only byproduct of the reaction. Since the most intense band of $B_{12}H_{12}^{2-}$ is located at 2480 cm^{-1} and the calculated spectra of $B_3H_8^-$, $B_{10}H_{10}^{2-}$ and $B_4H_{10}^{2-}$ presents bands in the 2500-2000 cm^{-1} range,[142,233] it is indeed possible that species containing these anions are formed. However, the amplitude of (I) seems to confirm the presence of multiple different phases.[144]

In the $Mg(BH_4)_2$ spectra, in addition to (I), two small bands at 1250 cm-1 and 1190 cm^{-1} (marked with *) are present. Also in sample 2:1 these peaks are recorded, together with two more peaks at 1109 cm^{-1} and 1074 cm^{-1} of difficult assignment. In $Ca(BH_4)_2$ spectra, two bands are observed (marked with +), the first one at 1235 cm^{-1}, which could be related to the $B_{12}H_{12}^{2-}$ anion,[142] and a second one at 736 cm^{-1} that does not correspond to none of the bands reported in the literature for closoborans.[233]

ATR spectra of 1:2 and 1:1 mixture are very similar to each other, presenting both a broadband at about 1000 cm^{-1} less intense than (I), and another closer to about 430 cm^{-1} (marked with #), also common to the 2:1 mixture. The # band could be connected with the formation of many different phases, which need to be defined precisely.

In conclusion, new phases appear to be involved in the decomposition of the mixtures, which certainly still contain B-H bonds.

Conclusions

Figure 56 shows a summary diagram of the results previously discussed for the $Mg(BH_4)_2$-$Ca(BH_4)_2$ system, which represents the phases present as a function of composition and temperature, at constant pressure of 2 bar of hydrogen. **Figure 56** also shows the peak temperatures (T_{peak} PT) and onset (T_{onset} PT) of the phase transitions α-β of $Mg(BH_4)_2$ and $Ca(BH_4)_2$. The peak (close triangle, T_{peak} dec) and onset temperatures (open triangle, T_{onset} dec) of the various steps of decomposition and magnesium rehydrogenation onset temperature (open star, T_{onset} Re-H_2) are reported as well.

$Mg(BH_4)_2$ and $Ca(BH_4)_2$ are completely immiscible in the solid state, as shown in **Figure 56**. In the XRD pattern of the three mixtures collected after ball-milling and after the heat treatment at 215 °C with p_{H2}=2 bar, in fact, the signals of the constituent phases are always distinguished. The ATR spectra and cell volumes also confirm this conclusion. Immiscibility is attributable and influenced not by the valence of ions (they are isovalent) but structural factors.

The decomposition of 2:1 mixture is similar to that of $Mg(BH_4)_2$, also originating the same crystalline products (Mg and MgH_2). For 1:1 and 1:2 mixture, the decomposition displays only two steps. The first is linked to the decomposition of $Mg(BH_4)_2$ and the second to that of $Ca(BH_4)_2$. It can be hypothesized that $Mg(BH_4)_2$, at 280 °C, originates species that react with $Ca(BH_4)_2$ and which then decompose at higher temperature. No product can be identified by diffraction patterns, apart from Mg and MgH_2. Probably amorphous phases or mixtures of different crystalline phases are formed. However, not only hydrides and borides are formed, but also species that contain the B-H bond. At 2 bar of H_2, only for $Mg(BH_4)_2$ and 2:1 mixture the reaction is partially reversible.

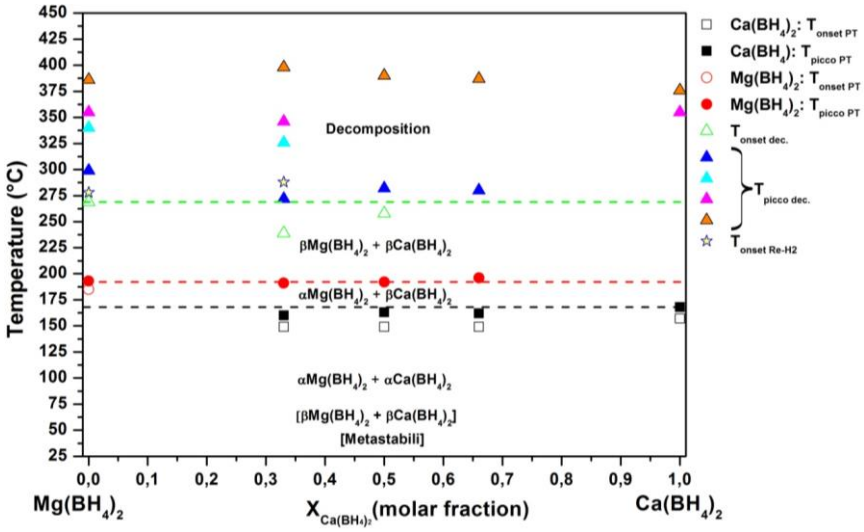

Figure 56 – Summary diagram of the phase stability in the $Mg(BH_4)_2$-$Ca(BH_4)_2$ system in function of temperature and composition, at a constant pressure of 2 bar of hydrogen.

The $Mg(BH_4)_2$-$Ca(BH_4)_2$ system begins to decompose at lower temperature than the parent borohydrides. However, the reaction is irreversible at 2 bar of hydrogen pressure, thus presenting many problems from the point of view of practical use. However, further studies are needed to precisely identify the decomposition products that have been formed, because among them some particularly stable species hinder reversibility. It is also essential to study in detail the mechanisms of decomposition and to investigate higher hydrogenation backpressure and the possible role of additives to further improve the properties of the system.

Ternary systems

Binary combination of borohydrides have been extensively investigated evidencing the formation of eutectics, bimetallic compounds or solid solutions. The investigation was extended to ternary systems in the $LiBH_4$-$NaBH_4$-KBH_4-$Mg(BH_4)_2$-$Ca(BH_4)_2$ system by exploring possible interaction among borohydrides in equimolar composition by mechanochemical treatment and in function of temperature. The mixture were synthetized from commercial $LiBH_4$, $NaBH_4$, KBH_4, γ-$Mg(BH_4)_2$ and α,β-$Ca(BH_4)_2$. The obtained phases were analysed at room temperature by X-ray diffraction to define the obtained crystal phases after ball milling and after thermal treatment up to 200 °C. HP-DSC and DTA-MS were used to study the thermal behaviour of the mixture defining temperature of transitions and decomposition reactions. Interaction among component both in the solid and liquid phase strongly depend on the mutual interaction.
As described in **Chapter 4**, the LiNaK system (**Figure 57**) was experimentally explored and fully assessed by the Calphad method revealing a ternary eutectic, fully liquid above 103 °C.[204]

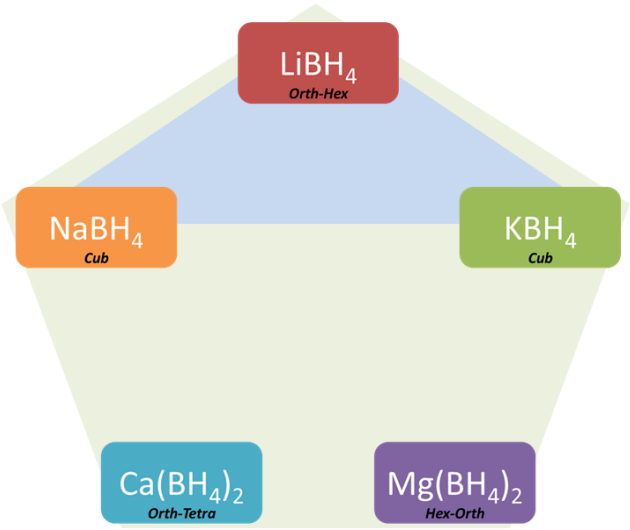

Figure 57 – Schematic representation of the binary $LiBH_4$-$NaBH_4$-KBH_4 system.

$LiBH_4$-$NaBH_4$-$Mg(BH_4)_2$

After ball milling, the LiNaMg system (**Figure 58, A**) presents all the starting materials, the γ-$Mg(BH_4)_2$ has partially converted into the α polymorph upon milling (**Figure 58, B, BM**). After the annealing (**Figure 58, B, 200 °C**), the intensity of the $Mg(BH_4)_2$ peaks are lower, the γ phase is no more present while peaks from the β phase can be recognised. Some broad peaks can be detected, indicating the possible partial decomposition of the mixture. In **Figure 58, C** two main reversible transitions can be recognised. On the second cycle, the peaks are more intense and sharp because they are measured on bulk mixture that have been molten and recrystallized. The first peak at T_{peak}= 99 °C (86 °C, on cooling) is related to the PT of $LiBH_4$ stabilized at lower temperature for the presence of an orthorhombic solid solution with $NaBH_4$.[124] The second peak at T_{peak}= 145 °C (135 °C, on cooling) can be assigned to a new ternary eutectic, while the liquidus temperature is detected around 160 °C.In the LiNaMg system, hydrogen release is observed at T_{peak}= 276 °C and 365 °C (**Figure 58, D**).

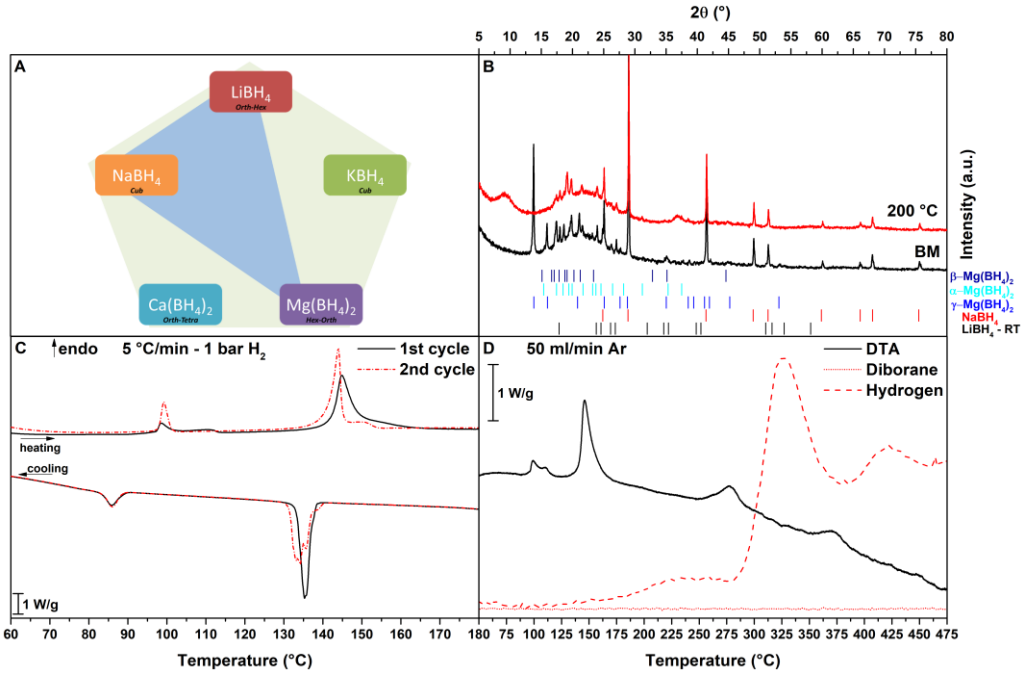

Figure 58 – LiNaMg system: A) Schematic representation of the system, B) PXD pattern of BM and annealed sample, C) HP-DSC trace, 2 cycle of heating and cooling under 1 bar of H_2, D) DTA-MS analysis up to 500 °C under 50 ml/min of Ar. Heating rate equal to at 5 °C/min, endo up.

$LiBH_4$-$NaBH_4$-$Ca(BH_4)_2$

If $Mg(BH_4)_2$ is replaced by $Ca(BH_4)_2$, in the LiNaCa system (**Figure 59, A**) no reactions occur upon milling nor annealing, $LiBH_4$, $NaBH_4$ and α-$Ca(BH_4)_2$ are present in the PXD pattern (**Figure 59, B, BM and 200 °C**). The DSC trace confirms that no interactions occur upon cycling, as previously reported in the literature,[234] the only peak observed is related to the PT of $LiBH_4$ at T_{peak}= 99 °C (81 °C, on cooling) (**Figure 59, C**). On the second cycle, the peak seems to present multiple transition, which can be related to a partial segregation of the compounds in the mixture and possible eutectic melting which however is not evident upon cooling.
The LiNaCa system releases hydrogen at temperature typical of $Ca(BH_4)_2$ and eutectic with $LiBH_4$ and $Ca(BH_4)_2$ (T_{peak}= 361 °C, 378 °C and 470 °C, **Figure 59, D**).

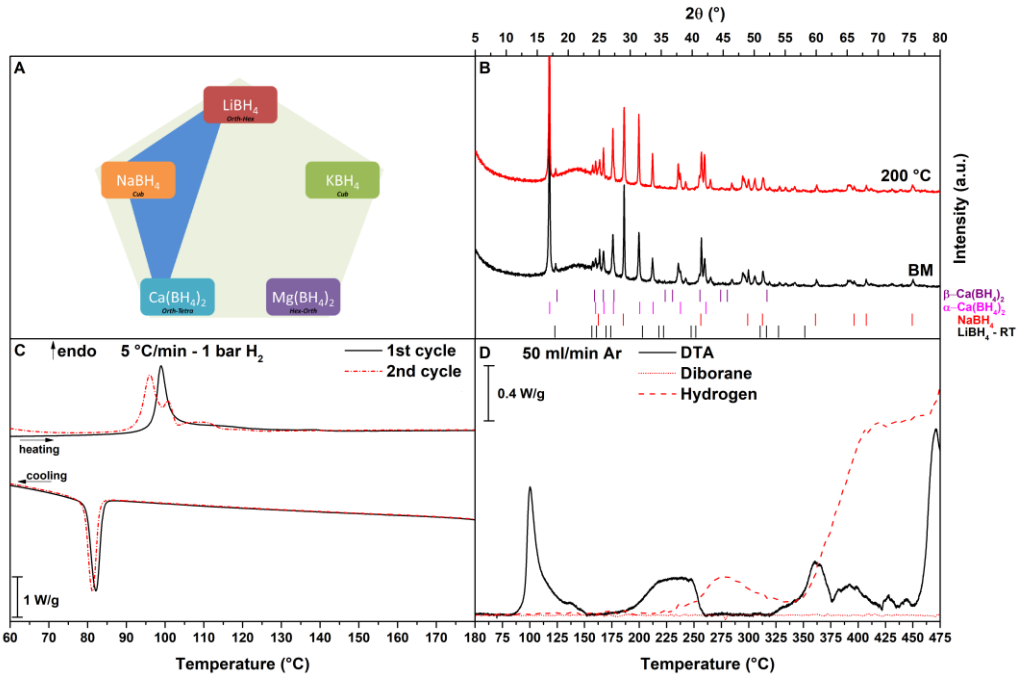

Figure 59 – LiNaCa system: A) Schematic representation of the system, B) PXD pattern of BM and annealed sample, C) HP-DSC trace, 2 cycle of heating and cooling under 1 bar of H_2, D) DTA-MS analysis up to 500 °C under 50 ml/min of Ar. Heating rate equal to at 5 °C/min, endo up.

$LiBH_4$-KBH_4-$Mg(BH_4)_2$

Moving to the LiKMg system (**Figure 60, A**), which was already studied in the literature,[235] we observed in the present milling condition, the formation of $LiKMg(BH_4)_4$ and $LiK(BH_4)_2$, together with the presence of an excess of $LiBH_4$, KBH_4, γ-$Mg(BH_4)_2$ and α-$Mg(BH_4)_2$ (**Figure 60, B, BM**). Upon cycling (**Figure 60, C**), we observed the PT of the $LiBH_4$, at T_{peak}= 95 °C, then a double peak can be observed, related to the reversible reaction to form $Li_2K_3Mg_2(BH_4)_9$[235] and the melting of the eutectic $LiBH_4$-KBH_4 at T_{peak}= 103 °C and 107 °C respectively (65 °C, on cooling). In fact, after annealing (**Figure 60, B, 200 °C**) the intensity of $LiKMg(BH_4)_4$ peaks are higher, while peaks from $LiBH_4$, KBH_4, γ-$Mg(BH_4)_2$, α-$Mg(BH_4)_2$ and $LiK(BH_4)_2$ decreases and almost disappears, underling a not complete reaction upon milling to form the trimetallic compound.
The LiKMg system releases hydrogen at T_{peak}= 311 °C and 390 °C because of the trimetallic compound and no further melting reaction seems to be involved (**Figure 60, D**).

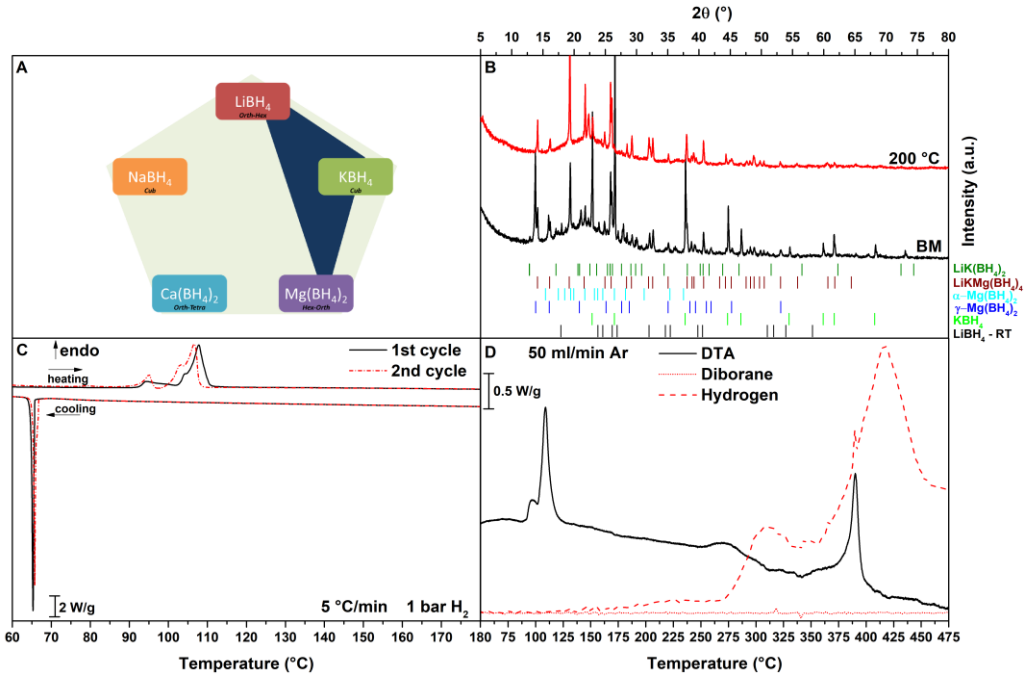

Figure 60 – LiKMg system: A) Schematic representation of the system, B) PXD pattern of BM and annealed sample, C) HP-DSC trace, 2 cycle of heating and cooling under 1 bar of H_2, D) DTA-MS analysis up to 500 °C under 50 ml/min of Ar. Heating rate equal to at 5 °C/min, endo up.

$LiBH_4$-KBH_4-$Ca(BH_4)_2$

In the LiKCa system (**Figure 61, A**), we observed the formation of the bimetallic $KCa(BH_4)_3$ and a little excess of $LiBH_4$ and KBH_4 after BM (**Figure 61, B, BM**), that decrease and almost disappears after annealing (**Figure 61, B, 200 °C**). From the DSC trace (**Figure 61, C**), at T_{peak}= 75 °C (68 °C on cooling) the PT of $KCa(BH_4)_3$ can be recognised, which is more intense and sharp on the second cycle. At T_{peak}= 106 °C (96 °C on cooling) and T_{peak}= 113 °C (107°C on cooling) the PT of $LiBH_4$ and eutectic melting of $LiBH_4$-KBH_4 occurs respectively. The liquidus temperature is detected at 177 °C (170°C on cooling) and could be an indication of a possible new ternary eutectic, indeed no PT of $Ca(BH_4)_2$ is observed because the compound is present in the liquid state.
The LiKCa system releases hydrogen from the liquid state above 280 °C, at T_{peak}= 343 °C and 471 °C (**Figure 61, D**).

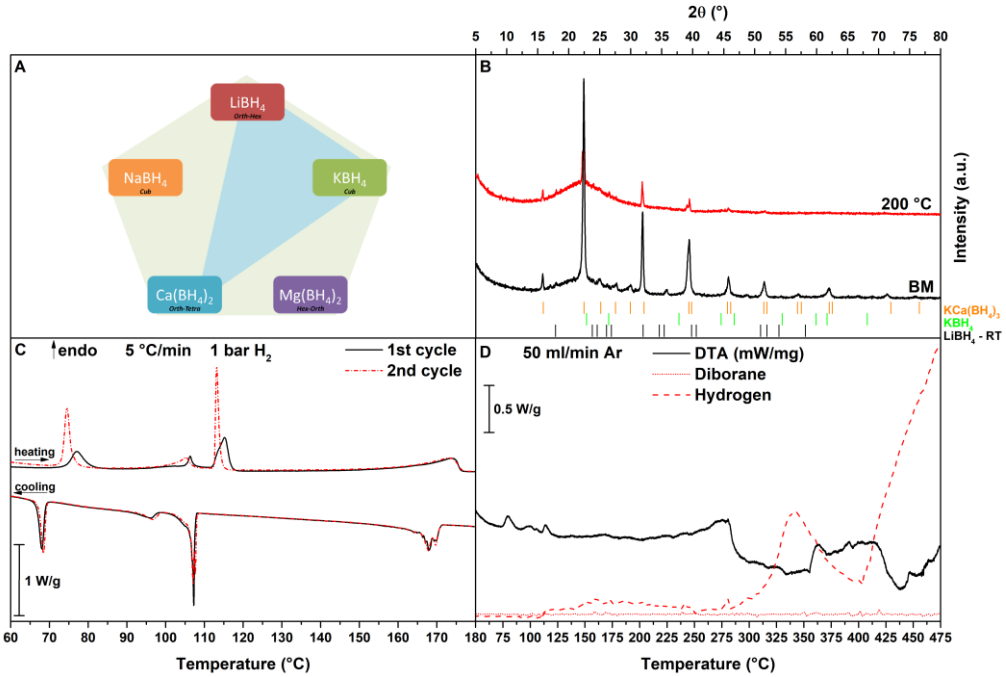

Figure 61 – LiKCa system: A) Schematic representation of the system, B) PXD pattern of BM and annealed sample, C) HP-DSC trace, 2 cycle of heating and cooling under 1 bar of H_2, D) DTA-MS analysis up to 500 °C under 50 ml/min of Ar. Heating rate equal to at 5 °C/min, endo up.

$LiBH_4$-$Mg(BH_4)_2$-$Ca(BH_4)_2$

If $LiBH_4$ is combine with two alkaline-earth borohydrides, in the LiMgCa system (**Figure 62, A**), after BM no reactions occurs and $LiBH_4$, γ-$Mg(BH_4)_2$, α-$Mg(BH_4)_2$ and α-$Ca(BH_4)_2$ are observed in the PXD pattern (**Figure 62, B, BM**). Nevertheless, after cycling (**Figure 62, B, 200 °C**) many unknown peaks are observed in the PXD pattern. At approx. 70 °C, an exothermic unexplained peak is observed, at T_{peak}= 114 °C (approx. 102 °C on cooling) we observe the PT of $LiBH_4$ followed by an endothermic event at T_{peak}= 126 °C, present only on the first cycle (**Figure 62, C**). This thermal event could be related to the formation of a MgCa solid solution never observed before and in which the γ-$Mg(BH_4)_2$ could play a role. At T_{peak}= 145 °C (approx. 115 °C on cooling) and T_{peak}= 153 °C (approx. 137 °C on cooling), some melting reactions are occurring, the liquidus temperature is observed approx. at T_{peak}= 173 °C, though some PT of $Mg(BH_4)_2$ and $Ca(BH_4)_2$ stabilized at lower temperature cannot be excluded (**Figure 62, C**). On cooling many transitions occurs which are of difficult identification.

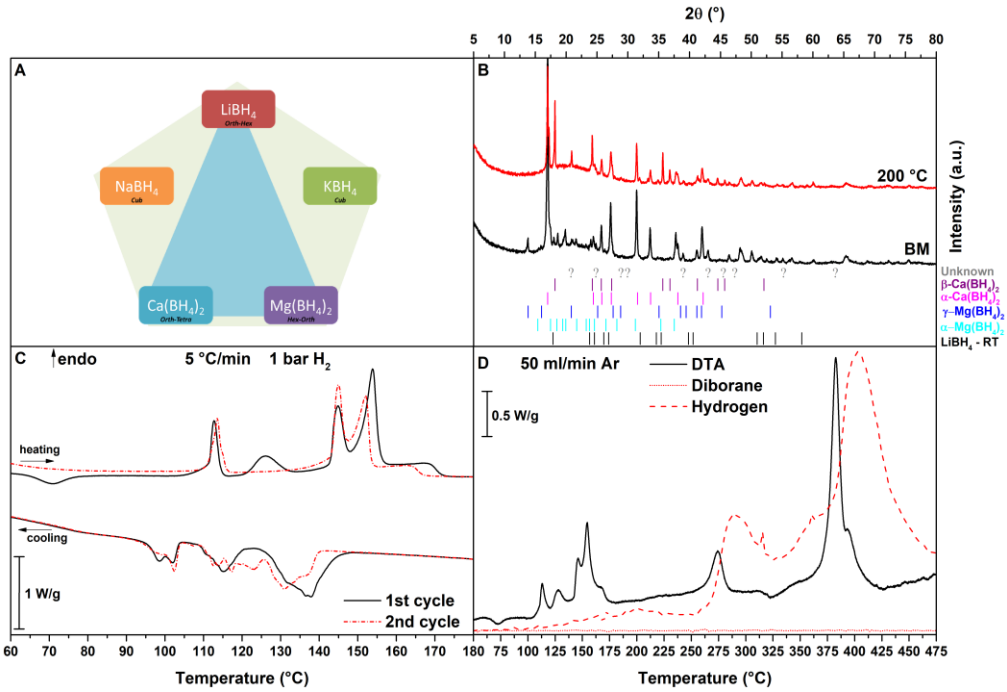

Figure 62 – LiMgCa system: A) Schematic representation of the system, B) PXD pattern of BM and annealed sample, C) HP-DSC trace, 2 cycle of heating and cooling under 1 bar of H_2, D) DTA-MS analysis up to 500 °C under 50 ml/min of Ar. Heating rate equal to at 5 °C/min, endo up.

After annealing (**Figure 62, B, 200 °C**), no $Mg(BH_4)_2$ is observed, peaks from $LiBH_4$, α-$Ca(BH_4)_2$, β-$Ca(BH_4)_2$ and the unknown phase are observed.
The LiMgCa system releases hydrogen at T_{peak}= 374 °C, 382 °C and 393 °C (**Figure 62, D**), at similar temperature as the MgCa system.

$NaBH_4$-KBH_4-$Mg(BH_4)_2$

Moving to ternary mixture without $LiBH_4$, in the NaKMg system (**Figure 63, A**), after BM only $NaBH_4$ and KBH_4 are observed in the pattern (**Figure 63, B, BM**), while after annealing the formation of the cubic $NaBH_4$-KBH_4 solid solution is occurring and can be identified by shoulders in the two pristine phases' peaks (**Figure 63, B, 200 °C**). The DSC trace presents only an exothermic peak around 90 °C on the first cycle (**Figure 63, C**).
The NaKMg system releases small amount of hydrogen above 200 °C in a large range of temperature, as for the pure $Mg(BH_4)_2$, no clear DTA signal are recorded (**Figure 63, D**). No melting of the NaK solid solution is observed.

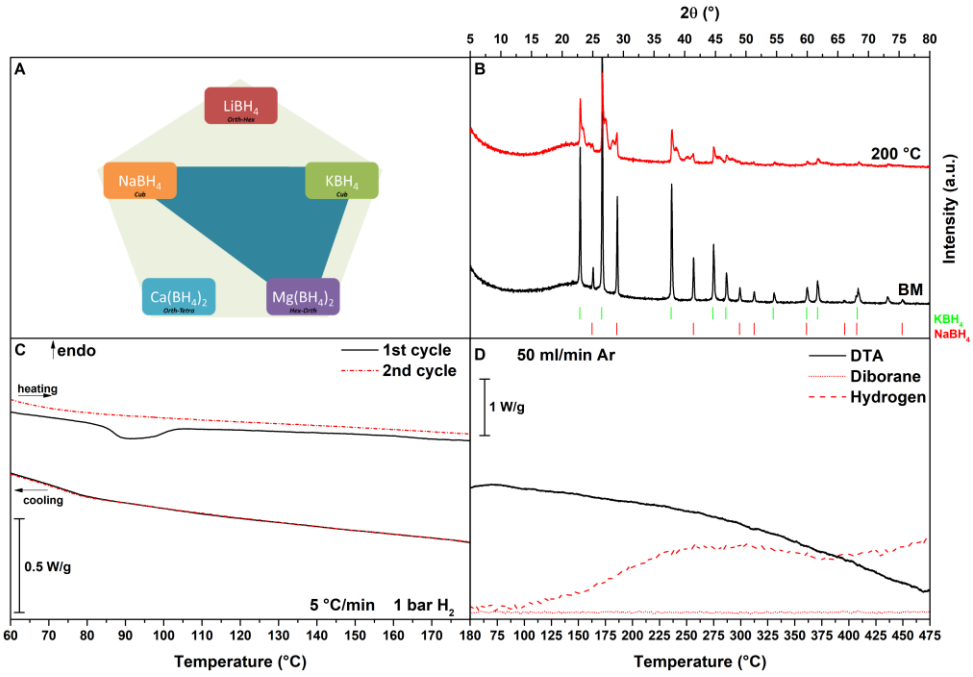

Figure 63 – NaKMg system: A) Schematic representation of the system, B) PXD pattern of BM and annealed sample, C) HP-DSC trace, 2 cycle of heating and cooling under 1 bar of H_2, D) DTA-MS analysis up to 500 °C under 50 ml/min of Ar. Heating rate equal to at 5 °C/min, endo up.

$NaBH_4$-KBH_4-$Ca(BH_4)_2$

In the NaKCa system (**Figure 64, A**), the formation of the bimetallic $KCa(BH_4)_3$ is observed again after BM together with an excess of $NaBH_4$, KBH_4 and α-$Ca(BH_4)_2$ (**Figure 64, B, BM**), after annealing the intensity of $KCa(BH_4)_3$ peaks increase while $NaBH_4$ and KBH_4 decrease and α-$Ca(BH_4)_2$ disappears (**Figure 64, B, 200 °C**). In the DSC trace only the PT of $KCa(BH_4)_3$ can be identified at T_{peak}= 72 °C (61 °C on cooling), more intense on the second cycle (**Figure 64, C**).
In the NaKCa system, the decomposition temperature of $KCa(BH_4)_3$ is lowered by the addition of $NaBH_4$ to T_{peak}= 311 °C, further decomposition occurs at T_{peak}= 382 °C and 439 °C (**Figure 64, D**).

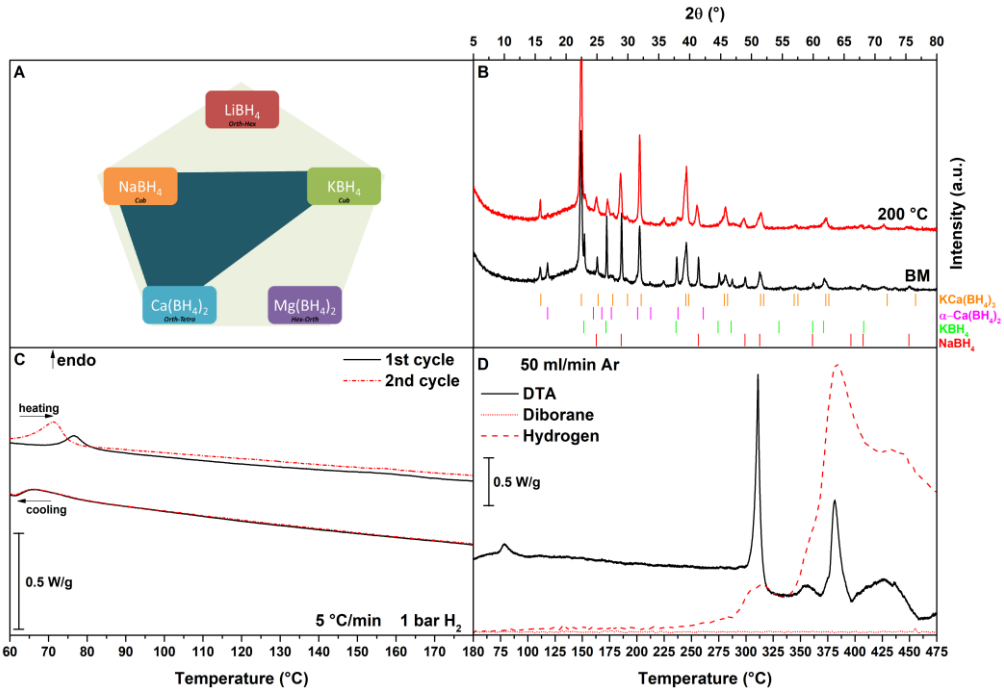

Figure 64 – NaKCa system: A) Schematic representation of the system, B) PXD pattern of BM and annealed sample, C) HP-DSC trace, 2 cycle of heating and cooling under 1 bar of H_2, D) DTA-MS analysis up to 500 °C under 50 ml/min of Ar. Heating rate equal to at 5 °C/min, endo up.

$NaBH_4$-$Mg(BH_4)_2$-$Ca(BH_4)_2$

The NaMgCa system (**Figure 65, A**) presents $NaBH_4$, γ-$Mg(BH_4)_2$ and α-$Ca(BH_4)_2$ after milling (**Figure 65, B, BM**). The DSC trace presents many broad peaks with low intensity on heating, and only the PT of $Ca(BH_4)_2$ can clearly be assigned around 160 °C, while on cooling only one broad peak is present below 100 °C (**Figure 65, C**). After annealing $NaBH_4$, γ-$Mg(BH_4)_2$ and α-$Ca(BH_4)_2$ are still present plus the presence of the same unknown phase of the LiMgCa (**Figure 65, B, 200 °C**).
In the NaMgCa system, hydrogen release occurs in three main events at T_{peak}= 261 °C, 369 °C and 436 °C (**Figure 65, D**).

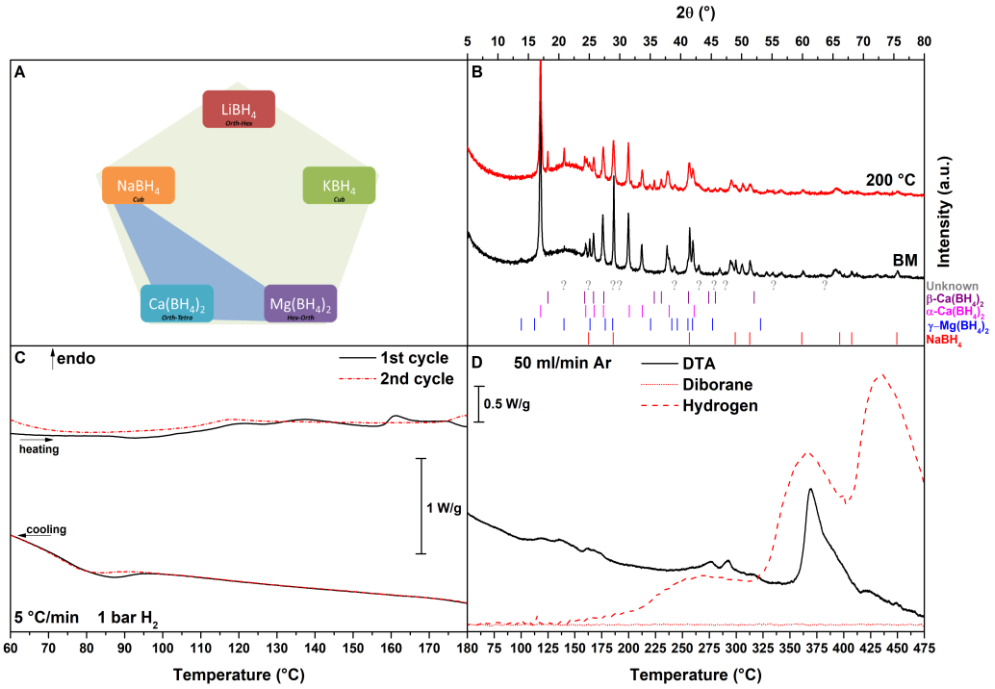

Figure 65 – NaMgCa system: A) Schematic representation of the system, B) PXD pattern of BM and annealed sample, C) HP-DSC trace, 2 cycle of heating and cooling under 1 bar of H_2, D) DTA-MS analysis up to 500 °C under 50 ml/min of Ar. Heating rate equal to at 5 °C/min, endo up.

KBH_4-$Mg(BH_4)_2$-$Ca(BH_4)_2$

In conclusion, in the KMgCa system (**Figure 66, A**), KBH_4, α-$Ca(BH_4)_2$ and $KCa(BH_4)_3$ are present after milling (**Figure 66, B, BM**), no peaks from $Mg(BH_4)_2$ are observed, while after annealing the intensity of $KCa(BH_4)_3$ peaks slightly increase, KBH_4 peaks decrease and trace of β-$Ca(BH_4)_2$ peaks can be recognised (**Figure 66, B, 200 °C**). As for the NaKCa system, in the DSC trace, only the PT of $KCa(BH_4)_3$ can be identified at T_{peak}= 72 °C (62 °C on cooling), slightly more intense on the second cycle (**Figure 66, C**).
In conclusion, in the KMgCa system, hydrogen release occurs at T_{peak}= 383 °C as for $KCa(BH_4)_3$ (**Figure 66, D**).

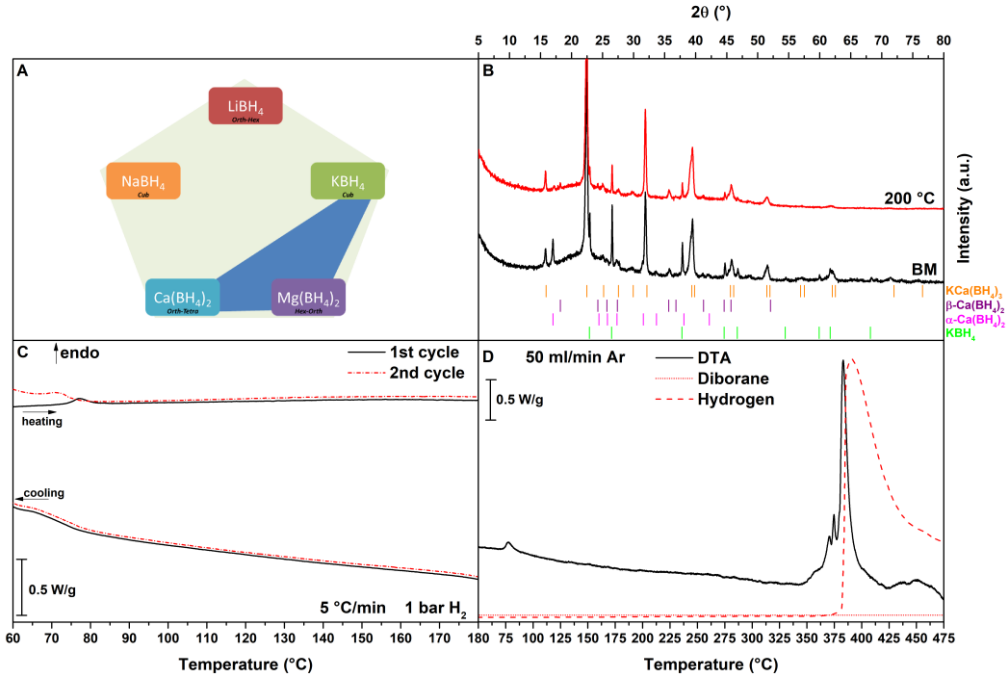

Figure 66 – KMgCa system: A) Schematic representation of the system, B) PXD pattern of BM and annealed sample, C) HP-DSC trace, 2 cycle of heating and cooling under 1 bar of H_2, D) DTA-MS analysis up to 500 °C under 50 ml/min of Ar. Heating rate equal to at 5 °C/min, endo up.

Quaternary systems

In binary and ternary systems, the formation of eutectics has been evidenced, so often the hydrogen release occurs involving a liquid phase, usually above 200 °C and at characteristic T_{peak} that are depending on the interaction among the cations and the complex BH_4^- anion in the liquid. Few bimetallic compound are also formed in ternary systems and play a role in decomposition processes.
Additionally, we extend the study towards higher system to understand if any entropy effects could improve the formation of solid solutions with simple structure and reduce the number of phases present in the mixture.

$LiBH_4$-$NaBH_4$-KBH_4-$Mg(BH_4)_2$

Starting from the LiNaKMg system (**Figure 67, A**), after BM we observe the formation of $LiKMg(BH_4)_4$ and $LiK(BH_4)_2$, together with $LiBH_4$, $NaBH_4$, KBH_4, γ-$Mg(BH_4)_2$ and α-$Mg(BH_4)_2$ (**Figure 67, B, BM**). The DSC trace is similar to the one of the LiKMg system, three main events can be observed on heating in the temperature range from 80 to 110 °C, consisting in the PT of $LiBH_4$, the reaction to form $Li_2K_3Mg_2(BH_4)_9$ and the melting of the $LiBH_4$-KBH_4 eutectic (**Figure 67, C**). Only on the first cooling ramp the reversible reaction of the trimetallic compound is observed at T_{peak}= 67 °C (**Figure 67, C**). Actually, $Li_2K_3Mg_2(BH_4)_9$ is observed after annealing in the PXD patter with $LiKMg(BH_4)_4$, $NaBH_4$, α-$Mg(BH_4)_2$, β-$Mg(BH_4)_2$ and small amount of KBH_4 (**Figure 67, B, 200 °C**).
The LiNaKMg system releases hydrogen at T_{peak}= 320 °C, 394 °C and 484 °C as for the LiKMg system (**Figure 67, C**).

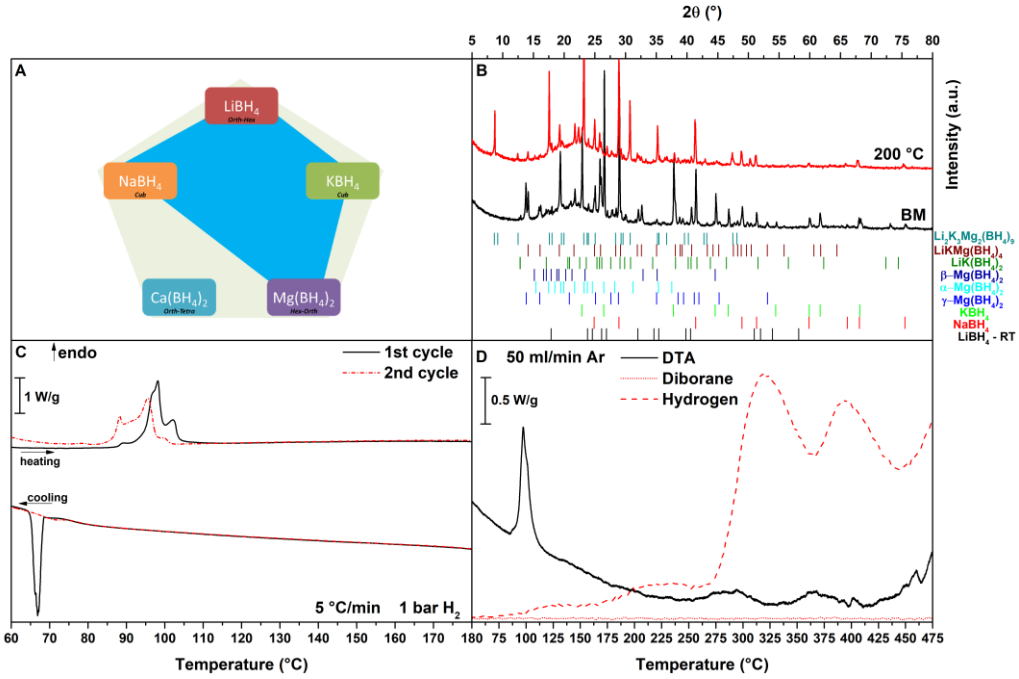

Figure 67 – LiNaKMg system: A) Schematic representation of the system, B) PXD pattern of BM and annealed sample, C) HP-DSC trace, 2 cycle of heating and cooling under 1 bar of H_2, D) DTA-MS analysis up to 500 °C under 50 ml/min of Ar. Heating rate equal to at 5 °C/min, endo up.

$LiBH_4$-$NaBH_4$-KBH_4-$Ca(BH_4)_2$

In the LiNaKCa system (**Figure 68, A**), the milled mixture presents $LiBH_4$, $NaBH_4$, KBH_4, α-$Ca(BH_4)_2$ and $KCa(BH_4)_3$ (**Figure 68, B, BM**). The phases do not change after annealing except for α-$Ca(BH_4)_2$ that disappears (**Figure 68, B, 200 °C**). The DSC trace shows the PT of $KCa(BH_4)_3$ at T_{peak}= 73 °C (66°C on cooling), the melting of LiNaK or LiNaCa ternary eutectic at T_{peak}= 99 °C (90°C on cooling) and the liquidus temperature at 156 °C (142°C on cooling). For the first time a liquid with four different borohydrides is clearly observed (**Figure 68, C**).
The LiNaKCa system releases hydrogen at T_{peak}= 295 °C and above 350 °C, the addition of $LiBH_4$ did improve the hydrogen release temperature (**Figure 68, D**).

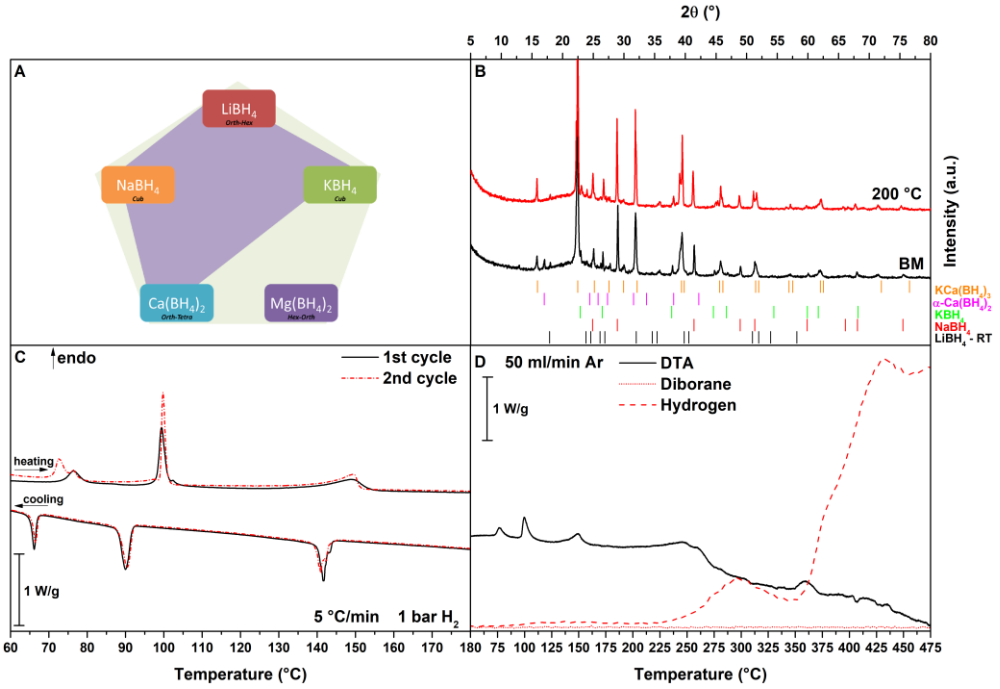

Figure 68 – LiNaKCa system: A) Schematic representation of the system, B) PXD pattern of BM and annealed sample, C) HP-DSC trace, 2 cycle of heating and cooling under 1 bar of H_2, D) DTA-MS analysis up to 500 °C under 50 ml/min of Ar. Heating rate equal to at 5 °C/min, endo up.

$LiBH_4$-$NaBH_4$-$Mg(BH_4)_2$-$Ca(BH_4)_2$

The LiNaMgCa system (**Figure 69, A**) presents $LiBH_4$, $NaBH_4$, γ-$Mg(BH_4)_2$, α-$Mg(BH_4)_2$ and α-$Ca(BH_4)_2$ after milling (**Figure 69, B, BM**), whereas after annealing only $NaBH_4$ and α-$Ca(BH_4)_2$ are clearly visible together with some halo that indicate partial decomposition of the mixtures after the thermal treatment (**Figure 69, B, 200 °C**). The thermal events recorded in the DSC (**Figure 69, C**) show the presence of three main melting at T_{peak}= 96 °C and 99 °C (85 °C on cooling), the liquidus temperature is recorded at 156 °C (99 °C on cooling), underlining again that a ternary and quaternary liquid is formed.
The LiNaMgCa system releases hydrogen at T_{peak}= 280 °C, 369 °C and 468 °C (**Figure 69, D**).

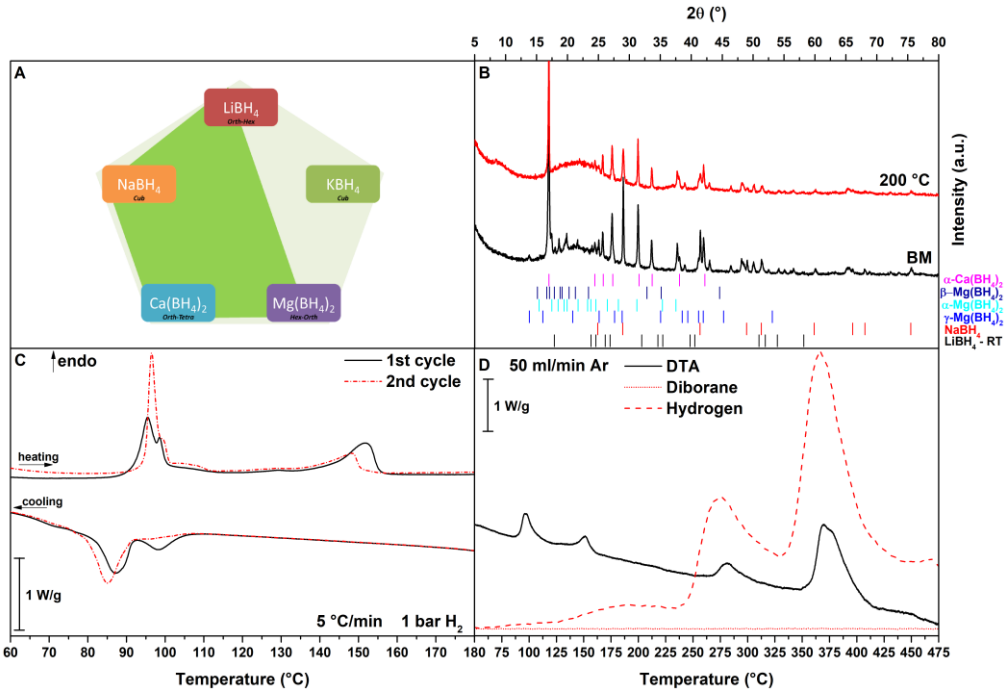

Figure 69 – LiNaMgCa system: A) Schematic representation of the system, B) PXD pattern of BM and annealed sample, C) HP-DSC trace, 2 cycle of heating and cooling under 1 bar of H_2, D) DTA-MS analysis up to 500 °C under 50 ml/min of Ar. Heating rate equal to at 5 °C/min, endo up.

$LiBH_4$-KBH_4-$Mg(BH_4)_2$-$Ca(BH_4)_2$

After milling, the LiKMgCa system (**Figure 70, A**) is characterized by the formation of $KCa(BH_4)_3$ and the presence of $LiBH_4$, KBH_4, and α-$Mg(BH_4)_2$ (**Figure 70, B, BM**). While, after annealing, only traces of $LiBH_4$ are present together with some peaks at low angles that indicate the formation of a small quantity of $LiKMg(BH_4)_4$ (**Figure 70, B, 200 °C**, $LiKMg(BH_4)_4$ not reported in legend). **Figure 70, C** shows the DSC trace of the mixture. It is characterized by the PT of $KCa(BH_4)_3$ at T_{peak}= 75 °C (65 °C on cooling), the PT of $LiBH_4$ at T_{peak}= 113 °C (104 °C on cooling), the melting of a ternary eutectic at T_{peak}= 126 °C (112 °C on cooling), that could be relate to the LiMgCa system, and the liquidus temperature at 157 °C (137 °C on cooling). The double peak at low temperature, on cooling, indicates the reaction of $LiKMg(BH_4)_4$ at T_{peak}= 67 °C.
The LiKMgCa system releases hydrogen at T_{peak}= 319 °C, 370 °C and 444 °C (**Figure 70, D**).

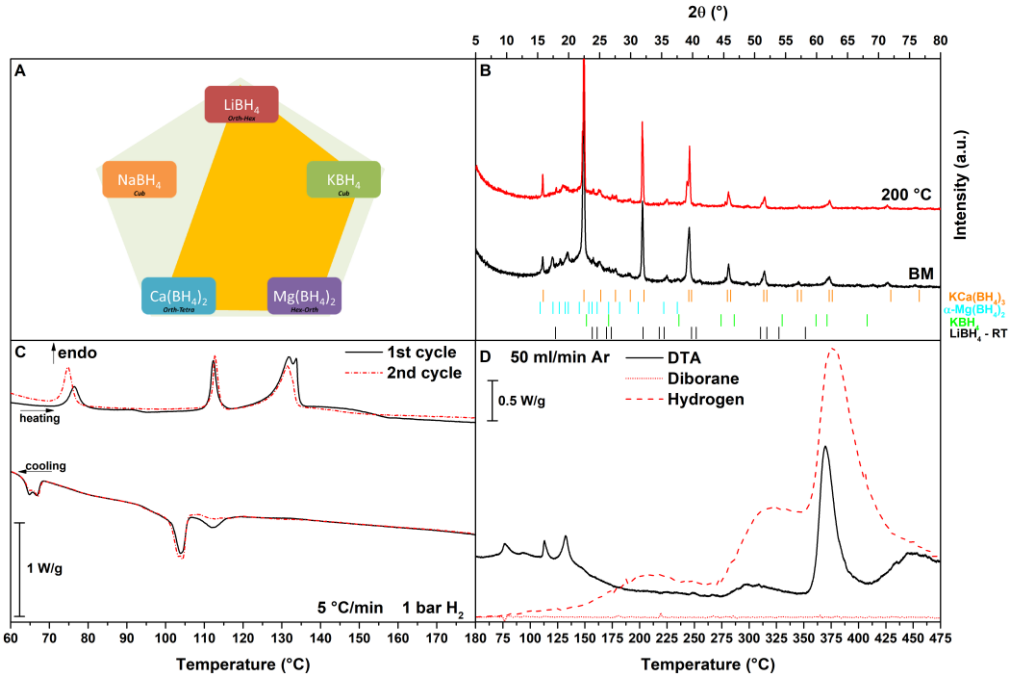

Figure 70 – LiKMgCa system: A) Schematic representation of the system, B) PXD pattern of BM and annealed sample, C) HP-DSC trace, 2 cycle of heating and cooling under 1 bar of H_2, D) DTA-MS analysis up to 500 °C under 50 ml/min of Ar. Heating rate equal to at 5 °C/min, endo up.

$NaBH_4$-KBH_4-$Mg(BH_4)_2$-$Ca(BH_4)_2$

The last quaternary system explored is the NaKMgCa system (**Figure 71, A**) that after milling shows $NaBH_4$, KBH_4, α-$Mg(BH_4)_2$, α-$Ca(BH_4)_2$ and $KCa(BH_4)_3$ (**Figure 71, B, BM**). After annealing only $NaBH_4$ and $KCa(BH_4)_3$ are left, halos indicate the partial decomposition of the mixture (**Figure 71, B, 200 °C**). In the DSC trace only the PT of $KCa(BH_4)_3$ and $Ca(BH_4)_2$ can be detected at T_{peak}= 75 °C and T_{peak}= 166 °C (129 °C on cooling) respectively, which could also be related to a melting reaction (**Figure 71, C**).
Finally, the NaKMgCa system releases hydrogen at T_{peak}= 293 °C, 367 °C and 477 °C (**Figure 71, D**).

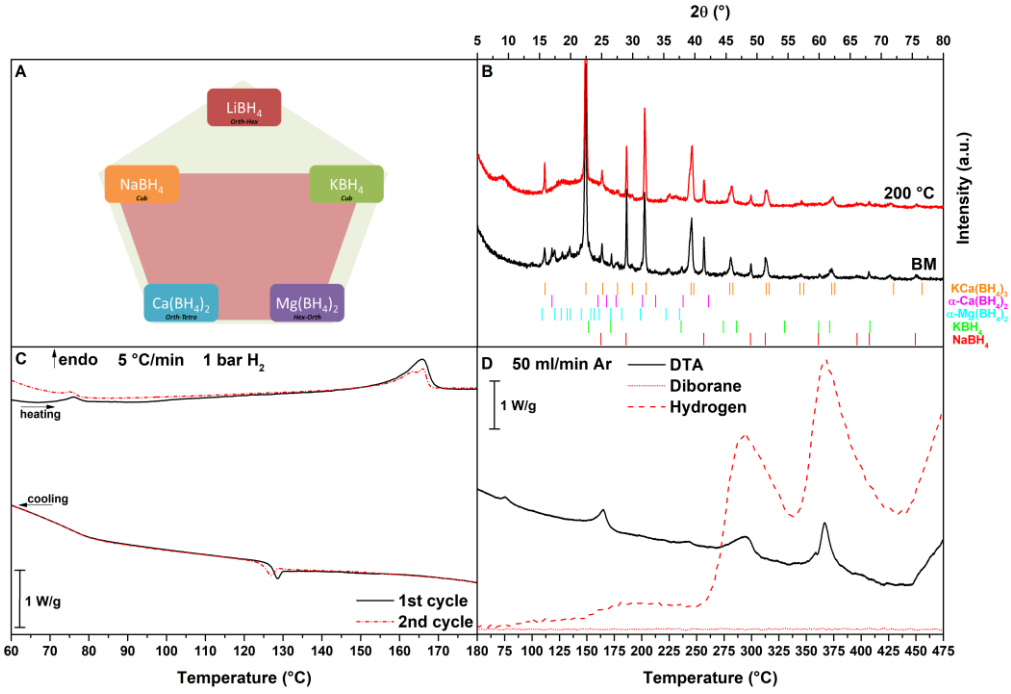

Figure 71 – NaKMgCa system: A) Schematic representation of the system, B) PXD pattern of BM and annealed sample, C) HP-DSC trace, 2 cycle of heating and cooling under 1 bar of H_2, D) DTA-MS analysis up to 500 °C under 50 ml/min of Ar. Heating rate equal to at 5 °C/min, endo up.

Conclusions

$KCa(BH_4)_3$ is the only bimetallic always formed when KBH_4 and $Ca(BH_4)_2$ are present. Its enthalpy of formation is likely strongly negative, limiting overcoming possible entropy contributions to the free energy of a solid solution based on multiple borohydrides. It has an orthorhombic face centred simple structure, which could be suitable to host other ions and form solid solutions. Sometimes also the trimetallic $LiKMg(BH_4)_4$ can be formed together with an excess of $LiK(BH_4)_2$. However, any other bi/tri-metallic borohydrides are observed (i.e. $K_3Mg(BH_4)_5$).

Furthermore, the investigation of equimolar ternary combinations in the $LiBH_4$-$NaBH_4$-KBH_4-$Mg(BH_4)_2$-$Ca(BH_4)_2$ system evidenced the presence of possible new ternary eutectics, such as in the LiMgCa, LiNaCa and LiNaMg systems. While NaMgCa, NaKMg and KMgCa systems present the formation of solid solutions.

In conclusion, hydrogen desorption usually occurs from the liquid phase in a complex multi-steps reaction and the presence of $LiBH_4$ generally promotes the release of H_2 at low temperatures. $KCa(BH_4)_3$ promotes the release in a single-step reaction but at higher temperature.

No new compounds seem to have been formed. However, high resolutions PXD and *in-situ* data will allow the determination of new ternary eutectic composition, and definition of solid solutions at higher temperature. Indeed the role of not crystalline compounds should be understood in relation with decomposition products.

Quinary system

The present study aims at extending the study on multi-metallic compounds and to explore, for the first time, a quinary mixture of borohydrides in the $LiBH_4$-$NaBH_4$-KBH_4-$Mg(BH_4)_2$-$Ca(BH_4)_2$ system (LiNaKMgCa system, **Figure 72**). In fact, this approach appears to be promising from the hydrogen release point of view, owing to the presence of cations of light-metals borohydrides, showing low decomposition temperatures.
The goal is to design combinations of borohydrides with multiple cations in equimolar ratio, following the concept of high entropy alloys. The equimolar composition of the $LiBH_4$-$NaBH_4$-KBH_4-$Mg(BH_4)_2$-$Ca(BH_4)_2$ system was synthetized by ball milling up to 50 hours under 10 bar of hydrogen. The obtained phases were analysed by X-ray diffraction and *in-situ* Synchrotron Radiation Powder X-ray Diffraction, in order to establish the amount of cations incorporated in the obtained crystalline phases, cell parameters and volumes of the phases, also as a function of temperature to study the thermal behaviour of the mixture. HP-DSC and DTA were also used to define the phase transformations and thermal decomposition reactions, leading to the release of hydrogen, which was detected by MS. Decomposition products were defined by PXD, ATR-IR and Raman spectroscopies. The existence of a quinary liquid borohydride phase is reported for the first time. Effects of the presence of multi-cations compounds or a liquid phase on the hydrogen desorption reactions are described.

Equilibrium phases in the quinary borohydride system

After 50 hours of ball milling, the equimolar mixture of $LiBH_4$-$NaBH_4$-KBH_4-$Mg(BH_4)_2$-$Ca(BH_4)_2$ still presents all the pristine compounds ($LiBH_4$, $NaBH_4$, KBH_4, α-$Mg(BH_4)_2$ and α-$Ca(BH_4)_2$) plus $KCa(BH_4)_3$, as can be observed in the PXD pattern shown in **Figure 73, A, BM**.
It is worth noting that, in the mixture, $Mg(BH_4)_2$ and $Ca(BH_4)_2$ are present only in the α polymorph, but γ-$Mg(BH_4)_2$ and β-$Ca(BH_4)_2$ are not detected, even if they are present in the starting materials. Similar behaviour was observed in the $LiBH_4$-$Mg(BH_4)_2$ system, where the α-β transition of $Mg(BH_4)_2$ is reversible.[202] No other bi- or tri-metallic compounds have been observed to form under ball milling. The Rietveld refinement and cell parameters of ball milled pure borohydrides are reported in **Figure 74-75** and they can be compared with the cell parameters

obtained from the Rietveld refinement of the LiNaKMgCa BM sample, reported in **Figure 76 A**.

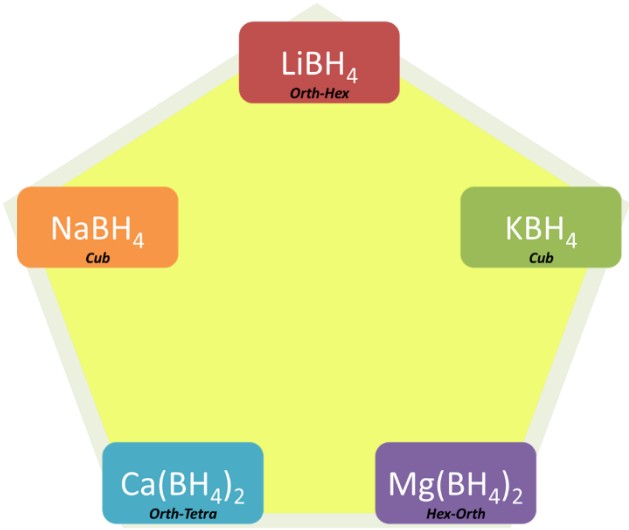

Figure 72 – Schematic representation of the quinary LiNaKMgCa system.

In the case of starting BM γ-$Mg(BH_4)_2$ (**Figure 75 D**), the PXD peaks are very weak because of the milling treatment, suggesting a significant reduction of long-range order in the structure upon mechano-chemical treatment.

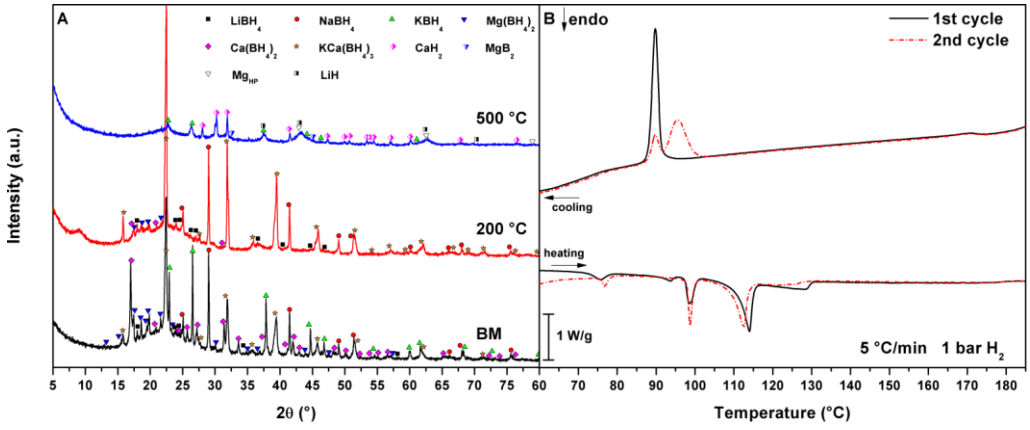

Figure 73 – LiNaKMgCa system: A) PXD pattern of samples ball milled (BM) and annealed in DSC up to 200 °C and 500 °C, B) HP-DSC trace, 2 cycle of heating and cooling at 5 °C/min and 1 bar of H_2.

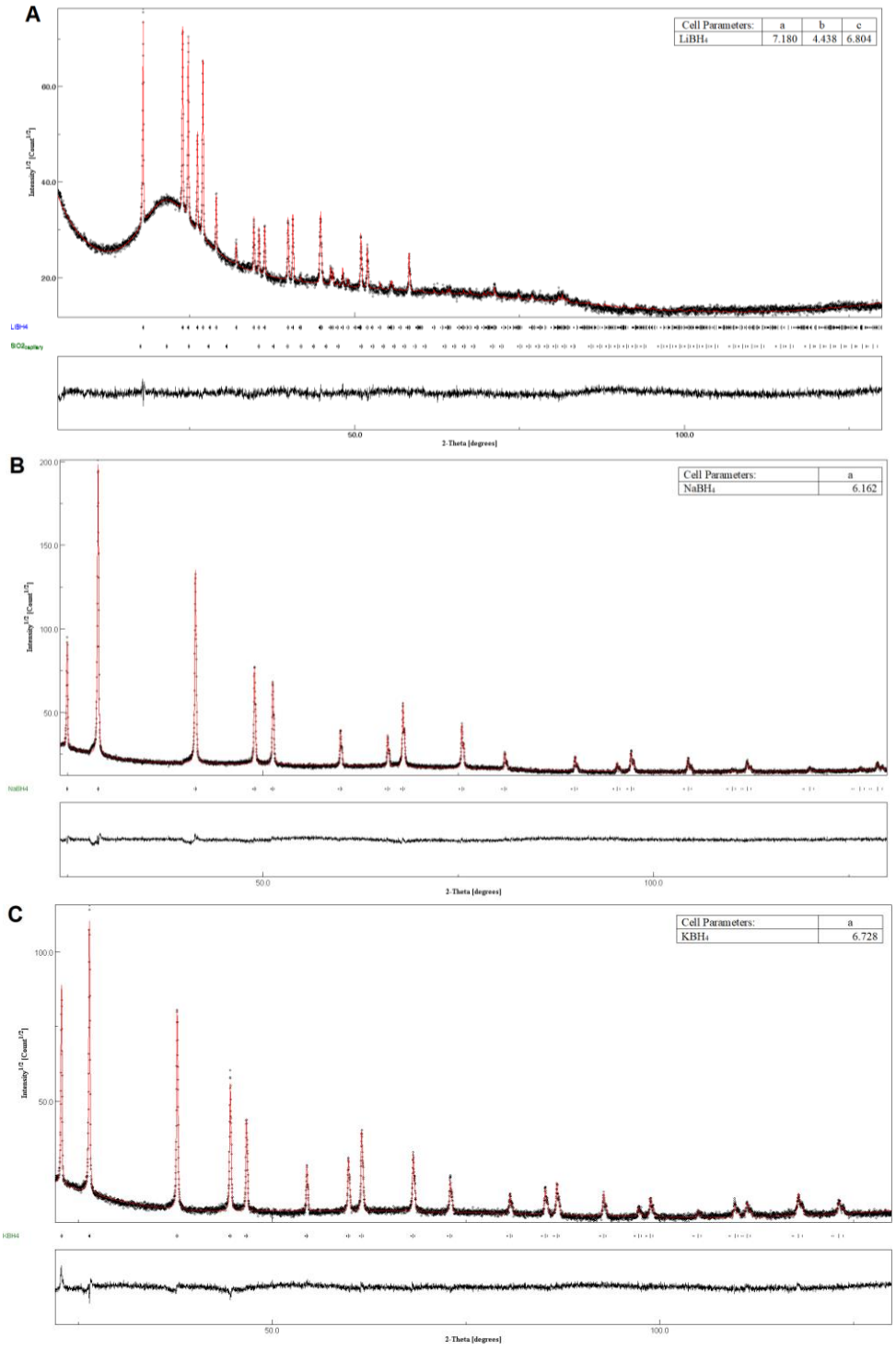

Figure 74 – X-ray diffraction and Rietveld analysis of ball milled pure borohydrides. A: LiBH4, B: $NaBH_4$, C: KBH_4. Lattice constant values are indicated in Å in the figures. (to be continued)

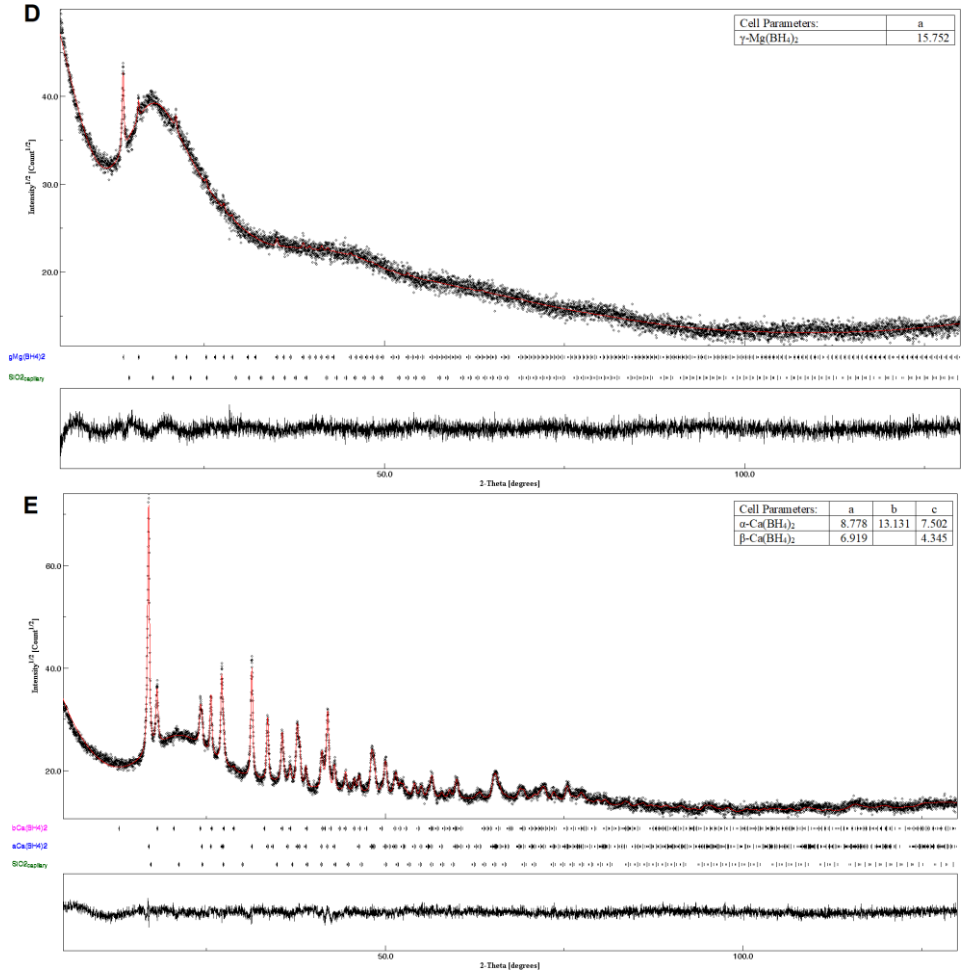

Figure 75 – X-ray diffraction and Rietveld analysis of ball milled pure borohydrides. D: $Mg(BH_4)_2$, E: $Ca(BH_4)_2$. Lattice constant values are indicated in Å in the figures.

This result can be related to the amorphous phase of $Mg(BH_4)_2$ observed under pressure.[236] Since the $KCa(BH_4)_3$ is the only bimetallic compound that has been observed, an equimolar mixture of KBH_4 and $Ca(BH_4)_2$ (KCa system) was synthetized and investigated. The weight fraction and cell parameters of the ball milled KCa system are reported in **Figure 77 A**.

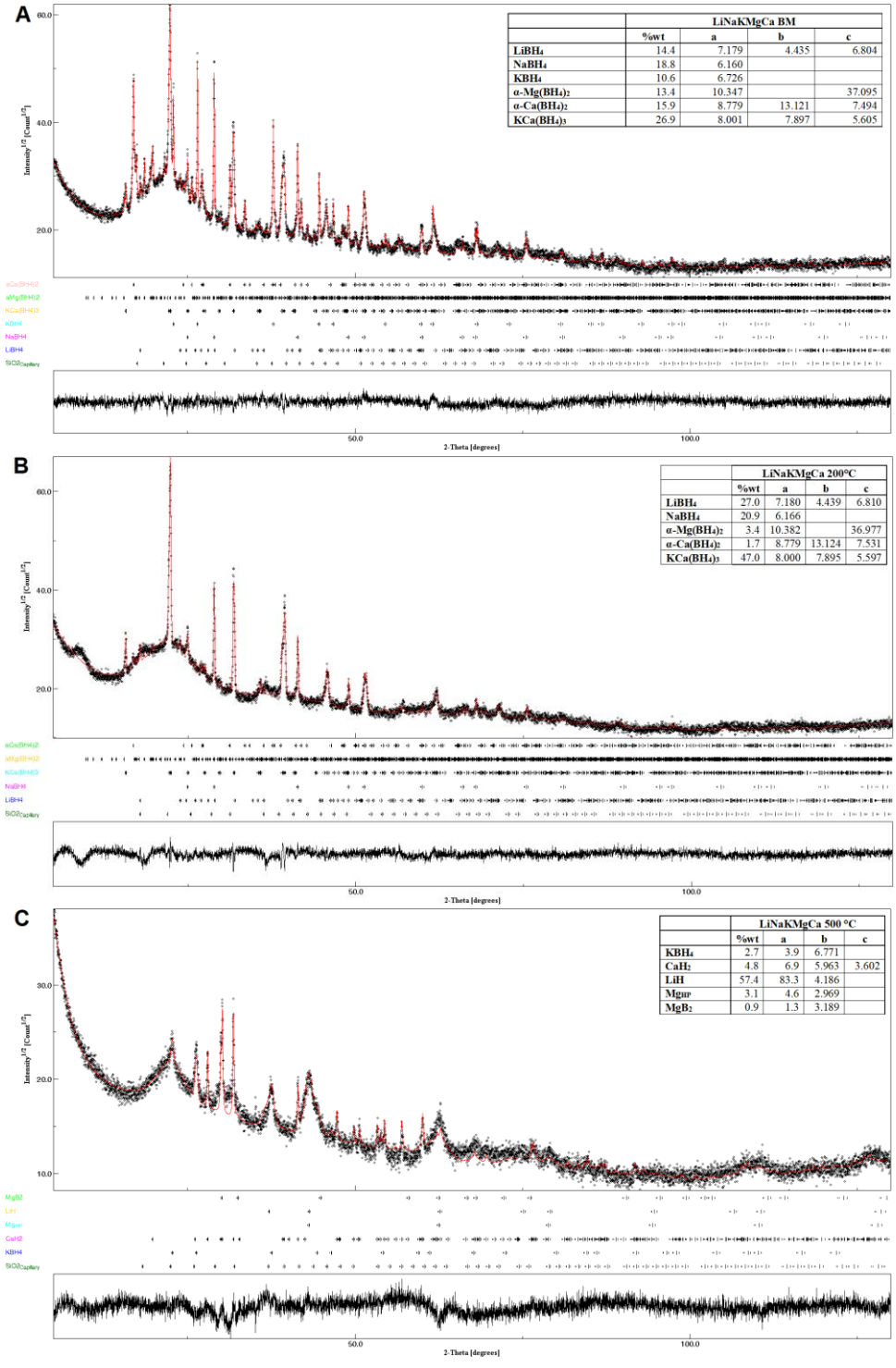

Figure 76 – Rietveld analysis of LiNaKMgCa system, ball milled (A), after DSC cycling up to 200 °C (B), after decomposition at 500 °C (C). Lattice constant values are indicated in Å in the figures.

In the KCa system, after milling, an excess of KBH_4 and $Ca(BH_4)_2$ is present, together with the $KCa(BH_4)_3$ compound, suggesting an incomplete reaction after ball milling at the present conditions. After thermal cycling up to 370 °C, i.e. over the melting temperature of the bimetallic compound (**Figure 77 B**), an excess of KBH_4 is still observed, as it was observed in the literature,[206] which suggests an off-stoichiometry of the compound.

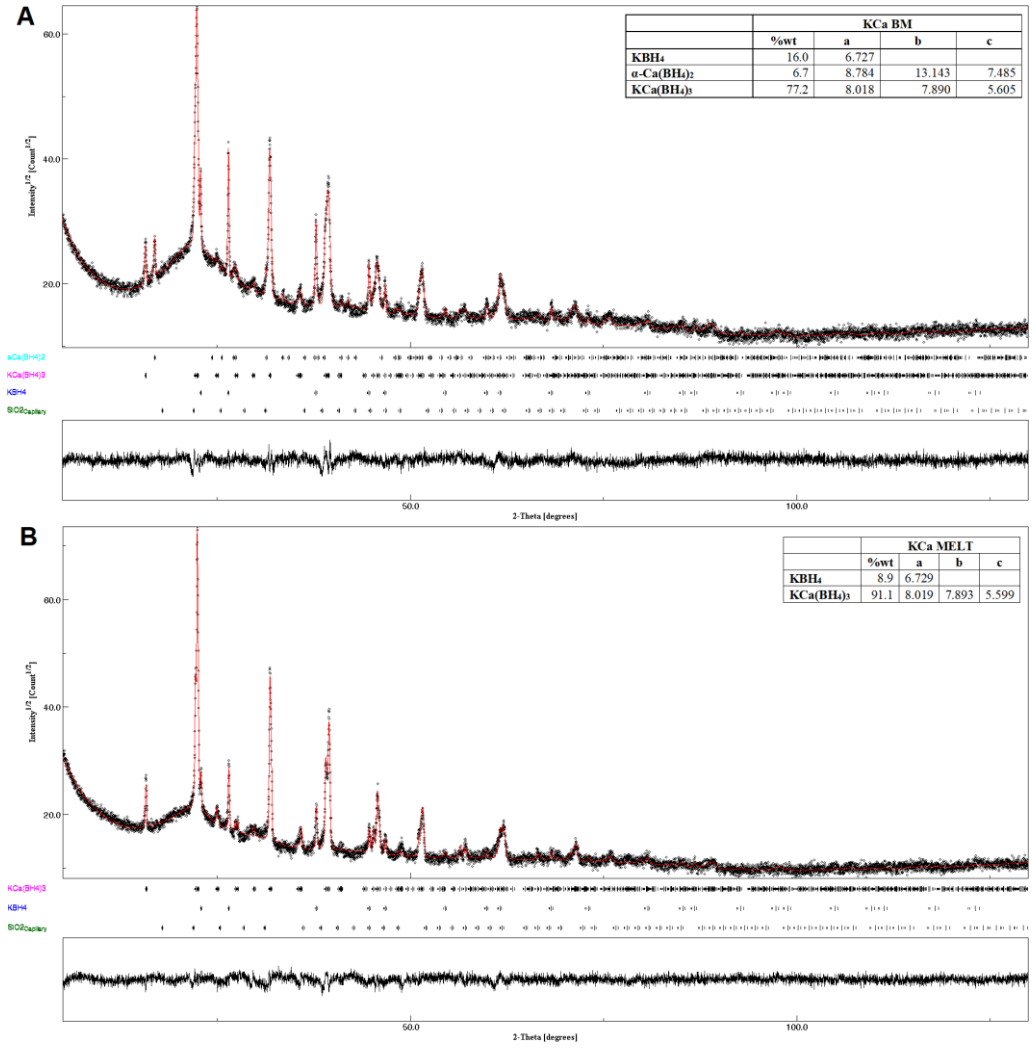

Figure 77 – Rietveld analysis of KCa system, ball milled (A) and after DSC cycling up to the melting temperature (B). Lattice constant values are indicated in Å in the figures.

Generally, no marked changes in the cell parameters of all phases are observed comparing the values observed for pure compounds and the LiNaKMgCa system,

evidencing no significant solid solutions formation upon milling. The only sensible variation that can be noticed is related to a decrease of the *a* lattice parameter of $KCa(BH_4)_3$ in the quinary system (8.001 Å), with respect to that observed in the KCa system after annealing (8.018 Å) and described in the previous chapter on the KCa system. The lower value of this cell parameter in the quinary mixture might be related to the dissolution, inside the crystal structure of the bimetallic compound, of a low amount of cations (e.g. Li^+, Na^+ and Mg^{2+}) with a smaller size with respect to K^+ and Ca^{2+}.

Ball milled pristine borohydrides have been also compared with the KCa and LiNaKMgCa systems by means of ATR-IR and Raman spectroscopies and results are reported in **Figure 78 A** and **Figure 78 B**, respectively.

In ATR-IR spectra, bands in the 2400-2000 cm^{-1} region are related to the B-H stretching, while those in the 1300-800 cm^{-1} region are related to H-B-H bending vibrational modes of ionic BH_4^-.[25,63,100] The stretching (v_1, v_3) and bending (v_2, v_4) modes of the BH_4^- anions are reported in **Figure 78 A** as dashed lines for comparison. The isolated BH_4^- anion has an ideal tetrahedral symmetry, but the vibrational modes can be split into several components in the crystalline state, due to lowering of its site symmetry. Generally, modes v_3 and v_4 are triply degenerate in free tetrahedral BH_4^- ions, and the v_2 is doubly degenerate.[63] The single broad band that can be observed in **Figure 78 A, BM** for the quinary mixture in the 2400-2000 cm^{-1} region may be related to a symmetry change of the BH_4^- site. However, since several phases are present simultaneously in the sample, there may be interaction among them, leading to disordering effects. So, the broad band extending in a wide energy region can be assigned to vibrational modes of BH_4^- ion in different borohydrides. Taking into account the results from PXD, broad bands observed in ATR-IR spectra are assigned to a physical mixture of different phases, rather than the presence of solid solutions.

Raman spectra confirm the presence of a single broad stretching band, in a frequency range similar to the ones of $LiBH_4$ and $Ca(BH_4)_2$, as it can be observed from dashed lines in **Figure 78 B, BM**.

In conclusion, a unique solid solution has not been obtained upon mixing five different borohydrides by mechanical milling. Only the $KCa(BH_4)_3$ bimetallic compound has been formed, suggesting that it has a strong negative enthalpy of formation, that overcomes possible entropy of mixing contributions to the free energy of the mixture.

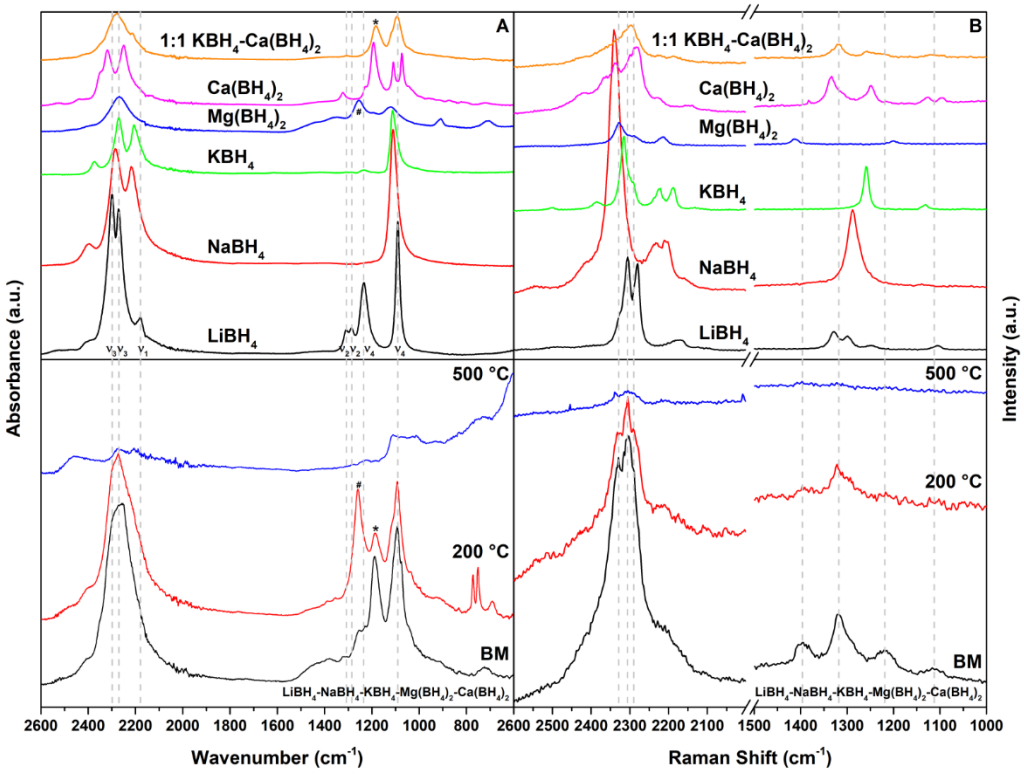

Figure 78 – ATR-IR (A) and Raman (B) spectra of ball milling pure borohydrides and KCa system (top) and LiNaKMgCa system after ball milling (BM) and after annealing at 200 °C and 500 °C (bottom).

Thermal stability of the quinary borohydride system

The DSC traces, obtained upon heating the LiNaKMgCa system up to 200 °C and then cooling down to 60 °C, are reported in **Figure 73 B**. Two cycles have been carried out and they evidence various events: the polymorphic transition of $KCa(BH_4)_3$ at T_{peak}= 76 °C (61 °C on cooling) and the melting of a eutectic at T_{peak}= 99 °C (90 °C on cooling). Another melting peak is observed at T_{peak}= 113 °C (95 °C on cooling), followed by another melting event ending at T= 130 °C. The liquidus temperature is observed at 180 °C (172 °C on cooling). On the first cooling ramp, only one peak is observed, possibly for segregation or kinetic reasons.

The PXD pattern of the quinary mixture after the DSC cycling up to 200 °C is shown in **Figure 73, A, 200 °C**, and corresponding Rietveld refinement analysis is reported in **Figure 76 B**. The PXD peaks of $KCa(BH_4)_3$ are rather intense and

those of $NaBH_4$ are clearly observed, while only traces of $LiBH_4$, KBH_4, α-$Mg(BH_4)_2$ and α-$Ca(BH_4)_2$ are still visible, together with a broad halo.
After thermal cycling the LiNaKMgCa system up to 200 °C, the ATR-IR bands in the 1300-800 cm^{-1} region became more intense and sharper with respect to those observed for the BM sample, as shown in **Figure 78 A, 200 °C**. Variations in the band intensity and shape due to thermal cycling of the BM sample can be related to the release of internal stress and to the formation of a coarser microstructure. A decrease in intensity of the 1185 cm^{-1} band (asymmetric bending) can be related to an modification of the BH_4^- surroundings, such as a change of neighbouring atoms or distances between the ions in the lattice, as observed for the bromide substitution in $LiBH_4$.[61] This band shows a redshift of 3 cm^{-1} with respect to the BM sample after thermal cycling. Generally, it can be observed that the typical IR bands due to the presence of $KCa(BH_4)_3$ (v_4 and *) can be clearly assigned in the LiNaKMgCa system after thermal cycling, as shown in **Figure 78 A, 200 °C**. Moreover, a strong band, marked #, similar to the one of $Mg(BH_4)_2$, is emerging together with two unidentified bands at 772 and 751 cm^{-1}. These are very sharp and could be related to the formation of a new unknown phase, which can be connected to the broad halo observed in the PXD pattern in **Figure 73, A, 200 °C**. Similar IR bands below 800 cm^{-1} have been observed in closoboranes,[233] however the observed frequencies do not correspond to those of any known closoboranes reported in the literature.
In the Raman spectra reported in **Figure 78 B, 200 °C**, some bands disappears after thermal cycling, while from the broad stretching band emerges a peak at 2306 cm^{-1}.
In order to confirm the interpretation of the observed DSC traces for the LiNaKMgCa system, the thermal behaviour of the KCa system was also investigated by DSC analysis, allowing to determine the enthalpy of the polymorphic transition and melting of the $KCa(BH_4)_3$ compound. **Figure 79** reports the DSC traces observed upon two cycles of heating up to 370 °C and cooling.
For the experiment, a backpressure of 50 bar of H_2 was applied to avoid the decomposition of the bimetallic compound, which was reported to occur strictly after melting.[206,234] The polymorphic transition occurs at an onset temperature of 67 °C on the second heating cycle (T_{peak}= 72 °C) and an onset temperature of 72 °C on the second cooling cycle (T_{peak}= 66 °C) with an enthalpy of 3.5±0.1 kJ/mol. The melting occurs at an onset temperature of 356 °C on the second heating cycle (T_{peak}= 363 °C) and an onset temperature of 361 °C on the second cooling cycle (T_{peak}= 359 °C), with an enthalpy of 6.3±0.1 kJ/mol.

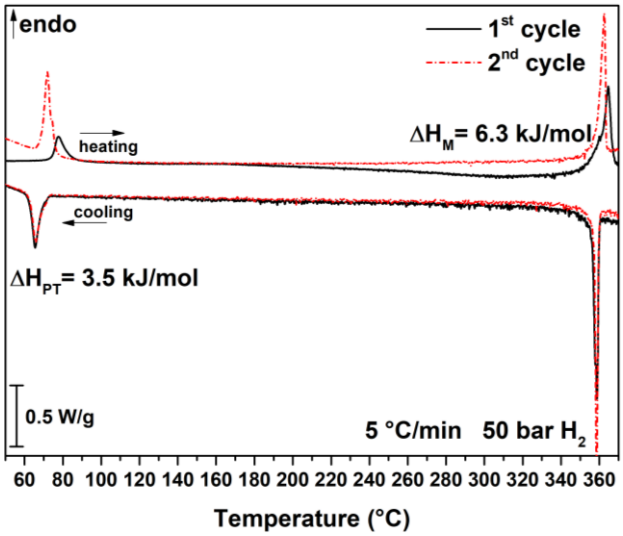

Figure 79 – KCa system: HP-DSC trace, 2 cycles of heating and cooling at 5 °C/min and 50 bar of H_2.

To better understand the thermal events observed in the DSC analysis, an *in-situ* SR-PXD experiment up to 250 °C has been performed for LiNaKMgCa system and results are shown in **Figure 80,** where the intensities of diffraction peaks are compared with HP-DSC traces upon cycling in the same temperature range. PXD patterns selected at various temperatures are reported in **Figure 81**.

From the *in-situ* analysis, it can be clearly observed the polymorphic transition of $KCa(BH_4)_3$ at T_{peak}= 78 °C on heating and T_{peak}= 59 °C on cooling. Starting from T_{peak}= 100 °C (T_{peak}= 88 °C on cooling), the PXD peak intensities of the high temperature polymorph of $KCa(BH_4)_3$ are increasing continually, while the intensity of $LiBH_4$ and KBH_4 are clearly decreasing, due to the eutectic melting of the LiNaK ternary eutectic. On the other hand, no significant change in the $NaBH_4$ peak intensity is observed, due to the small quantity that melts in the eutectic. At T_{peak}= 113 °C (T_{peak}= 108 °C on cooling), the PXD peaks of $LiBH_4$ disappear, since it is fully dissolved in the liquid phase. Up to 150 °C, also intensities of PXD peaks from KBH_4, $Mg(BH_4)_2$ and $Ca(BH_4)_2$ are decreasing. At 190 °C (T_{peak}= 184 °C on cooling) a broad melting peak ends in the DSC trace, and corresponding KBH_4 and $Mg(BH_4)_2$ melting is observed in SR-PXD patterns. Above 245 °C, the mixture is totally molten, and only broad peaks, that can be assigned to the liquid phase, are observed in the PXD patterns (see also **Figure 81**, from 250 °C and upon cooling).

$KCa(BH_4)_3$ and $NaBH_4$ recrystallize upon cooling at 234 °C (T_{peak}= 229 °C), as it can be observed combining the DSC trace and the SR-PXD patterns. Additionally,

the same transformations that are observed on heating are reversible upon cooling and can be detected in the DSC trace, but crystalline phases are hardly visible in the PXD.

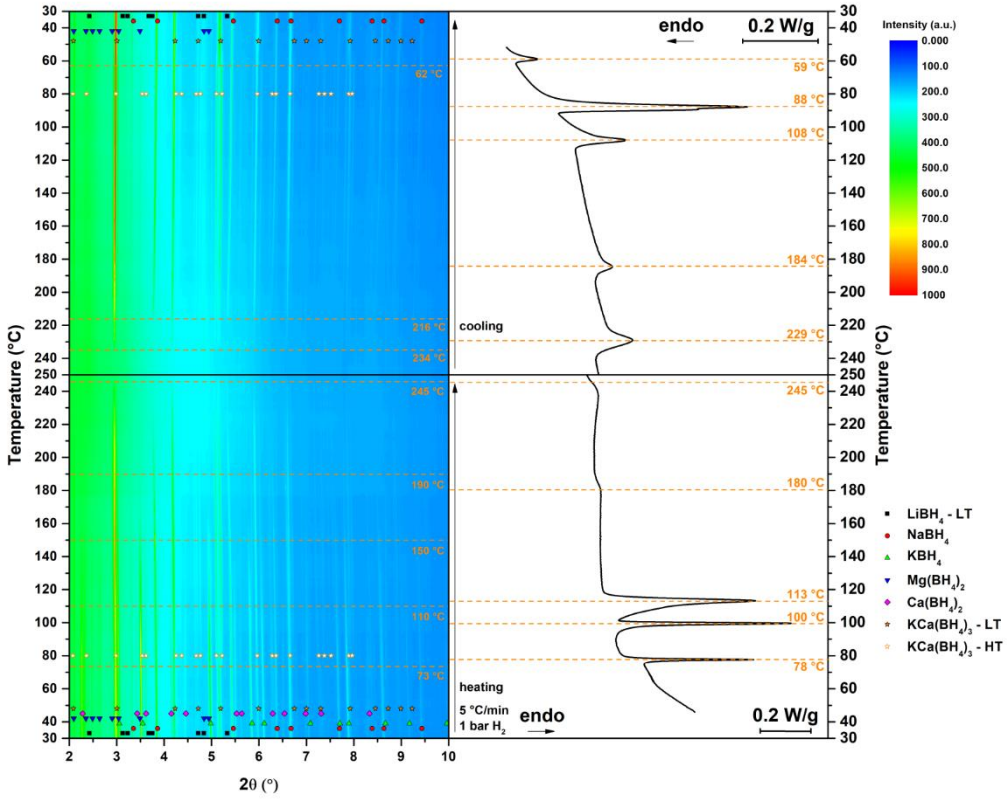

Figure 80 – LiNaKMgCa system: *in-situ* SR-PXD (left) up to 250 °C on heating and cooling at 5 °C/min and 1 bar of H_2 compared with HP-DSC trace (right) in the same condition.

Figure 82 compares the RT scans before (**black, dashed dot line**) and after (**red, continuous line**) the *in-situ* thermal cycling. After the annealing treatment, only $KCa(BH_4)_3$ and $NaBH_4$ are easily recognised, while no trace of KBH_4 and $Ca(BH_4)_2$ are observed. It is worth noting that at 2θ values of 1.3°, 2.5° and 4.7°, broad diffraction peaks are observed, maybe related to an unknown disordered phase. They are similar to the ones observed in the molten mixture (**Figure 81**) and are located in similar positions of diffraction peaks of $LiBH_4$ and $Mg(BH_4)_2$.

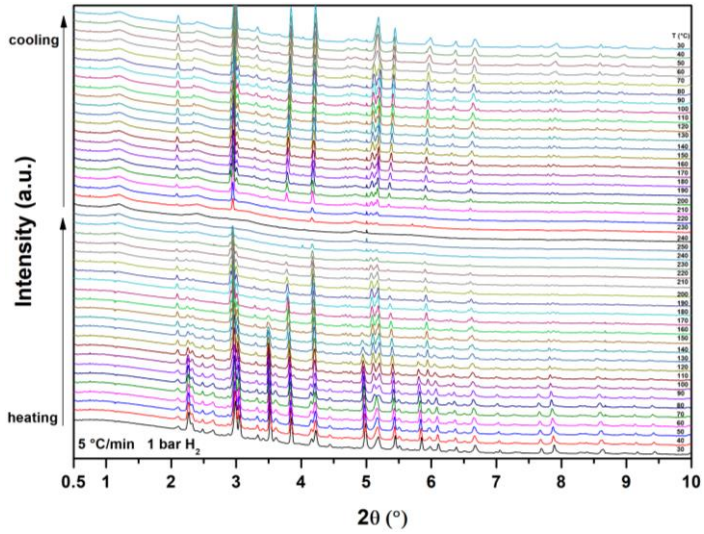

Figure 81 – LiNaKMgCa system: selected patterns, every 10 °C, of *in-situ* SR-PXD on heating and cooling at 5 °C/min and 1 bar of H_2.

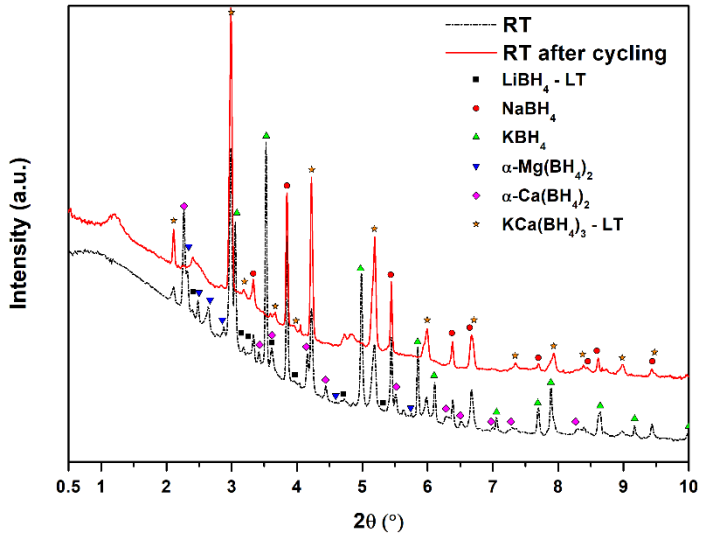

Figure 82 – LiNaKMgCa system: room temperature scans of *in-situ* SR-PXD analysis, before (dashed) and after cycling (line).

The combined DSC and SR-PXD analyses evidence the formation of a liquid borohydride phase, in which five cations are present simultaneously. The melting temperatures observed on heating in the LiNaKMgCa system are quite in good agreement with the eutectic temperatures present in binary system, as reported

in **Table 10**. In addition, it is clear that the melting sequence involves also the bimetallic borohydride, $KCa(BH_4)_3$. These results suggest limited interactions of borohydrides in the LiNaKMgCa system in the solid phase, where they result nearly immiscible. On the contrary, in the liquid phase, they interact, promoting miscibility and forming a quinary borohydride liquid phase, here observed for the first time. This liquid phase is likely promoted by a negative enthalpy of mixing.
In principle, sufficiently high temperatures would promote an entropy-driven transition to a structure containing a random cation occupancy in only one sub-lattice. However, sometimes, this temperature is too high and the material melts before reaching it, as it was observed for the selected system in this study. The failed formation of a unique solid solution phase could be additionally justified because of a not appropriate diversity in crystal structures, coordination and cationic radii of pure borohydrides. In fact, natural tendencies to minimize polyhedral distortions, maximize space filling and adopt polyhedral linkages that preserve electroneutrality required similar crystal structures, electronegativity and cation coordination. In addition, in order to form a solid solution, ions in the system should be isovalent, such that relative cation ratios can be varied continuously with a preserved electroneutrality. In this case, the addition of both mono-valent and bi-valent light-metals borohydrides to the mixture, likely hindered the occurrence of significant solubility.

Hydrogen desorption from the quinary borohydride system

Pure light-metals borohydrides have shown to release hydrogen at relatively high temperatures and the tailoring of their thermodynamics towards a room temperature and pressure hydrogen release is of interest for real applications of these systems for hydrogen storage.[28,34] Under argon flow, alkali-borohydrides decompose after melting: $LiBH_4$ is reported to slowly start to decompose above 300 °C, even after BM,[34,237] and its main decomposition occurs above 400 °C.[34] $NaBH_4$ decomposes slowly from the solid state and the main decomposition reaction occurs, after melting, slightly above 500 °C.[182,238] Decomposition occurs after melting and above 625 °C for KBH_4 as well.[182] $Mg(BH_4)_2$ and $Ca(BH_4)_2$ are reported to decompose above 250 °C and 350 °C, respectively, under argon flow.[34] Sometimes, ball milling and nanosizing of powder can modify the hydrogen release properties of those compounds.

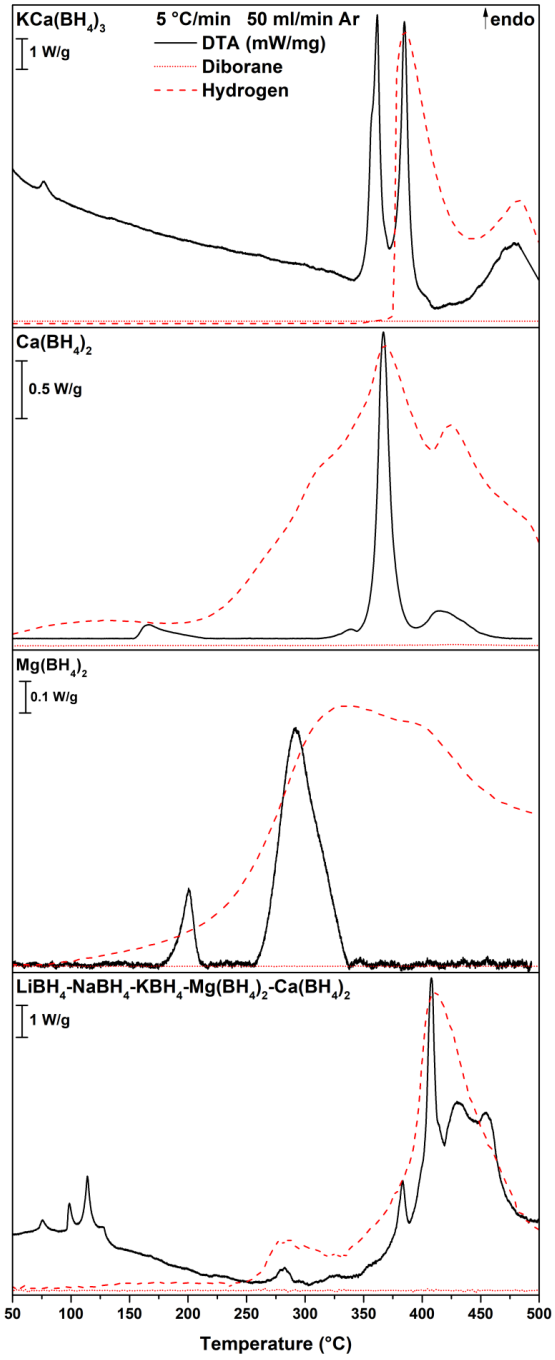

Figure 83 – DTA trace and MS of hydrogen and diborane up to 500°C, 5 °C/min, 50 mL/min Argon flow of LiNaKMgCa system compared with pure BM $Mg(BH_4)_2$, $Ca(BH_4)_2$ and the KCa system.

So, to understand if hydrogen release temperatures could have been modified because of BM, DTA-MS experiments on BM pure $Mg(BH_4)_2$, $Ca(BH_4)_2$ and the KCa system have been performed and results are reported in **Figure 83**. In all investigated samples, diborane gas was never detected in the MS analysis of decomposition gas. From the DTA-MS analysis of BM-$Mg(BH_4)_2$, the polymorphic transition of $Mg(BH_4)_2$ is observed at T_{peak}= 200 °C, together with the starting of hydrogen release from the solid state, that is recorded in a broad range of temperature. On the other hand, BM-$Ca(BH_4)_2$ shows the polymorphic transition at T_{peak}= 164 °C and the main hydrogen release occurs above 300 °C in two steps: the main one at T_{peak}= 366 °C and a second one at T_{peak}= 431 °C. In the KCa system, after the polymorphic transition and melting of $KCa(BH_4)_3$ at T_{peak}= 77 °C and T_{peak}= 362 °C, respectively, the hydrogen release starts strictly after the melting, with an intense release detected at T_{peak}= 385 °C and 479 °C.
Results of these DTA-MS measurements obtained for the quinary mixture are also reported in **Figure 83**. After DTA signals due to various phase transformations of borohydrides constitutive of the mixture, the DTA-MS peaks due to hydrogen release from the liquid phase are clearly observed. Thermal decomposition occurs in complex multistep reactions, starting from 250 °C at T_{peak}= 282, 383, 408, 430 and 454 °C, suggesting that the hydrogen release temperatures are not sensibly different from those of pure borohydrides.
In some pure borohydrides and eutectic mixtures, hydrogen release occurs from the liquid phase mainly because of kinetic reasons. When hydrogen release occurs from the liquid state, the characteristic T_{peak} of decomposition could be related on the interaction among the cations and the complex BH_4^- anion in the liquid.[201] In the case of the LiNaKMgCa system, the presence of many cations in the liquid phase seems not to influence significantly the bond strength in the complex BH_4^- anion.
After decomposition of the LiNaKMgCa system, IR and Raman spectroscopies do not detect any representative band (**Figure 78, 500 °C**). From PXD patterns (**Figure 73, A, 500 °C** and **Figure 76 C**) decomposition products, such as CaH_2, LiH, MgB_2 and the Mg high pressure cubic phase, can be identified. KBH_4 is still present, suggesting that the quinary mixture is not fully decomposed upon heating up to 500 °C.

Conclusions

In the study on the quinary mixture, phase stability and hydrogen release in a equimolar quinary mixture of borohydrides have been investigated for the first time. Following the concept of high entropy alloys, the investigated system is an equimolar mixture of $LiBH_4$, $NaBH_4$, KBH_4, $Mg(BH_4)_2$ and $Ca(BH_4)_2$.
The mixture was synthetized by ball milling and characterized to investigate the possible formation of new phases or solid solutions. The borohydrides result to be immiscible upon mechanical treatment up to 50 hours: pristine borohydrides are detected in the PXD after milling, together with $KCa(BH_4)_3$, whose enthalpy of formation likely overcomes entropy effect, limiting solid solubility. The thermal behaviour of the mixture has been characterized by *in-situ* SR-PXD and HP-DSC. The thermal analysis reveals several melting events, up to 250 °C. So, above 250 °C, a five-component liquid borohydride has been obtained for the first time, via eutectic reactions involving a bimetallic borohydride.
After thermal cycling up to 200 °C, IR spectroscopy reveals the presence of two unknown sharp bands below 800 cm^{-1} that could be related to broad peaks observed in the PXD, suggesting the formation of an unknown phase.
Dehydrogenation from the liquid phase containing five different borohydrides occurs in a complex multistep reaction. Hydrogen release temperatures are not significantly lowered with respect to those of pure borohydrides. Not all the borohydrides have been decomposed during the thermal treatment up to 500 °C.
In conclusion, this study showed the existence of ternary or higher eutectic mixtures of borohydrides, that might be further characterised to determine the exact composition and melting temperature. In addition, the occurrence of a new unknown phase has been observed, suggesting further studies to characterized it. More fundamental thermodynamic studies and assessments of complex systems might lead to a better understanding of phase mixtures formed upon mixing different borohydrides. Studies on their hydrogen release properties might be of interest for a further tailoring of borohydride systems for solid-state energy storage.

Chapter 6 – Reactive hydride composite with eutectic borohydrides

The development of materials showing hydrogen sorption reaction close to room temperature and ambient pressure will promote the use of hydrogen as energy carrier for mobile and stationary large-scale applications. In the present chapter, in order to reduce the thermodynamic stability of MgH_2, Ni has been added to form Mg_2NiH_4, which has been mixed with various borohydrides to further tune hydrogen release reactions. De-hydrogenation/re-hydrogenation properties of Mg_2NiH_4-$LiBH_4$-$M(BH_4)_x$ (M = Na, K, Mg, Ca) systems have been investigated. Mixtures of borohydrides have been selected to form eutectics, which provide a liquid phase at low temperatures, from 110 °C up to 216 °C. The presence of a liquid borohydride phase decreases the temperature of hydrogen release of Mg_2NiH_4, but only slight differences have been detected by changing the borohydrides in the eutectic mixture.

Introduction

To overcome the increasing worldwide demand of energy, the use of hydrogen as sustainable and efficient energy carrier plays an essential role. In this frame, the development of materials able to store hydrogen close to room temperature and ambient pressure will enable the use of hydrogen in mobile and stationary large-scale applications. Low cost and light weight hydrides are promising material for solid-state hydrogen storage, owing to their high gravimetric and volumetric hydrogen capacity.[23] The theoretical hydrogen content of $LiBH_4$ is 18.5%wt, i.e. the highest among metal borohydrides, while it is equal to 10.7%wt for $NaBH_4$, 7.5%wt for KBH_4, 14.9%wt for $Mg(BH_4)_2$ and 11.6%wt for $Ca(BH_4)_2$. Observed values are usually lower, depending on the experimental conditions.
Usually light metal hydrides absorb and release hydrogen through sluggish kinetics at relatively high temperatures. In order to reduce their thermodynamic stabilities, transition metals have been added to form complex metal hydrides,[27] such as in the case of MgH_2 mixed with Ni to form Mg_2NiH_4, with a theoretical hydrogen content equal to 3.6%wt. This complex metal hydride upon heating shows a polymorphic transition from a monoclinic to a hexagonal structure at 244 °C, together with the release of one hydrogen to form Mg_2NiH_3.[239,240] The main dehydrogenation reaction occurs at 305 °C under 5%H_2/95%N_2 flow or 1 bar H_2.[239,241] The thermodynamic properties of the Mg-Ni-H ternary system were

assessed by Zeng et al.,[242] where the values of temperature of decomposition as a function of hydrogen pressure are reported. Upon cycling at low hydrogen pressure, Mg_2Ni can absorb hydrogen (at T_{peak}= 247 °C, at 3 bar H_2) to form the partial hydrogenated hexagonal solid solution $Mg_2NiH_{0.3}$.[243]

Literature Survey

The so called Reactive Hydride Composites (RHC) allows mixtures of metal hydrides and borohydride to release hydrogen in a reversible manner under moderate temperature and hydrogen pressure conditions.[28]
The thermodynamic properties and phase diagrams of the $LiBH_4$-$NaBH_4$-KBH_4 system was recently assessed and it has been described in **Chapter 4**.[204] In this system, two eutectic compositions are present. 0.725$LiBH_4$-0.275KBH_4 (LiK) and 0.70$LiBH_4$-0.30$NaBH_4$ (LiNa) melt at an onset temperature of 105 °C and 216 °C, respectively. Even if the LiK eutectic shows a stable liquid above 105 °C, it does not decompose below 400 °C.[49] The decomposition of the 0.68$LiBH_4$-0.32$NaBH_4$ mixture was investigated in the literature, and it shows a release above 400 °C,[201] lowered to 250 °C when nanoconfined.[46] 0.55$LiBH_4$-0.45$Mg(BH_4)_2$ eutectic composition (LiMg) melts at 180 °C and releases hydrogen during melting and above 250 °C,[44,202,203] its decomposition is lowered to 150 °C upon nanoconfinement, thus suppressing the evolution of diborane and the formation of closoboranes.[50,244] 0.68$LiBH_4$-0.32$Ca(BH_4)_2$ eutectic composition (LiCa) melts at 200 °C and decomposes at 350 °C,[173] lowered down to 200 °C upon confinement.[46,245–247]
Recently various studies have explored the hydrogen release properties of mixtures of complex metal hydrides and borohydrides, such in the case of Mg_2FeH_6-$M(BH_4)_x$ systems (M = Li, Na, K, Mg, Ca).[248] Mg_2NiH_4-$M(BH_4)_x$ systems (M=Li,Na,Ca) have been studied as well, showing an improvement of the hydrogen release properties and cyclability.[249–253] The decomposition reactions can form boride species (e.g. $MgNi_{2.5}B_2$), which reversibly play as B-donors to form back the borohydride during the re-hydrogenation process. In the Mg_2NiH_4-$LiBH_4$ system, hydrogen release under argon flow starts at roughly 300 °C and it can be re-hydrogenated at 100 bar and 350 °C in about 4 hours.[249] The hydrogen release in the Mg_2NiH_4-$NaBH_4$ system has an onset temperature close to 250 °C under vacuum and it occurs in three different steps.[251] The Mg_2NiH_4-$Ca(BH_4)_2$ system releases hydrogen above 300 °C.[252] There is no report in the literature on the Mg_2NiH_4-KBH_4 system, since it is expected to release hydrogen at

temperatures that are considered not suitable for the employment of this material in real application. The Mg_2NiH_4-$Mg(BH_4)_2$ system has not been studied yet.
As reported above, mixtures of borohydrides have shown the formation of eutectic melts, which allow the release of hydrogen from the liquid state at low temperatures.[49,54] In the present study, we apply the RHC approach to eutectic mixtures of borohydrides, aiming to further improve hydrogen sorption properties of the mixed borohydrides. In order to compare our results with the literature, we investigated the as prepared Mg_2NiH_4 and the RHC mixture Mg_2NiH_4-$LiBH_4$. Then Mg_2NiH_4 was mixed with all the binary eutectic composition of $LiBH_4$ and $M(BH_4)_x$ (M = Na, K, Mg, Ca). The thermal behavior and decomposition temperature were analyzed by HP-DSC. Ball milled mixtures and samples after thermal cycling where analyzed by PXD to identify crystalline decomposition products. This study will allow an understanding of the behavior of a RHC mixture with a liquid phase and its role in the thermodynamic destabilization of hydrogen sorption reactions.

Results

An overview of the investigated samples and corresponding compositions is reported in **Table 14**. The investigated mixtures will be named by the main metals that are present (e.g. the $LiBH_4$ and KBH_4 in eutectic composition will be named LiK and its mixture with Mg_2NiH_4 will be named MgNiLiK).

Table 14 – Borohydrides structures and details on pure compounds, binary mixtures, bimetallics, solid solutions (SS), enthalpy [kJ/mol] and temperature [°C] of polymorphic transition (PT), eutectic melting (EU), thermal minima (TM), and decomposition (DEC).

Sample	Borohydrides composition (Molar Fraction)	RHC composition (Molar Fraction)
MgNiLi	$LiBH_4$	0.56 Mg_2NiH_4, 0.44 $LiBH_4$
MgNiLiK	0.72 $LiBH_4$, 0.28 KBH_4	0.56 Mg_2NiH_4, 0.32 $LiBH_4$, 0.12 KBH_4
MgNiLiNa	0.70 $LiBH_4$, 0.30 $NaBH_4$	0.56 Mg_2NiH_4, 0.31 $LiBH_4$, 0.13 $NaBH_4$
MgNiLiMg	0.55 $LiBH_4$, 0.45 $Mg(BH_4)_2$	0.64 Mg_2NiH_4, 0.20 $LiBH_4$, 0.16 $Mg(BH_4)_2$
MgNiLiCa	0.68 $LiBH_4$, 0.32 $Ca(BH_4)_2$	0.62 Mg_2NiH_4, 0.27 $LiBH_4$, 0.11 $Ca(BH_4)_2$

Figures 84-89a, report PXD patterns of the as-prepared samples, which can be compared with the patterns collected after thermal cycling. **Figures 84-89b** show the DSC traces upon cycling.

Mg_2NiH_4

As a consequence of the synthesis procedure, the diffraction pattern of Mg_2NiH_4 (**Figure 84a, as synthetized**) presents broad diffraction peaks of the monoclinic phase stable at room temperature, LT1. The orange-reddish colour of the powder indicates the presence of a microtwinned modification of the room-temperature phase, called LT2,[254] as confirmed by PXD pattern. As previously reported for a similar synthesis route,[255] even if a molar ratio 2:1 of starting MgH_2 and Ni have been used to obtain the complex metal hydride, traces of unreacted Ni are present in the sample.

In the DSC trace of pure Mg_2NiH_4 on heating (**Figure 84b, 1st cycle**), at T_{peak}= 244 °C, the monoclinic-to-cubic polymorphic phase transition can be observed. This transition is reversible, as clearly shown by the exothermic peak upon cooling at T_{peak}= 234 °C, due to the cubic high temperature phase forming LT1 and LT2.[239,240] In the 2nd cycle (**Figure 84b, 2nd cycle**), the polymorphic transition is observed again and upon further heating an endothermic peak related to hydrogen release can be detected. The complex metal hydride decompose to Mg_2Ni[255], under a hydrogen backpressure of 2.7 bar, at T_{peak}= 372 °C. Upon cooling, in the 2nd cycle, a broad exothermic peak of hydrogenation to form $Mg_2NiH_{0.3}$ can be observed below 235 °C.[243] Upon further cycling (**Figure 84b, 3rd cycle**), the sample releases hydrogen starting from 280 °C (T_{peak}= 296 °C), from $Mg_2NiH_{0.3}$.

$Mg_2NiH_{0.3}$, together with traces of Mg_2NiH_4, is observed in PXD after cooling (**Figure 84a, after DSC**).

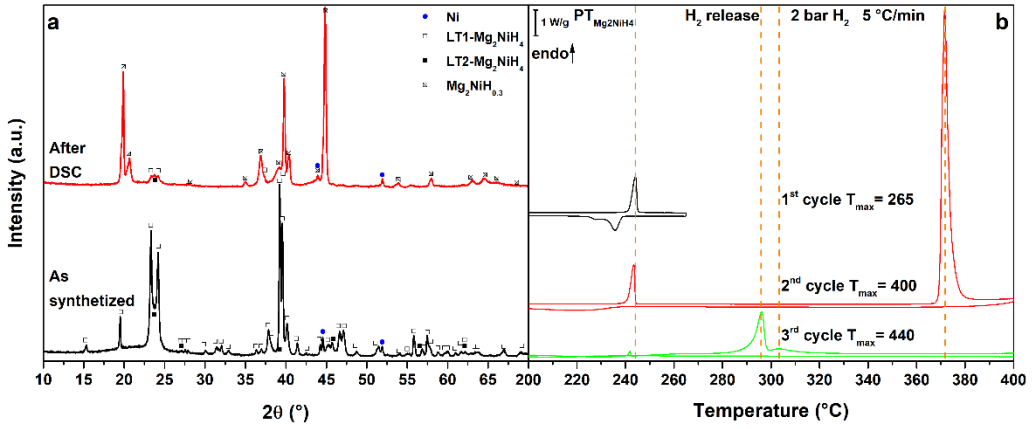

Figure 84 – (a) PXD of the as synthetized Mg_2NiH_4 (black, down) and after cycling in HP-DSC (red, up); b) HP-DSC cycling of Mg_2NiH_4 at 5 °C/min under a static pressure of 2.2 bar of H_2.

RHC mixtures

In almost all the diffraction patterns of Mg_2NiH_4 mixed with borohydrides, the composing phases are visible (**Figures 85-89a, BM**). However, in the MgNiLiK system (**Figure X86, BM**), the milling causes the formation of the $LiK(BH_4)_2$ bimetallic phase, in agreement with the literature.[54] In the MgNiLiMg system (**Figure 88a, BM**), $LiBH_4$ and $Mg(BH_4)_2$ are hardly visible after milling.

Mg_2NiH_4–$LiBH_4$

Figure 85b shows the DSC signals for the RHC mixture MgNiLi upon cycling. In the 1st cycle (**Figure 85b, 1st cycle**), the polymorphic transition of $LiBH_4$ is identified T_{peak}= 117 °C, which is reversible upon cooling. In the 2nd cycle (**Figure 85b, 2nd cycle**), after the polymorphic transition of $LiBH_4$, also the polymorphic phase transition of Mg_2NiH_4 is observed as a broad peak around 245 °C. Both DSC signals can be observed also on cooling. Furthermore, in the 3rd cycle (**Figure 85b, 3rd cycle**), after the polymorphic transition peaks, the melting of $LiBH_4$ can be detected at T_{peak}= 279 °C. All transitions are reversible and well visible during the cooling process, and temperature values are in good agreement with the literature.[78,239,240] In the 4th cycle (**Figure 85b, 4th cycle**), after the polymorphic transition peaks and $LiBH_4$ melting, at T_{peak}= 308 °C a broad endothermic peak due to hydrogen release from $LiBH_4$ can be observed under 2.7 bar H_2. In this case, on cooling, only small peaks from the polymorphic transitions can be observed, suggesting the occurrence of a reaction. In fact, in the last cycle (**Figure 85b, 5th cycle**) only small DSC peaks of Mg_2NiH_4 polymorphic transition, $LiBH_4$ polymorphic transition and melting can be observed on heating, evidencing the presence of a small quantity of parent hydrides in the sample. At higher temperatures, at T_{peak}= 335 °C, the main hydrogen release from the RHC mixture can be observed, with $LiBH_4$ and Mg_2NiH_4 forming $MgNi_{2.5}B_2$ and Mg. Upon cooling below 307 °C, Mg absorbs hydrogen to form MgH_2.
The PXD pattern after the DSC analysis (**Figure 85a, after DSC**) confirms the total decomposition of $LiBH_4$ and Mg_2NiH_4. In fact $MgNi_{2.5}B_2$, MgH_2 and a small quantity of unreacted Mg are observed, but no Li-containing phases are evidenced, likely because of the light scattering factor. $LiBH_4$ cannot be reformed because of the low hydrogen pressure applied. The obtained results are in good agreement with the literature[249] and confirms the decrease of the decomposition temperature of both Mg_2NiH_4 and $LiBH_4$ when mixed together into a RHC.

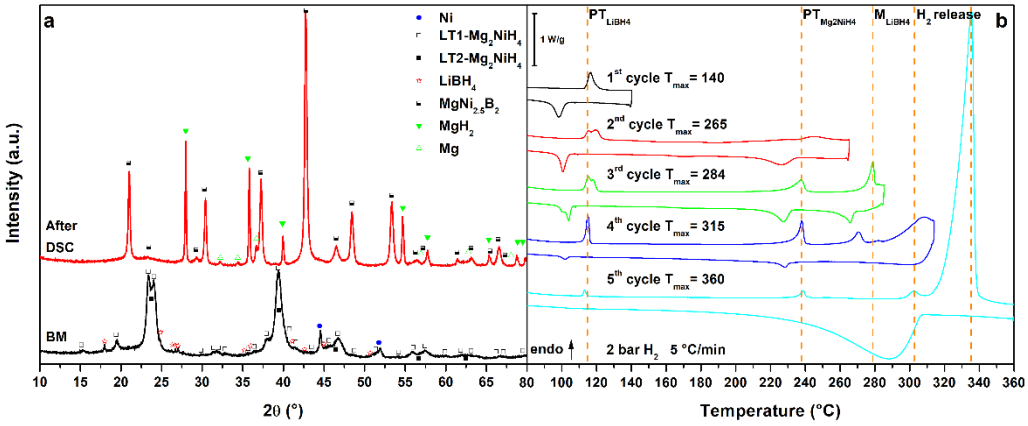

Figure 85 – (a) PXD of the ball milled MgNiLi system (black, down) and after cycling in HP-DSC (red, up); b) HP-DSC cycling of MgNiLi at 5 °C /min under a static pressure of 2.2 bar of H_2.

Mg_2NiH_4– $LiBH_4$–KBH_4 eutectic composition

Figure 86X reports the results obtained for the MgNiLiK system. Upon heating, in the 1st cycle (**Figure 86b, 1st cycle**), the melting of the LiK eutectic can be observed at T_{peak}= 110 °C, which is reversible upon cooling.[204] In the 2nd cycle (**Figure 86b, 2nd cycle**), after the eutectic melting, the polymorphic transition of Mg_2NiH_4 is observed as a broad peak at T_{peak}= 246 °C. Above 290 °C (T_{peak}= 325 °C) the main hydrogen release from the RHC mixture can be observed under 2.7 bar H_2. The mixture has decomposed into $MgNi_{2.5}B_2$, Mg_2Ni and Mg. In fact, a broad peak of hydrogenation can be detected, upon cooling, below 300 °C to form $Mg_2NiH_{0.3}$ and MgH_2. In the 3rd cycle (**Figure 86b, 3rd cycle**), no transitions from LiK eutectic and Mg_2NiH_4 are observed, endorsing their decomposition. Hydrogen release is observed in a broad peak around 292 °C, related to the hydrogen release from $Mg_2NiH_{0.3}$, and above 310 °C, related to decomposition of MgH_2. In this case, the hydrogen release temperature of the RHC mixture is lower of about 10 °C compared to the MgNiLi system. Upon cooling, the Mg hydrogenation peak is more defined in the 3th cycle because of a possible activation upon previous thermal cycling.

$Mg_2NiH_{0.3}$, MgH_2 and $MgNi_{2.5}B_2$ are present in the PXD pattern after DSC (**Figure 86a, after DSC**), together with an unknown phase. The XRD peak positions of this unknown phase correspond to those observed after decomposition of the Mg_2NiH_4-$Ca(BH_4)_2$ system.[252] The presence of KBH_4 in the mixture suggests that not all the borohydride present in the mixture has been decomposed upon

thermal cycling. So, from the liquid eutectic mixture of borohydrides, only $LiBH_4$ actively reacts with Mg_2NiH_4, whereas the most stable KBH_4 remains unaffected.

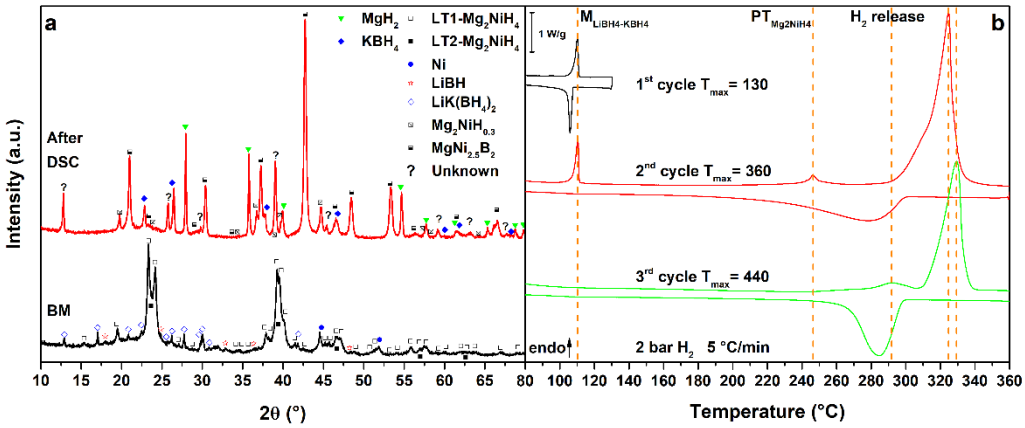

Figure 86 – (a) PXD of the ball milled MgNiLiK (black, down) and after cycling in HP-DSC (red, up); b) HP-DSC cycling of MgNiLiK at 5 °C/min under a static pressure of 2.2 bar of H_2.

Mg_2NiH_4– $LiBH_4$–$NaBH_4$ eutectic composition

Figure 87 presents the results obtained for the MgNiLiNa system. Upon heating in the 1st cycle (**Figure 87b, 1st cycle**), we observe the polymorphic transition of $LiBH_4$ at T_{peak}= 98 °C, stabilized for the presence of $NaBH_4$,[124] and the melting of the LiNa eutectic at T_{peak}= 228 °C. Both phase transformations are reversible and slightly undercooled on cooling. In the 2nd cycle (**Figure 87b, 2nd cycle**), after the previous phase transformations, also the polymorphic transition of Mg_2NiH_4 is observed at T_{peak}= 246 °C, followed by the main hydrogen release from the RHC mixture at T_{peak}= 327 °C under 2.7 bar H_2. The RHC mixture decomposes similarly to the MgNiLiK system, and on cooling, Mg_2Ni and Mg are hydrogenated to form $Mg_2NiH_{0.3}$ and MgH_2 below 302 °C. In the 3rd cycle (**Figure 87b, 3rd cycle**), previous transitions from LiNa and Mg_2NiH_4 are hardly visible, confirming their decomposition. In fact, the hydrogen release from $Mg_2NiH_{0.3}$ and MgH_2 are observed at T_{peak}= 290 °C and 331 °C, respectively. No improvement in the hydrogenation of Mg can be seen on cooling in the 3th cycle. In comparison to the starting components, the hydrogen release temperature of the RHC mixture has not been lowered by the substitution of KBH_4 with $NaBH_4$.

The decomposition products of the MgNiLiNa system are similar to those of MgNiLiK, as evidenced by the PXD analysis (**Figure 87a, after DSC**). Even in this case, the most stable $NaBH_4$ borohydride is still present after thermal cycling.

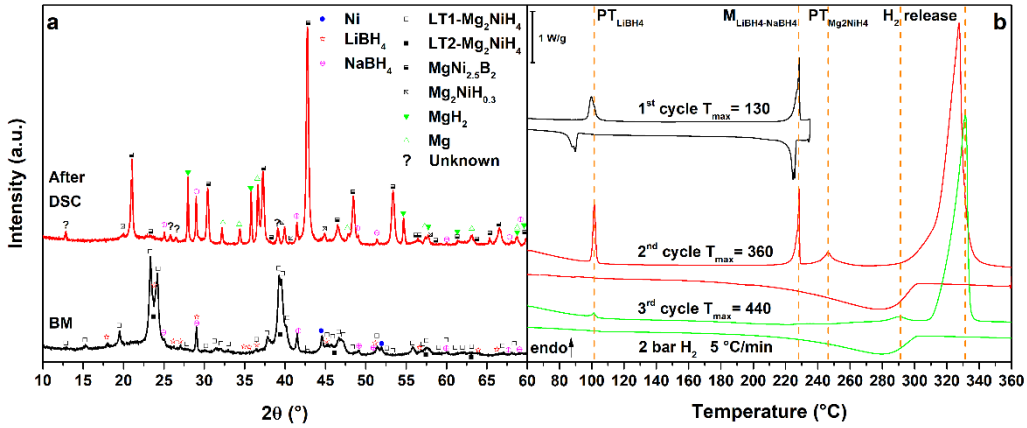

Figure 87 – (a) PXD of the ball milled MgNiLiNa (black, down) and after cycling in HP-DSC (red, up); b) HP-DSC cycling of MgNiLiNa at 5 °C/min under a static pressure of 2.2 bar of H_2.

Mg_2NiH_4– $LiBH_4$–$Mg(BH_4)_2$ eutectic composition

Results obtained for the MgNiLiMg system are shown in **Figure 88.** In the 1st cycle (**Figure 88b, 1st cycle**), the polymorphic transition of $LiBH_4$ is observed as a broad peak at T_{peak}= 111 °C, followed by the melting of the eutectic at T_{peak}= 176 °C. Upon cooling the crystallization of the eutectic is not clearly detected, possibly because some $Mg(BH_4)_2$ has already reacted, enriching the $LiBH_4$ fraction in the composition of the borohydride mixture.[44,202,203] In fact, the DSC peak due to the $LiBH_4$ phase transformation appears more intense on cooling with respect to that observed on heating. As a consequence, in the 2nd cycle (**Figure 88b, 2nd cycle**), the polymorphic transition of $LiBH_4$ is more defined and the LiMg eutectic melting is hardly detected as a broad peak. At higher temperatures, the Mg_2NiH_4 polymorphic transition is detected at T_{peak}= 246 °C, together with a small peak of hydrogen release from the liquid borohydride, as previously observed in the literature.[50] Furthermore, the main hydrogen release from the RHC mixture starts above 290 °C under 2.7 bar H_2 (T_{peak}= 336 °C). In this temperature range, the decomposition of $Mg(BH_4)_2$ is also expected.[34] On the other hands, after the decomposition of the mixture, $MgNi_{2.5}B_2$ and Mg are expected to be formed, so that the decomposition of $Mg(BH_4)_2$ to Mg, B and H_2 is limited. Upon cooling in the 2nd cycle, a broad hydrogenation peak is observed at T_{peak}= 260 °C related to the formation of MgH_2. Actually, in the 3rd cycle **(Figure 88b, 3rd cycle**), no peaks related to $LiBH_4$ or Mg_2NiH_4 phase transformations are observed, but several peaks related to hydrogen release are observed above 231 °C, in a

complex multi-steps reaction (T_{peak}= 302 °C, 315 °C and 323 °C). These peaks are related to the full decomposition of residual $Mg(BH_4)_2$,[34] together with hydrogen release from $Mg_2NiH_{0.3}$ and MgH_2. Hydrogenation of Mg_2Ni and Mg is clearly observed upon cooling below 300 °C. Finally, in the 4th cycle (**Figure 88b, 4th cycle**), only hydrogen release peaks from $Mg_2NiH_{0.3}$ (T_{peak}= 293 °C) and MgH_2 (T_{peak}= 317 °C) are observed and, during cooling, a peak related to hydrogenation can be detected again below 297 °C.

The decomposition products detected in the PXD patter after thermal cycling (**Figure 88a, after DSC**) are always the same, as observed for the MgNiLiK and MgNiLiNa systems. However, in this case, no traces of residual borohydrides are observed, suggesting the full reaction of $Mg(BH_4)_2$. It is worth to note that the intensity of the diffraction peaks of the unknown phase is higher with respect to the previous systems. The high content of Mg and B in this system suggests that the unknown phase could be related to the Mg-Ni-B system.

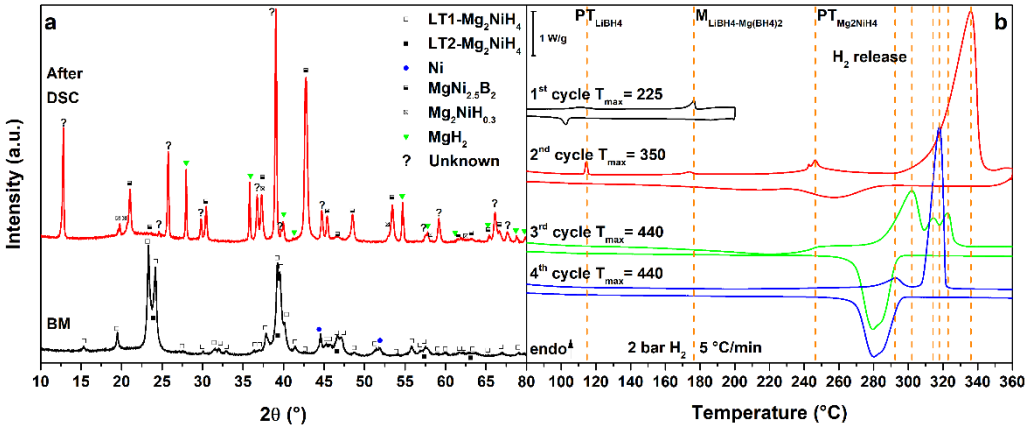

Figure 88 – (a) PXD of the ball milled MgNiLiMg (black, down) and after cycling in HP-DSC (red, up); b) HP-DSC cycling of MgNiLiMg at 5 °C/min under a static pressure of 2.2 bar of H_2.

Mg_2NiH_4– $LiBH_4$–$Ca(BH_4)_2$ eutectic composition

Finally, the results obtained for the MgNiLiCa system are reported in **Figure 89**. The DSC trace of the 1st cycle (**Figure 89b, 1st cycle**) presents the polymorphic transition of $LiBH_4$ at T_{peak}= 115 °C, the polymorphic transition of $Ca(BH_4)_2$ at T_{peak}= 150 °C and the melting of the LiCa eutectic at T_{peak}= 202 °C. Only the polymorphic transition of $Ca(BH_4)_2$ cannot be observed by DSC on cooling, because of sluggish kinetics.[173] In the 2nd cycle (**Figure 89b, 2nd cycle**), all the previous transitions of the LiCa system are observed. At higher temperatures, the

polymorphic transition of Mg_2NiH_4 is detected at T_{peak}= 243 °C, together with a small peak of hydrogen release from the liquid borohydride, as previously observed in the MgNiLiMg system and in the literature.[256] Furthermore, a DSC endothermic peak due to hydrogen release starts above 300 °C (T_{peak}= 332 °C), under 2.7 bar H_2, so that heating has been stopped at 350 °C, in order to separate hydrogen release reactions. The DSC exothermic DSC peaks due to hydrogenation reactions of Mg_2Ni and Mg can be observed on cooling below 304 °C. In the 3rd cycle (**Figure 89b, 3rd cycle**), no peaks from the LiCa system are observed, suggesting the occurrence of reactions between Mg_2NiH_4 and the borohydride mixture in the previous cycle. A DSC peak at T_{peak}= 298 °C is clearly related to the hydrogen release from $Mg_2NiH_{0.3}$, followed by the decomposition of MgH_2 and, at higher temperatures, by the decomposition of $Ca(BH_4)_2$ to CaH_2 up to 440 °C. In fact, in the 4th cycle (**Figure 89b, 4th cycle**), the decomposition of the $Mg_2NiH_{0.3}$ is hardly observed, but the decomposition of MgH_2 is clearly occurring at T_{peak}= 335 °C. During cooling, a broad peak of hydrogenation can be detected below 304 °C both in the 3rd and 4th cycle.
CaH_2 is observed, in addition to the previously observed mixture decomposition products, in the PXD pattern after cycling (**Figure 89a, after DSC**).

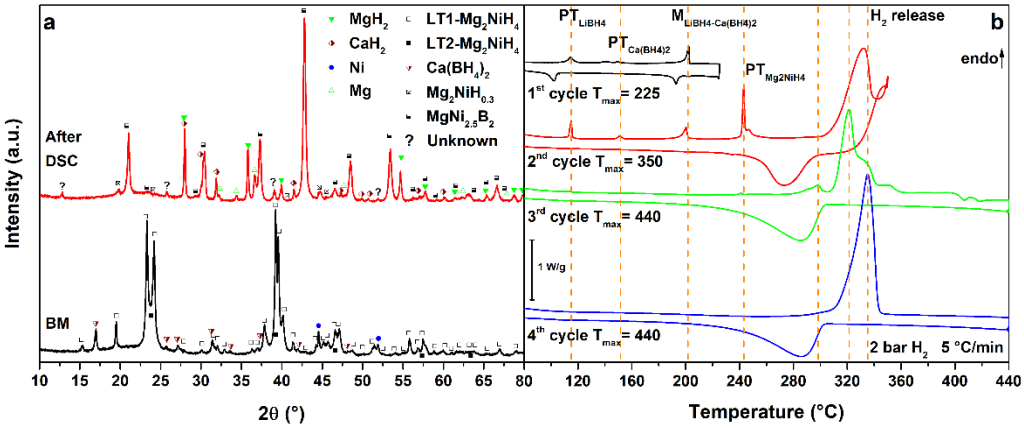

Figure 89 – (a) PXD of the ball milled MgNiLiCa (black, down) and after cycling in HP-DSC (red, up); b) HP-DSC cycling of MgNiLiCa at 5 °C/min under a static pressure of 2.2 bar of H_2.

Discussion

The results obtained in this work for the Mg_2NiH_4 and the Mg_2NiH_4–$LiBH_4$ (MgNiLi) system are in good agreement with previous studies reported in the literature.[239,243,249]

Table 15 – Peak temperatures of transitions and reactions for all the investigated systems (H: heating, C: cooling, PT: polymorphic transition, M: melting, Cr: crystallization). Part I.

			PT	PT	M/Cr	PT	H_2 Release				H_2 Uptake
System	Cycle	Ramp	$LiBH_4$	$Ca(BH_4)_2$	MBH_4	Mg_2NiH_4	MBH_4	$Mg_2NiH_{0.3}$	MgH_2	RHC	
MgNi	**1**	**H**				244					
	1	**C**				234					
	2	**H**				243				372	
	2	**C**									<235
	3	**H**				242		296	303		
	3	**C**									<235
MgNiLi	**1**	**H**	117								
	1	**C**	98								
	2	**H**	115			245					
	2	**C**	104			226					
	3	**H**	115		279	238					
	3	**C**	102		265	227					
	4	**H**	113		271	238				308	
	4	**C**				228					
	5	**H**				238			302	335	
	5	**C**									<307
MgNiLiK	**1**	**H**			110						
	1	**C**			106						
	2	**H**			110	246				325	
	2	**C**									<300
	3	**H**						292	329		
	3	**C**									<300
MgNiLiNa	**1**	**H**	98		228						
	1	**C**	90		226						
	2	**H**	102		228	246				327	
	2	**C**									<302
	3	**H**	101					290	331		
	3	**C**									<302

Mg_2NiH_4 releases hydrogen under 2.7 bar of H_2 at relatively high temperature (T_{peak}= 372 °C) and it is partially hydrogenated to $Mg2NiH_{0.3}$ on cooling. However, this temperature can be lowered by the addition of $LiBH_4$. In fact, in the RHC mixture MgNiLi, the release of hydrogen, under a backpressure of 2.7 bar, starts above 330 °C. Compared with the pristine compounds, their mixture leads to a release of hydrogen at lower temperature for both $LiBH_4$ and Mg_2NiH_4 to form $MgNi_{2.5}B_2$, Mg_2Ni and Mg.

Mg_2NiH_4 was then mixed with all the binary eutectic composition of $LiBH_4$ and $M(BH_4)_x$ (M = Na, K, Mg, Ca). In all systems, the decomposition of both $LiBH_4$

and Mg_2NiH_4 is evidenced by a broad DSC peak, localized around T_{peak}=320-330 °C. Upon cooling, in the present conditions, the decomposed samples, in all RHC studied mixtures, can be re-hydrogenated to form $Mg_2NiH_{0.3}$ and MgH_2. In further thermal cycles, two decomposition peaks are observed, related to $Mg_2NiH_{0.3}$ and MgH_2 hydrogen release, respectively. **Table 15** and **16** summarize the peak temperatures of transitions and reactions for all the investigated systems.

Table 16 – Peak temperatures of transitions and reactions for all the investigated systems (H: heating, C: cooling, PT: polymorphic transition, M: melting, Cr: crystallization). Part II.

			PT	PT	M/Cr	PT	H_2 Release				H_2 Uptake
System	Cycle	Ramp	$LiBH_4$	$Ca(BH_4)_2$	MBH_4	Mg_2NiH_4	MBH_4	$Mg_2NiH_{0.3}$	MgH_2	RHC	
MgNiLiMg	1	H	111		176						
	1	C	103								
	2	H	114		174	246	243			336	
	2	C									<286
	3	H					>231				
	3	C									<297
	4	H						293	317		
	4	C									<297
MgNiLiCa	1	H	115	150	202	243	246				
	1	C	102		193						
	2	H	115	151	200	241	>306			332	
	2	C									<304
	3	H					> 290				
	3	C									<304
	4	H								335	
	4	C									<304

All the systems investigated in this work present the decomposition of borohydrides from the liquid state, which appears to play a role on the temperature of decomposition of the RHC mixtures. When only $LiBH_4$ is present, the decomposition peak is at a slightly higher temperature with respect to RHC mixtures containing eutectic borohydrides mixtures, though it does not change significantly in all different systems. When a highly stable borohydride (i.e. $NaBH_4$ and KBH_4) is present in the eutectic mixture, only $LiBH_4$ plays and active role in the mixture and the RHC mixture does not decompose completely, so that the stable borohydride is still present in the decomposition products after thermal cycling. On the other hand, if an alkali-earth borohydride (i.e. $Mg(BH_4)_2$ and

$Ca(BH_4)_2$) is mixed with $LiBH_4$ to form an eutectic, the liquid phase fully decomposes, namely at lower temperature if compared to the pure eutectic mixture alone, but complex multi-steps reaction are taking place.
In all systems, when the borohydrides and the Mg_2NiH_4 decompose, they always react to form $MgNi_{2.5}B_2$ and Mg. The presence of an unknown decomposition product has also been observed in all RHC mixtures with eutectic borohydride mixtures. The low backpressure applied in this case is not high enough to form back the starting borohydrides, though it is able to hydrogenate the decomposed Mg_2Ni and Mg to form the $Mg_2NiH_{0.3}$ and MgH_2.
The decomposition temperatures in investigated systems have not been lowered significantly compared to previous studies of Mg_2NiH_4-MBH_4 mixtures. In fact, the hydrogen release temperature is still far from ambient conditions. A full rehydrogenation has not been obtained because of the limited H_2 pressure applied in the experimental conditions. As for previous studied mixtures,[249–253] a hydrogen pressure of 100 bar is expected to fully rehydrogenate the systems. The nanoconfinement of the studied mixtures into nanoporous scaffold to obtain nanostructured materials[46,49,50,54,244–247,253] might be explored to improve the thermodynamics and kinetics of hydrogen sorption reactions.

Conclusions

In this study, RHC systems obtained by mixing Mg_2NiH_4 and eutectic mixtures of borohydrides have been investigated, to explore possible improvements in hydrogen release properties of those systems.
In the investigated RHC mixtures, when $LiBH_4$ is in eutectic mixture with borohydrides that contain stable single charged metal cation, a slight improvement in the decomposition temperature of the RHC mixture is observed, but a leftover of the more stable borohydrides is detect after cycling.
The presence of double charged metal cation in the eutectic mixture causes a full decomposition of the borohydrides in complex multi-steps reactions. The presence of a stable liquid at low temperature promotes the decrease of the hydrogen release temperature, if compared to that of pure Mg_2NiH_4.

Chapter 7 – Conclusions and Outlook

The studies performed during this PhD project were focused on the determination of thermodynamic properties of complex hydrides for energy storage applications. The definition of properties-structures relations is a milestone to understand and further develop these materials. Thermodynamic properties and their implication in decomposition reactions and material stability enable the full description and understanding of complex systems and mixtures. The stability and energies involved in the decomposition process are key parameters to be considered for a real application of these systems in energy storage, taking into account the full life cycle assessment of the compounds and devices.

The studies performed during this PhD project were carried out at the Department of Chemistry of the University of Turin, under the supervision of Prof. Marcello Baricco, aims to accurately determine thermodynamic properties of complex hydrides, especially boron-compounds as borohydrides and closoboranes, in wide composition, temperature and pressure ranges to fill the lack of thermodynamic data of those systems. The study involved thermodynamics and theoretical assessment and development of databases for thermodynamic calculations.

Heat capacities of borohydrides were experimentally determined and assessed. This study enable the description of their thermodynamics as a function of temperature. The implementation of their database allow the exploration of more complex systems to further understand their role in hydrogen storage applications, heat storage in thermal solar concentration plans, and as solid-state electrolytes. This determination is fundamental for a deep understanding of the thermodynamics of hydrogen release and uptake reactions and to develop and design new promising solid-state hydrogen storage systems, solid-state electrolytes or for concentrating solar thermal power energy storage.

The thermodynamics of boron-based compounds and systems was extensively evaluated. In this study, computation and experiments are important companion. For this reason, the performed experiment were assessed by the use of computation thermodynamics software such as Thermo-Calc (based on the Calphad approach) and *ab-initio* calculation (DFT) of thermodynamic properties, using the CRYSTAL code (in collaboration with the theoretical and computational chemistry group).

The results clarify the bond between values of thermodynamic properties and chemical properties of those systems. The combination of the thermodynamic and mechanical properties with the chemistry of boron-based material will further

improve their application as solid-state hydrogen storage materials and open the way and the understanding of structure-properties relationships in the use of those materials in other possible new applications that have been cited above.

Complex hydrides are characterized by a cationic and an anionic sublattice, as expected for ionic compounds. Solubility of complex hydrides in the solid state can be obtained in a single or in both sublattices. Generally, complex hydrides shows different crystal structures at room temperature and often are subjected to polymorphic phase transitions upon heating, eventually leading to melting before decomposition. Mixtures of complex hydrides may show the formation of solid solutions, i.e. cationic or anionic fully disordered structures. On the other hand, as already described before, they can form compounds, i.e. cationic or anionic ordered structures. These compounds can be bimetallic, trimetallic or multimetallic, and they can show different anions in the structure. A systematic description of compounds observed upon mixing complex hydrides is reported in [25]. In case of immiscibility among complex hydrides, an eutectic melting can be observed. Full solubility is generally observed for complex hydrides in the liquid phase.
Solubility may be represented by the enthalpy and entropy of mixing. In the case of a regular solution model, the enthalpy of mixing can be easily represented by a single interaction parameter. In the solid state, it is related to the crystal structure and corresponding coordination of parent compounds. In the liquid phase, the occurrence of a short-range order may promote the formation of solutions. In all cases, phase diagrams of complex hydrides provide information on solubility in solid phases, as well as in the liquid. In this conclusion chapter, an overview of solubility in both cationic and anionic sublattices for borohydrides will be presented and the role of chemical bonds and coordination in the crystal structure will be highlighted.

Interaction in the solid state

Binary combinations between borohydrides or with halides have been extensively investigated, showing the formation of solid solutions, resulting from cationic [46,124,257,258] or anionic [55–63] substitutions, as well as hydrogen-fluorine exchange [64,65,67,259]. For some binary and ternary mixtures of borohydrides, corresponding thermodynamic properties and phase diagrams have been recently assessed allowing the determination of the enthalpy of mixing in solid and liquid phases.[124,204]

Examples of cationic solid solutions in borohydrides are limited to the $Mg(BH_4)_2$-$Zn(BH_4)_2$,[257] $Mg(BH_4)_2$-$Mn(BH_4)_2$,[258] $LiBH_4$-$NaBH_4$[124] and $NaBH_4$-KBH_4[172] systems. In other cases, a nearly full immiscibility is observed [36,42,44,49,54,173,202,203], suggesting structural and electronic constrains in the formation of solid solution in cationic sublattice in the case of borohydrides.

Considering the $LiBH_4$-$NaBH_4$-KBH_4 system, $LiBH_4$ can form a cubic phase with limited solid solubility in $NaBH_4$ and KBH_4. As a consequence, a positive interaction parameter of 5887 J/mol and 10000 J/mol, respectively, has been assessed.[204] In the $NaBH_4$-KBH_4 system, the assessed interaction parameter for the cubic phase turns out to be equal to 7893 J/mol, which explains the occurrence of a full solubility at high temperatures, but a miscibility gap at room temperature. No solid solutions have been observed in the orthorhombic and hexagonal phase, resulting in a high positive interaction parameter in the solid state, except for the $LiBH_4$-$NaBH_4$ system where an ideal behaviour have been observed with an extensive dissolution of $NaBH_4$ in the hexagonal phase. The higher solubility in the hexagonal phase with respect to the orthorhombic one is likely related to structural factors, such as the higher available free volume, fast reorientation of the BH_4^- anion and more favourable coordination in the hexagonal structure than in the orthorhombic one, allowing easy cationic exchange and motion.

The investigation of a quinary borohydride mixture showed a limited interaction of the different borohydrides in the $LiBH_4$-$NaBH_4$-KBH_4-$Mg(BH_4)_2$-$Ca(BH_4)_2$ system in the solid phase.[144]

Figure 90 A resumes available information on the results of cations interactions in the solid phase in the $LiBH_4$-$NaBH_4$-KBH_4-$Ca(BH_4)_2$-$Mg(BH_4)_2$ system. It can be observed that in addition of the previously reported interaction no miscibility is observed in other binary or higher combination. Thus, KBH_4 strongly interact with other borohydrides to form bimetallic compound or solid solution.

An anionic substitution of the BH_4^- group by halides is widely favoured in binary systems. In $LiBH_4$-$LiBr$[61] and $LiBH_4$-LiI,[56] hexagonal solid solution are stable at room temperature and they have been widely explored and characterized. A limited orthorhombic solid solution is present in the $LiBH_4$-$LiBr$ system, while possible solid solutions in the cubic structure have never been characterized in details. In the $LiBH_4$-$LiCl$ system,[62,63] no significant solubility in the orthorhombic phase is evidenced, while in the hexagonal phase limited solubility is detected at high temperature. A solubility in the solid state is confirmed for many binary systems between borohydrides and metal halides: $NaBH_4$-$NaCl$,[57,60] $NaBH_4$-$NaBr$,[260] $Ca(BH_4)_2$-$CaCl_2$,[58] $Ca(BH_4)_2$-CaI_2[58,59], $Mg(BH_4)_2$-$MgCl_2$[55], $Mg(BH_4)_2$-

$MgBr_2$[55]. In case of metal borohydride-borofluorides composites, MBH_4-MBF_4, M = Li, Na, K, a hydrogen-fluorine exchange occurs and short-lived $MBH_{4-x}F_x$ are formed, but fast decomposition to metal fluoride, diborane and *closo*-borane is observed.[64,65,67,259]

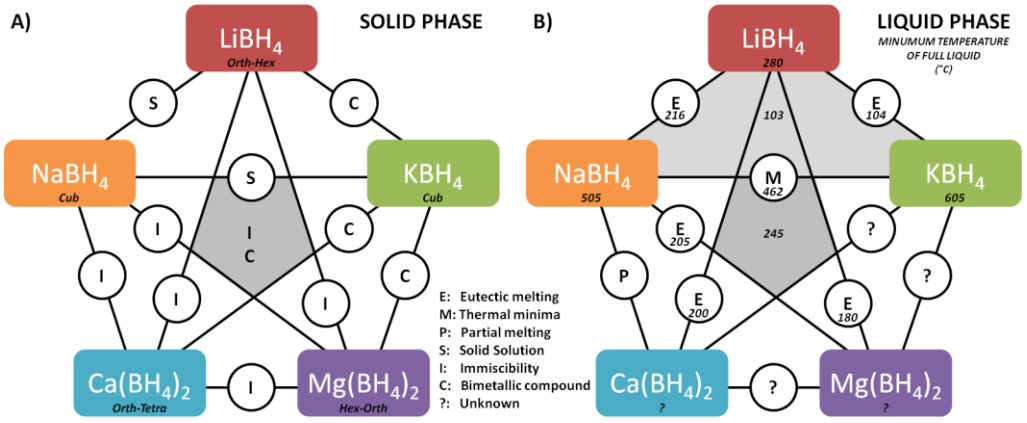

Figure 90 – Summary on the cation interactions in the LiBH4-NaBH4-KBH4-Mg(BH4)2-Ca(BH4)2 system, both in the solid (a) and liquid (b) phases. In Fig. 4a, crystal structures of pure borohydrides, showing allotropic transformations, and results of interactions are reported. In Fig. 4b, melting temperature of pure borohydrides, as well as minimum temperature for the existence of a pure liquid in mixtures, are reported, together with the description of the melting reactions.

Interaction in the liquid state

The enthalpies of mixing of the liquid phase for the assessed systems based on borohydrides[124,204] shows negative or low positive values, suggesting an attractive interaction among different borohydrides in the liquid phase. Experimental values of the enthalpy of mixing are hard to be measured and the lack of information for such important thermodynamic properties leave a gap in the full description of thermodynamics of these systems. However, by the Calphad approach, borohydride systems can be assessed taking into account different contribution to the excess Gibbs free energy, can be described in the whole temperature, pressure and compositional range. In the case of an ideal solution model, the enthalpy of mixing for a solution is equal to zero. If an ideal behaviour for both solid and liquid phases is considered for a binary A-B system, the enthalpy of mixtures is the weighted average of that of pure components. As a consequence, the enthalpy of melting varies linearly, as a function of composition, between those of pure components. Neglecting the temperature dependence of enthalpy,

the deviation from the ideal behaviour of the liquid phase can be outlined by a simple thermodynamic cycle, if the solid solutions are taken as ideal. In fact, the enthalpy of mixing for the liquid phase (ΔH_{mix}) can be estimated from the difference between the enthalpy of melting of the AB mixture (ΔH_{mAB}) and of the weighted average of that of pure components (ΔH_{mA} and ΔH_{mB}):

$$\Delta H_{mix} = \Delta H_{mAB} - x_A \Delta H_{mA} - x_B \Delta H_{mB} \quad \boldsymbol{Eq}.27$$

where x_A and x_B are the molar fractions of the A and B components, respectively. The regular solution model defines the enthalpy of mixing as a function of composition for a binary A-B system by the equation:

$$\Delta H_{mix} = x_A x_B \Omega \quad \boldsymbol{Eq}.28$$

where Ω is the interaction parameter, which can be easily estimated according to:

$$\Omega = \frac{\Delta H_{mAB} - x_A \Delta H_{mA} - x_B \Delta H_{mB}}{x_A x_B} \quad \boldsymbol{Eq}.29$$

By the integration of the DSC signal of the melting reactions in mixtures of borohydrides, the enthalpy change from solid to liquid phases can be measured. So, possible interactions in the liquid phase can be evidenced and the value for the enthalpy of mixing can be estimated. For binary systems showing thermal minima (e.g. $NaBH_4$-KBH_4), the solid solution can be considered as ideal.
In case of a eutectic melting (e.g. $LiBH_4$-$NaBH_4$ and $LiBH_4$-KBH_4) the solid phases can be considered fully immiscible, so that the enthalpy of the solid mixture is obtained by averaging that of that of pure components.
The Calphad method allows assessment of these parameters using a least square method and taking into account all available data on the system or pure compound from the available database or new experimental data.[34] Following the thermodynamic cycle described above, an estimation of the interaction parameter Ω for the liquid phase in the $LiBH_4$-$NaBH_4$-KBH_4 system is reported in **Table 17** and it is compared with assessed values.
For the $LiBH_4$-$NaBH_4$ the assessed and estimated values of Ω have a reasonable agreement, being both negative, confirming the presence of a strong interaction in the liquid phase. For the $LiBH_4$-KBH_4 system, estimated value is positive, whereas the assessed on is strongly negative.

Table 17 – Experimental (ΔH_{mEXP}) and assessed (ΔH_{mASS}) values (in J/mol) for the enthalpy of melting in pure and mixed borohydrides. Assessed (Ω_{ASS}) and estimated (Ω_{EST}) values (in J/mol) of the interaction parameters for the liquid phase, according the regular solution model.

Composition	ΔH_{mEXP}	ΔH_{mASS}	Ω_{ASS}	Ω_{EST}
$LiBH_4$		7200		
$NaBH_4$		16900		
KBH_4		19200		
0.70$LiBH_4$ 0.30$NaBH_4$	6990	6520	-19604*	-14857
0.725$LiBH_4$ 0.275KBH_4	11025	9828	-13016	2633
0.682$NaBH_4$ 0.318KBH_4	17028	15331	1056	-2782

(*) A temperature dependency and sub-regular model were used to describe the LiBH4-NaBH4 system. The reported values have been recalculated as if the system was described by a regular model.

The observed discrepancy can be due to an overestimation of the assessed value, as evidenced by the lower value of ΔH_{mASS} with respect to ΔH_m. In addition, because of the presence of a deep eutectic, a temperature dependence of thermodynamic properties may play a role. Finally, for the $NaBH_4$-KBH_4 system, both Ω_{ASS} and Ω_{EST} are close to zero and the deviation from the ideality of the cubic solid solution can explain the observed discrepancy. Even if the estimated values can provide a first hint on the enthalpy of mixing for the liquid phase, the assessed value are more reliable, because they take into account possible variation of enthalpy as a function of temperature and possible deviations for ideality of the solid solutions.

For the quinary $LiBH_4$-$NaBH_4$-KBH_4-$Mg(BH_4)_2$-$Ca(BH_4)_2$ borohydride mixture, a multi-cation liquid phase has been observed for the first time, underling a strong interaction among borohydrides that could be related both to strong negative enthalpy of mixing or entropy effects.[144]

Figure 90 B summarizes the melting reactions occurring in the $LiBH_4$-$NaBH_4$-KBH_4-$Ca(BH_4)_2$-$Mg(BH_4)_2$ system, evidencing the lowest temperature for the occurrence of a single liquid phase.

Generally, in the liquid phase, a full solubility in the cation sublattice is observed, with a stabilization of the liquid mixture with respect to pure liquid borohydrides, as evidenced by the occurrence of eutectics or thermal minima.

Conclusions and Outlook

In borohydride mixtures, all binary multi-cationic systems investigated so far shown a stabilisation of the liquid phase, forming eutectic mixtures with negative or low positive enthalpy of mixing of the liquid phase. Meanwhile, binary multi-anionic system of borohydrides and halides evidenced a strong interaction in the solid phases, while no eutectic have been reported. It can be concluded that, in borohydride systems, the cationic and anionic sublattices play a different role in the interaction in solid and liquid phase upon mixing. Their thermodynamics is strongly related to structures, coordination number, temperature, enthalpy and entropy of the transitions.
The stability of a phase is related to the reciprocal interaction among the ionic sublattices and electronegativity of the ions involved in the structure. As reported before, in the case of anionic substitutions, the formation of a solid solution is favoured, which may indicate that the anionic sublattices of borohydrides is characterized of equivalent sites, which can host randomly different anions with similar size. Nevertheless, the cation sublattices is more related to its characteristic coordination number, limiting the formation of solid solutions, but allowing destabilizing the sublattices towards a liquid phase. The stabilisation of the liquid phase at low temperature can be partially understood taking into account a variation of the charge distribution in the physical mixture of different borohydrides. Short-range order and entropy could play a role as well in the formation of a multi-cation liquid phase, which should be further investigated.
A detailed description of the structure and thermodynamics of the liquid phase in borohydrides is still missing. Experimental values of thermodynamic properties of eutectics and liquid borohydrides would be of interest to further understand the role of the liquid in the thermal decomposition or hydrogen release reactions.
The hydrogen release properties strongly depend on the interaction between the two sublattices, mainly taking into account the variation of the B-H bond strength. For this reason, a detailed study of the thermodynamics and structures of both solid and liquid phase in borohydride mixtures should be carefully deepen to further develop and tailor the hydrogen storage properties in complex hydrides.

To conclude and resume, during this PhD project, the $LiBH_4$-$NaBH_4$-KBH_4 ternary system was deeply investigated, combining experimental and theoretical investigations. The Calphad method was used to assess the thermodynamics of $LiBH_4$-$NaBH_4$, $LiBH_4$-KBH_4 and $NaBH_4$-KBH_4 pseudo binary systems, as well as a full investigation and assessment of the ternary system. The evaluation of the

hydrogen release reactions from different mixtures in the system was not deeply investigated. A prediction of the decomposition reactions in the system can be done with the current optimised database. However, it should be coupled with experimental evaluation of these reactions. Further studies can be performed and would be of interest.

Extended experimental investigations of the interaction between borohydrides in equimolar ratio in ternary or higher mixtures (up to quinary) were performed. Furthermore, the MgCa binary system, which description was still missing, was characterized in function of temperature and composition.

This study could be further expanded considering different borohydrides, which have not been taken into account, or by the understanding of the correct composition of new eutectic mixtures and solid solutions. These mixtures can be used for the production of other single-crystal borohydrides with the flux-assisted method[261] or for melt infiltration in nanoporous scaffolds. Eutectic mixtures of borohydrides could be of interest because liquid hydrogen carries can allow fast refuelling of cars and the stabilisation of the liquid state down to room temperature could be a direction of possible future investigations (i.e. other mixtures to obtain ionic liquids).

Eutectic mixtures of borohydrides have been mixed with Mg_2NiH_4 to form reactive hydride composite and tailor their hydrogen storage properties to improve hydrogen release temperatures and cyclability. However only a slight improvement of the hydrogen release reactions have been evidenced.

The study of the structure of liquid borohydrides and eutectic mixture should be integrated with PDF measurements on the liquid to further understand the role of a short-range order in these compounds. The study is currently on going in collaboration with Dr. Mauro Coduri in ESRF.

The heat capacity of some borohydrides have been experimentally determined, and an insight on different polymorphs of closoboranes have been performed studying the polymorphic transition mechanism and enthalpies by HP-DSC.

Those values are important and useful information for the thermodynamic assessment of these compounds. Correlation and structure-properties relation have been evidences and discussed. The heat capacities and vibrational study of closoborane would be of interest for a complete description of these promising compounds.

In conclusion, it has been demonstrated that a combined use of *ab-initio* (in collaboration with Dr. Marta Corno and Prof. Piero Ugliengo, at the University of Piemonte Orientale and Turin) and Calphad thermodynamic calculations, supported and confirmed by experimental measurements (in collaboration with

Prof. Michele Chierotti and Prof. Giuseppe Spoto for the spectroscopies analysis, at the University of Turin), especially *in-situ* techniques, is a powerful tool for a complete description of thermodynamic properties of mixtures of borohydrides. The proficient results from this PhD project have been possible thanks to a wide scientific network and many international collaborations. It must be underlined how much is important to support international collaborations and efforts in basic research to further enlarge the knowledge on these topics and to further tailor and improve those systems for real applications.

Further research must be directed towards accurately measuring the properties and suitability of complex hydrides, since preliminary techno-economic investigations demonstrate high potential and competitiveness for thermal energy systems based on metal hydrides materials compared with traditional molten salt systems (cost of 25–30 $/kWhth for currently available metal hydrides materials against 30–32 $/kWhth for molten salt systems).[128]

References

(1) Armaroli, N.; Balzani, V. The Future of Energy Supply: Challenges and Opportunities. *Angew. Chemie Int. Ed.* **2007**, *46* (1–2), 52–66.

(2) Züttel, A.; Remhof, A.; Borgschulte, A.; Friedrichs, O. Hydrogen: The Future Energy Carrier. *Philos. Trans. R. Soc. A Math. Phys. Eng. Sci.* **2010**, *368* (1923), 3329–3342.

(3) UNDP, Human Development Report. **2014**.

(4) Gender and Climate Change - Thematic Issue Briefs and Training Modules (accessed July 2018) http://www.undp.org/content/undp/en/home/librarypage/womens-empowerment/gender-and-climate-change.html.

(5) Arora-Jonsson, S. Virtue and Vulnerability: Discourses on Women, Gender and Climate Change. *Glob. Environ. Chang.* **2011**, *21* (2), 744–751.

(6) Wong, S. Can Climate Finance Contribute to Gender Equity in Developing Countries? *J. Int. Dev.* **2016**, *28* (3), 428–444.

(7) Shankar, A. Strategically Engaging Women in Clean Energy Solutions for Sustainable Development and Health. *Glob. Sustain. Dev. Rep. Br.* **2015**.

(8) Carlsson-Kanyama, A.; Lindén, A.-L. Energy Efficiency in Residences—Challenges for Women and Men in the North. *Energy Policy* **2007**, *35* (4), 2163–2172.

(9) Rehman, S.; Al-Hadhrami, L. M.; Alam, M. M. Pumped Hydro Energy Storage System: A Technological Review. *Renew. Sustain. Energy Rev.* **2015**, *44*, 586–598.

(10) Armaroli, N.; Balzani, V. The Hydrogen Issue. *ChemSusChem* **2011**, *4* (1), 21–36.

(11) Lai, Q.; Paskevicius, M.; Sheppard, D. A.; Buckley, C. E.; Thornton, A. W.; Hill, M. R.; Gu, Q.; Mao, J.; Huang, Z.; Liu, H. K.; et al. Hydrogen Storage Materials for Mobile and Stationary Applications: Current State of the Art. *ChemSusChem* **2015**, *8* (17), 2789–2825.

(12) Peter, S. C. Reduction of CO2 to Chemicals and Fuels: A Solution to Global Warming and Energy Crisis. *ACS Energy Lett.* **2018**, 1557–1561.

(13) Kato, S.; Matam, S. K.; Kerger, P.; Bernard, L.; Battaglia, C.; Vogel, D.; Rohwerder, M.; Züttel, A. The Origin of the Catalytic Activity of a Metal Hydride in CO2 Reduction. *Angew. Chemie* **2016**, *128* (20), 6132–6136.

(14) Ley, M. B.; Jepsen, L. H.; Lee, Y.-S. S.; Cho, Y. W.; Bellosta von Colbe, J. M.; Dornheim, M.; Rokni, M.; Jensen, J. O.; Sloth, M. M.; Filinchuk, Y.; et al. Complex Hydrides for Hydrogen Storage – New Perspectives. *Mater. Today* **2014**, *17* (3), 122–128.

(15) Møller, K.; Sheppard, D.; Ravnsbæk, D.; Buckley, C.; Akiba, E.; Li, H.-W.; Jensen, T. Complex Metal Hydrides for Hydrogen, Thermal and Electrochemical Energy Storage. *Energies* **2017**, *10* (10), 1645.

(16) Gallandat, N.; Romanowicz, K.; Züttel, A. An Analytical Model for the Electrolyser Performance Derived from Materials Parameters. *J. Power Energy Eng.* **2017**, *05* (10), 34–49.

(17) Broom, D. P. *Hydrogen Storage Materials The Characterization of Their Storage Properties*; Springer, 2010.

(18) FCHJU Multi-Annual Work Plan (MAWP) - accessed July 2018 https://www.fch.europa.eu.

(19) DoE Targets (accessed June 2018) https://www.energy.gov/eere/fuelcells/doe-technical-targets-onboard-hydrogen-storage-light-duty-vehicles.

(20) "FCHJU Multi-Annual Work Plan (MAWP)."

(21) Jepsen, L. H.; Ley, M. B.; Lee, Y. S.; Cho, Y. W.; Dornheim, M.; Jensen, J. O.; Filinchuk, Y.; Jørgensen, J. E.; Besenbacher, F.; Jensen, T. R. Boron–nitrogen Based Hydrides and Reactive Composites for Hydrogen Storage. *Mater. Today* **2014**, *17* (3), 129–135.

(22) Li, H. W.; Yan, Y.; Orimo, S. I.; Züttel, A.; Jensen, C. M. Recent Progress in Metal Borohydrides for Hydrogen Storage. *Energies* **2011**, *4* (1), 185–214.

(23) Callini, E.; Atakli, Z. Ö. K.; Hauback, B. C.; Orimo, S. I.; Jensen, C.; Dornheim, M.; Grant, D.; Cho, Y. W.; Chen, P.; Hjörvarsson, B.; et al. Complex and Liquid Hydrides for Energy Storage. *Appl. Phys. A* **2016**, *122* (4), 353.

(24) Sakituna, B.; Lamaridarkrim, F.; Hirscher, M. Metal Hydride Materials for Solid Hydrogen

Storage: A Review. *Int. J. Hydrogen Energy* **2007**, *32* (9), 1121–1140.
(25) Paskevicius, M.; Jepsen, L. H.; Schouwink, P.; Černý, R.; Ravnsbæk, D. B.; Filinchuk, Y.; Dornheim, M.; Besenbacher, F.; Jensen, T. R. Metal Borohydrides and Derivatives – Synthesis, Structure and Properties. *Chem. Soc. Rev.* **2017**, *46* (5), 1565–1634.
(26) Materials-Based Hydrogen Storage (accessed June 2018) https://www.energy.gov/eere/fuelcells/materials-based-hydrogen-storage.
(27) Dornheim, M. Thermodynamics of Metal Hydrides: Tailoring Reaction Enthalpies of Hydrogen Storage Materials. In *Thermodynamics - Interaction Studies - Solids, Liquids and Gases*; InTech, 2011; Vol. Dr. Juan C, pp 891–918.
(28) Rude, L. H.; Nielsen, T. K.; Ravnsbæk, D. B.; Bösenberg, U.; Ley, M. B.; Richter, B.; Arnbjerg, L. M.; Dornheim, M.; Filinchuk, Y.; Besenbacher, F.; et al. Tailoring Properties of Borohydrides for Hydrogen Storage: A Review. *Phys. status solidi* **2011**, *208* (8), 1754–1773.
(29) Bennington, S.; Lovell, A.; Headen, T.; Royse, D.; Nathanson, A.; Voller, S. Spacecraft and Spacesuit Shield. US20130095307A1, 2013.
(30) Züttel, A. Materials for Hydrogen Storage. *Mater. Today* **2003**, *6* (9), 24–33.
(31) Nakamori, Y.; Miwa, K.; Ninomiya, A.; Li, H.; Ohba, N.; Towata, S.; Züttel, A.; Orimo, S. I. Correlation between Thermodynamical Stabilities of Metal Borohydrides and Cation Electronegativites: First-Principles Calculations and Experiments. *Phys. Rev. B* **2006**, *74* (4), 045126.
(32) Orimo, S. I.; Nakamori, Y.; Ohba, N.; Miwa, K.; Aoki, M.; Towata, S. I.; Züttel, A. Experimental Studies on Intermediate Compound of LiBH4. *Appl. Phys. Lett.* **2006**, *89* (2), 26–28.
(33) Züttel, A.; Borgschulte, A.; Orimo, S. I. Tetrahydroborates as New Hydrogen Storage Materials. *Scr. Mater.* **2007**, *56* (10), 823–828.
(34) Paskevicius, M.; Ley, M. B.; Sheppard, D. A.; Jensen, T. R.; Buckley, C. E. Eutectic Melting in Metal Borohydrides. *Phys. Chem. Chem. Phys.* **2013**, *15* (45), 19774.
(35) Roedern, E.; Jensen, T. R. Thermal Decomposition of Mn(BH 4) 2 –M(BH 4) x and Mn(BH 4) 2 –MH x Composites with M = Li, Na, Mg, and Ca. *J. Phys. Chem. C* **2014**, *118* (41), 23567–23574.
(36) Ley, M. B.; Roedern, E.; Thygesen, P.; Jensen, T. R. Melting Behavior and Thermolysis of NaBH4−Mg(BH4)2 and NaBH4−Ca(BH4)2 Composites. *Energies* **2015**, *8* (4), 2701–2713.
(37) Puszkiel, J.; Garroni, S.; Milanese, C.; Gennari, F.; Klassen, T.; Dornheim, M.; Pistidda, C. Tetrahydroborates: Development and Potential as Hydrogen Storage Medium. *Inorganics* **2017**, *5* (4), 74.
(38) Nakamori, Y.; Li, H. W.; Kikuchi, K.; Aoki, M.; Miwa, K.; Towata, S. I.; Orimo, S. I. Thermodynamical Stabilities of Metal-Borohydrides. *J. Alloys Compd.* **2007**, *446–447*, 296–300.
(39) Nakamori, Y.; Li, H. W.; Matsuo, M.; Miwa, K.; Towata, S. I.; Orimo, S. I. Development of Metal Borohydrides for Hydrogen Storage. *J. Phys. Chem. Solids* **2008**, *69* (9), 2292–2296.
(40) Ravnsbæk, D. B.; Jensen, T. R. Tuning Hydrogen Storage Properties and Reactivity: Investigation of the LiBH4-NaAlH4 System. *J. Phys. Chem. Solids* **2010**, *71* (8), 1144–1149.
(41) Nickels, E. A.; Jones, M. O.; David, W. I. F.; Johnson, S. R.; Lowton, R. L.; Sommariva, M.; Edwards, P. P. Tuning the Decomposition Temperature in Complex Hydrides: Synthesis of a Mixed Alkali Metal Borohydride. *Angew. Chemie Int. Ed.* **2008**, *47* (15), 2817–2819.
(42) Lee, H. S.; Lee, Y. S.; Suh, J. Y.; Kim, M.; Yu, J. S.; Cho, Y. W. Enhanced Desorption and Absorption Properties of Eutectic LiBH4-Ca(BH4)2 Infiltrated into Mesoporous Carbon. *J. Phys. Chem. C* **2011**, *115* (40), 20027–20035.
(43) Gosalawit-Utke, R.; Milanese, C.; Nielsen, T. K.; Karimi, F.; Saldan, I.; Pranzas, K.; Jensen, T. R.; Marini, A.; Klassen, T.; Dornheim, M. Nanoconfined 2LiBH4–MgH2 for Reversible Hydrogen Storages: Reaction Mechanisms, Kinetics and Thermodynamics. *Int. J. Hydrogen Energy* **2013**, *38* (4), 1932–1942.

(44) Liu, X.; Peaslee, D.; Sheehan, T. P.; Majzoub, E. H. Decomposition Behavior of Eutectic LiBH4–Mg(BH4)2 and Its Confinement Effects in Ordered Nanoporous Carbon. *J. Phys. Chem. C* **2014**, *118* (47), 27265–27271.
(45) Lee, H. S.; Lee, Y.-S.; Suh, J.-Y.; Kim, M.; Yu, J.-S.; Cho, Y. W. Enhanced Desorption and Absorption Properties of Eutectic LiBH 4 –Ca(BH 4) 2 Infiltrated into Mesoporous Carbon. *J. Phys. Chem. C* **2011**, *115* (40), 20027–20035.
(46) Javadian, P.; Sheppard, D. A.; Buckley, C. E.; Jensen, T. R. Hydrogen Storage Properties of Nanoconfined LiBH4-Ca(BH4)2. *Int. J. Hydrogen Energy* **2015**, *11* (43), 96–103.
(47) Gosalawit-Utke, R.; Nielsen, T. K.; Saldan, I.; Laipple, D.; Cerenius, Y.; Jensen, T. R.; Klassen, T.; Dornheim, M. Nanoconfined 2LiBH4–MgH 2 Prepared by Direct Melt Infiltration into Nanoporous Materials. *J. Phys. Chem. C* **2011**, *115* (21), 10903–10910.
(48) Vajo, J. J. Influence of Nano-Confinement on the Thermodynamics and Dehydrogenation Kinetics of Metal Hydrides. *Curr. Opin. Solid State Mater. Sci.* **2011**, *15* (2), 52–61.
(49) Roedern, E.; Hansen, B. R. S.; Ley, M. B.; Jensen, T. R. Effect of Eutectic Melting, Reactive Hydride Composites, and Nanoconfinement on Decomposition and Reversibility of LiBH 4 – KBH 4. *J. Phys. Chem. C* **2015**, *119* (46), 25818–25825.
(50) Javadian, P.; Jensen, T. R. Enhanced Hydrogen Reversibility of Nanoconfined LiBH4–Mg(BH4)2. *Int. J. Hydrogen Energy* **2014**, *39* (18), 9871–9876.
(51) Doroodian, A.; Dengler, J. E.; Genest, A.; Rösch, N.; Rieger, B. Methylguanidinium Borohydride: An Ionic-Liquid-Based Hydrogen-Storage Material. *Angew. Chemie Int. Ed.* **2010**, *49* (10), 1871–1873.
(52) Li, S.; Gao, H.; Shreeve, J. M. Borohydride Ionic Liquids and Borane/Ionic-Liquid Solutions as Hypergolic Fuels with Superior Low Ignition-Delay Times. *Angew. Chemie - Int. Ed.* **2014**, *53* (11), 2969–2972.
(53) Li, H.-W. W. H. W.; Orimo, S. I.; Nakamori, Y.; Miwa, K.; Ohba, N.; Towata, S. I.; Züttel, A. Materials Designing of Metal Borohydrides: Viewpoints from Thermodynamical Stabilities. *J. Alloys Compd.* **2007**, *446–447*, 315–318.
(54) Ley, M. B.; Roedern, E.; Jensen, T. R. Eutectic Melting of LiBH4–KBH4. *Phys. Chem. Chem. Phys.* **2014**, *16* (44), 24194–24199.
(55) Hino, S.; Fonneløp, J. E.; Corno, M.; Zavorotynska, O.; Damin, A.; Richter, B.; Baricco, M.; Jensen, T. R.; Sørby, M. H.; Hauback, B. C. Halide Substitution in Magnesium Borohydride. *J. Phys. Chem. C* **2012**, *116* (23), 12482–12488.
(56) Rude, L. H.; Groppo, E.; Arnbjerg, L. M.; Ravnsbæk, D. B.; Malmkjær, R. A.; Filinchuk, Y.; Baricco, M.; Besenbacher, F.; Jensen, T. R. Iodide Substitution in Lithium Borohydride, LiBH4–LiI. *J. Alloys Compd.* **2011**, *509* (33), 8299–8305.
(57) Olsen, J. E.; Karen, P.; Sørby, M. H.; Hauback, B. C. Effect of Chloride Substitution on the Order-Disorder Transition in NaBH4 and Na11BD4. *J. Alloys Compd.* **2014**, *587* (2027), 374–379.
(58) Grove, H.; Rude, L. H.; Jensen, T. R.; Corno, M.; Ugliengo, P.; Baricco, M.; Sørby, M. H.; Hauback, B. C. Halide Substitution in Ca(BH 4) 2. *RSC Adv.* **2014**, *4* (9), 4736–4742.
(59) Rude, L. H.; Filinchuk, Y.; Sørby, M. H.; Hauback, B. C.; Besenbacher, F.; Jensen, T. R. Anion Substitution in Ca(BH 4) 2 –CaI 2 : Synthesis, Structure and Stability of Three New Compounds. *J. Phys. Chem. C* **2011**, *115* (15), 7768–7777.
(60) Ravnsbæk, D. B.; Rude, L. H.; Jensen, T. R. Chloride Substitution in Sodium Borohydride. *J. Solid State Chem.* **2011**, *184* (7), 1858–1866.
(61) Rude, L. H.; Zavorotynska, O.; Arnbjerg, L. M. M.; Ravnsbæk, D. B.; Malmkjær, R. A. A.; Grove, H.; Hauback, B. C.; Baricco, M.; Filinchuk, Y.; Besenbacher, F.; et al. Bromide Substitution in Lithium Borohydride, LiBH4-LiBr. *Int. J. Hydrogen Energy* **2011**, *36* (24), 15664–15672.
(62) Arnbjerg, L. M.; Ravnsbæk, D. B.; Filinchuk, Y.; Vang, R. T.; Cerenius, Y.; Besenbacher, F.; Jørgensen, J.-E.; Jakobsen, H. J.; Jensen, T. R. Structure and Dynamics for LiBH4−LiCl Solid Solutions. *Chem. Mater.* **2009**, *21* (24), 5772–5782.
(63) Zavorotynska, O.; Corno, M.; Pinatel, E. R.; Rude, L. H.; Ugliengo, P.; Jensen, T. R.;

Baricco, M. Theoretical and Experimental Study of LiBH4-LiCl Solid Solution. *Crystals* **2012**, *2* (4), 144–158.
(64) Pinatel, E. R.; Corno, M.; Ugliengo, P.; Baricco, M. Effects of Metastability on Hydrogen Sorption in Fluorine Substituted Hydrides. *J. Alloys Compd.* **2014**, *615*, S706–S710.
(65) Corno, M.; Pinatel, E. R.; Ugliengo, P.; Baricco, M. A Computational Study on the Effect of Fluorine Substitution in LiBH4. *J. Alloys Compd.* **2011**, *509* (SUPPL. 2), S679–S683.
(66) Rude, L. H.; Filsø, U.; D'Anna, V.; Spyratou, a.; Richter, B.; Hino, S.; Zavorotynska, O.; Baricco, M.; Sørby, M. H.; Hauback, B. C.; et al. Hydrogen–fluorine Exchange in NaBH4–NaBF4. *Phys. Chem. Chem. Phys.* **2013**, *15* (41), 18185.
(67) Richter, B.; Ravnsbæk, D. B.; Sharma, M.; Spyratou, A.; Hagemann, H.; Jensen, T. R. Fluoride Substitution in LiBH 4 ; Destabilization and Decomposition. *Phys. Chem. Chem. Phys.* **2017**, *19* (44), 30157–30165.
(68) Pitt, M. P.; Paskevicius, M.; Brown, D. H.; Sheppard, D. A.; Buckley, C. E. Thermal Stability of Li 2 B 12 H 12 and Its Role in the Decomposition of LiBH 4. *J. Am. Chem. Soc.* **2013**, *135* (18), 6930–6941.
(69) Hansen, B. R. S.; Paskevicius, M.; Li, H. W.; Akiba, E.; Jensen, T. R. Metal Boranes: Progress and Applications. *Coord. Chem. Rev.* **2016**, *323*, 60–70.
(70) Hansen, B. R. S.; Paskevicius, M.; Li, H.-W.; Akiba, E.; Jensen, T. R. Metal Boranes: Progress and Applications. *Coord. Chem. Rev.* **2015**.
(71) Paskevicius, M.; Pitt, M. P.; Brown, D. H.; Sheppard, D. a.; Chumphongphan, S.; Buckley, C. E. First-Order Phase Transition in the Li2B12H12 System. *Phys. Chem. Chem. Phys.* **2013**, *15* (38), 15825.
(72) Wilmer, D.; Feldmann, H.; Lechner, R. E. Ion Dynamics in Solid Solutions of Sodium Phosphate and Sodium Sulfate. *Phys. Chem. Chem. Phys.* **2002**, *4* (14), 3260–3265.
(73) Lundén, A. On the Paddle-Wheel Mechanism for Cation Conduction in Lithium Sulphate. *Zeitschrift für Naturforsch.* **1995**, *1076* (50a), 1067–1076.
(74) Song, L.; Wang, S.; Jiao, C.; Si, X.; Li, Z.; Liu, S.; Liu, S.; Jiang, C.; Li, F.; Zhang, J.; et al. Thermodynamics Study of Hydrogen Storage Materials. *J. Chem. Thermodyn.* **2012**, *46*, 86–93.
(75) Siegel, D. J.; Wolverton, C.; Ozolins, V. Thermodynamic Guidelines for the Prediction of Hydrogen Storage Reactions and Their Application to Destabilized Hydride Mixtures. *Phys. Rev. B - Condens. Matter Mater. Phys.* **2007**, *76* (13), 1–6.
(76) Lukas, H. L.; Fries, S. G.; Sundman, B. *Computational Thermodynamics, the Calphad Method*; Press, C. U., Ed.; 2007.
(77) Saunders, N.; Fahrmann, M.; Small, C. J. The Application of Calphad Calculations to Ni-Based Superalloys. *Superalloy 2000* **2000**, No. 803.
(78) El Kharbachi, A.; Pinatel, E. R.; Nuta, I.; Baricco, M. A Thermodynamic Assessment of LiBH4. *Calphad* **2012**, *39*, 80–90.
(79) Pinatel, E. R. E. R.; Albanese, E.; Civalleri, B.; Baricco, M. Thermodynamic Modelling of Mg(BH4)2. *J. Alloys Compd.* **2015**, *645* (S1), S64–S68.
(80) Fonneløp, J. E.; Corno, M.; Grove, H.; Pinatel, E. R.; Sørby, M. H.; Ugliengo, P.; Baricco, M.; Hauback, B. C. Experimental and Computational Investigations on the AlH3/AlF3 System. *J. Alloys Compd.* **2011**, *509* (1), 10–14.
(81) Ravnsbæk, D. B.; Sørensen, L. H.; Filinchuk, Y.; Besenbacher, F.; Jensen, T. R. Screening of Metal Borohydrides by Mechanochemistry and Diffraction. *Angew. Chemie - Int. Ed.* **2012**, *51* (15), 3582–3586.
(82) Li, Y.; Zhao, M.; Ding, X.; Liu, D.; Zhang, Q. Direct Mechanochemical Formation of Alkali Metal Borohydrides Nanocrystals Exhibiting Kinetic and Thermodynamic Destabilizations. *Int. J. Hydrogen Energy* **2016**, *41* (4), 2807–2813.
(83) Mal'tseva, N. N.; Generalova, N. B.; Masanov, a. Y.; Zhizhin, K. Y.; Kuznetsov, N. T. Mechanochemical Synthesis of Complex Hydrides. *Russ. J. Inorg. Chem.* **2012**, *57* (13), 1631–1652.
(84) Huot, J.; Ravnsbæk, D. B.; Zhang, J.; Cuevas, F.; Latroche, M.; Jensen, T. R.

Mechanochemical Synthesis of Hydrogen Storage Materials. *Prog. Mater. Sci.* **2013**, *58* (1), 30–75.
(85) Doppiu, S.; Schultz, L.; Gutfleisch, O. In Situ Pressure and Temperature Monitoring during the Conversion of Mg into MgH2 by High-Pressure Reactive Ball Milling. *J. Alloys Compd.* **2007**, *427* (1–2), 204–208.
(86) Clegg, W.; Blake, A. J.; Cole, J. M.; Evans, J. S. O.; Main, P.; Parsons, S.; Watkin, D. J. *Crystal Structure Analysis Principles and Practice*, Second.; 2009.
(87) Giacovazzo, C.; Monaco, H. L.; Artioli, G.; Viterbo, D.; Milanesio, M.; Gilli, G.; Gilli, P.; Zanotti, G.; Ferraris, G.; Catti, M. *Fundamentals of Crystallography*, Third.; 2011.
(88) Ravnsbæk, D. B.; Filinchuk, Y.; Cerný, R.; Jensen, T. R. Powder Diffraction Methods for Studies of Borohydride-Based Energy Storage Materials. *Zeitschrift für Krist.* **2010**, *225* (12), 557–569.
(89) Møller, K. T.; Hansen, B. R. S.; Dippel, A.-C.; Jørgensen, J.-E. E.; Jensen, T. R. Characterization of Gas-Solid Reactions Using In Situ Powder X-Ray Diffraction. *Zeitschrift für Anorg. und Allg. Chemie* **2014**, *640* (15), 3029–3043.
(90) Hammersley, A. P. FIT2D: An Introduction and Overview. *Eur. Synchrotron Radiat. Facil. Intern. Rep. ESRF97HA02T* **1997**, *68* (58).
(91) Hammersley, A. P.; Svensson, S. O.; Hanfland, M.; Fitch, A. N.; Hausermann, D. Two-Dimensional Detector Software: From Real Detector to Idealised Image or Two-Theta Scan. *High Press. Res.* **1996**, *14* (4–6), 235–248.
(92) Snyder, R. L.; Bunge, H. J.; Fiala, J. *Defect and Microstructure Analysis by Diffraction*; Oxford Univ. Press, 1999.
(93) Lutterotti, L.; Matthies, S.; Wenk, H. R. MAUD: A Friendly Java Program for Material Analysis Using Diffraction. *IUCr Newsl. CPD* **1999**, *21*, 14–15.
(94) Cerenius, Y.; Ståhl, K.; Svensson, L. A.; Ursby, T.; Oskarsson, Å.; Albertsson, J.; Liljas, A. The Crystallography Beamline I711 at MAX II. *J. Synchrotron Radiat.* **2000**, *7* (4), 203–208.
(95) Jensen, T. R.; Nielsen, T. K.; Filinchuk, Y.; Jørgensen, J. E.; Cerenius, Y.; Gray, E. M.; Webb, C. J. Versatile in Situ Powder X-Ray Diffraction Cells for Solid-Gas Investigations. *J. Appl. Crystallogr.* **2010**, *43* (6), 1456–1463.
(96) Bösenberg, U.; Pistidda, C.; Tolkiehn, M.; Busch, N.; Saldan, I.; Suarez-Alcantara, K.; Arendarska, A.; Klassen, T.; Dornheim, M. Characterization of Metal Hydrides by In-Situ XRD. *Int. J. Hydrogen Energy* **2014**, *39* (18), 9899–9903.
(97) Hansen, B. R. S.; Møller, K. T.; Paskevicius, M.; Dippel, A.-C.; Walter, P.; Webb, C. J.; Pistidda, C.; Bergemann, N.; Dornheim, M.; Klassen, T.; et al. In Situ X-Ray Diffraction Environments for High-Pressure Reactions. *J. Appl. Crystallogr.* **2015**, *48* (4), 1234–1241.
(98) Montanari, R.; Baricco, M.; Angella, G.; Kaciulis, S.; Riccardi, B. *Tecniche Sperimentali per La Caratterizzazione Dei Materiali Dal Laboratorio Alla Produzione*; Associazione Italiana di metallurgia, 2005.
(99) Chase, M. W.; Davies, C. A.; Downey, J. R.; Frurip, D. J.; McDonald, R. A.; Syverud, A. N. JANAF Thermochemical Tables. *J. Phys. Chem.* **1998**, *Part I Al-* (Data 9), 1–957.
(100) D'Anna, V.; Spyratou, A.; Sharma, M.; Hagemann, H. FT-IR Spectra of Inorganic Borohydrides. *Spectrochim. Acta Part A Mol. Biomol. Spectrosc.* **2014**, *128*, 902–906.
(101) D'Anna, V.; Lawson Daku, L. M.; Hagemann, H. Quantitative Spectra–Structure Relations for Borohydrides. *J. Phys. Chem. C* **2015**, *119* (38), 21868–21874.
(102) D'Anna, V.; Lawson Daku, L. M.; Hagemann, H. Vibrational Spectra and Structure of Borohydrides. *J. Alloys Compd.* **2013**, *580* (SUPPL1), S122–S124.
(103) Renaudin, G.; Gomes, S.; Hagemann, H.; Keller, L.; Yvon, K. Structural and Spectroscopic Studies on the Alkali Borohydrides MBH4 (M = Na, K, Rb, Cs). *J. Alloys Compd.* **2004**, *375* (1–2), 98–106.
(104) Sethio, D.; Lawson Daku, L. M.; Hagemann, H. A Theoretical Study of the Spectroscopic Properties of B2H6 and of a Series of BxHy Z- Species (x = 1-12, y = 3-14, Z= 0-2): From BH3 to B12H12 2-. *Int. J. Hydrogen Energy* **2016**, *41* (16), 6814–6824.

(105) Sharma, M.; Sethio, D.; D'Anna, V.; Hagemann, H. Theoretical Study of B12HnF2-(12-n) Species. *Int. J. Hydrogen Energy* **2015**, *40* (37), 12721–12726.
(106) Sethio, D.; Lawson Daku, L. M.; Hagemann, H. Computational Study of the Vibrational Spectroscopy Properties of Boron-Hydrogen Compounds: Mg(B3H8)2, CB9H10−and CB11H12−. *Int. J. Hydrogen Energy* **2017**, *42* (35), 22496–22501.
(107) Hagemann, H.; Gomes, S.; Renaudin, G.; Yvon, K. Raman Studies of Reorientation Motions of [BH4]- Anionsin Alkali Borohydrides. *J. Alloys Compd.* **2004**, *363* (1–2), 126–129.
(108) Reed, D.; Book, D. Recent Applications of Raman Spectroscopy to the Study of Complex Hydrides for Hydrogen Storage. *Curr. Opin. Solid State Mater. Sci.* **2011**, *15* (2), 62–72.
(109) Kister, A. T.; Redlich, O. Algebraic Representation of Thermodynamic Properties and the Classification. *Ind. Eng. Chem.* **1948**, *40* (2), 345–348.
(110) Andersson, J. O.; Helander, T.; Hoglund, L.; Shi, P.; Sundman, B. THERMO-CALC & DICTRA, Computational Tools For Materials Science. *Calphad* **2002**, *26* (2), 273–312.
(111) ThermoCalc software (accessed July 2018) http://www.thermocalc.se.
(112) Pandat Software (Accessed July 2018).
(113) FactSage Software (Accessed July 2018).
(114) Dinsdale, A. T. SGTE Data For Pure Elements. *Calphad* **1991**, *15* (4), 317–425.
(115) SGTE Substance Database V 4.1. *SGTE Subst. database V 4.1. - http//www.crct.polymtl.ca/fact/documentation/sgps_list.htm*.
(116) NIST (accessed July 2018) http://www.nist.gov/.
(117) Dovesi, R.; Saunders, V. R.; Roetti, C.; Orlando, R.; Zicovich-Wilson, C. M.; Pascale, F.; Civalleri, B.; Doll, K.; Harrison, N. M.; Bush, I. J.; et al. *CRYSTAL14 User's Manual, University of Torino*; 2014.
(118) Dovesi, R.; Orlando, R.; Erba, A.; Zicovich-Wilson, C. M.; Civalleri, B.; Casassa, S.; Maschio, L.; Ferrabone, M.; De La Pierre, M.; D'Arco, P.; et al. CRYSTAL14: A Program for the Ab Initio Investigation of Crystalline Solids. *Int. J. Quantum Chem.* **2014**, *114* (19), 1287–1317.
(119) Perdew, J. P.; Burke, K.; Ernzerhof, M. Generalized Gradient Approximation Made Simple. *Phys. Rev. Lett.* **1996**, *77* (18), 3865–3868.
(120) Adamo, C.; Barone, V. Toward Reliable Density Functional Methods without Adjustable Parameters: The PBE0 Model. *J. Chem. Phys.* **1999**, *110* (13), 6158–6170.
(121) Lee, C.; Yang, W.; Parr, R. G. Development of the Colle-Salvetti Correlation-Energy Formula into a Functional of the Electron Density. *Phys. Rev. B* **1988**, *37* (2), 785–789.
(122) Becke, A. D. Density-Functional Thermochemistry. III. The Role of Exact Exchange. *J. Chem. Phys.* **1993**, *98* (7), 5648.
(123) Grimme, S. Semiempirical GGA-Type Density Functional Constructed with a Long-Range Dispersion Correction. *J. Comput. Chem.* **2006**, *27* (15), 1787–1799.
(124) Dematteis, E. M.; Roedern, E.; Pinatel, E. R.; Corno, M.; Jensen, T. R.; Baricco, M. A Thermodynamic Investigation of the LiBH4–NaBH4 System. *RSC Adv.* **2016**, *6* (65), 60101–60108.
(125) Zavorotynska, O.; Corno, M.; Damin, A.; Spoto, G.; Ugliengo, P.; Baricco, M. Vibrational Properties of MBH4 and MBF4 Crystals (M = Li, Na, K): A Combined DFT, Infrared, and Raman Study. *J. Phys. Chem. C* **2011**, *115* (38), 18890–18900.
(126) Pascale, F.; Zicovich-Wilson, C. M.; Lopez Gejo, F.; Civalleri, B.; Orlando, R.; Dovesi, R. The Calculation of the Vibrational Frequencies of Crystalline Compounds and Its Implementation in the CRYSTAL Code. *J. Comput. Chem.* **2004**, *25* (6), 888–897.
(127) Zicovich-Wilson, C. M.; Torres, F. J.; Pascale, F.; Valenzano, L.; Orlando, R.; Dovesi, R. Ab Initio Simulation of the IR Spectra of Pyrope, Grossular, and Andradite. *J. Comput. Chem.* **2008**, *29* (13), 2268–2278.
(128) Sheppard, D. A.; Paskevicius, M.; Humphries, T. D.; Felderhoff, M.; Capurso, G.; Bellosta von Colbe, J.; Dornheim, M.; Klassen, T.; Ward, P. A.; Teprovich, J. A.; et al. Metal Hydrides for Concentrating Solar Thermal Power Energy Storage. *Appl. Phys. A* **2016**, *122* (4), 395.
(129) Grimvall, G. *Thermophysical Properties of Materials*; 1999.

(130) Gavrichev, K. S. Heat Capacity and Thermodynamic Properties of Inorganic Compounds Containing Tetrahedral Anions (BH - 4 , AlH - 4 , GaH - 4 , BF - 4 , ClO - 4 , BrO - 4 , and IO - 4). *Inorg. Mater.* **2003**, *39* (SUPPL.), S89–S112.
(131) El Kharbachi, A.; Nuta, I.; Hodaj, F.; Baricco, M. Above Room Temperature Heat Capacity and Phase Transition of Lithium Tetrahydroborate. *Thermochim. Acta* **2011**, *520* (1–2), 75–79.
(132) Johnston, H.; Hallett, N. Low Temperature Heat Capacities of Inorganic Solids. XIV. Heat Capacity of Sodium Bororhydride from 15-300K. *J. Am. Chem* **1953**, *75* (Table 111), 1467–1468.
(133) Gorbunov, V. E.; Gavrichev, K. S.; Lazarev, V. B. Thermodynamic Properties and Phase Transitions of Alkali Metal Borohydrides. *Russ. J. Phys. Chem.* **1988**, *60* (8), 1240–1242.
(134) Boodman, D. Thermal Properties of Some Hydrides. *Univ. Pitts., ONR Contract Sumber N6 ori 43, T.O.1, Tech. Rep.* **1949**, *Oct. 10*.
(135) Douglas, T. B.; Harman, A. W. Heat Content of Sodium Borohydride and of Potassium Borohydride from 0 ° to 400 ° C C : *J. Res. Natl. Bur. Stand. (1934).* **1958**, *60* (2), 117–124.
(136) Furukawa, G. T.; Reilly, M. L.; Piccirelli, J. H. Heat Capacity of Potassium Borohydride (KBH4) from 15 to 375 °K. Thermodynamic Properties from 0 to 700 °K. *J. Res. Natl. Bur. Stand. Sect. A Phys. Chem.* **1964**, *68A* (6), 651.
(137) Pinatel, E. R.; Albanese, E.; Civalleri, B.; Baricco, M. Thermodynamic Modelling of Mg(BH4)2. *J. Alloys Compd.* **2015**, *645* (S1), S64–S68.
(138) Udovic, T. J. V.A.1 National Institute of Standards and Technology (NIST). *FY 2008 Annu. Prog. Rep.* **2008**, 504–509.
(139) Gorbunov, V. E.; Gavrichev, K. S.; Bakum, S. I. Low-Temperature Specific Heat of Rubidium Borohydride RbBH4. *Russ. J. Phys. Chem.* **1985**, *59* (12), 1754–1756.
(140) Gorbunov, V. E.; Gavrichev, K. S.; Totrova, G. A.; Bakum, S. I. Low-Temperature Specific Heat of Caesium Borohydride CsBH4. *Russ. J. Phys. Chem.* **1986**, *60* (2), 296–298.
(141) Dimitrievska, M.; White, J. L.; Zhou, W.; Stavila, V.; Klebanoff, L. E.; Udovic, T. J. Structure-Dependent Vibrational Dynamics of Mg(BH 4) 2 Polymorphs Probed with Neutron Vibrational Spectroscopy and First-Principles Calculations. *Phys. Chem. Chem. Phys.* **2016**, *18* (36), 25546–25552.
(142) Vitillo, J. G. J. G.; Bordiga, S.; Baricco, M. Spectroscopic and Structural Characterization of Thermal Decomposition of γ-Mg(BH 4) 2 : Dynamic Vacuum versus H 2 Atmosphere. *J. Phys. Chem. C* **2015**, *119* (45), 25340–25351.
(143) Paskevicius, M.; Jepsen, L. H.; Schouwink, P.; Černý, R.; Ravnsbæk, D. B.; Filinchuk, Y.; Dornheim, M.; Besenbacher, F.; Jensen, T. R. Metal Borohydrides and Derivatives-Synthesis, Structure and Properties. *Chem. Soc. Rev.* **2017**, *46* (5), 1565–1634.
(144) Dematteis, E. M. E. M.; Santoru, A.; Poletti, M. G. G. M. G.; Pistidda, C.; Klassen, T.; Dornheim, M.; Baricco, M. Phase Stability and Hydrogen Desorption in a Quinary Equimolar Mixture of Light-Metals Borohydrides. *Int. J. Hydrogen Energy* **2018**, *Submitted* (Special Issue-E-MRS Fall 2017 Symposium), 1–11.
(145) Vitillo, J. G.; Groppo, E.; Bardají, E. G.; Baricco, M.; Bordiga, S. Fast Carbon Dioxide Recycling by Reaction with γ-Mg(BH4)2. *Phys. Chem. Chem. Phys.* **2014**, *16* (41), 22482–22486.
(146) Eagles, M.; Sun, B.; Richter, B.; Jensen, T. R.; Filinchuk, Y.; Conradi, M. S. NMR Investigation of Nanoporous γ-Mg(BH 4) 2 and Its Thermally Induced Phase Changes. *J. Phys. Chem. C* **2012**, *116* (24), 13033–13037.
(147) Paskevicius, M.; Pitt, M. P.; Webb, C. J.; Sheppard, D. A.; Filsø, U.; Gray, E. M.; Buckley, C. E. In-Situ X-Ray Diffraction Study of γ-Mg(BH4)2 Decomposition. *J. Phys. Chem. C* **2012**, *116*, 15231–15240.
(148) Filinchuk, Y.; Ronnebro, E.; CHANDRA, D. Crystal Structures and Phase Transformations in Ca(BH4)2. *Acta Mater.* **2009**, *57* (3), 732–738.
(149) Llamas-Jansa, I.; Friedrichs, O.; Fichtner, M.; Bardaji, E. G.; Züttel, A.; Hauback, B. C. The

Role of Ca(BH4)2 Polymorphs. *J. Phys. Chem. C* **2012**, *116* (25), 13472–13479.
(150) Riktor, M. D.; Sørby, M. H.; Chłopek, K.; Fichtner, M.; Buchter, F.; Züttel, A.; Hauback, B. C. In Situ Synchrotron Diffraction Studies of Phase Transitions and Thermal Decomposition of Mg(BH4)2 and Ca(BH4)2. *J. Mater. Chem.* **2007**, *17* (47), 4939.
(151) Riktor, M. D.; Filinchuk, Y.; Vajeeston, P.; Bardají, E. G.; Fichtner, M.; Fjellvåg, H.; Sørby, M. H.; Hauback, B. C. The Crystal Structure of the First Borohydride Borate, Ca3(BD4)3(BO3). *J. Mater. Chem.* **2011**, *21* (20), 7188.
(152) Borgschulte, A.; Gremaud, R.; Züttel, A.; Martelli, P.; Remhof, A.; Ramirez-Cuesta, A. J.; Refson, K.; Bardaji, E. G.; Lohstroh, W.; Fichtner, M.; et al. Experimental Evidence of Librational Vibrations Determining the Stability of Calcium Borohydride. *Phys. Rev. B* **2011**, *83* (2), 024102.
(153) Stockmayer, W. H.; Rice, D. W.; Stephenson, C. Thermodynamic Properties of Sodium Borohydride and Aqueous Borohydride Ion Ang8. **1955**, *77*, 1980–1983.
(154) Verdal, N.; Udovic, T. J.; Zhou, W.; Rush, J. J.; De Vries, D. J.; Hartman, M. R. Vibrational Spectroscopic Study of Subtle Phase Transitions in Alkali Borohydrides: Comparison with First-Principles Calculations. *J. Phys. Chem. C* **2013**, *117* (2), 876–883.
(155) Petit, A.-T.; Dulong, P.-L. Recherches Sur Quelques Points Importants de La Théorie de La Chaleur. *Ann. Chim. Phys.* **1819**, *10*, 395–413.
(156) Mnyukh, Y. On the Phase Transitions That Cannot Materialize. *Am. J. Condens. Matter Phys.* **2013**, *4* (1), 1–12.
(157) Mnyukh, Y. *Fundamentals of Solid-State Phase Transitions, Ferromagnetism and Ferroelectricity*, second edi.; 2009.
(158) Porter, D. A.; Easterling, K. E. *Phase Transformations in Metals and Alloys*, second edi.; Springer-Science+Business Media, B. Y., Ed.; Springer US: Boston, MA, 1992.
(159) Wu, H.; Tang, W. S.; Stavila, V.; Zhou, W.; Rush, J. J.; Udovic, T. J. Structural Behavior of Li2B10H10. *J. Phys. Chem. C* **2015**, *119* (12), 6481–6487.
(160) Hofman, K.; Albert, B. Crystal Structures of M2[B10H10](M= Na, K, Rb) via Real-Space Simulated Annealing Powder Techniques. *Z. Krist.* **2005**, *220*, 142–146.
(161) Bonnetot, B.; Mongeot, H.; Aboukhassib, A.; Lefebvre, F. Phase Transition Investigations of Closo-Hydroborates. *Inorganica Chim. Acta* **1992**, *193* (1), 21–26.
(162) Muetterties, E. L.; Balthis, J. H.; Chia, Y. T.; Knoth, W. H.; Miller, H. C. Chemistry of Boranes. VIII. Salts and Acids of B 10 H 10 -2 and B 12 12 -2. *Inorg. Chem.* **1964**, *3* (3), 444–451.
(163) Her, J.-H.; Yousufuddin, M.; Zhou, W.; Jalisatgi, S. S.; Kulleck, J. G.; Zan, J. A.; Hwang, S.-J.; Bowman, R. C.; Udovic, T. J. Crystal Structure of Li 2 B 12 H 12 : A Possible Intermediate Species in the Decomposition of LiBH 4. *Inorg. Chem.* **2008**, *47* (21), 9757–9759.
(164) Verdal, N.; Her, J.-H.; Stavila, V.; Soloninin, A. V.; Babanova, O. a.; Skripov, A. V.; Udovic, T. J.; Rush, J. J. Complex High-Temperature Phase Transitions in Li2B12H12 and Na2B12H12. *J. Solid State Chem.* **2014**, *212*, 81–91.
(165) Sadikin, Y.; Schouwink, P.; Brighi, M.; Łodziana, Z.; Černý, R. Modified Anion Packing of Na 2 B 12 H 12 in Close to Room Temperature Superionic Conductors. *Inorg. Chem.* **2017**, *56* (9), 5006–5016.
(166) Tiritiris, I.; Schleid, T. Die Dodekahydro-Closo-Dodekaborate M2[B12H12] Der Schweren Alkalimetalle (M+ = K+, Rb+, NH4+, Cs+) Und Ihre Formalen Iodid-Addukte M3I[B12H12] (≡ MI · M2[B12H12]). *Zeitschrift für Anorg. und Allg. Chemie* **2003**, *629* (78), 1390–1402.
(167) Verdal, N.; Wu, H.; Udovic, T. J.; Stavila, V.; Zhou, W.; Rush, J. J. Evidence of a Transition to Reorientational Disorder in the Cubic Alkali-Metal Dodecahydro-Closo-Dodecaborates. *J. Solid State Chem.* **2011**, *184* (11), 3110–3116.
(168) Mulliken, R. S. A New Electroaffinity Scale; Together with Data on Valence States and on Valence Ionization Potentials and Electron Affinities. *J. Chem. Phys.* **1934**, *2* (11), 782–793.
(169) Mulliken, R. S. Electronic Structures of Molecules XI. Electroaffinity, Molecular Orbitals and

Dipole Moments. *J. Chem. Phys.* **1935**, *3* (9), 573–585.
(170) Allred, A. L. Electronegativity Values from Thermochemical Data. *J. Inorg. Nucl. Chem.* **1961**, *17*, 215–221.
(171) Mann, J. B.; Meek, T. L.; Allen, L. C. Configuration Energies of the Main Group Elements. *J. Am. Chem. Soc.* **2000**, *122* (12), 2780–2783.
(172) Jensen, S. R. H.; Jepsen, L. H.; Skibsted, J.; Jensen, T. R. Phase Diagram for the NaBH4-KBH4 System and the Stability of a Na(1– x)K(x)BH4 Solid Solution. *J. Phys. Chem. C* **2015**, *119* (50), 27919–27929.
(173) Lee, J. Y.; Ravnsbæk, D. B.; Lee, Y. S.; Kim, Y.; Cerenius, Y.; Shim, J.; Jensen, T. R.; Hur, N. H.; Cho, Y. W. Decomposition Reactions and Reversibility of the LiBH4 -Ca(BH4)2 Composite. *J. Phys. Chem. C* **2009**, *113* (33), 15080–15086.
(174) Adams, R. M. Borax to Boranes. *Adv. Chem.* **1961**, *32*, 60–68.
(175) Semenenko, K. N.; Chavgun, a P.; Surov, V. N. Interaction of Sodium Tetrahydroborate with Potassium and Lithium Tetrahydroborates. *Russ. J. Inorg. Chem.* **1971**, *16* (2), 271–273.
(176) Skripov, A. V.; Soloninin, A. V.; Rude, L. H.; Jensen, T. R.; Filinchuk, Y. Nuclear Magnetic Resonance Studies of Reorientational Motion and Li Diffusion in LiBH 4 –LiI Solid Solutions. *J. Phys. Chem. C* **2012**, *116* (50), 26177–26184.
(177) Miyazaki, R.; Karahashi, T.; Kumatani, N.; Noda, Y.; Ando, M.; Takamura, H.; Matsuo, M.; Orimo, S.; Maekawa, H. Room Temperature Lithium Fast-Ion Conduction and Phase Relationship of LiI Stabilized LiBH4. *Solid State Ionics* **2011**, *192* (1), 143–147.
(178) Maekawa, H.; Matsuo, M.; Takamura, H.; Ando, M.; Noda, Y.; Karahashi, T.; Orimo, S. I. Halide-Stabilized LiBH4, a Room-Temperature Lithium Fast-Ion Conductor. *J. Am. Chem. Soc.* **2009**, *131* (3), 894–895.
(179) Huff, G. F. US 2.935.428. *US 2.935.428* **1960**.
(180) Pinatel, E. R. Thermodynamic Modelling of Hydrogen Storage Materials. *PhD Thesis, Univ. Turin* **2012**, Thermodynamic Modelling of Hydrogen Storage Materi.
(181) Milanese, C.; Garroni, S.; Girella, A.; Mulas, G.; Berbenni, V.; Bruni, G.; Suriñach, S.; Baró, M. D.; Marini, A. Thermodynamic and Kinetic Investigations on Pure and Doped NaBH 4 −MgH 2 System. *J. Phys. Chem. C* **2011**, *115* (7), 3151–3162.
(182) Stasinevich, D. S.; Egorenko, G. A. Thermographic Investigation of Alkali Metal and Magnesium Tetrahydroborates at Pressures up to 10 Atm. *Russ. J. Inorg. Chem.* **1968**, *13* (3), 341–343.
(183) Kim, K. C.; Sholl, D. S. Crystal Structures and Thermodynamic Investigations of LiK(BH4)2 , KBH4 , and NaBH4 from First-Principles Calculations. *J. Phys. Chem. C* **2010**, *114* (1), 678–686.
(184) Yves-Marie, M.; Gambino, M.; Bros, J.-P. Enthalpies de Formation Des Alliages Liquides Bismuth-Ethain-Gallium a 723 K. Choix d'une Representation Analytique Des Grandeurs d'exces Integrales et Partielles de Melange. *J. Chim. Phys.* **1975**, *72* (1), 83–88.
(185) Cantor, B.; Chang, I. T. H.; Knight, P.; Vincent, A. J. B. Microstructural Development in Equiatomic Multicomponent Alloys. *Mater. Sci. Eng. A* **2004**, *375–377* (1–2 SPEC. ISS.), 213–218.
(186) Poletti, M. G.; Battezzati, L. Electronic and Thermodynamic Criteria for the Occurrence of High Entropy Alloys in Metallic Systems. *Acta Mater.* **2014**, *75*, 297–306.
(187) Yeh, J.-W.; Chen, S.-K.; Lin, S.-J.; Gan, J.-Y.; Chin, T.-S.; Shun, T.-T.; Tsau, C.-H.; Chang, S.-Y. Nanostructured High-Entropy Alloys with Multiple Principal Elements: Novel Alloy Design Concepts and Outcomes. *Adv. Eng. Mater.* **2004**, *6* (5), 299–303.
(188) Laurent-Brocq, M.; Akhatova, A.; Perrière, L.; Chebini, S.; Sauvage, X.; Leroy, E.; Champion, Y. Insights into the Phase Diagram of the CrMnFeCoNi High Entropy Alloy. *Acta Mater.* **2015**, *88*, 355–365.
(189) Senkov, O. N.; Woodward, C.; Miracle, D. B. Microstructure and Properties of Aluminum-Containing Refractory High-Entropy Alloys. *Jom* **2014**, *66* (10), 2030–2042.
(190) Senkov, O. N.; Wilks, G. B.; Scott, J. M.; Miracle, D. B. Mechanical Properties of

Nb25Mo25Ta25W25 and V20Nb20Mo20Ta20W20 Refractory High Entropy Alloys. *Intermetallics* **2011**, *19* (5), 698–706.
(191) Li, Z.; Pradeep, K. G.; Deng, Y.; Raabe, D.; Tasan, C. C. Metastable High-Entropy Dual-Phase Alloys Overcome the Strength–ductility Trade-Off. *Nature* **2016**, *534* (7606), 227–230.
(192) Miracle, D.; Miller, J.; Senkov, O.; Woodward, C.; Uchic, M.; Tiley, J. Exploration and Development of High Entropy Alloys for Structural Applications. *Entropy* **2014**, *16* (12), 494–525.
(193) Miracle, D. B.; Senkov, O. N. A Critical Review of High Entropy Alloys and Related Concepts. *Acta Mater.* **2017**, *122*, 448–511.
(194) Rogal, L.; Bobrowski, P.; Körmann, F.; Divinski, S.; Stein, F.; Grabowski, B. Computationally-Driven Engineering of Sublattice Ordering in a Hexagonal AlHfScTiZr High Entropy Alloy. *Sci. Rep.* **2017**, *7* (1), 2209.
(195) Santodonato, L. J.; Zhang, Y.; Feygenson, M.; Parish, C. M.; Gao, M. C.; Weber, R. J. K.; Neuefeind, J. C.; Tang, Z.; Liaw, P. K. Deviation from High-Entropy Configurations in the Atomic Distributions of a Multi-Principal-Element Alloy. *Nat. Commun.* **2015**, *6* (1), 5964.
(196) Feuerbacher, M. Dislocations and Deformation Microstructure in a B2-Ordered Al28Co20Cr11Fe15Ni26 High-Entropy Alloy. *Sci. Rep.* **2016**, *6* (1), 29700.
(197) Andersson, J.-O.; Guillermet, A. F.; Hillert, M.; Jansson, B.; Sundman, B. A Compound-Energy Model of Ordering in a Phase with Sites of Different Coordination Numbers. *Acta Metall.* **1986**, *34* (3), 437–445.
(198) Rost, C. M.; Sachet, E.; Borman, T.; Moballegh, A.; Dickey, E. C.; Hou, D.; Jones, J. L.; Curtarolo, S.; Maria, J.-P. Entropy-Stabilized Oxides. *Nat. Commun.* **2015**, *6*, 8485.
(199) Gild, J.; Zhang, Y.; Harrington, T.; Jiang, S.; Hu, T.; Quinn, M. C.; Mellor, W. M.; Zhou, N.; Vecchio, K.; Luo, J. High-Entropy Metal Diborides: A New Class of High-Entropy Materials and a New Type of Ultrahigh Temperature Ceramics. *Sci. Rep.* **2016**, *6* (July), 2–11.
(200) Orimo, S. I.; Nakamori, Y.; Kitahara, G.; Miwa, K.; Ohba, N.; Towata, S.; Züttel, A. Dehydriding and Rehydriding Reactions of LiBH4. *J. Alloys Compd.* **2005**, *404–406* (SPEC. ISS.), 427–430.
(201) Liu, Y.; Reed, D.; Paterakis, C.; Contreras Vasquez, L.; Baricco, M.; Book, D. Study of the Decomposition of a 0.62LiBH4–0.38NaBH4 Mixture. *Int. J. Hydrogen Energy* **2017**, *42* (35), 22480–22488.
(202) Bardají, E. G.; Zhao-Karger, Z.; Boucharat, N.; Nale, A.; van Setten, M. J.; Lohstroh, W.; Röhm, E.; Catti, M.; Fichtner, M. LiBH 4 −Mg(BH 4) 2 : A Physical Mixture of Metal Borohydrides as Hydrogen Storage Material. *J. Phys. Chem. C* **2011**, *115* (13), 6095–6101.
(203) Fang, Z.-Z.; Kang, X.-D.; Wang, P.; Li, H.-W.; Orimo, S.-I. Unexpected Dehydrogenation Behavior of LiBH4/Mg(BH4)2 Mixture Associated with the in Situ Formation of Dual-Cation Borohydride. *J. Alloys Compd.* **2010**, *491* (1–2), L1–L4.
(204) Dematteis, E. M.; Pinatel, E. R.; Corno, M.; Jensen, T. R.; Baricco, M. Phase Diagrams of the LiBH4–NaBH4–KBH4 System. *Phys. Chem. Chem. Phys.* **2017**, *19* (36), 25071–25079.
(205) Schouwink, P.; D'Anna, V.; Ley, M. B.; Lawson Daku, L. M.; Richter, B.; Jensen, T. R.; Hagemann, H.; Černý, R. Bimetallic Borohydrides in the System M (BH 4) 2 –KBH 4 (M = Mg, Mn): On the Structural Diversity. *J. Phys. Chem. C* **2012**, *116* (20), 10829–10840.
(206) Schouwink, P.; Ley, M. B.; Tissot, A.; Hagemann, H.; Jensen, T. R.; Smrčok, L.; Černý, R. Structure and Properties of Complex Hydride Perovskite Materials. *Nat. Commun.* **2014**, *5706* (5), 1–10.
(207) Mao, J.; Guo, Z.; Poh, C. K.; Ranjbar, A.; Guo, Y.; Yu, X.; Liu, H. Study on the Dehydrogenation Kinetics and Thermodynamics of Ca(BH4)2. *J. Alloys Compd.* **2010**, *500* (2), 200–205.
(208) Jiang, S.; Hu, T.; Gild, J.; Zhou, N.; Nie, J.; Qin, M.; Harrington, T.; Vecchio, K.; Luo, J. A New Class of High-Entropy Perovskite Oxides. *Scr. Mater.* **2018**, *142*, 116–120.
(209) Ozolins, V.; Majzoub, E. H.; Wolverton, C. First-Principles Prediction of Thermodynamically Reversible Hydrogen Storage Reactions in the Li-Mg-Ca-B-H System. *J. Am. Chem. Soc.*

2009, *131* (1), 230–237.
(210) Orimo, S.-I.; Nakamori, Y.; Eliseo, J. R.; Züttel, A.; Jensen, C. M. Complex Hydrides for Hydrogen Storage. *Chem. Rev.* **2007**, *107* (10), 4111–4132.
(211) Kulkarni, A. D.; Wang, L.-L.; Johnson, D. D.; Sholl, D. S.; Johnson, J. K. First-Principles Characterization of Amorphous Phases of MB 12 H 12 , M = Mg, Ca. *J. Phys. Chem. C* **2010**, *114* (34), 14601–14605.
(212) Wang, L.; Graham, D. D.; Robertson, I. M.; Johnson, D. D. On the Reversibility of Hydrogen-Storage Reactions in Ca(BH4)2 : Characterization via Experiment and Theory. *J. Phys. Chem. C* **2009**, *113*, 20088–20096.
(213) Rönnebro, E. Development of Group II Borohydrides as Hydrogen Storage Materials. *Curr. Opin. Solid State Mater. Sci.* **2011**, *15* (2), 44–51.
(214) Liu, Y.; Giri, S.; Zhou, J.; Jena, P. Intermediate Phases during Decomposition of Metal Borohydrides, M(BH4)n (M = Na, Mg, Y). *J. Phys. Chem. C* **2014**, *118* (49), 28456–28461.
(215) Zavorotynska, O.; Deledda, S.; Hauback, B. C. B. C. Kinetics Studies of the Reversible Partial Decomposition Reaction in Mg(BH4)2. *Int. J. Hydrogen Energy* **2016**, *41* (23), 9885–9892.
(216) Soloveichik, G. L.; Gao, Y.; Rijssenbeek, J.; Andrus, M.; Kniajanski, S.; Bowman, R. C.; Hwang, S. J.; Zhao, J. C. Magnesium Borohydride as a Hydrogen Storage Material: Properties and Dehydrogenation Pathway of Unsolvated Mg(BH4)2. *Int. J. Hydrogen Energy* **2009**, *34* (2), 916–928.
(217) Riktor, M. D.; Sørby, M. H.; Muller, J.; Bardají, E. G.; Fichtner, M.; Hauback, B. C. On the Rehydrogenation of Decomposed Ca(BH4)2. *J. Alloys Compd.* **2015**, *632*, 800–804.
(218) Minella, C. B.; Garroni, S.; Olid, D.; Teixidor, F.; Pistidda, C.; Lindemann, I.; Gut, O.; Bar, M. D.; Klassen, T.; Dornheim, M. Experimental Evidence of Ca [B12H12] Formation During Decomposition of a Ca(BH4)2+MgH2 Based Reactive Hydride Composite. *J. Phys. Chem. C* **2011**, *115*, 18010–18014.
(219) Saldan, I.; Hino, S.; Humphries, T. D.; Zavorotynska, O.; Chong, M.; Jensen, C. M.; Deledda, S.; Hauback, B. C. Structural Changes Observed during the Reversible Hydrogenation of Mg(BH4)2 with Ni-Based Additives. *J. Phys. Chem. C* **2014**, *118*, 23376–23384.
(220) He, L.; Li, H.-W.; Tumanov, N.; Filinchuk, Y.; Akiba, E. Facile Synthesis of Anhydrous Alkaline Earth Metal Dodecaborates MB12H12 (M=Mg,Ca) from M(BH4)2. *Dalt. Trans.* **2015**, *44* (36), 15882–15887.
(221) Rueda, M.; Sanz-Moral, L. M.; Girella, A.; Cofrancesco, P.; Milanese, C.; Martï¿½n, ï¿½ngel. Reversible Hydrogen Sorption in the Composite Made of Magnesium Borohydride and Silica Aerogel. *Int. J. Hydrogen Energy* **2016**, *41* (34), 15245–15253.
(222) Kim, J.; Shim, J.; Cho, Y. W. On the Reversibility of Hydrogen Storage in Ti- and Nb-Catalyzed Ca(BH4)2. *J. Power Sources* **2008**, *181*, 140–143.
(223) Ibikunle, A. A.; Goudy, A. J. Kinetics and Modeling Study of a Mg(BH4)2/Ca(BH4)2 Destabilized System. *Int. J. Hydrogen Energy* **2012**, *37* (17), 12420–12424.
(224) Durojaiye, T.; Ibikunle, A.; Goudy, A. J. Hydrogen Storage in Destabilized Borohydride Materials. *Int. J. Hydrogen Energy* **2010**, *35* (19), 10329–10333.
(225) Fichtner, M.; Chlopek, K.; Longhini, M.; Hagemann, H. Vibrational Spectra of Ca(BH4)2. *J. Phys. Chem. C* **2008**, *112*, 11575–11579.
(226) Liu, A.; Xie, S.; Dabiran-Zohoory, S.; Song, Y. High-Pressure Structures and Transformations of Calcium Borohydride Probed by Combined Raman and Infrared Spectroscopies. *J. Phys. Chem. C* **2010**, *114* (26), 11635–11642.
(227) Stadie, N. P.; Callini, E.; Richter, B.; Jensen, T. R.; Borgschulte, A.; Züttel, A. Supercritical N2 Processing as a Route to the Clean Dehydrogenation of Porous Mg(BH4)2. *J. Am. Chem. Soc.* **2014**, *136* (23), 8181–8184.
(228) Chong, M.; Abhi, K.; Tom, A.; Shin-ichi, O.; Satish, J.; Jensen, C. M. Reversible Dehydrogenation of Magnesium Borohydride to Magnesium Triborane in the Solid State under Moderate Conditions. *Chem. Commun.* **2011**, *47*, 1330–1332.

(229) Chong, M.; Matsuo, M.; Orimo, S.; Autrey, T.; Jensen, C. M. Selective Reversible Hydrogenation of Mg(B3H8)2/MgH2 to Mg(BH4)2: Pathway to Reversible Borane-Based Hydrogen Storage? *Inorg. Chem.* **2015**, *54*, 4120–4125.
(230) Kim, Y.; Reed, D.; Lee, Y.; Lee, J. Y.; Shim, J.; Book, D.; Cho, Y. W. Identification of the Dehydrogenated Product of Ca(BH4)2. *J. Phys. Chem. C* **2009**, *113*, 5865–5871.
(231) Kim, Y.; Hwang, S.; Lee, Y. S.; Suh, J.; Han, H. N.; Cho, Y. W. Hydrogen Back-Pressure Effects on the Dehydrogenation Reactions of Ca(BH 4) 2. *J. Phys. Chem. C* **2012**, *116* (49), 25715–25720.
(232) Minella, C. B.; Pistidda, C.; Garroni, S.; Nolis, P.; Baro, M. D.; Gut, O.; Klassen, T.; Bormann, R.; Dornheim, M. Ca(BH4)2+MgH2: Desorption Reaction and Role of Mg on Its Reversibility. *J. Phys. Chem. C* **2013**, *117*, 3846–3852.
(233) Muetterties, E. L.; Merrifield, R. E.; Miller, H. C.; Knoth, W. H.; Downing, J. R. Chemistry of Boranes. III. 1 The Infrared and Raman Spectra of B 12 H 12 - and Related Anions. *J. Am. Chem. Soc.* **1962**, *84* (13), 2506–2508.
(234) Schouwink, P.; Ramel, A.; Giannini, E.; Radovan, Č. Flux-Assisted Single Crystal Growth and Heteroepitaxy of Perovskite-Type Mixed-Metal Borohydrides. **2015**.
(235) Schouwink, P.; Ley, M. B.; Jensen, T. R.; Smrčok, L.; Černý, R. Borohydrides: From Sheet to Framework Topologies. *Dalt. Trans.* **2014**, *43* (21), 7726.
(236) Filinchuk, Y.; Richter, B.; Jensen, T. R.; Dmitriev, V.; Chernyshov, D.; Hagemann, H. Porous and Dense Magnesium Borohydride Frameworks: Synthesis, Stability, and Reversible Absorption of Guest Species. *Angew. Chemie Int. Ed.* **2011**, *50* (47), 11162–11166.
(237) Lang, J.; Gerhauser, A.; Filinchuk, Y.; Klassen, T.; Huot, J. Differential Scanning Calorimetry (DSC) and Synchrotron X-Ray Diffraction Study of Unmilled and Milled LiBH4: A Partial Release of Hydrogen at Moderate Temperatures. *Crystals* **2011**, *2* (4), 1–21.
(238) Urgnani, J.; Torres, F. J.; Palumbo, M.; Baricco, M. Hydrogen Release from Solid State NaBH4. *Int. J. Hydrogen Energy* **2008**, *33* (12), 3111–3115.
(239) Martínez-Coronado, R.; Retuerto, M.; Torres, B.; Martínez-Lope, M. J.; Fernández-Díaz, M. T.; Alonso, J. A. High-Pressure Synthesis, Crystal Structure and Cyclability of the Mg2NiH4 Hydride. *Int. J. Hydrogen Energy* **2013**, *38* (14), 5738–5745.
(240) Noréus, D. Properties of Formal Low-Valence Transition Metal - Hydrogen Complexes in Mg2NiH4 and Na2PdH2. *Zeitschrift für Phys. Chemie* **1989**, *163* (Part_2), 575–578.
(241) Čermák, J.; Král, L.; David, B. Hydrogen Diffusion in Mg2NiH4 Intermetallic Compound. *Intermetallics* **2008**, *16* (4), 508–517.
(242) Zeng, K.; Klassen, T.; Oelerich, W.; Bormann, R. Thermodynamic Analysis of the Hydriding Process of Mg–Ni Alloys. *J. Alloys Compd.* **1999**, *283* (1–2), 213–224.
(243) Révész, Á.; Gajdics, M.; Schafler, E.; Calizzi, M.; Pasquini, L. Dehydrogenation-Hydrogenation Characteristics of Nanocrystalline Mg2Ni Powders Compacted by High-Pressure Torsion. *J. Alloys Compd.* **2017**, *702*, 84–91.
(244) Zhao-Karger, Z.; Witter, R.; Bardaji, E. G.; Wang, D.; Cossement, D.; Fichtner, M. Altered Reaction Pathways of Eutectic LiBH4-Mg(BH4)2 by Nanoconfinement. *J. Mater. Chem. A* **2013**, *1* (10), 3379.
(245) Lee, Y.-S.; Filinchuk, Y.; Lee, H. S.; Suh, J.-Y.; Kim, J. W.; Yu, J.-S.; Cho, Y. W. On the Formation and the Structure of the First Bimetallic Borohydride Borate, LiCa 3 (BH 4)(BO 3) 2. *J. Phys. Chem. C* **2011**, *115* (20), 10298–10304.
(246) Ampoumogli, A.; Charalambopoulou, G.; Javadian, P.; Richter, B.; Jensen, T. R.; Steriotis, T. Hydrogen Desorption and Cycling Properties of Composites Based on Mesoporous Carbons and a LiBH4–Ca(BH4)2 Eutectic Mixture. *J. Alloys Compd.* **2015**, *645*, S480–S484.
(247) Lee, H. S.; Hwang, S.-J.; Kim, H. K.; Lee, Y.-S.; Park, J.; Yu, J.-S.; Cho, Y. W. In Situ NMR Study on the Interaction between LiBH 4 –Ca(BH 4) 2 and Mesoporous Scaffolds. *J. Phys. Chem. Lett.* **2012**, *3* (20), 2922–2927.
(248) Chaudhary, A.-L.; Li, G.; Matsuo, M.; Orimo, S.; Deledda, S.; Sørby, M. H.; Hauback, B. C.; Pistidda, C.; Klassen, T.; Dornheim, M. Simultaneous Desorption Behavior of M Borohydrides and Mg2FeH6 Reactive Hydride Composites (M = Mg, Then Li, Na, K, Ca).

Appl. Phys. Lett. **2015**, *107* (7), 073905.
(249) Vajo, J. J.; Li, W.; Liu, P. Thermodynamic and Kinetic Destabilization in LiBH4/Mg2NiH4: Promise for Borohydride-Based Hydrogen Storage. *Chem. Commun.* **2010**, *46* (36), 6687.
(250) Li, W.; Vajo, J. J.; Cumberland, R. W.; Liu, P.; Hwang, S.-J.; Kim, C.; Bowman, R. C. Hydrogenation of Magnesium Nickel Boride for Reversible Hydrogen Storage. *J. Phys. Chem. Lett.* **2010**, *1* (1), 69–72.
(251) Afonso, G.; Bonakdarpour, A.; Wilkinson, D. P. Hydrogen Storage Properties of the Destabilized 4NaBH4/5Mg2NiH4 Composite System. *J. Phys. Chem. C* **2013**, *117* (41), 21105–21111.
(252) Bergemann, N.; Pistidda, C.; Milanese, C.; Emmler, T.; Karimi, F.; Chaudhary, A.-L.; Chierotti, M. R.; Klassen, T.; Dornheim, M. Ca(BH4)2–Mg2NiH4: On the Pathway to a Ca(BH4)2 System with a Reversible Hydrogen Cycle. *Chem. Commun.* **2016**, *52* (26), 4836–4839.
(253) Javadian, P.; Zlotea, C.; Ghimbeu, C. M.; Latroche, M.; Jensen, T. R. Hydrogen Storage Properties of Nanoconfined LiBH 4 –Mg 2 NiH 4 Reactive Hydride Composites. *J. Phys. Chem. C* **2015**, *119* (11), 5819–5826.
(254) Blomqvist, H.; Noréus, D. Mechanically Reversible Conductor–insulator Transition in Mg2NiH4. *J. Appl. Phys.* **2002**, *91* (8), 5141–5148.
(255) Polanski, M.; Nielsen, T. K.; Kunce, I.; Norek, M.; Płociński, T.; Jaroszewicz, L. R.; Gundlach, C.; Jensen, T. R.; Bystrzycki, J. Mg2NiH4 Synthesis and Decomposition Reactions. *Int. J. Hydrogen Energy* **2013**, *38* (10), 4003–4010.
(256) Javadian, P.; GharibDoust, S. P.; Li, H.-W.; Sheppard, D. A.; Buckley, C. E.; Jensen, T. R. Reversibility of LiBH4 Facilitated by the LiBH4–Ca(BH4)2 Eutectic. *J. Phys. Chem. C* **2017**, *121* (34), 18439–18449.
(257) Albanese, E.; Kalantzopoulos, G. N.; Vitillo, J. G.; Pinatel, E.; Civalleri, B.; Deledda, S.; Bordiga, S.; Hauback, B. C.; Baricco, M. Theoretical and Experimental Study on Mg(BH4)2–Zn(BH4)2 Mixed Borohydrides. *J. Alloys Compd.* **2013**, *580*, S282–S286.
(258) Černý, R.; Penin, N.; D'Anna, V.; Hagemann, H.; Durand, E.; Růžička, J. MgxMn(1−x)(BH4)2 (X=0–0.8), a Cation Solid Solution in a Bimetallic Borohydride. *Acta Mater.* **2011**, *59* (13), 5171–5180.
(259) Rude, L. H.; Filsø, U.; D'Anna, V.; Spyratou, A.; Richter, B.; Hino, S.; Zavorotynska, O.; Baricco, M.; Sørby, M. H.; Hauback, B. C.; et al. Hydrogen–fluorine Exchange in NaBH4–NaBF4. *Phys. Chem. Chem. Phys.* **2013**, *15* (41), 18185.
(260) Paterakis, C.; Guo, S.; Heere, M.; Liu, Y.; Contreras, L. F.; Sørby, M. H.; Hauback, B. C.; Reed, D.; Book, D. Study of the NaBH 4 –NaBr System and the Behaviour of Its Low Temperature Phase Transition. *Int. J. Hydrogen Energy* **2017**, *42* (35), 22538–22543.
(261) Schouwink, P.; Ramel, A.; Giannini, E.; Černý, R.; Radovan, Č.; Černý, R.; Radovan, Č. Flux-Assisted Single Crystal Growth and Heteroepitaxy of Perovskite-Type Mixed-Metal Borohydrides. *CrystEngComm* **2015**, *17* (13), 2682–2689.

Take home messages

Do Science! Travel, Live, Love, Communicate. Science is everywhere and for everyone, especially for woman!

"You can make more friends in two months by becoming interested in other people than you can in two years by trying to get other interested in you"
– Dale Carnegie

Cheers, to HYDROGEN! --- Be amorphous, stay cool!
- Cit.

"Prendi il largo!"

"Duc in altum!"

Luke 5:4